SAE Aerospace
An SAE International Group

AEROSPACE INFORMATION REPORT

SAE AIR1419 | REV. B

Issued 1983-05
Reaffirmed 2011-07
Revised 2013-05

Superseding AIR1419A

(R) Inlet Total-Pressure-Distortion Considerations for Gas-Turbine Engines

RATIONALE

The intent of this document is to provide a basic understanding of the effects of inlet total-pressure distortion on the performance of gas turbine engines, particularly in military applications.

FOREWORD

Changes in this revision have been made to reflect new knowledge in the following areas:

- Computational Fluid Dynamics, CFD, has become widely used for design and analysis
- Highly offset inlets have imposed additional challenges
- Full Authority Digital Electronic Control, FADEC, systems have become commonplace
- New methods of distortion synthesis have been developed
- New instrumentation techniques have been developed
- New techniques for data acquisition, storage, and processing have been developed
- Testing methodology/procedures have changed
- Some previously state-of-the-art techniques have become obsolete

The philosophy that was adopted to implement changes was:

- Only added material that didn't exist in original document
- Revised dated references to "state-of-the-art," "current technology," etc.
- Removed discussion of analog computers and other technological sections that are no longer applicable
- Generally avoided text-editing existing sections that are still applicable
- Made terminology consistent with recent ARP1420 revisions

This document has been cleared for public release with PA number AEDC2012-091.

TO PLACE A DOCUMENT ORDER: Tel: 877-606-7323 (inside USA and Canada)
Tel: +1 724-776-4970 (outside USA)
Fax: 724-776-0790
Email: CustomerService@sae.org
SAE WEB ADDRESS: http://www.sae.org

SAE values your input. To provide feedback on this Technical Report, please visit
http://www.sae.org/technical/standards/AIR1419B

PREFACE

Industry and government agencies concerned with aircraft design and operation recognize a need to improve methodology and communication on spatial total-pressure distortion aspects of the inlet/engine compatibility problem. The appearance of modern turbofan engines in the late 1960s focused attention on this need, and there followed a period of intense activity to develop engineering techniques for assuring adequate stability. These techniques were identified, formulated and exercised independently in various parts of industry to solve flow distortion problems on specific systems. The aircraft and engine companies form a matrix of cooperative engineering activity in the international military and civil aircraft market, and a third dimension is added by the group of customers. The three groups needed to consolidate individual experience, establish common ground, and gain a perspective concerning the applicability and accuracy of these techniques. Adequate resolution of the aircraft/engine stability problem would depend upon generating generally usable guidelines addressing analysis, test, data processing, and information transfer which would be applied in a manner consistent with the expected severity of the problem.

The SAE International Aerospace Council Divisional Technical Committee S-16 (Turbine Engine Inlet Flow Distortion Committee) was formed in 1972 to examine the aircraft gas turbine engine/inlet compatibility development process, as affected by flow distortion, to assess what experience was common throughout industry or what could be agreed as desirable to make common. The Committee formulated a number of guidelines to improve communications and minimize repetitive workloads among program participants. It recognized that practices employed to cope with flow distortion effects were young and changing and that in several critical areas, practice was not sufficiently common or defined to warrant establishing guidelines. For these reasons the guidelines were purposely limited, and were organized and published in March 1978 as Aerospace Recommended Practice ARP1420, Gas Turbine Engine Inlet Flow Distortion Guidelines. ARP1420 was circulated widely in the U.S. and European aeronautical industries. Significant comments and opinions were expressed, and were carefully considered by the Committee prior to submitting the ARP to the SAE Aerospace Council for publication.

The S-16, in its proceedings, produced a wealth of information which, in its entirety, contained a significant part of the flow-distortion-related corporate knowledge of the industry as it existed in the mid-1970s time period. The Committee decided that this information, organized into a generally available document, would provide a source of knowledge for engineers new to the problems of inlet-engine compatibility. The Committee, therefore, compiled Aerospace Information Report AIR1419 Inlet-Total-Pressure Distortion Considerations for Gas-Turbine Engines to amplify the information contained in ARP1420 and to provide a corporate memory.

SAE Technical Committee S-16, through its members and liaison representatives, represents a cross section of the part of government and industry having the major share of the responsibility for assuring economical, safe, and instability-free propulsion systems. The organizations that sponsor S-16 and make possible, through the members and representatives, ARP1420, AIR1419, and other inlet distortion documents, should be commended. These documents exist today because of their active concern for the distortion problem and their willingness to provide resources to obtain solutions. The members and representatives collectively contributed hundreds of hours of work between Committee meetings to assure worthwhile results and productive meetings.

TABLE OF CONTENTS

1. SCOPE

This document addresses many of the significant issues associated with effects of inlet total-pressure distortion on turbine-engine performance and stability. It provides a review of the development of techniques used to assess engine stability margins in the presence of inlet total-pressure distortion. Specific performance and stability issues that are covered by this document include total-pressure recovery and turbulence effects and steady and dynamic inlet total-pressure distortion.

1.1 Purpose

The purpose of this document is to provide specific information about determining the effects of inlet total-pressure distortion on turbine-engine performance and stability. Testing methodologies and computational fluid dynamics (CFD) approaches are described. Types and scales of testing hardware are discussed with applications for each.

2. REFERENCES

2.1 Applicable Documents

The following publications form a part of this document to the extent specified herein. The latest issue of SAE publications shall apply. The applicable issue of other publications shall be the issue in effect on the date of the purchase order. In the event of conflict between the text of this document and references cited herein, the text of this document takes precedence. Nothing in this document, however, supersedes applicable laws and regulations unless a specific exemption has been obtained.

2.1.1 SAE Publications

Available from SAE International, 400 Commonwealth Drive, Warrendale, PA 15096-0001, Tel: 877-606-7323 (inside USA and Canada) or 724-776-4970 (outside USA), www.sae.org.

2.1.1.1 ARP1420B, “Gas Turbine Engine Inlet Flow Distortion Guidelines.”

2.1.1.2 SAE 680286, “Integration of Inlet and Engine - An Engine Man’s Point of View.”

2.1.1.3 AIR5656, “Statistical Stability Assessment.”

2.1.1.4 AS681J, “Gas Turbine Engine Performance Presentation for Computer Programs.”

2.1.1.5 ARP246C, “Orientation of Engine Axis, Coordinate and Numbering Systems for Aircraft Gas Turbine Engines.”

2.1.1.6 ARP1210D, “Gas Turbine Engine Interface Test Data Reduction Computer Programs.”

2.1.1.7 AS755D, “Aircraft Propulsion System Performance Station Designation and Nomenclature.”

2.1.1.8 SAE 740824, “Supersonic Inlet Simulator - A Tool for Simulation of Realistic Engine Entry Flow Conditions.”

2.1.1.9 AIR5687, “Inlet/Engine Compatibility - From Model to Full Scale Development."

2.1.1.10 AIR5686, “A Methodology for Assessing Inlet Swirl Distortion.”

2.1.1.11 AIR5866, “An Assessment of Planar Waves.”

2.1.1.12 ARP5826, "Distortion Synthesis/Estimation Techniques."

2.1.1.13 AIR5396, "Characterizations of Aircraft Icing Conditions."

2.2 Applicable References

2.2.1 Brimelow, B. and Steenken, W. G., “Compatibility Technology Requirements, Proceedings of the Project Squid Workshop on Engine-Airframe Integration - Short Haul Aircraft,” Purdue University, Report No. PU-R1-78, May 1977.

2.2.2 Braithwaite, W. M., Graber, E. J., Jr., and Mehalic, C. M., “The Effect of Inlet Temperature and Pressure Distortion on Turbojet Performance,” AIAA 73-1316, November 1973.

2.2.3 Brimelow, B., Collins, T. P., and Pfefferkorn, G. A., “Engine Testing in a Dynamic Environment,” AIAA 74-1198, October 1974.

2.2.4 Plourde, G. A. and Brimelow, B., “Pressure Fluctuations Cause Compressor Instability,” Proceedings of the Air Force Airframe-Propulsion Compatibility Symposium, AD0876608, June 1970.

2.2.5 Calogeras, J. E., Mehalic, C. M., and Burstadt, P. L., “Experimental Investigation of the Effect of Screen Induced Total Pressure Distortion on Turbojet Stall Margin,” NASA-TM-X-2239, March 1971.

2.2.6 Williams, D. D. and Yost, J. O., “Some Aspects of Inlet/Engine Flow Compatibility," Aeronautical Journal, September 1973.

2.2.7 Gray, W. G., “Propulsion System Flow Stability Program (Dynamic),” AFAPL-TR-68-142, Part IV, December 1968.

2.2.8 Reynolds, G. G., Vier, W. F., and Collins, T. P., “An Experimental Evaluation of Unsteady Flow Effects on an Axial Compressor - P^3 Generator Program,” AD0767615, July 1973.

2.2.9 Hodder, B. K., “An Investigation of Engine Influence on Inlet Performance,” NASA-CR-166136, January 1981.

2.2.10 Johnson, R. H., “Inlet Distortion Scaling of Wind Tunnel Model Results,” NASA-CR-143840, December 1976.

2.2.11 Spong, E. D., Hammock, M. S., and Stevens, C. H., “F-15 Inlet/Engine Test Techniques and Distortion Methodology Studies,” Volume I, Technical Discussion, NASA-CR-144866, June 1978.

2.2.12 Johnson, R. H., “Comparison of Inlet Distortion from Flight and Wind Tunnel Tests,” NASA-CR-144864, April 1978.

2.2.13 MacMiller, C. J., “Investigation of Subsonic Duct Distortion,” AD0859930, March 1969.

2.2.14 Armstrong, E. K. and Williams, D. D., “Some Intake Flow Maldistribution Effects on Compressor Rotor Blade Vibration,” Journal of Sound and Vibration, Vol. 3, pp. 349-354, May 1966.

2.2.15 Danforth, C. E., “Distortion Induced Vibration in Fan and Compressor Blading,” AIAA-1974-232, January 1974.

2.2.16 Sisto, F., “Aeromechanical Response,” AGARD Lecture Series No. 72 on Distortion Induced Engine Stability, AGARD-LS-72, Paper No. 4, October 1974.

2.2.17 Mikolojczak, A. A., Arnoldi, R. A., Snyder, L. E., and Stargardter, H., “Advances in Fan and Compressor Blade Flutter Analysis and Predictions,” Journal of Aircraft, Vol. 12, pp. 325-332, April 1975.

2.2.18 Huffman, G. D., Ostdiek, F. R., and Rivir, R. B., "An Assessment of Flow Quality Requirements for the Compressor Research Facility," ADA023888, January 1976.

2.2.19 Overall, B. W. and Harper, R. E., "The Air Jet Distortion Generator System - A New Tool for Aircraft Turbine Engine Testing," AIAA 77-993, July 1977.

2.2.20 Korn, J. A. and McKain, T. F., "Exploratory Research Into Turbofan Stability Performance," Vol. I and II, AD0771073 and AD0771074, November 1973.

2.2.21 Braithwaite, W. M., Dicus, J. H., and Moss, J. E., Jr., "Evaluation with a Turbofan Engine of Air Jets as a Steady State Inlet Flow Distortion Device," NASA-TM-X-1955, January 1970.

2.2.22 Collins, T. P., "The Aerothermodynamics of Aircraft Gas Turbine Engines: Engine Stability Considerations," Oates, G. C., Editor, ADA059784, pp. 23-1 to 23-9, July 1978.

2.2.23 Ogorodnikov, D. A. and Yanchuck, V. A., "Investigation of Flow Pattern Simulation at Supersonic Flight Speed," International Symposium of Air Breathing Engines, March 1976.

2.2.24 Lazalier, G. R. and Tate, J. T., "Development of a Prototype Discrete Frequency, Total Pressure Fluctuation Generator for Jet Engine/Inlet Compatibility Investigation," Proceedings of the Air Force Airframe-Propulsion Compatibility Symposium, AD0876608, June 1970.

2.2.25 Crites, R. C. and Heckert, M. V., "Application of Random Data Techniques to Aircraft Inlet Diagnostics," AIAA 70-597, May 1970.

2.2.26 Schweikard, W. G., "Test Techniques, Instrumentation, and Data Processing," AGARD Lecture Series No. 72 on Distortion Induced Engine Stability, AGARD-LS-72 Paper No. 6, October 1974.

2.2.27 Motycka, D. L., "Ground Vortex - Limit to Engine/Reverser Operation," Transactions of ASME, Journal of Engineering for Power, April 1976.

2.2.28 Billig, L. O., "Integrated Propulsion Control System (IPCS) Final Report," ADA032439, ADA033774, ADA034172, and ADA033062, August 1976.

2.2.29 Steenken, W. G., "Effect of Transducer Diameter on Resolution of Total Pressure Fluctuations in Turbulent Flow," Progress in Astronautics and Aeronautics, Volume 34, Instrumentation for Airbreathing Propulsion, 1974.

2.2.30 G Systems Inc., "Using LabVIEW Real-Time and Dynamic Signal Acquisition (DSA) for Propulsion Inlet Flow Distortion Pattern Assessment in Jet Engine Inlets," 2003.

2.2.31 Holzman, J. K. and Payne, G., "Design and Flight Testing of a Nullable Compressor Face Rake," NASA-TN-D-7162, January 1973.

2.2.32 Arend, D. J. and Saunders, J. D., "An Experimental Evaluation of the Performance of Two Combined Pitot Pressure Probes," AIAA 2009-1073, January 2009.

2.2.33 Malloy, D. J. and Minter, M. J., "New and Improved Test Technologies to Validate and Analyze High-Response Aerodynamic Test Data," AIAA 2008-1628, February 2008.

2.2.34 Shepard, D., "A Two-Dimensional Interpolation Function for Irregularly-Spaced Data," Proceedings of the 1968 23rd ACM National Conference, pp. 517-524, January 1968.

2.2.35 Oates, Gordon C., "Aircraft Propulsion Systems Technology and Design," AIAA, 1989.

2.2.36 Kostin, L. C. and Millstone, S. D., “Application of Statistical Parameters in Defining Inlet Airflow Dynamics,” AIAA-68-649, June 1968.

2.2.37 Cohen, H., Rogers, G. F. C., and Saravanamuttoo, H. I. H., “Gas Turbine Theory,” Longman, Third Edition, 1987.

2.2.38 Johnsen, I. A. and Bullock, R. O. “Aerodynamic Design of Axial-Flow Compressors,” NASA SP-36, 1965.

2.2.39 Tesch, W. A., Moszee, R. H., and Steenken, W. G., “Linearized Blade Row Compression Component Model: Stability and Frequency Response Analysis of a J85-13 Compressor,” NASA-CR-135162, Sept. 1976.

2.2.40 Cumpsty, N. A, “Compressor Aerodynamics,” Longman Scientific and Technical, 1989.

2.2.41 Hearsey, R. M., “HTO300 – A Computer Program for the Design and Analysis of Axial Turbomachinery,” 1970.

2.2.42 Boyer, K. M. and O’Brien, W. F. “An Improved Streamline Curvature Approach for Off-Design Analysis of Transonic Axial Compression Systems,” Transactions of the ASME, Journal of Turbomachinery, Vol. 125, pp. 475-481, July 2003.

2.2.43 Greitzer, E. M., “Surge and Rotating Stall in Axial Flow Compressors, Part I: Theoretical Compression System Model,” ASME Journal of Engineering for Power, Vol. 98, pp. 190-198, April 1976.

2.2.44 Greitzer, E. M., “Surge and Rotating Stall in Axial Flow Compressors, Part II: Experimental Results and Comparisons with Theory,” ASME Journal of Engineering for Power, Vol. 98, pp. 199-217, April 1976.

2.2.45 Hale, A. A. and Davis, M. W., Jr., "DYNamic Turbine Engine Compressor Code (DYNTECC) - Theory and Capabilities," AIAA-92-3190, July 1992.

2.2.46 Reynolds, G. G. and Steenken, W. G., “Dynamic Digital Blade Row Compression Component Stability Model: Model Validation and Analysis of Planar Pressure Pulse Generator and Two-Stage Fan Test Data,” AFAPL-TR-76-76, August 1976.

2.2.47 Hosney, W. M., Bitter, S. J., and Steenken, W. G., “Turbofan Engine Non-Recoverable Stall Computer Simulation Development and Validation,” AIAA-85-1432, July 1985.

2.2.48 Ward, G. G., “Compressor Stability Assessment Program (Techniques for Constructing Mathematical Models of Compression Systems and Propulsion Systems),” Air Force Aero Propulsion Laboratory, TR-74-107, Vol. II, Wright-Patterson Air Force Base, OH, December 1974.

2.2.49 Davis, M. W., Jr., “A Stage-by-Stage Dual-Spool Compression System Modeling Technique,” ASME 82-GT-189, March 1982.

2.2.50 Hosney, W. M. and Steenken, W. G., “Aerodynamic Instability Performance of an Advanced High-Pressure-Ratio Compression Component,” AIAA-86-1619, June 1986.

2.2.51 Mazzawy, R. S., “Multiple Segment Parallel Compressor Model for Circumferential Flow Distortion,” Transactions of the ASME, Journal of Engineering for Power, pp. 288-296, April 1977.

2.2.52 Tesch, W. A. and Steenken, W. G., “Blade Row Dynamic Digital Compressor Program, Vol. 1, J85, Clean Inlet Flow and Parallel Compressor Models,” NASA CR-134978, March 1976.

2.2.53 Longley, J. P. and Greitzer, E. M. “Inlet Distortion Effects in Aircraft Propulsion System Integration,” AGARD-LS-183, Advisory Group for Aerospace Research & Development Lecture Series, May 1992.

2.2.54 Shahrohki, K. A. and Davis, Jr., M. W., "Application of a Modified Dynamic Compression System Model to a Low-Aspect Ratio Fan: Effects of Inlet Distortion," AIAA-95-0301, January 1995.

2.2.55 Davis, M. W., Jr., "Parametric Investigation into the Combined Effects of Pressure and Temperature Distortion on Compression System Stability," AIAA-91-1895, June 1991.

2.2.56 Cousins, William T., et al., "Inlet Distortion Testing and Analysis of a High-Bypass Ratio Turbofan Engine," Presented at the 16th International Symposium on Air Breathing Engines, ISABE-2003-1110, August, 2003.

2.2.57 Hynes, T. P. and Greitzer, E. M., "A Method for Assessing Effects of Inlet Flow Distortion on Compressor Stability," Transactions of the ASME, Journal of Turbomachinery, Vol. 109, pp. 371-379, 1987.

2.2.58 Davis, Milt and Hale, Alan, "A Parametric Study on the Effects of Inlet Swirl on Compression System Performance and Operability Using Numerical Simulations," GT2007-27033, May 2007.

2.2.59 Davis, Milt, Jr., Beale, Dave, and Sheoran, Yogi, "Integrated Test and Evaluation Techniques as Applied to an Inlet Swirl Investigation Using the F109 Gas Turbine Engine," GT2008-50074, June 2008.

2.2.60 Bouldin, B. and Sheoran, Y., "Impact of Complex Swirl Patterns on Compressor Performance and Operability Using Parallel Compressor Analysis," ISABE2007-1140, September 2007.

2.2.61 Hale, A. A. and O'Brien, W. F., "A Three-Dimensional Turbine Engine Analysis Compressor Code (TEACC) for Steady-State Inlet Distortion," Transactions of the ASME, Journal of Turbomachinery, Vol. 120, pp. 422-430, July 1998.

2.2.62 Gong, Y., Tan, C., Gordon, K. A., and Greitzer, E. M., "A Computational Model for Short-Wavelength Stall Inception and Development in Multistage Compressors," Transactions of the ASME, Journal of Turbomachinery, Vol. 121, pp. 726-734, October 1999.

2.2.63 Chima, R. "A Three-Dimensional Unsteady CFD Model of Compressor Stability," ASME GT2006-90040, May 2006.

2.2.64 Davis, Milt, Hale, Alan, and Beale, Dave. "An Argument for Enhancement of the Current Inlet Distortion Ground Test Practice for Aircraft Gas Turbine Engines," Transactions of the ASME, Journal of Turbomachinery, pp. 235-241, April 2002.

2.2.65 Hale, Alan, Davis, Milt, and Sirbaugh, Jim, "A Numerical Simulation Capability for Analysis of Aircraft Inlet-Engine Compatibility," Journal of Engineering for Gas Turbines and Power, Vol. 128, pp. 473-481, July 2006.

2.2.66 Yao, J., Gorrell, S. E., and Wadia, A. R., "High-Fidelity Numerical Analysis of Per-Rev-Type Inlet Distortion Transfer in Multistage Fans – Part I: Simulations with Selected Blade Rows," ASME GT2008-50812, June 2008.

2.2.67 Yao, J., Gorrell, S. E., and Wadia, A. R., "High-Fidelity Numerical Analysis of Per-Rev-Type Inlet Distortion Transfer in Multistage Fans – Part II: Entire Component Simulation and Investigation," ASME GT2008-50813, June 2008.

2.2.68 Wallner, L. E., Useller, J. W., and Saari, M. J., "A Study of Temperature Transients at the Inlet of a Turbojet Engine," NACA RM E57C22, June 1957.

2.2.69 DiPietro, A. L., Jr., and O'Brien, W. F., "Design and Experimental Evaluation of a Dynamic Thermal Distortion Generator for Turbomachinery Research," AIAA 94-0149, January 1994.

2.2.70 Aini, Y., deLaneuville, R., Stoner, A., and Capece, V., “High Cycle Fatigue of Turbomachinery Components - Industry Perspective,” AIAA-1997-3365, July 1997.

2.2.71 Manwaring, S., Rabe, D., Lorence, C., and Wadia, A., “Inlet Distortion Generated Forced Response of a Low-Aspect-Ratio, Transonic Fan,” Journal of Turbomachinery, Vol. 119, pp. 665-676, October 1997.

2.2.72 Hamed, A., and Numbers, K. “Inlet Distortion Considerations for High Cycle Fatigue in Gas Turbine Engines,” AIAA-1997-3364, July 1997.

2.2.73 Jones, H., “Development of a Noninterference Technique for Measuring Turbine Engine Rotor Blade Stresses,” AIAA-1985-1472, July 1985.

2.2.74 Chi, R., and Jones, H., “Demonstration Testing of a Noninterference Technique for Measuring Turbine Engine Rotor Blade Stresses,” AIAA-1988-3143, July 1988.

2.2.75 Vining, C., Arnold, S., Hayes, B., and Howard, R., “PC-Based Generation 4 Non-Contact Stress Measurement System,” Proceedings of the 10th National Turbine Engine High-Cycle Fatigue Conference, March 2005.

2.2.76 Emmons, H. W., Pearson, C. E., and Grant, H. P., “Compressor Surge and Stall Propagation,” Transactions of the ASME, Vol. 77, No. 4, pp. 455-467, May 1955.

2.2.77 Day, I. J., and Cumpsty, N. A., “The Measurement and Interpretation of Flow within Rotating Stall Cells in Axial Compressors,“ Journal of Mechanical Engineering Sciences, The Institution of Mechanical Engineers, Vol. 20, No. 2, 1978.

2.2.78 Day, I. J., “Axial Compressor Stall,” Ph. D. Dissertation, Christ’s College (Cambridge University), 1976.

2.2.79 Burwell, A. E., and Patterson, G. T., “Dynamic Engine Behavior During Post Surge Operation of a Turbofan Engine,” AIAA 85-1430, July 1985.

2.2.80 Moore, F. K., “A Theory of Rotating Stall of Multistage Axial Compressors,” NASA CR-3685, July 1983.

2.2.81 Greitzer, E. M., “Review – Axial Compressor Stall Phenomena,” Journal of Fluids Engineering, Vol. 102, pp. 134-151, June 1980.

2.2.82 Pampreen, R., “Compressor Surge and Stall,” Concepts ETI, Inc., ISBN 0-933283-05-9,1993.

2.2.83 Davis, M. W., Jr., "A Stage-by-Stage Post-Stall Compression System Modeling Technique: Methodology, Validation, and Application," Ph.D. Dissertation, Virginia Polytechnic Institute and State University, December 1986.

2.2.84 Davis, M. W., Jr., "A Post-Stall Compression System Modeling Technique," AEDC-TR-86-34, February 1987.

2.2.85 Davis, M. W., Jr., and O'Brien, W. F., "Stage-by-Stage Poststall Compression System Modeling Technique," Journal of Propulsion and Power, Vol. 7, Number 6, pp. 997-1005, November-December 1991.

2.2.86 Owen, A. K., Mattern, D. L., and Le, K. D., “Comparisons of Rig and Engine Dynamic Events in the Compressor of an Axi-Centrifugal Turboshaft Engine,” ASME 96-GT-239, June 1996.

2.2.87 "Recommended Practices for the Assessment of the Effects of Atmospheric Water Ingestion on the Performance and Operability of Gas Turbine Engines," Propulsion and Energetics Panel Working Group 24, Advisory Group for Aerospace Research and Development, NATO, 1995.

2.2.88 Hale, Alan, Klepper, Jason, and Hurwitz, Wayne, "A Numerical Capability to Analyze the Effects of Water Ingestion on Compression System Performance and Operability," ASME GT2005-68480, June 2005.

2.3 Related Publications

The following publications are provided for information purposes only and are not a required part of this SAE Aerospace Technical Report.

2.3.1 Crites, R. C., "The Philosophy of Analog Techniques Applied to the Analysis and High Speed Screening of Dynamic Data," AIAA 70-595, May 1970.

2.3.2 Ellis, S. and Brownstein, Capt. B., "A Procedure for Estimating Maximum Time-Variant Distortion with Limited Instrumentation," AIAA 72-1099, December 1972.

2.3.3 Jacocks, J. L. and Kneile, K. R., "Statistical Prediction of Maximum Time-Variant Inlet Distortion Levels," AEDC-TR-74-121, January 1975.

2.3.4 Motycka, D. L., "Determination of Maximum Instantaneous Distortion Patterns from Statistical Properties of Inlet Pressure Data," AIAA 76-705, July 1976.

2.3.5 Melick, H. C., Ybarra, A. H., and Bencze, D. R., "Estimating Maximum Instantaneous Distortion from Inlet Total Pressure RMS and PSD Measurements," AIAA 75-1213, September 1975.

2.3.6 Chung, K., Hosny, W. M., and Steenken, W. G., "Aerodynamic Stability Analysis of NASA J85-13/Planar Pressure Pulse Generator Installation," NASA-CR-165141, November 1980.

2.3.7 Chamblee, C. E., Davis, M. W., and Kimzey, W. F., "A Multi-Stage Axial Flow Compressor Mathematical Modeling Technique with Application to Two Current Turbofan Compression Systems," AIAA 80-0054, January 1980.

2.3.8 Mehalic, C. M. and Lottig, R. A., "Steady-State Inlet Temperature Distortion Effects on the Stall Limits of a J85-GE-13 Turbojet Engine," NASA-TM-X-2990, February 1974.

2.3.9 Baghdadi, S. and Lueke, J. E., "Compressor Stability Analysis," ASME 81-WA/FE-18, November 1981.

2.3.10 Burstadt, P. L. and Wenzel, L. M., "A Method to Account for Variation of Average Compressor Inlet Pressure During Instantaneous Distortion Analysis," AIAA 76-703, July 1976.

2.3.11 Surber, L. and Sedlock, D., "Effects of Airframe Inlet Integration on Half-Axisymmetric and Two-Dimensional Supersonic Inlet Performance," AIAA 78-960, July 1978.

2.3.12 Stock, C. P. and Bissinger, N. C., "The Design and Development of the Tornado Engine Air Intake," AGARD Fluid Dynamics Symposium on Aerodynamics of Power Plant Installation, Paper No. 10, May 1981.

2.3.13 Mitchell, G. A., "Effect of Inlet Ingestion of a Wing Tip Vortex on Turbojet Stall Margin," NASA-TM-X-71610, September 1974.

2.3.14 Motycka, D. L. and Walter, W. A., "An Experimental Investigation of Ground Vortex Formation During Reverse Engine Operation," AIAA 75-1322, October 1975.

2.3.15 Wallace, R., Kenyon, J., King, P., and O'Brien, W., "Assessing Fan and Compressor Blade HCF Sensitivity to Non-Uniform Inlet Flows," ASME GT2004-54264, June 2004.

2.3.16 Longley, J. P., Shin, H-W, Plumley, R. E., Silkowski, P. D., Day, I. J., Greitzer, E. M., Tan, C. S., and Wisler, D. C., "Effects of Rotating Inlet Distortion on Multistage Compressor Stability," Transactions of the ASME, Journal of Turbomachinery, 1996.

2.3.17 Greitzer, E. M., Mazzawy, R. S., and Fulkerson, D. A., "Flow Field Coupling Between Compression Components in Asymmetric Flow," ASME 77-GT-17, March 1977.

2.3.18 Greitzer, E. M., and Griswold, H. R., "Coupled Compressor-Diffuser Interaction with Circumferential Flow Distortion," Journal of Mechanical Engineering Sciences, Vol. 18, pp. 25-38, February 1976.

2.3.19 Ward, G. C., "Compressor Stability Assessment: Dual Spool Compressor System Test and Data Analysis," AFAPL-TR-74, Vol. 1, December 1974.

2.3.20 Smith, R. E., "Marrying Airframes and Engines in Ground Test Facilities – An Evolutionary Revolution", AIAA 95-0950, 1995 Wright Brothers Lectureship in Aeronautics, September 1995.

2.3.21 Childs, H. J., Kichendorfer, F. D., Lubick, R. J., and Friedman, R., "Stall and Flameout Resulting from Firing of Armament," NACA RM E55E25, August 1955.

2.3.22 Welch, Gerard E., "Determination of Critical Sector Angle of Inlet Swirl Distortion Using Actuator-Duct Model," AIAA-2007-5057, July 2007.

2.4 Symbols and Abbreviations

1-D	One dimensional
3D, 3-D	Three dimensional
A	Area
A/B	Afterburner
AC	Alternating current
A/C	Aircraft
A/D	Analog-to-digital
AEDC	Arnold Engineering Development Center
AGARD	Advisory Group for Aerospace Research and Development
AIP	Aerodynamic interface plane
AIR	Aerospace Information Report
AOA	Angle of attack, deg
AOS	Sideslip angle, deg
APD	Amplitude probability density
ARP	Aerospace Recommended Practice
ASME	American Society of Mechanical Engineers
ATF	Altitude test facility
A_P	Pressure distortion transfer function
A_T	Temperature distortion transfer function
b	Stability limit line loss weighting or superposition factor
B	AIP distortion parameter weighting or superposition factor
BLC	Boundary layer control
b_p	The ratio of the loss of stability pressure ratio due to a 180-degree one-per-rev low pressure region with radial distortion to the loss of stability pressure ratio due to a pure circumferential 180-degree one-per-rev pattern
b_T	Superposition function which accounts for coupling effects between the circumferential and radial components of total-temperature distortion
CC_P	Circumferential total-pressure distortion offset coefficient for sensitivity or portion of sensitivity lines not passing through the origin

CC_T	Circumferential total-temperature distortion offset coefficient for sensitivity or portion of sensitivity lines not passing through the origin
$CDGC_p$	Distortion generation coefficient
$CDTC_p$	Distortion transfer coefficient
CFD	Computational fluid dynamics
C_h	Radial offset term for the hub
C_i	Constant (offset) for ring i
CR_p, C_R	Radial total-pressure distortion offset coefficient for sensitivity or portion of sensitivity lines not passing through the origin
CR_T	Tip radial total-pressure distortion offset coefficient for sensitivity or portion of sensitivity lines not passing through the origin; radial total-temperature distortion offset coefficient for sensitivity or portion of sensitivity lines not passing through the origin
C_t	Radial offset term for the tip
D	Diameter
DFRC	Dryden Flight Research Center
DPC	Circumferential distortion parameter
DPR	Radial distortion parameter
DPS	AIP distortion screening parameter
DTC	Temperature distortion parameter
ECS	Environmental control system
EX_p	Extent function which accounts for change in loss of stability pressure ratio due to the extent of the total-pressure pattern differing from 180 degrees
EX_T	Extent function which accounts for change in loss of stability pressure ratio due to the extent of the total-temperature pattern differing from 180 degrees
f	Frequency
F	Force
FADEC	Full authority digital electronic control
F_g	Gross thrust
FOD	Foreign object damage
$f(\theta)$	Combined pressure and temperature distortion superposition and spatial orientation function
$f(\theta_i^-)$	Extent function
FX	Axial force distribution
g	Acceleration due to gravity
HCF	High cycle fatigue
HP	High-pressure
HPC	High-pressure compressor
ID	Inner diameter
IGV	Inlet guide vanes
I_R	Radial intensity parameter
JSF	Joint Strike Fighter
KC_i	Circumferential distortion sensitivity for ring i
KC_P	Circumferential total-pressure distortion sensitivity
KC_T	Circumferential total-temperature distortion sensitivity
K_r	Average radial sensitivity
KRAD	Radial distortion factor
KR_i	Radial distortion sensitivity for ring i
KR_p	Radial total-pressure distortion sensitivity
KR_T	Tip radial total-pressure distortion sensitivity
K_T	Temperature distortion sensitivity
K_θ	Circumferential distortion factor
L	Characteristic length
LP	Low-pressure
LPC	Low-pressure compressor
LWC	Liquid water content, the mass of the supercooled liquid in a unit volume of dry air
m	Mass

M	Mach number
$\dot{m}$	Mass flux
MFR	Mass flow ratio
MLC	Meanline code
MPR	Multiple per revolution
MVD	Median volumetric diameter (half of the LWC is of greater diameter and half of the LWC is of lower diameter)
N	Number of instrumentation rings; turbine engine RPM
NACA	National Advisory Committee for Aeronautics
NAPC	Naval Air Propulsion Center
NASA	National Aeronautics and Space Administration
NATO	North Atlantic Treaty Organization
NC	Core speed, rpm
N_C	Engine RPM corrected to standard sea level conditions
NF	Fan speed, rpm
NR	Non-random
NSMS	Noninterference Stress Measuring System
OD	Outer diameter
P	Static pressure
PAV	Average pressure, usually for a ring
P_{AVG}	Average total pressure of the AIP
PAVLOW	Average pressure in the extent
PFAV	AIP average total pressure
PLA	Power lever angle
P_{MAX}	Maximum total pressure of the AIP
P_{MIN}	Minimum total pressure of the AIP
PR1	Pressure ratio on undistorted flow stability limit line
PRDS	Distorted flow pressure ratio
PRi, PR(i), PR_i	Pressure ratio i
PRDS	Pressure ratio on distorted flow stability limit line
PRO	Pressure ratio on undistorted operating line
PSD	Power spectral density
P_t'	Relative total pressure
Q	Rate of heat added to a fluid
r	Radius
RANS	Reynolds averaged Navier-Stokes
RFG	Random frequency generator
RMS	Root mean square
RPM	Revolutions per minute
RSS	Root-sum-square
S	Superposition function which accounts for coupling effects between total-pressure distortion and total-temperature distortion
SFC	Specific fuel consumption
SLCC	Streamline curvature code
SM	Stability margin
SSA	Statistical stability assessment
S-16	SAE Turbine Engine Inlet Flow Distortion Committee
SW	Shaft work
T	Temperature
TDC	Top dead center
TR	Total temperature ratio
U	Velocity, local wheel speed
U_C	Convective velocity
V	Velocity; absolute velocity
V_m	Axial velocity

V_R	Relative velocity
VSTOL	Vertical/Short Takeoff and Landing
V_t	Tangential velocity
WA, WA2	Compressor inlet corrected airflow
W_B	Mass transfer rate across boundary
α, AOA	Test article angle of attack; absolute air angle
α_i	Weighting factor for ring i
β, AOS	Test article angle of sideslip; relative air angle
β_{metal}	Blade metal angle
γ	Ratio of specific heats
δ	Temperature ratio; deviation
ΔPC/P	Circumferential pressure distortion intensity element
ΔP/PC	Circumferential total pressure distortion term
ΔP/PR	Radial total pressure distortion term
ΔPR/P	Radial pressure distortion intensity element
ΔPRS	Loss of stability pressure ratio
ΔPRS_C	Stability pressure ratio loss due to circumferential total pressure distortion
ΔPRS_R	Stability pressure ratio loss due to radial total pressure distortion
ΔPRS_T	Stability pressure ratio loss due to temperature distortion
ΔSM	Loss in stability margin
ΔT/TC	Circumferential total temperature distortion term
ΔT/TR	Radial total temperature distortion term
$(\Delta T/TC)_{25}$	Level of HPC inlet circumferential total-temperature distortion
η	Efficiency
θ^-	Extent in degrees of a low-pressure region
θ^+	Extent in degrees of a high-pressure region
λ	Wavelength
ρ	Density of air
σ	One standard deviation
τ	Characteristic time or time constant
ϕ	Auto-power spectra
ω	Pressure ratio loss

Subscripts:

1	Blade entrance
180	Related to a 180-degree pattern
2	Blade exit
25	Inlet/engine station 25
c	Circumferential
h	Hub
HPC	High-pressure compressor
HUB	Related to the hub
i	Ring number
p	Pressure
r	Radial
t, TIP	Related to the tip
T	Temperature
U	Associated with velocity component U
θ	Related to extent

3. STABILITY MARGIN AND LOSS OF STABILITY PRESSURE RATIO

Compressor stability margin definitions fall into two general classes: stability margin defined at constant corrected airflow, usually at the compressor inlet, and stability margin defined at constant corrected rotor speed.

Stability margin defined at constant airflow has advantages for inlet-engine airflow matching and stability assessment. With this definition both inlet distortion and engine distortion tolerance can be expressed as functions of airflow. Consequently, the corrected airflow passing through the interface plane can be used as the common denominator for both inlet distortion and engine distortion tolerance.

Stability margin defined at constant rotor speed has advantages for the engine manufacturer; most compressor design procedures and testing are carried out at constant rotor speed. Also, stability margin at limiting rotor speed can be defined without extrapolation.

The inlet/engine compatibility guidelines of ARP1420, Reference 2.1.1.1, recommend a total-pressure-distortion methodology which utilizes one definition of stability margin as a basis. This section discusses that definition and the rationale for its choice against a background of some alternative definitions currently used in industry.

3.1 ARP1420 Definitions and Rationale

ARP1420 stability margin is defined at constant corrected airflow at the inlet of the compression component, with variable geometry, if any, in the scheduled position. ARP1420 stability margin is the difference between the stability pressure ratio and the operating pressure ratio, normalized by the operating pressure ratio. Referring to Figure 1, the ARP1420 undistorted stability margin is defined as:

$$SM = \frac{PR1 - PRO}{PRO} \times 100 \qquad \text{(Eq. 1)}$$

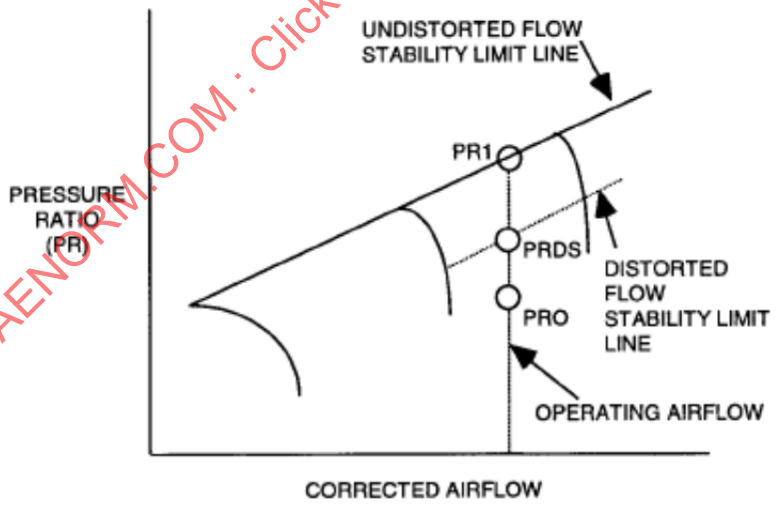

FIGURE 1 - ARP1420 STABILITY MARGIN DEFINITION

The ARP1420 loss in stability pressure ratio due to inlet total pressure distortion (ΔPRS) also is measured at constant inlet corrected airflow with the variable geometry, if any, in the scheduled position. ΔPRS is the loss in stability pressure ratio due to inlet distortion normalized by the undistorted stability pressure ratio. With reference to Figure 1:

$$\Delta PRS = \frac{PR1 - PRDS}{PR1} \times 100 \quad \text{(Eq. 2)}$$

The loss in stability pressure ratio is normalized by the undistorted stability pressure ratio rather than by the operating pressure ratio because the operating pressure ratio may not have been defined when compressor rig tests are made to determine the effect of distortion on compressor stability. Also, a better comparison among compressors from different engines can be made using a distortion sensitivity that is independent of the operating point.

Fan data, both with and without inlet distortion, are shown in Figure 2 to illustrate the definitions of stability margin and loss of stability pressure ratio due to inlet distortion. Using the nomenclature of Figure 2, ARP1420 stability margin, with no inlet distortion, at 96.4% airflow is:

$$SM = \frac{PR(3) - PR(8)}{PR(8)} \times 100 = 15\% \quad \text{(Eq. 3)}$$

In the example shown in Figure 2, the dashed lines represent a shift in performance due to circumferential inlet distortion. The loss in stability pressure ratio due to distortion is calculated at the stability limit airflow with inlet distortion. At 89.3% inlet airflow:

$$\Delta PRS = \frac{PR(1) - PR(4)}{PR(1)} \times 100 = 1.2\% \quad \text{(Eq. 4)}$$

At this airflow, the clean flow stability margin is:

$$SM = \frac{PR(1) - PR(6)}{PR(6)} \times 100 = 20.29\% \quad \text{(Eq. 5)}$$

With reference to Figures 1 and 2, the stability margin with distorted flow is:

$$SM_{dist} = \frac{PRDS - PRO}{PRO} \times 100 = \frac{PR(4) - PR(6)}{PR(6)} \times 100 = 18.84\% \quad \text{(Eq. 6)}$$

The change in stability margin for a fixed operating pressure ratio is related to the loss of stability pressure ratio, ΔPRS, by

$$\Delta SM = \frac{PR1}{PRO}\Delta PRS = \left(1 + \frac{SM}{100}\right)\Delta PRS \quad \text{(Eq. 7)}$$

For example, at 89.3% airflow:

$$\Delta SM = 1.203 \times 1.2 = 1.44\% \quad \text{(Eq. 8)}$$

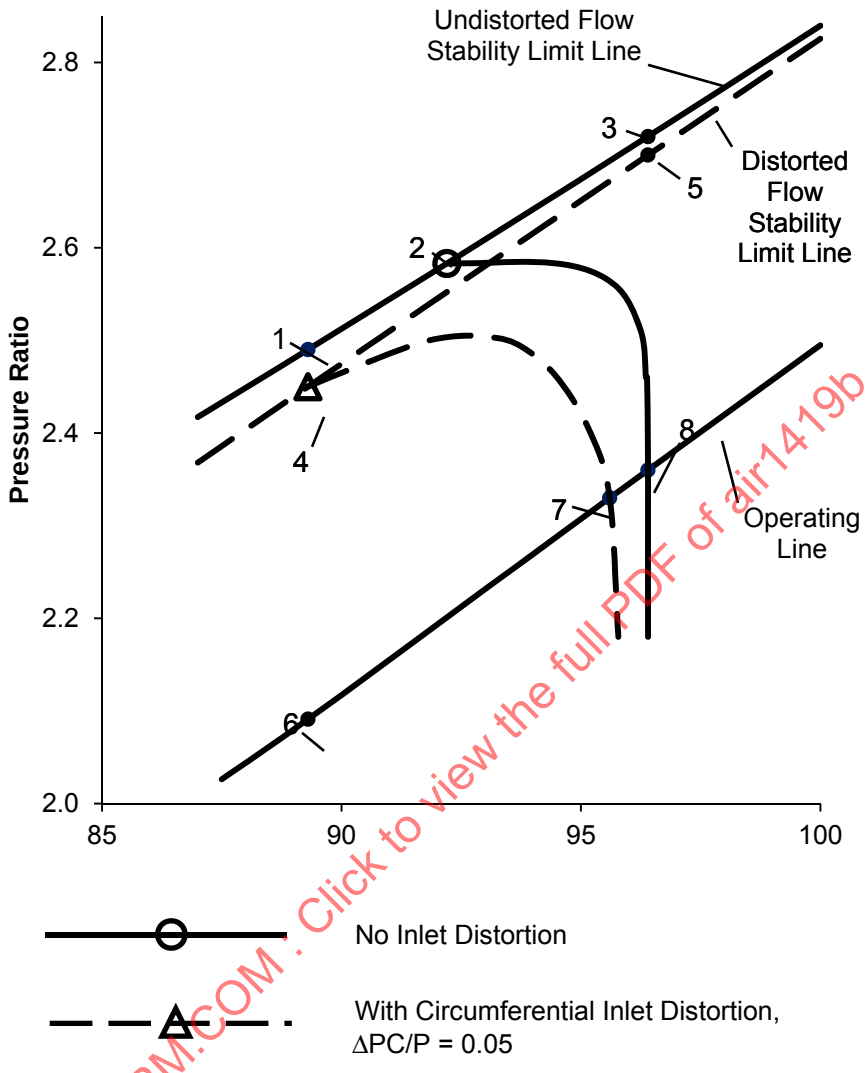

Point Number	Pressure Ratio	Airflow
1	2.49	89.3
2	2.58	92.2
3	2.72	96.4
4	2.46	89.3
5	2.70	96.4
6	2.07	89.3
7	2.33	95.6
8	2.36	96.4

FIGURE 2 - FAN MAP TO ILLUSTRATE STABILITY MARGIN DEFINITION

3.2 Other Definitions of Stability Margin

Many definitions of stability margin have been used. Some of these are used in compressor design and development. Some of the more common definitions are given in Table 1, in terms of the nomenclature and numerical values of the undistorted flow lines in Figure 2, to illustrate that the numerical value of stability margin is dependent on stability margin definition.

The list of stability margin definitions in Table 1 is not comprehensive; other definitions exist, utilizing, for example, compressor exit static pressure.

TABLE 1 - ALTERNATIVE STABILITY MARGIN DEFINITIONS

Number	Definition	Percent Stability Margin	
1	$\frac{PR(3)-PR(8)}{PR(8)}\times 100$	15.2 (ARP1420)	Constant Airflow
2	$\frac{PR(3)-PR(8)}{PR(3)}\times 100$	13.2	
3	$\frac{PR(3)-PR(8)}{PR(8)-1}\times 100$	26.5	
4	$\frac{\left(\frac{PR}{WA}\right)_2-\left(\frac{PR}{WA}\right)_8}{\left(\frac{PR}{WA}\right)_8}\times 100$	14.3	Constant Speed
5†	$\frac{\left(\frac{PR}{WA\sqrt{TR}}\right)_2-\left(\frac{PR}{WA\sqrt{TR}}\right)_8}{\left(\frac{PR}{WA\sqrt{TR}}\right)_2}\times 100$	11.2*	
6†	$\frac{\left(\frac{PR}{WA}\right)_2-\left(\frac{PR}{WA}\right)_8}{\left(\frac{PR}{WA}\right)_2}\times 100$	12.5	
7	$\frac{PR(2)-PR(8)}{PR(8)}\times 100$	9.3	
8	$\frac{PR(2)-PR(8)}{PR(2)}\times 100$	8.5	
9	$\frac{PR(2)-PR(8)}{PR(8)-1}\times 100$	16.2	

† WA denotes compressor inlet corrected airflow. TR denotes compressor total temperature ratio.
* Assuming 80% adiabatic efficiency.

The definitions fall into two general classes: (1) stability margin evaluated at constant airflow (definitions 1-3) which may require an increase in rotor speed between the operating point and the stability limit point and (2) stability margin evaluated at constant rotor speed (definitions 4-9) which may have a reduction in airflow between the operating point and the stability limit point. For a vertical compressor rotor speed line, when constant rotor speed and constant corrected inlet airflow are achieved simultaneously (compressor choke), the constant rotor speed definitions will calculate the same stability margin as the corresponding constant airflow definitions. For example, definitions 1, 4, and 7 will calculate the same stability margin with a vertical speed line, while definitions 2, 6, and 8 are another such set of corresponding definitions.

Every stability margin definition that is normalized by the operating point has a corresponding definition normalized by the stability limit point. Three of these corresponding pairs appear in Table 1, namely 1 and 2, 4 and 6, and 7 and 8. Definitions 3 and 9 are normalized by compressor total pressure rise rather than total pressure ratio. Definition 5 is proportional to compressor exit throttle closure; it is the percentage reduction in compressor exit corrected airflow from the operating point to the stability limit point at constant corrected rotor speed. Definition 6 is derived from 5 by neglecting temperature ratio differences between stability limit and operating points.

Stability margin values vary between 8.5% and 26.5% for the examples shown in Table 1. This wide variation for the same compressor, at the same operating condition, illustrates the need for a preferred stability margin definition.

3.3 Stability Margin with Inlet Distortion

Clean-flow stability margin, distorted-flow stability margin and the loss in stability margin due to inlet distortion calculated for the nine definitions of stability margin presented in Table 1 are compared in Table 2. Clean-flow stability margins in Table 2 range from 8.5% to 26.5%, while the corresponding loss in stability margin due to the test level of circumferential distortion ranges from 0.5% to 6.4%.

TABLE 2 - DIFFERENT STABILITY MARGIN DEFINITIONS RESULT IN DIFFERENT DISTORTION ACCOUNTING

Definition Number	Data Points		Clean-Flow Stability Margin, Percent	Distorted-Flow Stability Margin, Percent	Loss in Stability Margin Due to Distortion, Percent
	Clean Flow	Distorted Flow			
1	3, 8	5, 8	15.2	14.4	0.8 (ARP1420)
2	3, 8	5, 8	13.2	12.6	0.6
3	3, 8	5, 8	26.5	25.0	1.5
4	2, 8	4, 7	14.3	13.0	1.3
5	2, 8	4, 7	11.2	10.7	0.5
6	2, 8	4, 7	12.5	11.5	1.0
7	2, 8	4, 7	9.3	5.6	3.7
8	2, 8	4, 7	8.5	5.3	3.2
9	2, 8	4, 7	16.2	9.8	6.4

The effects of inlet total-pressure distortion on engine stability can be accounted for consistently using any of the above compressor stability margin definitions. Definitions which give higher values of stability margin usually have greater sensitivity to distortion so that all definitions reproduce the test stability limit point for the test level of inlet distortion. However, each method may estimate a different stability limit point for distortions different from the test level.

Rotor speed and airflow relationships are required, both with and without inlet distortion, to match inlet operating airflow for constant speed stability margin definitions. Constant airflow stability margin definitions, on the other hand, enable rapid assessments of distortion effects on stability margin to be made at the matched inlet and engine airflow. Stability assessments made at constant inlet corrected airflow, defined at the interface plane, simplify communication across the interface plane since inlet performance, inlet stability, inlet distortion, engine performance, and engine stability are all functions of the corrected airflow at the interface plane.

Different definitions of stability margin give different numerical values for stability margin and loss in stability margin, as illustrated by Table 2. This can cause appreciable confusion in inlet/engine compatibility studies because each definition provides a different numerical description of stability. Consequently, an engineer trying to compare the stability of propulsion systems that utilize different definitions of stability margin and different accounting procedures has to understand different methodologies and then translate stability margins into a common base. This translation may require data that are not readily available, such as compressor maps with and without distortion. Translation will certainly require a significant amount of additional work.

The ARP1420 stability margin definition and the associated ΔPRS definition were recommended by the SAE S-16 committee to meet the need for a consistent approach to quantifying inlet/engine stability assessment with inlet total-pressure distortion. Stability accounting systems based on these definitions are widely used and have been successful on all applications to date.

The use of the ARP1420 definition of stability margin for inlet total pressure distortion assessment does not preclude the use of alternative stability margin definitions for compressor design and development purposes. As stated in ARP1420, a particular engine configuration may require an alternative stability margin definition. In this case, the stability margin definition, stability margin loss, and stability assessment procedure need to be specified.

3.4 Stability Limit Line Extrapolation in the Compressor Overspeed Region

In the example of Figure 2, the stability limit line was defined up to the operating airflow by testing at higher rotor speeds on the compressor rig. In some test rig situations, the achievement of high corrected rotor speeds and corresponding airflows may not be possible. For example, rig power supply constraints may make it impossible to determine experimentally a stability limit line at high airflows in the compressor overspeed regime. If the operational limit rotor speed is achievable, extrapolation of the stability limit line still may be required to extend the stability limit line to the highest operating airflow.

It is common practice to test compression components without distortion and at one level of distortion. Linear interpolation is used to estimate the loss of stability pressure ratio due to differing inlet distortion intensities. The following example shows how different stability limit line extrapolations can affect this estimation procedure. The same undistorted speed line in Figure 2 also appears in Figure 3, but in Figure 3 it is assumed that the speed line shown is a limiting speed line. A speed line with radial distortion intensity of 0.10 also is shown in Figure 3. Stability limit line extrapolation 1 is the same stability limit line as shown in Figure 2 for undistorted operation. Stability limit line extrapolation 2 is a higher stability limit line extrapolation. The matched inlet-engine airflow has been selected as the test airflow with inlet distortion, 94.9% airflow, so that stability accounting can reproduce the test conditions.

The effect of these different stability limit line extrapolations on estimates of the ARP1420 stability margin for various levels of distortion are shown in Table 3.

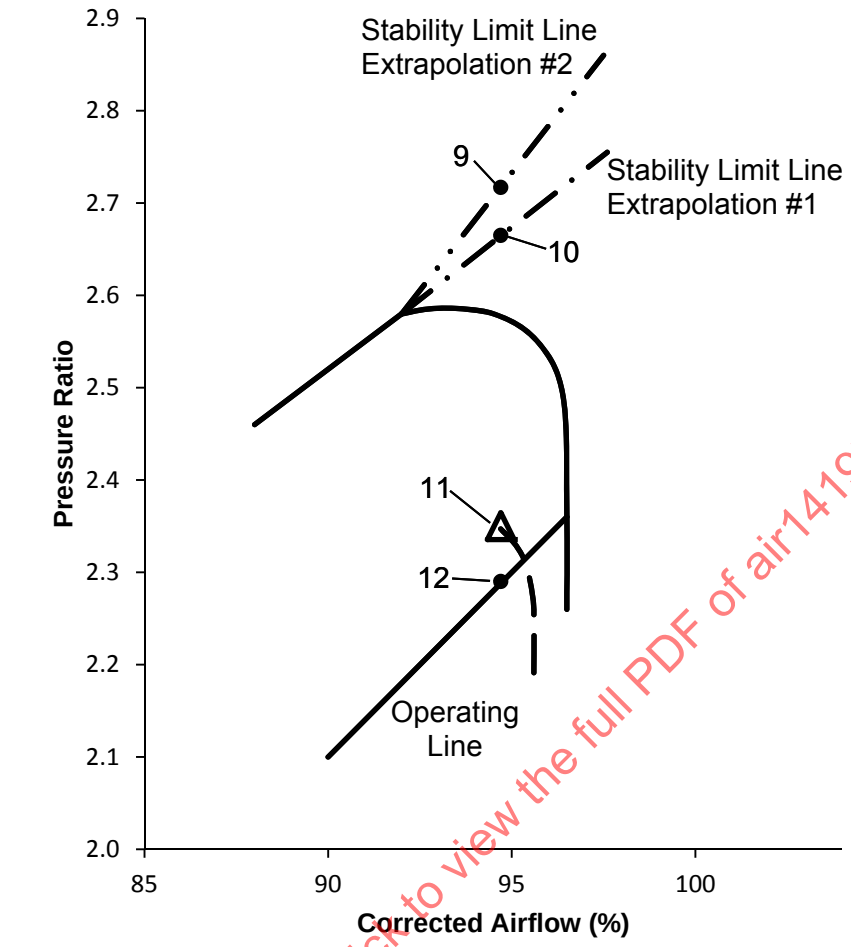

No Inlet Distortion Limiting Speed

With Radial Inlet Distortion Limiting Speed, ΔPR/P = 0.10

Point Number	Pressure Ratio	Airflow
9	2.71	94.9
10	2.67	94.9
11	2.35	94.9
12	2.30	94.9

FIGURE 3 - FAN MAP TO ILLUSTRATE EFFECT OF STABILITY LIMIT LINE EXTRAPOLATION

TABLE 3 - EFFECT OF STABILITY LIMIT LINE EXTRAPOLATION ON STABILITY ACCOUNTING

Inlet Distortion Level (ΔPR/P)	SM – Stability Margin with Inlet Distortion		ΔPRS – Loss in Stability Pressure Ratio Due to Inlet Distortion	
	Stability Limit Line 1	Stability Limit Line 2	Stability Limit Line 1	Stability Limit Line 2
0	16.1	17.8	0	0
0.05	9.1	10.0	6.0	6.6
0.10	2.2	2.2	12.0	13.3
0.11	0.8	0.6	13.2	14.6

It can be seen by examining Table 3:

- A higher undistorted stability limit line is compensated by an increased loss in stability pressure ratio with inlet distortion, so that both stability limit line extrapolations produce the same distorted stability margin for the test conditions of ΔPR/P = 0.10.

- A high stability limit line extrapolation (2) gives higher stability margin estimates for distortion levels that are lower than tested and lower stability margin estimates for distortions higher than tested.

Distortion tests should be conducted at or above maximum anticipated distortion levels because interpolation is safer than extrapolation.

4. STABILITY PRESSURE RATIO CORRELATION

Estimation of the loss of stability pressure ratio (ΔPRS) due to inlet total-pressure distortion is fundamental to accomplishing a stability assessment (Section 5). ΔPRS, defined in Section 3, can be correlated using the distortion descriptor elements described in this section. This section also discusses the rationale underlying the selection of these distortion descriptor elements.

Sample probe readings based upon screen test data are given for a variety of patterns useful for constructing a stability pressure-ratio correlation system and for checking out a distortion descriptor element computation program. To aid this process, the data are given in terms of probe-by-probe total-pressure readings and the associated contour plot; the results are presented as descriptor element values and illustrated with bar charts.

Three correlation systems are described to familiarize the reader with the type of data required for constructing a stability pressure ratio distortion correlation system and to illustrate achievable accuracies. Section 4 ends with discussions of methods for and problems of screening inlet data and formulating a universal screening procedure.

4.1 Distortion Descriptor Element Definitions

Aerodynamic Interface Plane total-pressure probe data are used to describe inlet distortion directly in terms of the probe readings (pattern) and numerically in terms of distortion descriptors that are related to the severity of the distortion. Distortion descriptors provide a means of identifying critical distorted inlet-flow conditions and of communicating during propulsion system development. A universal distortion descriptor is beyond the state-of-the-art; however, distortion descriptor elements have been identified (Reference 2.1.1.1) for use in structuring a distortion descriptor for a particular engine. These elements are used to define each distortion descriptor system and its associated computation procedure. The distortion descriptor elements are used to quantify the distortion at the AIP. Fundamental to the distortion-descriptor elements is the set of pressure-probe readings that are used to describe the total-pressure distribution. The pressure probes usually are arranged in rake and ring arrays, as described in Section 8. Circumferential and radial distortion elements, which are calculated using the pressure-probe readings, are defined on a ring-by-ring basis. Inlet spatial distortion is described in terms of circumferential and radial elements and is discussed in detail in the following paragraphs.

Circumferential distortion is described for each instrumentation ring in terms of intensity, extent and multiple-per-revolution elements.

Intensity: The circumferential distortion intensity element (ΔPC/P) is a numerical indication of the magnitude of the pressure defect for each ring.

Extent: The circumferential distortion extent element (θ^-) is the angular region, in degrees, in which the pressure is below ring average pressure.

Multiple-per-Revolution: The circumferential distortion multiple-per-revolution element (MPR) is a numerical indication of the "effective" number of low-pressure regions for each ring.

The radial distortion intensity element (ΔPR/P) describes the difference between the ring-average pressure and the face-average pressure for each ring. Both positive and negative values of radial intensity are possible. Positive values reflect a ring-average pressure that is below the face-average pressure.

4.1.1 Circumferential Distortion Elements - One-Per-Rev Patterns

The "intensity" and "extent" elements of circumferential distortion are obtained by linear interpolation of the pressures in a given instrumentation ring i. Typical pressures for the probes in the i^{th} ring for a representative one-per-revolution pattern (one pressure defect in 360 degrees) are shown in Figure 4. Theta minus, θ_i^-, is the circumferential extent of the low-pressure region measured in degrees. It is defined by the intersection between the ring average pressure and the linear interpolation which subtends the low-pressure region.

$$Extent = (\theta^-)_i = \theta_{2_i} - \theta_{1_i} \quad \text{(Eq. 9)}$$

Intensity,

$$\left(\frac{\Delta PC}{P}\right)_i = \frac{(PAV)_i - (PAVLOW)_i}{(PAV)_i} \quad \text{(Eq. 10)}$$

where:

$$(PAV)_i = \frac{1}{360}\int_0^{360} P(\theta)_i \, d\theta = ring\ i\ average\ pressure \quad \text{(Eq. 11)}$$

$$(PAVLOW)_i = \frac{1}{\theta_i^-}\int_{\theta_i^-} P(\theta)_i d\theta \quad \text{(Eq. 12)}$$

$P(\theta)_i$ is a function resulting from a linear fit between the data points.

The intensity element is equal to the shaded area of Figure 4 divided by the product of θ_i^- times $(PAV)_i$, and

$$\text{Multiple-Per-Rev} = (MPR)_i = 1 \quad \text{(Eq. 13)}$$

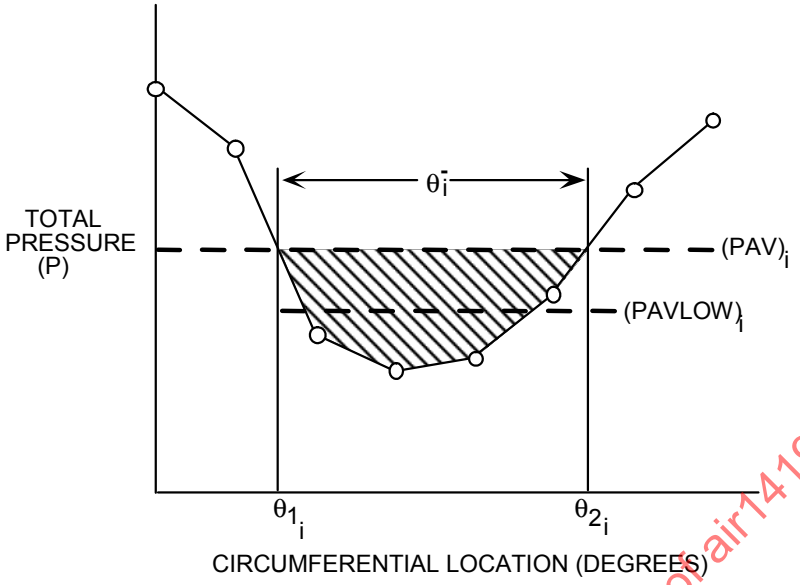

FIGURE 4 - RING CIRCUMFERENTIAL DISTORTION FOR A ONE-PER-REV PATTERN

4.1.2 Circumferential Distortion Elements - Multiple-Per-Rev Patterns

The circumferential distortion intensity and extent elements for multi-lobe distortion patterns also are determined by a linear interpolation procedure. A pattern with two low-pressure regions separated by two high-pressure regions of extents θ_{i1}^+ and θ_{i2}^+ appears in Figure 5. In all that follows, the analytical expressions are written for the kth low-pressure region for Q low-pressure regions for each ring. The extent and intensity elements of each low pressure region are calculated using Equations 9 and 10.

4.1.2.1 Patterns with $\theta_{ik}^+ \leq \theta_{min}^+$

If the pattern has low-pressure regions circumferentially separated by high-pressure regions with extents less than or equal to θ_{min}^+, it is considered as an equivalent one-per-revolution low-pressure region. θ_{min}^+ is specified by the descriptor developer and is a function of the predicted or measured engine response to distortion. A value of θ_{min}^+ of approximately 25 degrees is suggested in the absence of other information.

In Figure 5,

$$Extent = \theta_i^- = \sum_{k=1}^{Q} \theta_{ik}^- = (\theta_2 - \theta_1)_i + (\theta_4 - \theta_3)_i \quad \text{(Eq. 14)}$$

$$Intensity = \left(\frac{\Delta PC}{P}\right)_i = \frac{(PAV)_i - (PAVLOW)_i}{(PAV)_i} \quad \text{(Eq. 15)}$$

where:

$$(PAVLOW)_i = \frac{1}{\theta_i^-}\sum_{k=1}^{Q}\int_{\theta_{ik}^-} P(\theta)_i d\theta \qquad \text{(Eq. 16)}$$

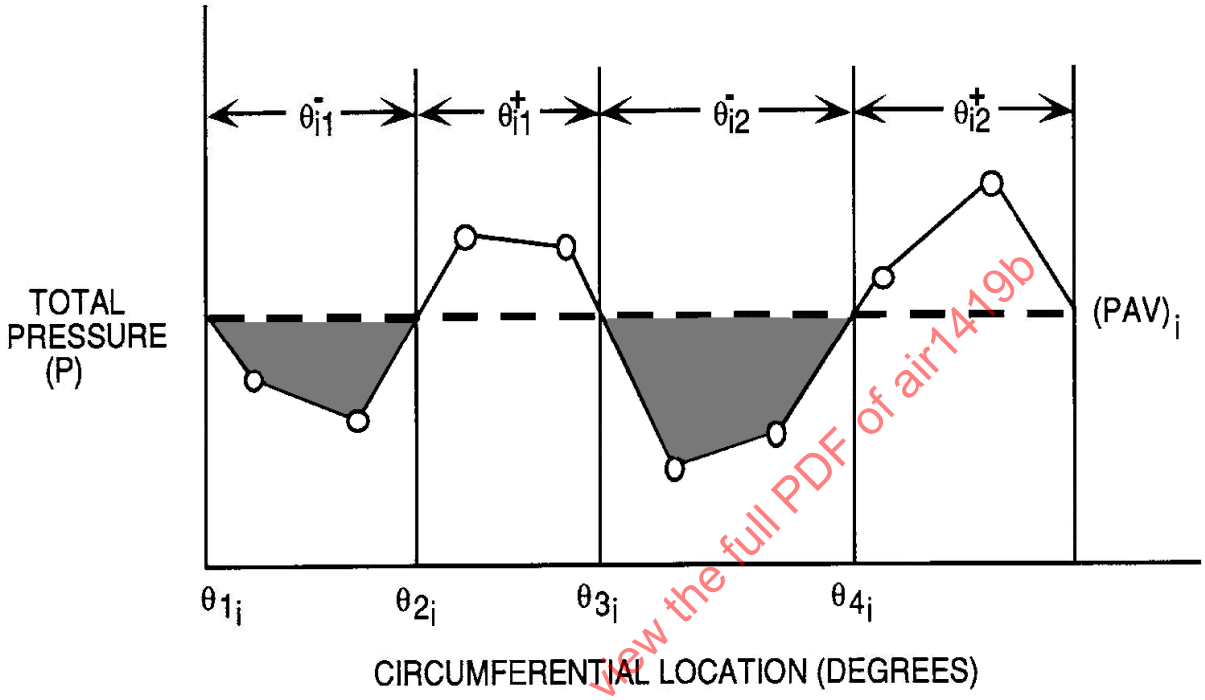

FIGURE 5 - RING CIRCUMFERENTIAL DISTORTION FOR A MULTIPLE-PER-REV PATTERN

Hence,

$$\left(\frac{\Delta PC}{P}\right)_i = \frac{\sum_{k=1}^{Q}\left(\frac{\Delta PC}{P}\right)_{ik}\theta_{ik}^-}{\sum_{k=1}^{Q}\theta_{ik}^-} \qquad \text{(Eq. 17)}$$

Multiple-Per-Rev = MPR = 1 for this case.

4.1.2.2 Patterns with $\theta_{ik}^+ > \theta_{min}^+$

If the pattern has low-pressure regions circumferentially separated by high-pressure regions with extents greater than θ_{min}^+, then the multiple-per-revolution element is greater than one.

Intensity $\left(\frac{\Delta PC}{P}\right)_i$ is the $\left(\frac{\Delta PC}{P}\right)_{ik}$ corresponding to the maximum value of $\left[\left(\frac{\Delta PC}{P}\right)_{ik}\theta_{ik}^-\right]$.

Extent θ_i^- is the θ_{ik}^- corresponding to the maximum value of $\left[\left(\frac{\Delta PC}{P}\right)_{ik}\theta_{ik}^-\right]$.

The multiple-per-revolution term is defined as the number of equivalent low-pressure regions, the equivalence being based on the ratio of the total integrated area beneath $(PAV)_i$ in Figure 5 to the largest single area beneath $(PAV)_i$. This is given by the equation:

$$Multiple-per-revolution = (MPR)_i = \frac{\sum_{k=1}^{Q}\left[\left(\frac{\Delta PC}{P}\right)_{ik}\theta_{ik}^{-}\right]}{max\left[\left(\frac{\Delta PC}{P}\right)_{ik}\theta_{ik}^{-}\right]} \quad \text{(Eq. 18)}$$

4.1.3 Radial Distortion Elements

The radial distortion intensity of a ring is defined as the difference between the face-average pressure and the ring-average pressure divided by the face-average pressure. Both positive and negative values of radial intensity therefore occur; positive values reflect a ring-average pressure that is below the face average. A typical tip-radial distortion pattern is shown in Figure 6. The arrows indicate the difference in radial pressure for ring 5. For the general ring, i, the radial intensity is given as:

$$\left(\frac{\Delta PR}{P}\right)_i = \frac{(PFAV)-(PAV)_i}{(PFAV)} \quad \text{(Eq. 19)}$$

where (PFAV) is the area-weighted face-average pressure. For N rings at centers of equal areas:

$$(PFAV) = \frac{1}{N}\sum_{i=1}^{N}(PAV)_i \quad \text{(Eq. 20)}$$

It should be noted that the definition of the radial intensity implies that $\frac{1}{N}\sum_{i=1}^{N}\left(\frac{\Delta PR}{P}\right)_i = 0$.

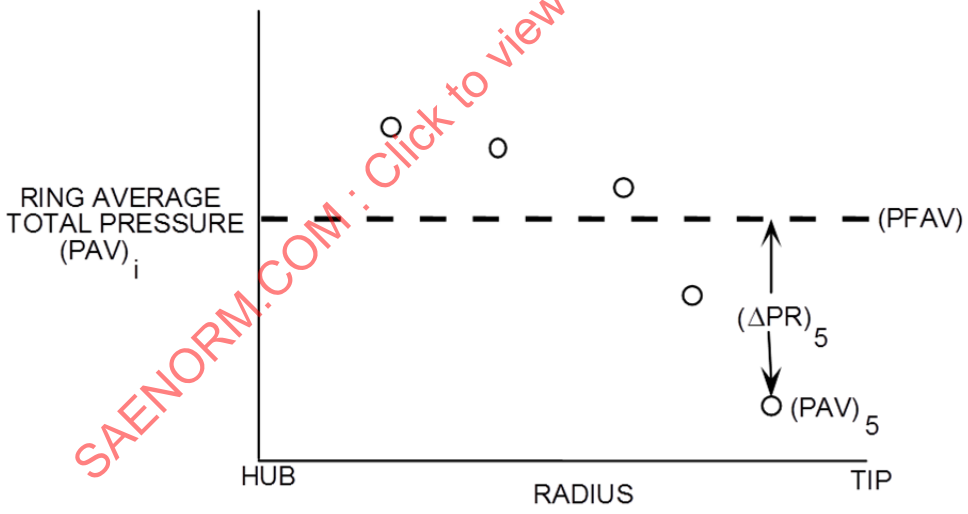

FIGURE 6 - RADIAL DISTORTION PATTERN

4.2 Rationale for Element Definitions

The definitions of the distortion-descriptor elements given in 4.1 were chosen for a number of reasons. The most important requirement was that the elements should describe well-established facts, that is, the stability of an engine compression component is sensitive to the magnitude of a circumferentially varying total-pressure defect (circumferential intensity), the time a blade spends in the defect region (extent), the number of defects encountered by a blade in one revolution (multiple-per-rev), the magnitude of a radially-varying total-pressure defect (radial intensity), and whether the circumferential and/or radial defects occur in the hub, mid-span, or tip regions of the compression-component inlet (Reference 2.1.1.2).

The particular form of the circumferential distortion intensity element was chosen to aid in making hand calculations by avoiding complicated mathematical expansions and to avoid sensitivity to a single-probe low total-pressure reading. The latter was accomplished by averaging the pressures in the low total-pressure region, thus avoiding an expression such as $(P_{MAX} - P_{MIN})/P_{AVG}$ which is descriptive of the flow, but does not take the response of the turbomachinery into account. The circumferential intensity element was nondimensionalized by the ring-average total pressure rather than face-average total pressure in an attempt to reduce the apparent "double bookkeeping" that occurs when analyzing complex aircraft patterns. This "double bookkeeping" occurs when the low total-pressure region may contribute to both the circumferential and radial intensity elements so as to effectively make the defect appear more severe than it actually is.

To reduce the computation time for the time-variant distortion descriptor elements, linear interpolation is considered adequate for determining the angular extent (θ^-) of a low pressure region, thus avoiding differing results due to the type of interpolation used (Fourier curve fit, polynomial, spline). This pragmatic approach to handling large amounts of data produces results that correlate to an acceptable degree of accuracy.

A continuous functional representation, indicating the presence of multiple-per-rev regions, rather than an integer jump function, was chosen because the stability response of compression components varies in a continuous manner, depending on the relationship between the intensity-extent products for each of the low-pressure regions.

4.3 Sample Element Calculations

As an aid to interpreting and calculating the distortion-descriptor elements, an example inlet pattern, illustrated in Figure 7, is examined in detail. The corresponding probe readings, normalized by face-average total pressure, are given in Figure 8. The pattern has two low pressure regions separated by more than 25 degrees in the outer rings and is termed a "two-per-rev pattern." The ARP1420 recommended probe array is superposed. The calculation of the circumferential distortion elements for the inner ring where the circumferential profile is only a one-per-rev profile is illustrated in Figure 9. The intensity element ($\Delta PC/P$) is 0.02 per Equations 10 and 12. The extent element (θ^-) is 157 degrees and the multiple-per-rev element (MPR) is 1.0 per Equation 13. The calculation of the circumferential distortion elements for the outer ring is illustrated in Figure 10. This ring has two low-pressure regions separated by more than θ^+_{min}. In this case, the intensity is equal to the value associated with the largest area under the ring-average total pressure. The multiple-per-rev factor is equal to 1.1 per Equation 18. The values of the radial distortion elements, as calculated according to Equation 19, are illustrated in Figure 11.

All distortion elements for each ring of this pattern can be illustrated using a bar graph display as shown in Figure 12. This type of display makes it possible to obtain quickly the following characteristics of the pattern:

a. The circumferential intensity is greatest at the tip.

b. The circumferential extent is greatest at the hub.

c. The only multiple-per-rev content exists at the tip.

d. The radial intensity is greatest at the tip.

This format gives the data and the results in both tabular and pictorial form and will be used to summarize the data and the results for the sample distortion patterns of the next subsection. The data for this example as well as the results are given in Figure 8.

A pattern with two low-pressure regions separated by less than θ^+_{min} is illustrated in Figure 13. The circumferential distortion intensity element for the outer ring was calculated according to Equation 15 and has a value of 0.026.

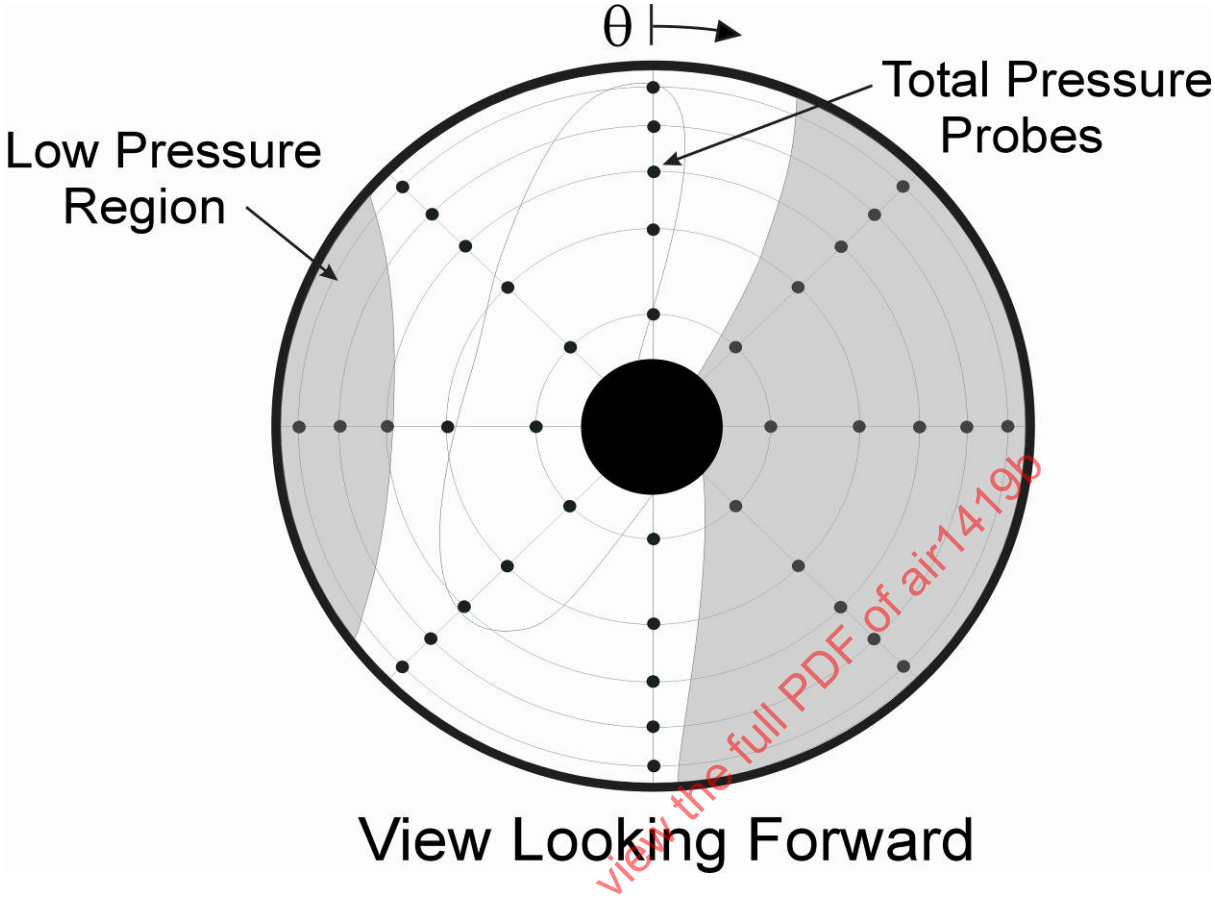

FIGURE 7 - EXAMPLE OF INLET PATTERN

Probe by Probe
Clockwise from TDC

	rake 1	rake 2	rake 3	rake 4	rake 5	rake 6	rake 7	rake 8
ring 1 (hub)	1.021	0.987	0.976	0.985	1.010	1.028	1.024	1.028
ring 2	1.024	0.980	0.960	0.970	1.005	1.020	1.008	1.018
ring 3	1.027	0.972	0.948	0.960	1.001	1.017	0.995	1.010
ring 4	1.025	0.963	0.938	0.950	1.000	1.006	0.985	1.004
ring 5 (tip)	1.020	0.957	0.930	0.942	1.000	1.024	0.952	0.998

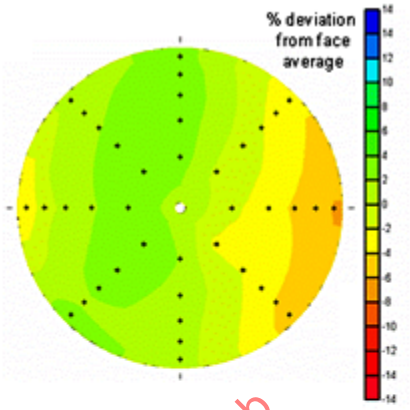

Distortion Descriptor Elements

	$\left(\frac{\Delta PC}{P}\right)_i$	$(\theta^*)_i$	$(MPR)_i$	$\left(\frac{\Delta PR}{P}\right)_i$
ring 1	0.0196	157.2	1.0000	-0.0158
ring 2	0.0238	144.7	1.0000	-0.0065
ring 3	0.0272	140.0	1.0000	0.0005
ring 4	0.0298	135.6	1.0000	0.0079
ring 5	0.0315	132.7	1.1313	0.0139

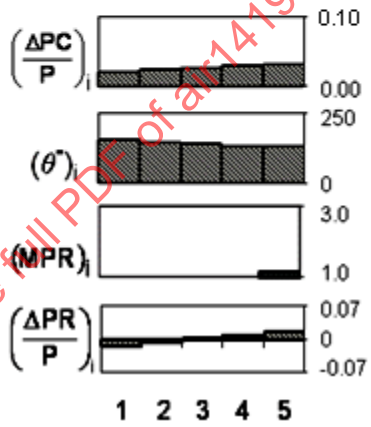

FIGURE 8 - SAMPLE PATTERN DEFINITION AND RESULTS

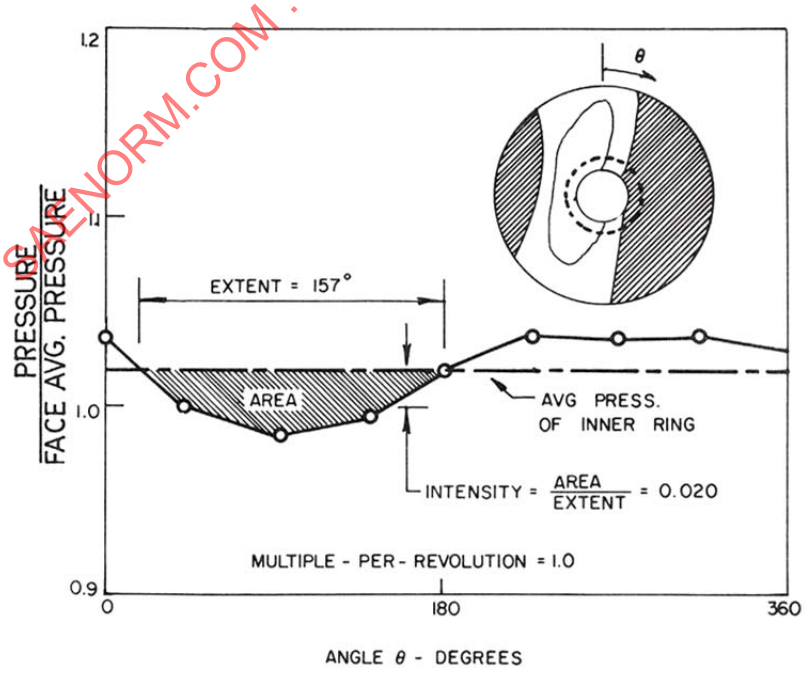

FIGURE 9 - CIRCUMFERENTIAL DISTORTION ELEMENTS FOR INNER RING

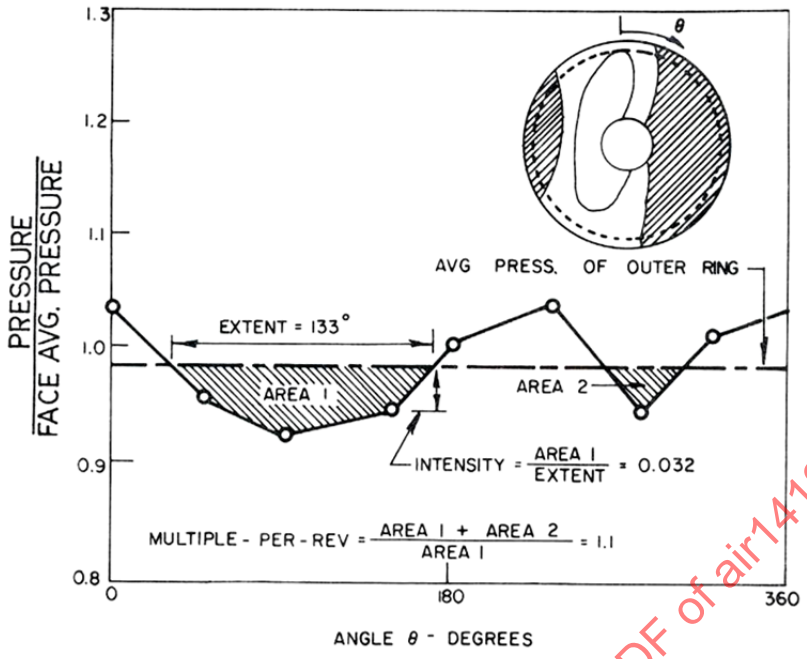

FIGURE 10 - CIRCUMFERENTIAL DISTORTION ELEMENTS FOR OUTER RING

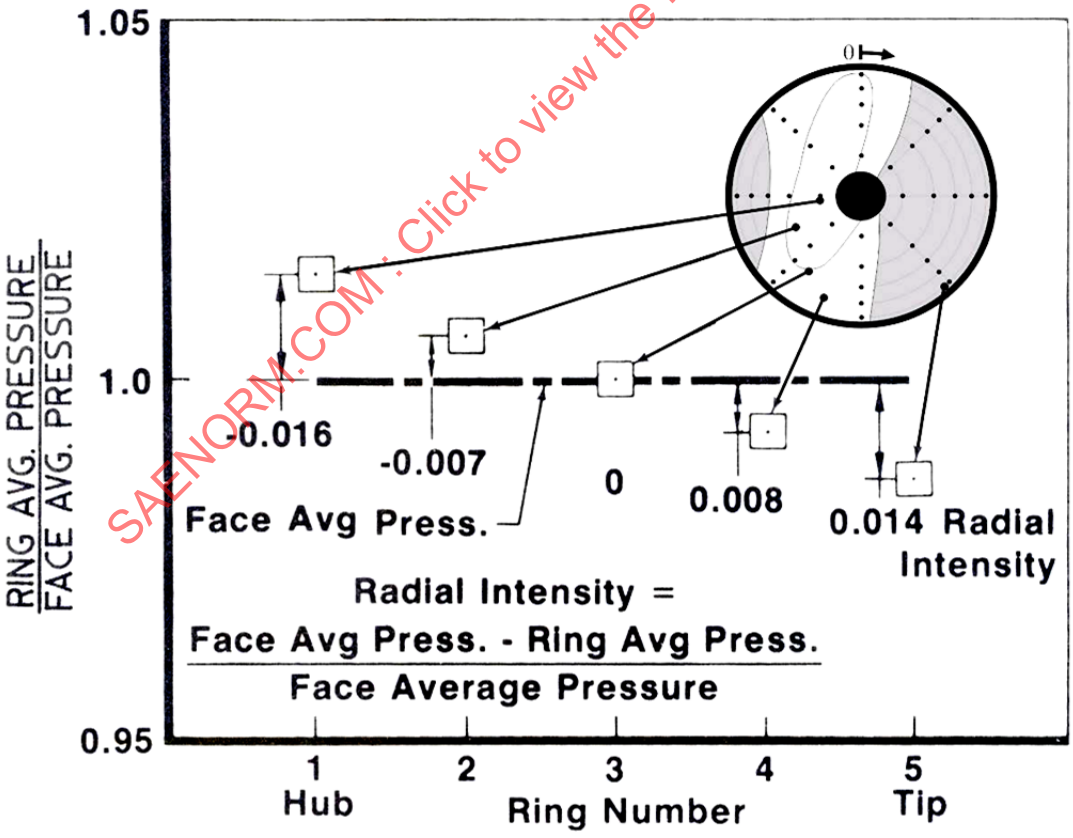

FIGURE 11 - RADIAL DISTORTION ELEMENTS

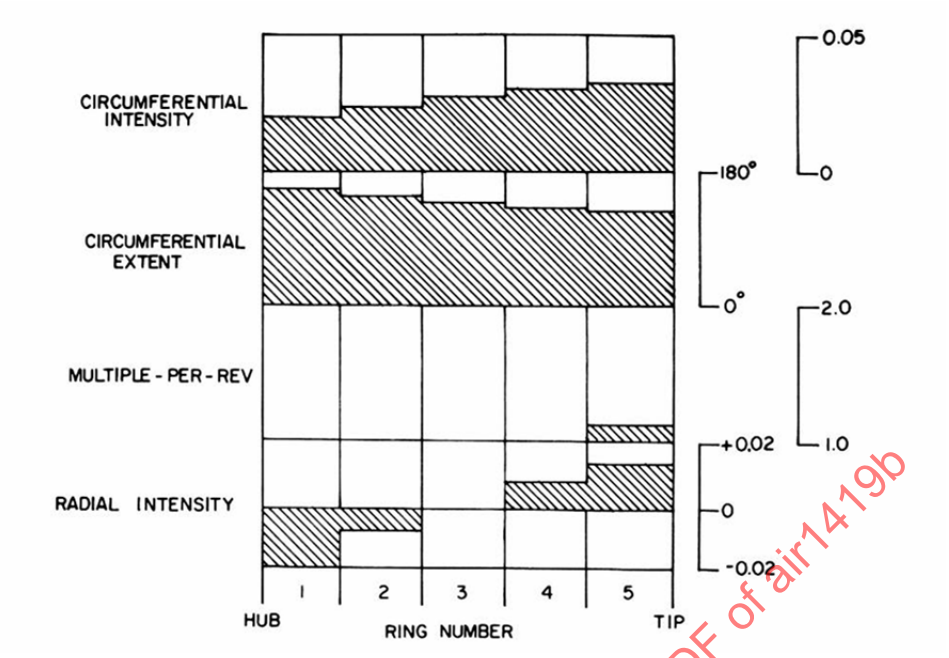

FIGURE 12 - DISTORTION-DESCRIPTOR ELEMENTS FOR THE EXAMPLE INLET PATTERN

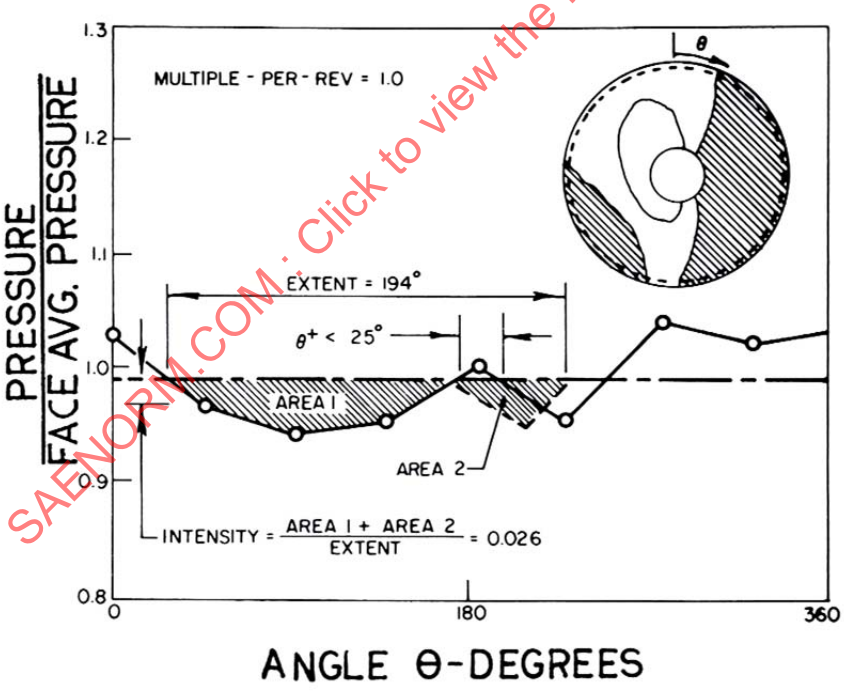

FIGURE 13 - EQUIVALENT ONE-PER-REV PATTERN

4.4 Example Distortion Patterns

Example distortion patterns are given in this paragraph for use in checking computer program results and to illustrate the results obtained when calculating the distortion descriptor elements for each of the patterns. The elements of the probe-by-probe data arrays are the probe readings normalized by the area-weighted face-average total pressure.

Each of these patterns is taken from screen test data. Although the patterns of 4.4.1 through 4.4.6 were intended to be classical patterns (180-degree one-per-rev square wave, hub-radial, and tip-radial), and/or stylized combined patterns (180-degree one-per-rev + hub-radial, 180-degree one-per-rev + tip-radial, and 90-degree one-per-rev + tip-radial), the actual patterns often had significant differences from the intended patterns. Careful attention to detail is required when designing a distortion screen if the desired pattern shapes and distortion element values are to be achieved for all test conditions.

4.4.1 180-Degree One-Per-Rev Circumferential Distortion Pattern

The information relevant to this pattern is given in Figure 14. The ring circumferential intensity values are nearly constant and the angular extent of the circumferential distortion is uniform from ring-to-ring. There is no multiple-per-rev content and very little radial distortion content.

Probe by Probe
Clockwise from TDC

	rake 1	rake 2	rake 3	rake 4	rake 5	rake 6	rake 7	rake 8
ring 1 (hub)	0.906	0.912	0.962	1.101	1.116	1.079	0.924	0.915
ring 2	0.903	0.897	1.075	1.119	1.103	1.139	0.946	0.902
ring 3	0.905	0.904	1.048	1.076	1.096	1.107	0.935	0.907
ring 4	0.906	0.899	1.058	1.090	1.107	1.115	0.943	0.905
ring 5 (tip)	0.908	0.914	1.028	1.069	1.071	1.090	0.949	0.925

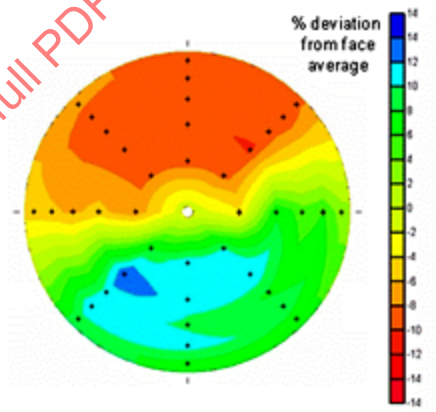

Distortion Descriptor Elements

	$\left(\frac{\Delta PC}{P}\right)_i$	$(\theta^*)_i$	$(MPR)_i$	$\left(\frac{\Delta PR}{P}\right)_i$
ring 1	0.0652	207.8	1.0000	0.0095
ring 2	0.0877	178.7	1.0000	-0.0117
ring 3	0.0755	180.4	1.0000	0.0016
ring 4	0.0800	180.1	1.0000	-0.0040
ring 5	0.0634	181.1	1.0000	0.0046

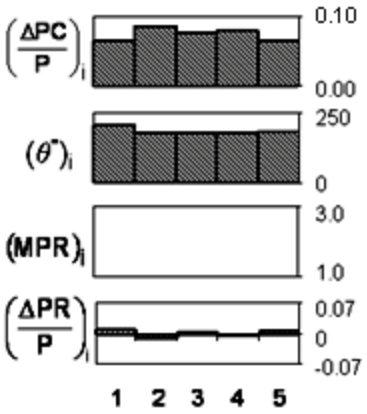

FIGURE 14 - 180-DEGREE 1/REV CIRCUMFERENTIAL DISTORTION PATTERN

4.4.2 Hub-Radial Distortion Pattern

The information relevant to this pattern is given in Figure 15. This hub-radial pattern has almost no circumferential distortion. The angular extent and multiple-per-rev elements have little physical significance.

Probe by Probe
Clockwise from TDC

	rake 1	rake 2	rake 3	rake 4	rake 5	rake 6	rake 7	rake 8
ring 1 (hub)	0.943	0.944	0.938	0.942	0.945	0.946	0.947	0.938
ring 2	0.972	0.955	0.982	0.967	0.957	0.968	0.959	0.941
ring 3	1.023	1.013	1.017	1.011	1.021	1.003	1.020	1.007
ring 4	1.058	1.038	1.053	1.045	1.048	1.050	1.063	1.051
ring 5 (tip)	1.031	1.026	1.030	1.020	1.019	1.043	1.032	1.035

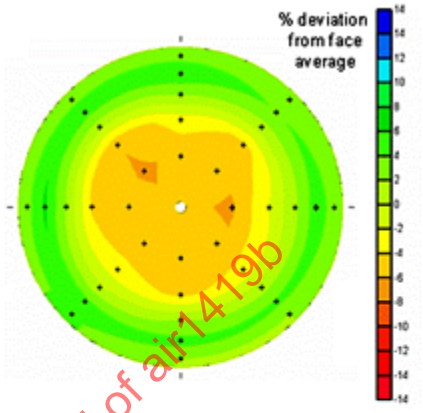

Distortion Descriptor Elements

	$\left(\frac{\Delta PC}{P}\right)_i$	$(\theta^*)_i$	$(MPR)_i$	$\left(\frac{\Delta PR}{P}\right)_i$
ring 1	0.0025	94.7	1.7419	0.0571
ring 2	0.0103	94.5	1.2779	0.0374
ring 3	0.0056	58.5	1.7627	-0.0143
ring 4	0.0039	191.9	1.0000	-0.0507
ring 5	0.0048	178.3	1.0000	-0.0295

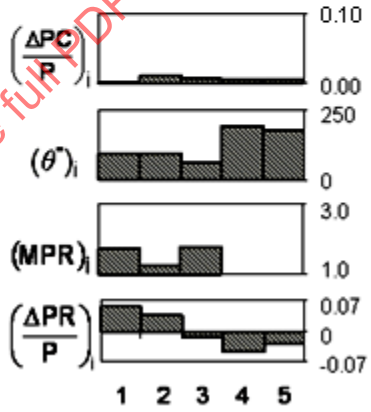

FIGURE 15 - HUB-RADIAL DISTORTION PATTERN

4.4.3 Tip-Radial Distortion Pattern

The information relevant to this pattern is given in Figure 16. This tip-radial pattern has essentially no circumferential distortion. The angular extent and multiple-per-rev elements have little physical significance.

Probe by Probe
Clockwise from TDC

	rake 1	rake 2	rake 3	rake 4	rake 5	rake 6	rake 7	rake 8
ring 1 (hub)	1.044	1.037	1.028	1.030	1.038	1.032	1.043	1.032
ring 2	1.054	1.033	1.051	1.040	1.035	1.048	1.045	1.034
ring 3	1.000	1.010	0.997	1.029	1.002	1.022	1.008	1.021
ring 4	0.970	0.960	0.961	0.960	0.954	0.976	0.960	0.975
ring 5 (tip)	0.948	0.943	0.943	0.943	0.945	0.954	0.952	0.945

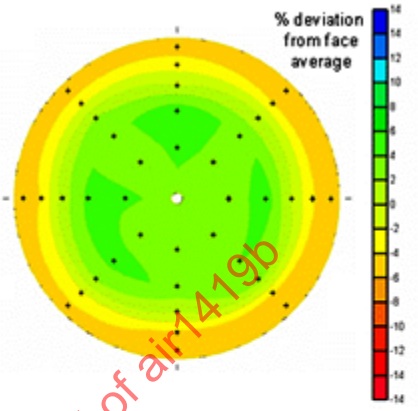

Distortion Descriptor Elements

	$\left(\frac{\Delta PC}{P}\right)_i$	$(\theta^*)_i$	$(MPR)_i$	$\left(\frac{\Delta PR}{P}\right)_i$
ring 1	0.0044	113.4	1.2297	-0.0354
ring 2	0.0040	81.2	2.3086	-0.0424
ring 3	0.0066	133.7	1.2195	-0.0111
ring 4	0.0050	176.7	1.0687	0.0356
ring 5	0.0031	175.7	1.0555	0.0534

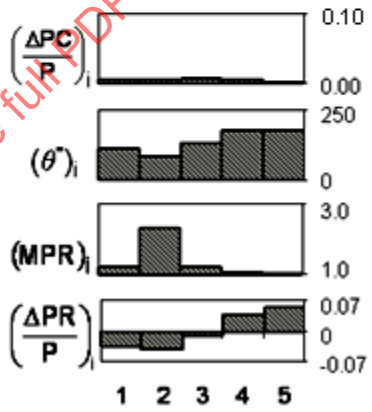

FIGURE 16 - TIP-RADIAL DISTORTION PATTERN

4.4.4 180-Degree One-Per-Rev + Hub-Radial Combined Distortion Pattern

The information relevant to this pattern is given in Figure 17. This 180-degree one-per-rev + hub-radial combined distortion pattern has fairly uniform circumferential angular extent, and tip-radial distortion intensity elements. There is minor multiple-per-rev content in the tip.

Probe by Probe
Clockwise from TDC

	rake 1	rake 2	rake 3	rake 4	rake 5	rake 6	rake 7	rake 8
ring 1 (hub)	0.874	0.874	0.941	1.035	1.050	1.037	0.910	0.877
ring 2	0.884	0.898	0.996	0.988	1.009	1.013	0.965	0.889
ring 3	0.925	0.930	1.067	1.086	1.077	1.090	0.961	0.920
ring 4	0.940	0.938	1.124	1.151	1.143	1.140	0.986	0.942
ring 5 (tip)	0.938	0.930	1.104	1.010	1.086	1.120	1.007	0.949

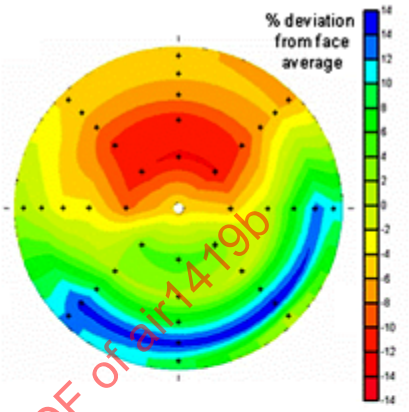

Distortion Descriptor Elements

	$\left(\frac{\Delta PC}{P}\right)_i$	$(\theta^{\circ})_i$	$(MPR)_i$	$\left(\frac{\Delta PR}{P}\right)_i$
ring 1	0.0610	198.3	1.0000	0.0456
ring 2	0.0541	155.5	1.0000	0.0400
ring 3	0.0660	176.3	1.0000	-0.0120
ring 4	0.0808	178.4	1.0000	-0.0506
ring 5	0.0603	162.1	1.0034	-0.0230

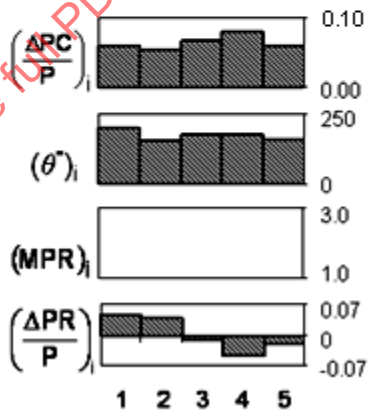

FIGURE 17 - 180-DEGREE 1/REV + HUB-RADIAL COMBINED DISTORTION PATTERN

4.4.5 180-Degree One-Per-Rev + Tip-Radial Combined Distortion Pattern

The information relevant to this pattern is given in Figure 18. This 180-degree one-per-rev + tip-radial combined distortion pattern has fairly uniform circumferential and angular extent distortion elements. There is no multiple-per-rev content. The tip-radial-distortion content is not as uniform as might be desired.

Probe by Probe
Clockwise from TDC

	rake 1	rake 2	rake 3	rake 4	rake 5	rake 6	rake 7	rake 8
ring 1 (hub)	0.961	0.936	1.024	1.144	1.175	1.120	0.988	0.947
ring 2	0.939	0.943	1.128	1.131	1.143	1.166	1.000	0.930
ring 3	0.927	0.910	1.102	1.131	1.104	1.082	0.958	0.924
ring 4	0.876	0.885	1.062	1.041	1.050	1.057	0.931	0.889
ring 5 (tip)	0.873	0.871	1.002	1.006	1.032	1.006	0.921	0.868

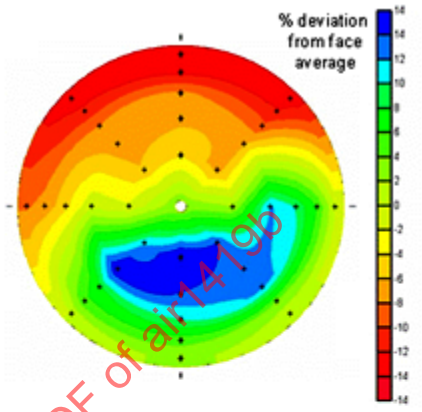

Distortion Descriptor Elements

	$\left(\frac{\Delta PC}{P}\right)_i$	$(\theta^{\sim})_i$	$(MPR)_i$	$\left(\frac{\Delta PR}{P}\right)_i$
ring 1	0.0662	201.5	1.0000	-0.0322
ring 2	0.0839	173.3	1.0000	-0.0427
ring 3	0.0757	181.6	1.0000	-0.0126
ring 4	0.0744	172.9	1.0000	-0.0306
ring 5	0.0628	175.2	1.0000	0.0569

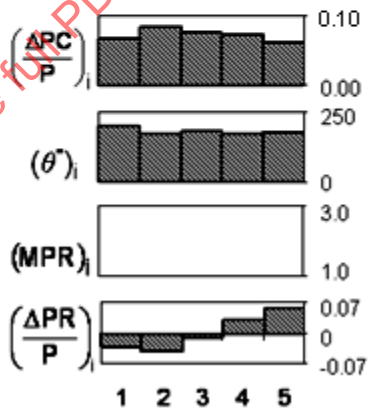

FIGURE 18 - 180-DEGREE 1/REV + TIP-RADIAL COMBINED DISTORTION PATTERN

4.4.6 90-Degree One-Per-Rev + Tip-Radial Combined Distortion Pattern

The information relevant to this pattern is given in Figure 19. This 90-degree one-per-rev + tip-radial combined distortion pattern has essentially uniform circumferential and angular extent distortion elements. There is no multiple-per-rev content in this pattern. The nonuniformity of the tip-radial content is similar to that of the 180-degree one-per-rev + tip-radial combined distortion pattern.

Probe by Probe
Clockwise from TDC

	rake 1	rake 2	rake 3	rake 4	rake 5	rake 6	rake 7	rake 8
ring 1 (hub)	0.987	0.962	0.982	1.068	1.086	1.061	1.076	1.069
ring 2	0.961	0.939	1.091	1.072	1.086	1.064	1.080	1.064
ring 3	0.911	0.913	1.020	1.034	1.010	1.046	1.012	1.026
ring 4	0.878	0.873	0.989	1.002	0.984	0.987	0.985	0.997
ring 5 (tip)	0.872	0.858	0.970	0.983	0.981	0.985	0.972	0.961

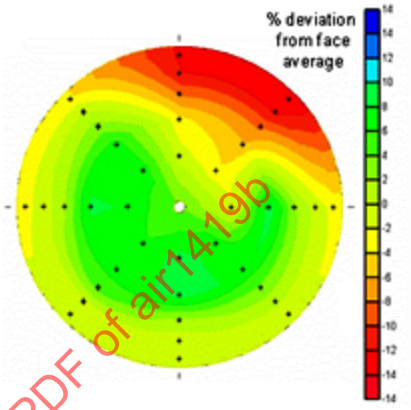

Distortion Descriptor Elements

	$\left(\frac{\Delta PC}{P}\right)_i$	$(\theta^{\sim})_i$	$(MPR)_i$	$\left(\frac{\Delta PR}{P}\right)_i$
ring 1	0.0472	145.5	1.0000	-0.0390
ring 2	0.0631	112.8	1.0000	-0.0473
ring 3	0.0592	113.6	1.0000	0.0009
ring 4	0.0631	111.2	1.0000	0.0356
ring 5	0.0600	119.4	1.0000	0.0498

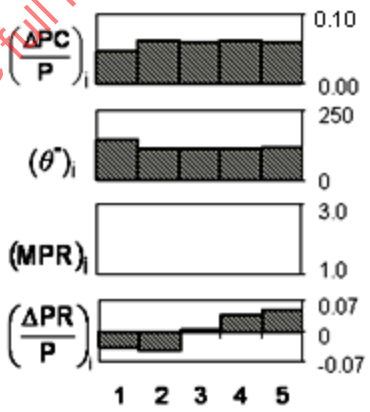

FIGURE 19 - 90-DEGREE 1/REV + TIP-RADIAL COMBINED DISTORTION PATTERN

4.4.7 Two-Per-Rev with Lows Closer than 25 Degrees and with Tip-Radial Distortion Pattern

The information relevant to this pattern is given in Figure 20. This pattern is treated as a one-per-rev pattern which has a nearly uniform circumferential extent of approximately 140 degrees. The circumferential distortion level is nearly uniform ring-to-ring with a value of approximately 0.07, and the radial distortion is located at the tip with a value of approximately 0.02.

Probe by Probe
Clockwise from TDC

	rake 1	rake 2	rake 3	rake 4	rake 5	rake 6	rake 7	rake 8	rake 9	rake 10	rake 11	rake 12
ring 1 (hub)	1.060	0.911	0.911	1.056	0.905	0.905	1.055	1.055	1.056	1.056	1.057	1.060
ring 2	1.073	0.900	0.900	1.062	0.903	0.903	1.056	1.056	1.062	1.062	1.058	1.073
ring 3	1.060	0.911	0.911	1.057	0.907	0.907	1.059	1.059	1.057	1.057	1.056	1.060
ring 4	1.058	0.902	0.902	1.049	0.899	0.899	1.052	1.052	1.049	1.049	1.029	1.058
ring 5 (tip)	1.010	0.895	0.895	1.026	0.889	0.889	1.021	1.021	1.026	1.026	0.998	1.010

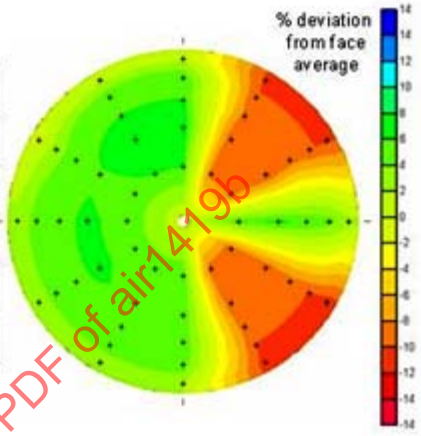

Distortion Descriptor Elements

	$\left(\frac{\Delta PC}{P}\right)_i$	$(\theta^-)_i$	$(MPR)_i$	$\left(\frac{\Delta PR}{P}\right)_i$
ring 1	0.0704	140.1	1.0000	-0.0072
ring 2	0.0761	139.9	1.0000	-0.0090
ring 3	0.0704	139.9	1.0000	-0.0084
ring 4	0.0712	138.7	1.0000	0.0002
ring 5	0.0614	138.0	1.0000	0.0245

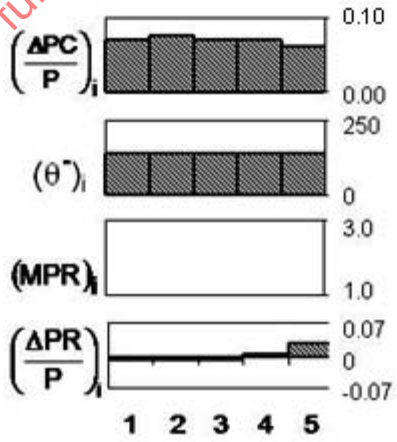

FIGURE 20 - TWO/REV WITH LOWS CLOSER THAN 25 DEGREES AND WITH TIP-RADIAL DISTORTION PATTERN

4.4.8 Two-Per-Rev with Lows Further Apart than 25 Degrees and with Tip-Radial Distortion Pattern

The information relative to this pattern is given in Figure 21. The multiple-per-rev descriptor element for this pattern has a value of almost two, making it a “bona fide” two-per-rev pattern. The extent of the largest low pressure region is approximately 71 degrees. The circumferential distortion is essentially uniform from hub to tip with a value of approximately 0.07 and a tip-radial-distortion value of approximately 0.02.

Probe by Probe
Clockwise from TDC

	rake 1	rake 2	rake 3	rake 4	rake 5	rake 6	rake 7	rake 8	rake 9	rake 10	rake 11	rake 12
ring 1 (hub)	1.060	0.911	0.911	1.056	1.056	1.056	1.057	0.905	0.905	1.055	1.055	1.060
ring 2	1.073	0.900	0.900	1.062	1.062	1.062	1.058	0.903	0.903	1.056	1.056	1.073
ring 3	1.060	0.911	0.911	1.057	1.057	1.057	1.054	0.907	0.907	1.059	1.059	1.060
ring 4	1.058	0.902	0.902	1.049	1.049	1.049	1.029	0.899	0.899	1.052	1.052	1.058
ring 5 (tip)	1.010	0.895	0.895	1.026	1.026	1.026	0.998	0.889	0.889	1.021	1.021	1.010

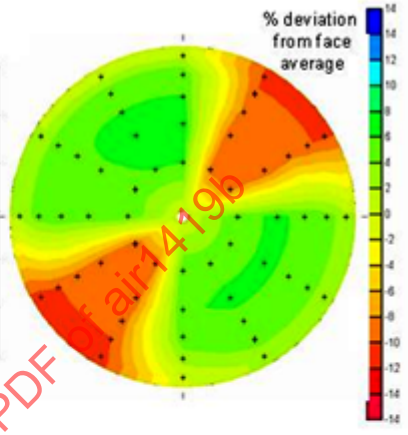

Distortion Descriptor Elements

	$\left(\frac{\Delta PC}{P}\right)_i$	$(\bar{\theta})_i$	$(MPR)_i$	$\left(\frac{\Delta PR}{P}\right)_i$
ring 1	0.0723	70.6	1.9288	-0.0073
ring 2	0.0775	69.1	1.9942	-0.0090
ring 3	0.0715	70.6	1.9502	-0.0083
ring 4	0.0711	73.0	1.9301	0.0001
ring 5	0.0624	73.5	1.8944	0.0245

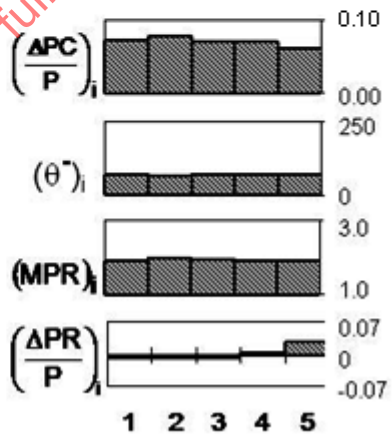

FIGURE 21 - TWO/REV WITH LOWS FURTHER APART THAN 25 DEGREES AND WITH TIP-RADIAL DISTORTION PATTERN

4.4.9 Aircraft Pattern

The information relevant to this pattern is given in Figure 22. This pattern has strong mid-span circumferential distortion and strong tip-radial content. The circumferential distortion is essentially 180 degrees in extent, and no multiple-per-rev content is present.

Probe by Probe
Clockwise from TDC

	rake 1	rake 2	rake 3	rake 4	rake 5	rake 6	rake 7	rake 8
ring 1 (hub)	1.124	1.089	1.010	0.947	1.017	1.037	1.039	1.082
ring 2	1.109	1.100	1.024	0.888	0.937	1.020	1.025	1.092
ring 3	1.088	1.075	1.030	0.891	0.896	0.972	0.980	1.088
ring 4	1.050	1.027	1.008	0.938	0.893	0.989	0.948	1.029
ring 5 (tip)	0.949	0.945	0.953	0.897	0.902	0.913	0.904	0.972

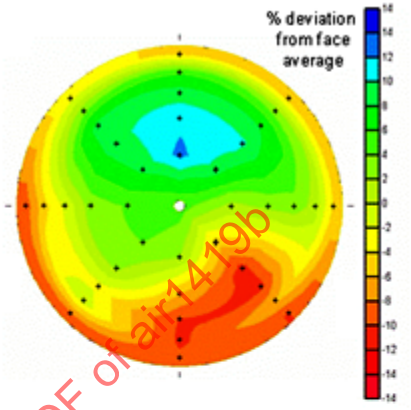

Distortion Descriptor Elements

	$\left(\frac{\Delta PC}{P}\right)_i$	$(\theta^{\sim})_i$	$(MPR)_i$	$\left(\frac{\Delta PR}{P}\right)_i$
ring 1	0.0327	203.2	1.0000	-0.0463
ring 2	0.0574	174.6	1.0000	-0.0275
ring 3	0.0624	180.5	1.0000	-0.0056
ring 4	0.0394	180.2	1.0000	0.0117
ring 5	0.0236	177.8	1.0000	0.0678

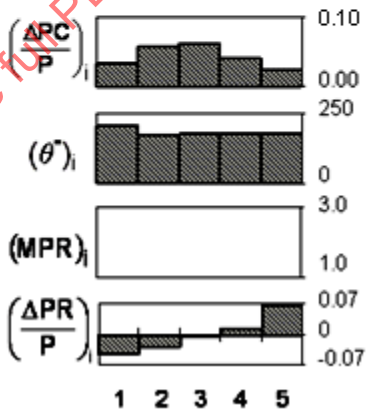

FIGURE 22 - AIRCRAFT PATTERN

4.5 Correlation Methods

The loss of compressor stability pressure ratio is related to the distortion-descriptor elements given in 4.1. There does not appear to be any simple or unique form for combining the elements to correlate the loss in stability pressure ratio that will meet the accuracy requirements for every compressor. However, the equation given below and in Figure 23 is general in nature and can be expanded to include nearly any distortion descriptor used to date:

$$\Delta PRS = \sum_{i=1}^{N}\left[KC_i\left(\frac{\Delta PC}{P}\right)_i + KR_i\left(\frac{\Delta PR}{P}\right)_i + C_i\right] \times 100 \quad \text{(Eq. 21)}$$

where ΔPRS is the loss of stability pressure ratio due to distortion, expressed as a percent of the undistorted stability pressure ratio and

N = the number of instrumentation rings

KC_i = the circumferential distortion sensitivity for ring i

KR_i = the radial distortion sensitivity for ring i

$\left(\frac{\Delta PC}{P}\right)_i$ = the circumferential distortion intensity for ring i, defined in 4.1.1

$\left(\frac{\Delta PR}{P}\right)_i$ = the radial distortion intensity for ring i, defined in 4.1.2

C_i = a constant (offset) term for ring i

$$\Delta PRS = [\text{Circumferential Term} + \text{Radial Term} + \text{Constant Term}]$$

$$\Delta PRS = \sum_{i=1}^{N}\left[KC_i\left(\frac{\Delta PC}{P}\right)_i + KR_i\left(\frac{\Delta PR}{P}\right)_i + C_i\right] \times 100$$

Circumferential Sensitivity

Circumferential Intensity

Radial Sensitivity

Radial Intensity

Constant Term

FIGURE 23 - BASIC EQUATION FOR CALCULATING STABILITY PRESSURE RATIO LOSS (ΔPRS)

The sensitivity and offset coefficients are generalized coefficients and will vary with distortion content (extent, multiple-per-rev), compression system design, and operating conditions. They are derived from test data and should be of sufficient accuracy to correlate the effect of critical distortion patterns within ±2% of stability pressure ratio. For practical purposes, the generalized coefficients are often expanded. An example of the expanded circumferential sensitivity is given in Figure 24. This expanded sensitivity is a function of the defect location (hub, mid-span, or tip), the extent and multiple-per-rev circumferential distortion descriptor elements, as well as the reference sensitivity. The reference sensitivity, usually based on a 180-degree one-per-rev circumferential distortion pattern, is generally represented by a constant at a given corrected speed. If significant nonlinearities occur in the loss of stability pressure ratio with the level of intensity relationship for the reference pattern, especially at high levels, the relationship can be treated as being piecewise linear. This then leads to reference sensitivities which vary with level of intensity and contribute to the offset term, C_i.

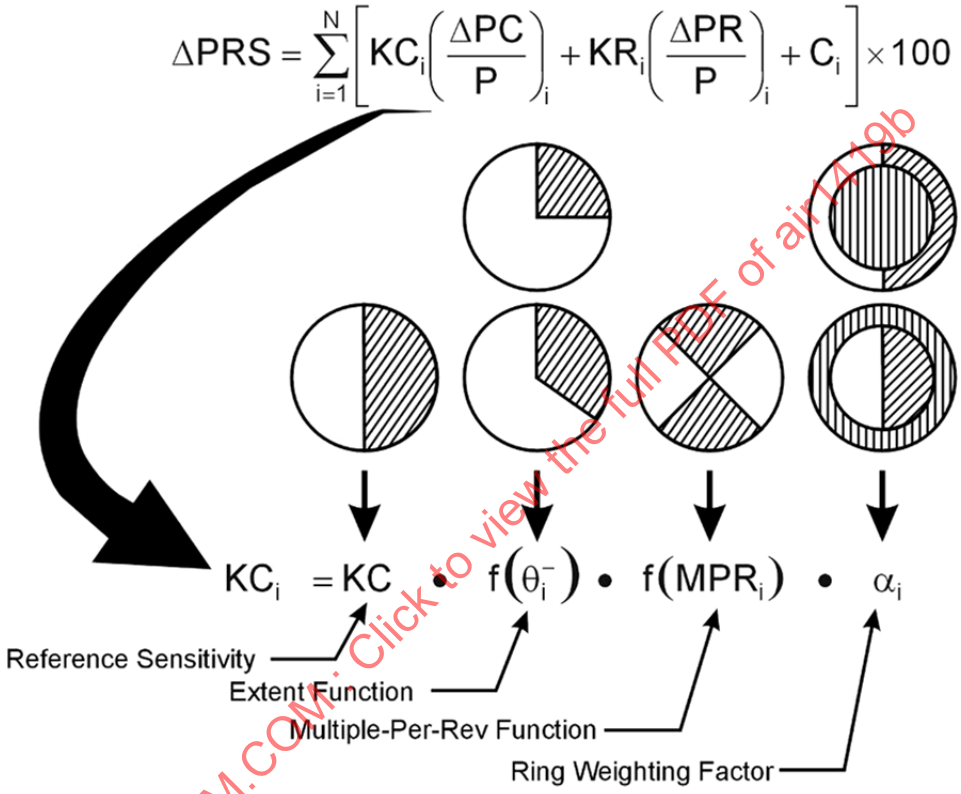

FIGURE 24 - EXAMPLE OF EXPANDED CIRCUMFERENTIAL SENSITIVITY

The loss in stability pressure ratio for downstream compression components can be calculated according to Equation 21 through the introduction of distortion transfer and generation coefficients in the sensitivity parameters. Methods for accomplishing this are discussed in 4.5.1 and 4.5.2.

The following paragraphs provide examples of three methods that have been used to correlate the loss of stability pressure ratio for compression components. In two cases, the correlation makes full use of ARP1420 distortion-descriptor elements, but the elements are not used in conjunction with an aircraft program. The third is in use with an aircraft program, but the circumferential distortion intensity is not the ARP1420 definition. Further, examples of correlations, based on distortion elements similar to those derived in ARP1420, are given to show the broad range of components that can be treated using this correlation method.

4.5.1 Method A

Method A has been used to correlate data from a three-stage fan in terms of ARP1420 distortion descriptor elements with the same accuracy as an existing distortion index that has been verified by distortion screen tests, propulsion system tests, and flight tests.

The example shows a data correlation in terms of four empirical correlation coefficients, namely circumferential sensitivity, radial sensitivity, hub-radial offset, and tip-radial offset. Fictional, but typical, values of these correlation coefficients are presented as functions of inlet corrected airflow.

The philosophy of Method A is:

a. The circumferential sensitivity of Equation 21 is expanded to include ring-weighting factors, an extent factor, and a multiple-per-revolution factor.

b. The loss in stability pressure ratio due to circumferential distortion is proportional to a weighted average of the distortion-descriptor elements over the entire interface plane.

c. The loss in stability pressure ratio due to radial distortion is evaluated for two annular regions. For an interface plane defined by five instrumentation rings, the hub region consists of the inner two instrumentation rings and the tip region consists of the outer two instrumentation rings.

d. The loss in stability pressure ratio due to radial distortion is the higher of the losses evaluated for the hub and tip regions.

e. The loss in stability pressure ratio due to combined circumferential and radial distortions is obtained by algebraic superposition of circumferential and radial terms.

f. Correlation coefficients are functions of corrected inlet airflow only, and are independent of the distortion pattern.

g. Loss in stability pressure ratio due to inlet distortion is measured from an undistorted stability limit line with uniform inlet flow as defined in 3.2.

4.5.1.1 Definition of Terms

ΔPRS_c = the loss in stability pressure ratio due to circumferential distortion expressed as a percentage of the undistorted stability pressure ratio

N = the number of instrumentation rings

α_i = the weighting factor for ring i. To represent an existing distortion index, α_i was selected to be inversely proportional to the instrumentation ring diameter, subject to $\sum_{i=1}^{N} \alpha_i = 1$.

K_c = the average circumferential sensitivity, determined empirically

$\left(\frac{\Delta PC}{P}\right)_i$ = the ARP1420 circumferential distortion intensity of ring i

θ_i^- = the ARP1420 circumferential extent of the distortion in ring i in degrees

MPR_i = the ARP1420 multiple-per-revolution element for ring i

ΔPRS_h = the loss in stability pressure ratio due to hub-radial distortion expressed in percent of the undistorted stability pressure ratio

ΔPRS_t = the loss in stability pressure ratio due to tip-radial distortion expressed in percent of the undistorted stability pressure ratio

ΔPRS = the loss in stability pressure ratio due to inlet distortion expressed in percent of the undistorted stability pressure ratio (ARP1420 definition)

ΔPRS_r = the loss in stability pressure ratio due to radial distortion expressed in percent of the undistorted stability pressure ratio

K_r = the average radial sensitivity, determined empirically

$\left(\frac{\Delta PR}{P}\right)_i$ = the ARP1420 radial distortion intensity of ring i. This intensity can be either positive or negative.

C_h, C_t = the radial offset terms for the hub and tip, respectively. Usually one is close to zero, denoting the region closest to stability pressure ratio loss, while the other is negative, reflecting the higher stability margin of the region furthest from stability pressure ratio loss.

4.5.1.2 Formulae for Loss of Stability Pressure Ratio

The loss in stability pressure ratio due to circumferential distortion is obtained from a weighted average of distortion-descriptor elements over the interface plane.

$$\Delta PRS_c = \left[\sum_{i=1}^{N} \alpha_i K_c \left(\frac{\Delta PC}{P}\right)_i \left(\frac{\bar{\theta_i}}{180}\right) \left(\frac{1}{MPR}\right)_i\right] \times 100 \quad \text{(Eq. 22)}$$

The ring weighting factor, extent function, and multiple-per-rev function of Equation 22 were based on experience with similar fans; consequently, the circumferential sensitivity, K_c, is the only empirically determined correlating parameter in Equation 22.

The loss in stability pressure ratio due to radial distortion is the higher of the loss of the hub or tip regions. Equation 23 describes the loss in stability pressure ratio in the hub region which consists of rings 1 and 2, weighted equally. Equation 24 describes the loss in stability pressure ratio in the tip region which consists of rings 4 and 5, weighted equally. Equation 25 determines whether the hub or tip region is critical for the stability of the particular radial inlet pattern and inlet airflow under investigation.

$$\Delta PRS_h = \left\{\left[\sum_{i=1}^{2} \frac{1}{2} K_r \left(\frac{\Delta PR}{P}\right)_i\right] + C_h\right\} \times 100 \quad \text{(Eq. 23)}$$

$$\Delta PRS_t = \left\{\left[\sum_{i=N-1}^{N} \frac{1}{2} K_r \left(\frac{\Delta PR}{P}\right)_i\right] + C_t\right\} \times 100 \quad \text{(Eq. 24)}$$

$$\Delta PRSr = \text{larger of } \Delta PRSh \text{ or } \Delta PRSt \quad \text{(Eq. 25)}$$

Circumferential and radial terms are added:

$$\Delta PRS = \Delta PRSc + \Delta PRSr \quad \text{(Eq. 26)}$$

The set of Equations 22, 23, 24, 25, and 26 are equivalent to general Equation 21. An example illustrating this equivalence is presented later in this section.

4.5.1.3 Correlation Coefficients

a. Circumferential Distortion

The circumferential sensitivity is established from tests with 180-degree classical inlet distortion screens. A typical variation of circumferential sensitivity with corrected airflow is shown in Figure 25.

b. Radial Distortion

Typical variations of radial sensitivity, hub-radial offset, and tip-radial offset are given in Figures 26, 27, and 28, respectively. The combination of radial sensitivity, hub-radial offset, and tip-radial offset is used to model the piecewise linear loss of stability pressure ratio with radial distortion, as discussed below. Under ideal conditions (no error), one radial offset should be zero while the other should be either zero or negative. From Figures 27 and 28, it can be seen that below 60% airflow the hub-radial offset is significantly negative while the tip-radial offset is not zero, but is between 0.0 and -0.02. This nonzero tip-radial offset reflects error in the undistorted stability-pressure-ratio measurement. This correlation assumes that the undistorted stability pressure ratio was measured between 0 and 2% lower than the true value in this airflow range. Similarly, the nonzero hub-radial offset above 95% airflow describes an undistorted stability margin that is assumed to be measured a fraction of a percent lower than the true value.

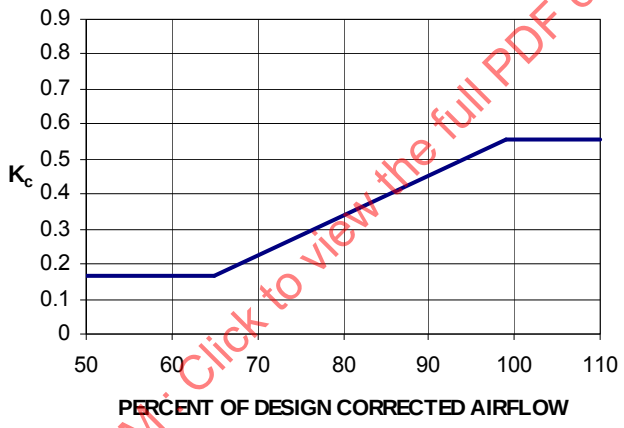

FIGURE 25 - CIRCUMFERENTIAL SENSITIVITY

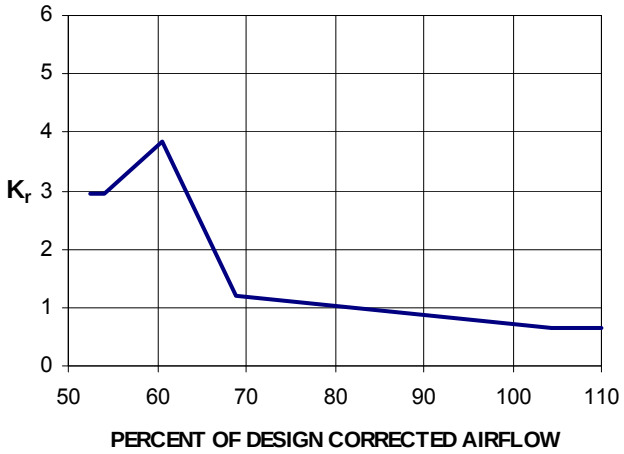

FIGURE 26 - RADIAL SENSITIVITY

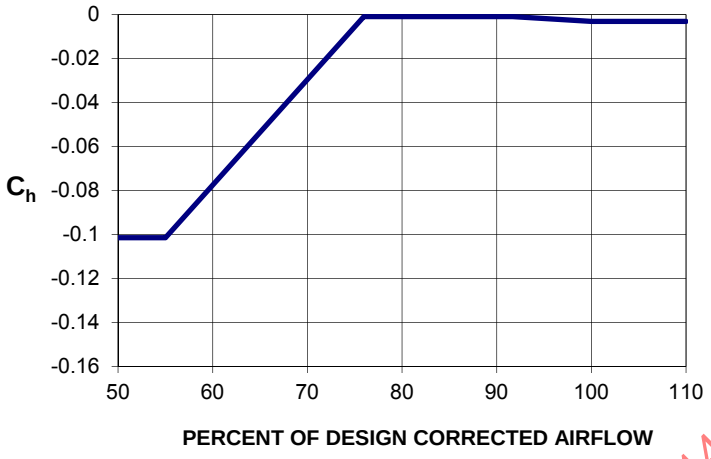

FIGURE 27 - HUB-RADIAL OFFSET

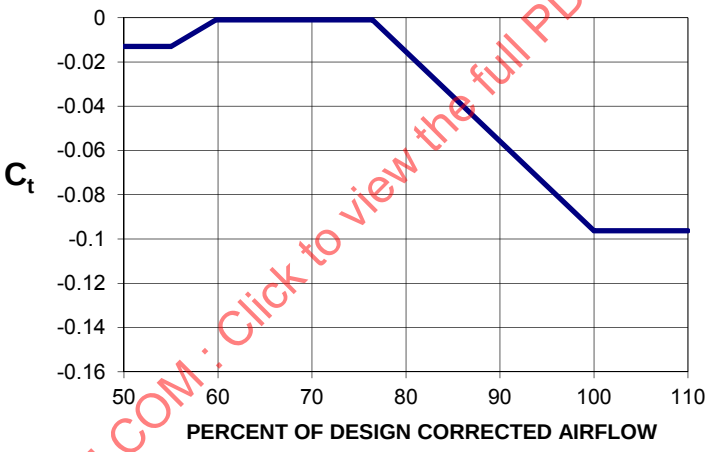

FIGURE 28 - TIP-RADIAL OFFSET

c. Piecewise-Linear Radial Distortion Correlation

The loss in stability pressure ratio due to hub-radial distortion usually has a significantly different characteristic than the loss in stability pressure ratio for a tip-radial distortion of the same magnitude, as illustrated in Figure 29. The stability limit line of a fan can usually be increased by a small amount of either hub-radial or tip-radial distortion. Consequently, the piecewise-linear curve shown in Figure 30 is faired through the data of Figure 29. An increase in the stability limit line (negative ΔPRS) over the undistorted stability limit line for hub distortions with an intensity of less than 0.1 is shown in Figure 30. The slope of the line (radial sensitivity) is assumed equal for both hub and tip distortions. If there were more data points to justify different slopes, then different sensitivities could be used for hub-radial and tip-radial distortions.

The use of hub- and tip-radial offset terms to describe the intercepts of the linear correlation lines on the zero distortion axis is illustrated in Figure 31. The equation used to correlate loss in stability pressure ratio due to radial distortion is illustrated in Figure 32. In this example, the hub constant C_h = -0.06 while the tip constant C_t = 0. This can be interpreted as the hub having 6% more stability margin than the tip, which can be used to offset the destabilizing effects of hub-radial and circumferential distortions. The loss in stability pressure ratio is the maximum value calculated from either the hub or tip correlation equations. For this example, the hub is critical for hub-distortion intensities greater than 0.05, while the tip is critical for hub distortions less than 0.05 and for all tip distortions.

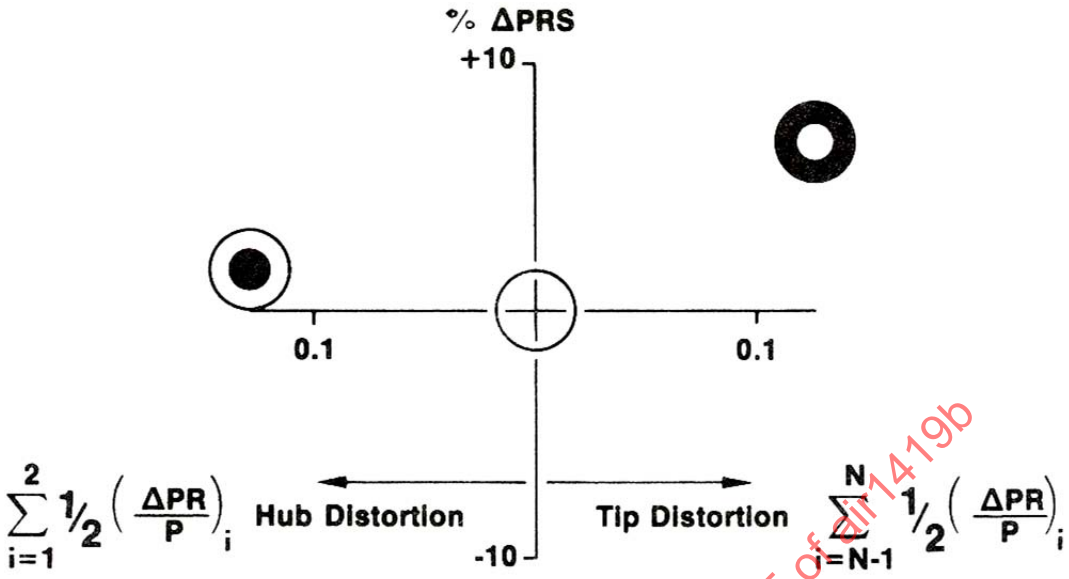

FIGURE 29 - EXAMPLE OF RADIAL DISTORTION DATA

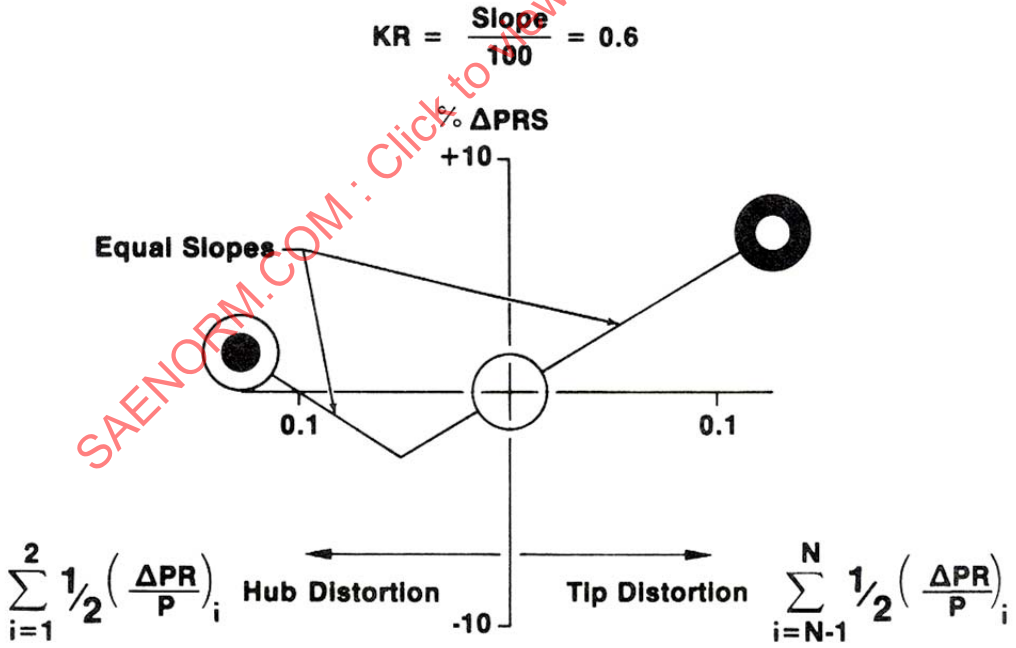

FIGURE 30 - RADIAL SENSITIVITY EVALUATION

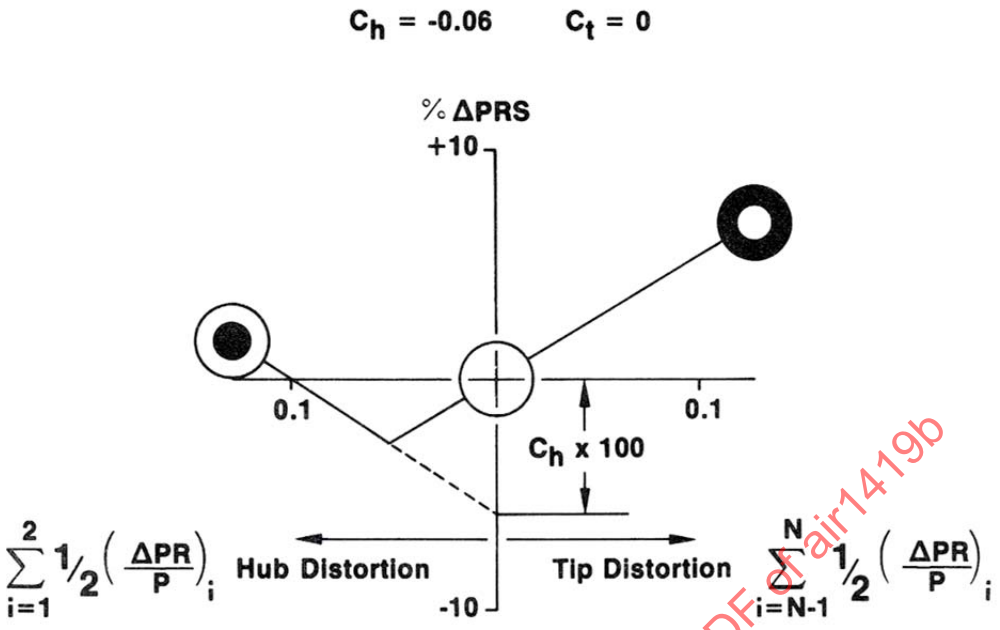

FIGURE 31 - CONSTANT TERM

$$\Delta PRS = Max\left\{\left[\sum \frac{1}{2} KR \left(\frac{\Delta PR}{P}\right)_i\right] + C\right\} \times 100$$

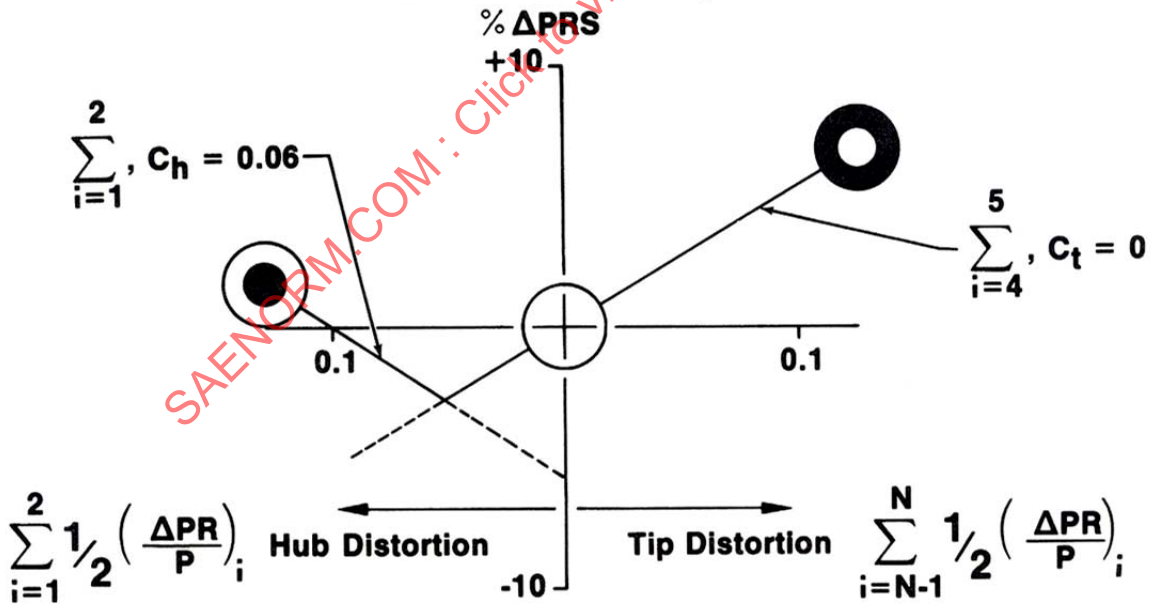

FIGURE 32 - MODELING RADIAL DISTORTION

4.5.1.4 Example Calculations

Evaluate the loss in stability pressure ratio for the aircraft pattern shown in Figure 22 at 100% airflow.

From Figures 25, 26, 27 and 28 at 100% airflow, K_c = 0.55, K_r = 0.7, C_h = -0.002, and C_t = -0.096.

For an annular AIP with a hub-to-tip ratio of 0.33 and rings on centers of equal area, circumferential weighting factors are α_i = 0.303, 0.219, 0.180, 0.157 and 0.141.

Evaluating Equation 22 for the pattern defined by Figure 22 gives ΔPRS_c = (0.00615 + 0.00671 + 0.00619 + 0.00341 + 0.00181) x 100 = 2.42.

Evaluating Equation 23 gives ΔPRS_h = (-0.0162 - 0.0096 - 0.002) x 100 = -2.78

Evaluating Equation 24 gives ΔPRS_t = (0.0041 + 0.0237 - 0.096) x 100 = -6.82

From Equation 25, the hub is critical, therefore ΔPRS_r = -2.78

From Equation 26, ΔPRS = 2.42 - 2.78 = -0.36

This particular pattern results in a small increase in stability pressure ratio at this operating condition because the gain in stability margin with hub-radial distortion more than offsets the loss in stability margin due to circumferential distortion.

4.5.1.5 Equivalence of Method A to the Basic Equation

Method A can be put into the form of the basic Equation 21, using Equation 27 which relates the ring sensitivity, KC_i, to the average sensitivity, KC, and by Equations 28 and 29 which set some of the terms to zero as a result of Equation 25.

$$KC_i = \alpha_i K_c \left(\frac{\theta_i^-}{180}\right)\left(\frac{1}{MPR_i}\right)^2 \quad \text{(Eq. 27)}$$

If Equation 25 indicates that the hub is critical, then

$$KR_1 = KR_2 = K_r/2$$

$$KR_3 = KR_4 = KR_5 = 0$$

$$C_1 = C_2 = C_h/2$$

$$C_3 = C_4 = C_5 = 0 \quad \text{(Eq. 28)}$$

If Equation 25 indicates that the tip is critical, then

$$KR_4 = KR_5 = K_r/2$$

$$KR_1 = KR_2 = KR_3 = 0$$

$$C_4 = C_5 = C_t/2$$

$$C_1 = C_2 = C_3 = 0 \quad \text{(Eq. 29)}$$

The basic Equation 21 is shown below together with an array which shows each of the terms of the equation evaluated for the example of 4.5.1. Each line of the array represents the terms of one ring of Equation 21 with the hub ring at the top.

For this example, Equation 25 indicates that the hub is critical, therefore:

$$KR_1 = KR_2 = 0.35$$

$$KR_3 = KR_4 = KR_5 = 0$$

$$C_1 = C_2 = -0.001$$

$$C_3 = C_4 = C_5 = 0 \quad \text{(Eq. 30)}$$

$$\Delta PRS = \sum_{i=1}^{N} \left[KC_i \left(\frac{\Delta PC}{P} \right)_i + KR_i \left(\frac{\Delta PR}{P} \right)_i + C_i \right] \times 100 \quad \text{(Eq. 31)}$$

$$\begin{aligned} \Delta PRS = [&0.188(0.0327) + 0.35(-0.0463) - 0.001 \\ &+0.117(0.0574) + 0.35(-0.0257) - 0.001 \\ &+0.099(0.0624) + 0(-0.0056) + 0 \\ &+0.086(0.0394) + 0(0.0117) + 0 \\ &+0.0767(0.0236) + 0(0.0687) + 0] \times 100 \end{aligned}$$

$$\Delta PRS = -0.30 \quad \text{(Eq. 32)}$$

The radial ring sensitivities and offset terms of Equation 21 can change with the inlet distortion pattern, whereas in the alternative, equivalent equations for calculating loss in stability pressure ratio (Equations 22, 23, 24, 25, and 26), the sensitivities and offset terms are functions of inlet corrected airflow only and are independent of the inlet distortion pattern.

4.5.2 Method B

In this paragraph, an expansion similar to that of Equation 21 is developed to show how each term may be obtained. Although the following method has been used for a number of compression components, the information contained herein has been developed for a fictionalized fan compression component with two stages. This distortion sensitivity methodology is based on decomposing any aircraft pattern into its circumferential and radial elements and estimating the loss in stability pressure ratio due to each element. The loss in stability pressure ratio for each distortion element is based on sensitivities determined from classical and stylized pattern testing.

4.5.2.1 Definition of Terms

Correlation of the loss of stability pressure ratio for the fan component is accomplished using the empirical relationship:

$$\Delta PRS = b_P \times EX_P \left[KC_P \left(\frac{\Delta P}{PC} \right) + CC_P \right] + \left[KR_P \left(\frac{\Delta P}{PR} \right) + CR_P \right] \quad \text{(Eq. 33)}$$

where:

ΔPRS = the loss in stability pressure ratio

b_p = superposition function which accounts for coupling effects between the circumferential and radial components of total-pressure distortion

EX_p = extent function which accounts for change in loss of stability pressure ratio due to the extent of the total-pressure pattern differing from 180 degrees

KC_p = circumferential total-pressure distortion sensitivity

ΔP/PC = level of inlet circumferential total-pressure distortion

CC_p = circumferential total-pressure distortion offset coefficient for sensitivity or portion of sensitivity lines not passing through the origin

KR_p = radial total-pressure distortion sensitivity

$\Delta P/PR$ = level of inlet radial total-pressure distortion

CR_p = radial total-pressure distortion offset coefficient for sensitivity or portion of sensitivity lines not passing through the origin

Equation 33, when it is written in the form of Equation 21, is similar to an expansion of Equation 21.

$$\Delta PRS = KC\left(\frac{\Delta P}{PC}\right) + KR\left(\frac{\Delta P}{PR}\right) + C \quad \text{(Eq. 34)}$$

where

$$KC = b_P \times EX_P \times KC_P \quad \text{(Eq. 35)}$$

$$KR = KR_P \quad \text{(Eq. 36)}$$

$$C = b_P \times EX_P \times CC_P + CR_P \quad \text{(Eq. 37)}$$

The bracketed terms (Equation 33) represent the loss in stability pressure ratio due to pure 180-degree one-per-rev circumferential and pure radial distortions, respectively. The circumferential total-pressure distortion term $\Delta P/PC$ was determined from the maximum value of the expression:

$$\frac{\Delta P}{PC} = \frac{1}{2}\sum_{i=1}^{2}\frac{(P\ RING\ AVG)_i - (P\ RING\ MIN)_i}{P\ FACE\ AVG} \quad \text{(Eq. 38)}$$

or

$$\frac{\Delta P}{PC} = \frac{1}{2}\sum_{i=4}^{5}\frac{(P\ RING\ AVG)_i - (P\ RING\ MIN)_i}{P\ FACE\ AVG} \quad \text{(Eq. 39)}$$

where i denotes a ring (the hub ring is denoted by 1 and the tip ring by 5). Note that the definition differs from the ARP1420 definition for the circumferential distortion level element, but is related to it for well-behaved patterns. The radial total-pressure distortion term $\Delta P/PR$ was determined from the maximum value of the expression

$$\frac{\Delta P}{PR} = max\left[\frac{(P\ FACE\ AVG) - (P\ RING\ AVG)_i}{P\ FACE\ AVG}\right] \quad \text{(Eq. 40)}$$

Only positive values are considered. The maximum value usually is contributed by either i=5 (tip-radial) or i=1 (hub-radial). This definition is identical to the ARP1420 radial distortion level element definition.

4.5.2.2 Coefficient Determination (Constant Corrected Speed)

This paragraph reviews the manner in which the coefficients of Equation 33 were determined. Prior to this discussion, it is instructive to examine the coefficients in more detail to determine what they represent. Equation 33 can be arranged to give the following form:

$$\Delta PRS = \left[KC_P\left(\frac{\Delta P}{PC}\right) + CC_P\right] b_P \times EX_P + \left[KR_P\left(\frac{\Delta P}{PR}\right) + CR_P\right] \quad \text{(Eq. 41)}$$

Equation 41 can be written in the following form:

$$\Delta PRS = \Delta PRS_{C,180}\left(\frac{\Delta PRS_{C,180,R}}{\Delta PRS_{C,180}}\right)\left(\frac{\Delta PRS_{C,\theta,R}}{\Delta PRS_{C,180,R}}\right) + \Delta PRS_R \quad \text{(Eq. 42)}$$

where:

$\Delta PRS_{C,180}$ = KC_p ($\Delta P/PC$) + CC_p and represents the loss of stability pressure ratio assuming the low pressure region has an extent of 180 degrees and that no radial distortion is present

$\frac{\Delta PRS_{C,180,R}}{\Delta PRS_{C,180}}$ = b_p and represents the ratio of the loss of stability pressure ratio due to a 180-degree one-per-rev low pressure region with radial distortion to the loss of stability pressure ratio due to a pure circumferential 180-degree one-per-rev pattern

$\frac{\Delta PRS_{C,\theta,R}}{\Delta PRS_{C,180,R}}$ = EX_p and represents the ratio of the loss in stability pressure ratio due to a circumferential low-pressure region of arbitrary angular extent with radial distortion to the loss in stability pressure ratio due to a 180-degree one-per-rev low-pressure region with radial distortion

ΔPRS_R = loss in stability pressure ratio due to radial distortion assuming no circumferential distortion is present

The methodology screens defined in Table 4 were used to establish the loss in stability pressure ratio at the given corrected speeds. Further, this table indicates which screens were used in determining each coefficient.

TABLE 4 - METHODOLOGY SCREENS AND COEFFICIENT DETERMINATION

TYPE	COEFFICIENTS
180-degree 1/rev	KC_p, CC_p
hub-radial	$KR_{P,Hub}$, $CR_{p,Hub}$
tip-radial	$KR_{p,Tip}$, $CR_{p,Tip}$
180-degree 1/rev + tip-radial	b_p
135-degree 1/rev + tip-radial 90-degree 1/rev + tip-radial	EX_p

Circumferential Distortion Sensitivities

The circumferential distortion sensitivity coefficients were determined from test data which were obtained using 180-degree one-per-rev screens. The data are shown in Figure 33. Straight lines have been faired through the data and the origin. It was assumed that the radial distortion levels are sufficiently low (0.015 on the average) such that any loss of stability pressure ratio due to radial distortion could be assumed to be zero. In this case, Equation 33 can be written in the form:

$$KC_P = \frac{\Delta PRS - CC_P}{\Delta P/PC} \quad \text{(Eq. 43)}$$

since the coefficients b_p and EX_p are identically equal to one. Because straight lines can be drawn through the data and the origin, the circumferential distortion offset coefficient is identically equal to zero. The manner in which the lines are faired is based upon experience and an examination of the degree of correlation at the completion of the first pass in this iteration process. The results of Figure 33 have been reduced to 180-degree one-per-rev circumferential distortion sensitivities using Equation 43 and are plotted as a function of corrected speed in Figure 34.

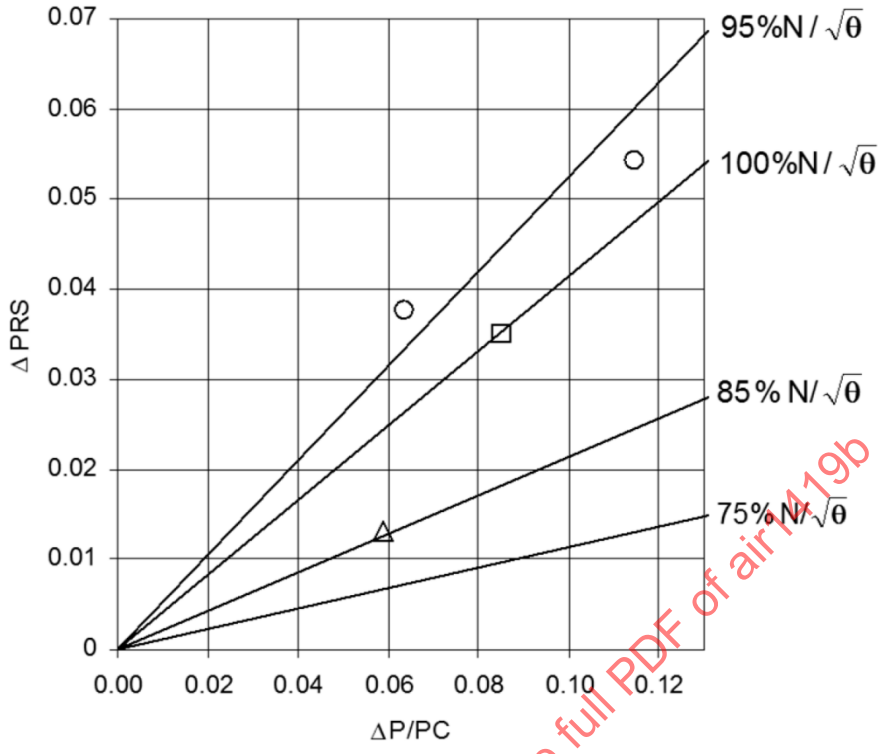

FIGURE 33 - LOSS OF STABILITY PRESSURE RATIO DUE TO 180-DEGREE 1/REV TOTAL-PRESSURE DISTORTION

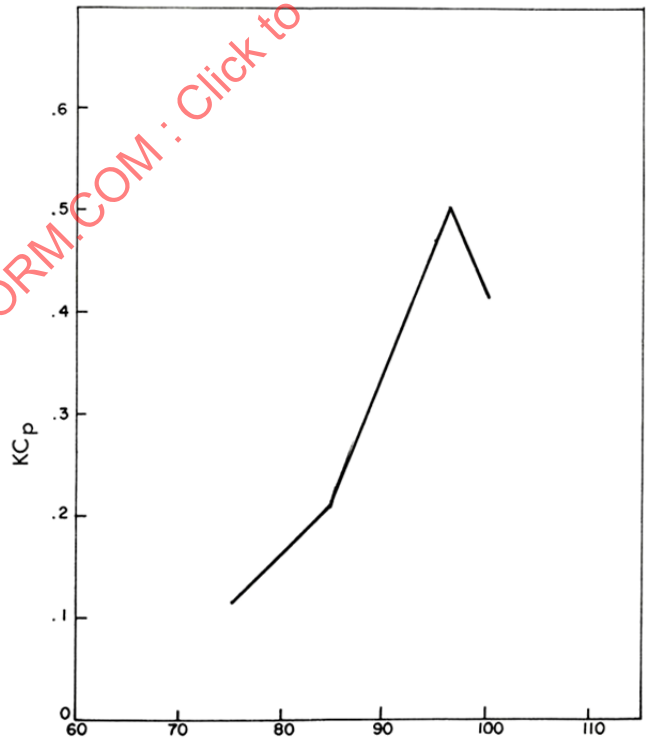

FIGURE 34 - ONE/REV TOTAL-PRESSURE DISTORTION SENSITIVITY

4.5.2.3 Radial Distortion Sensitivities

The radial distortion sensitivity coefficients were determined from test data that were obtained using graded[1] hub- or tip-radial screens. The data are shown in Figure 35. If the circumferential distortion is assumed to be negligible such that it produces no loss in stability pressure ratio, then Equation 33 can be written as

$$KR_P = \frac{\Delta PRS - CR_P}{\Delta P/PR} \quad \text{(Eq. 44)}$$

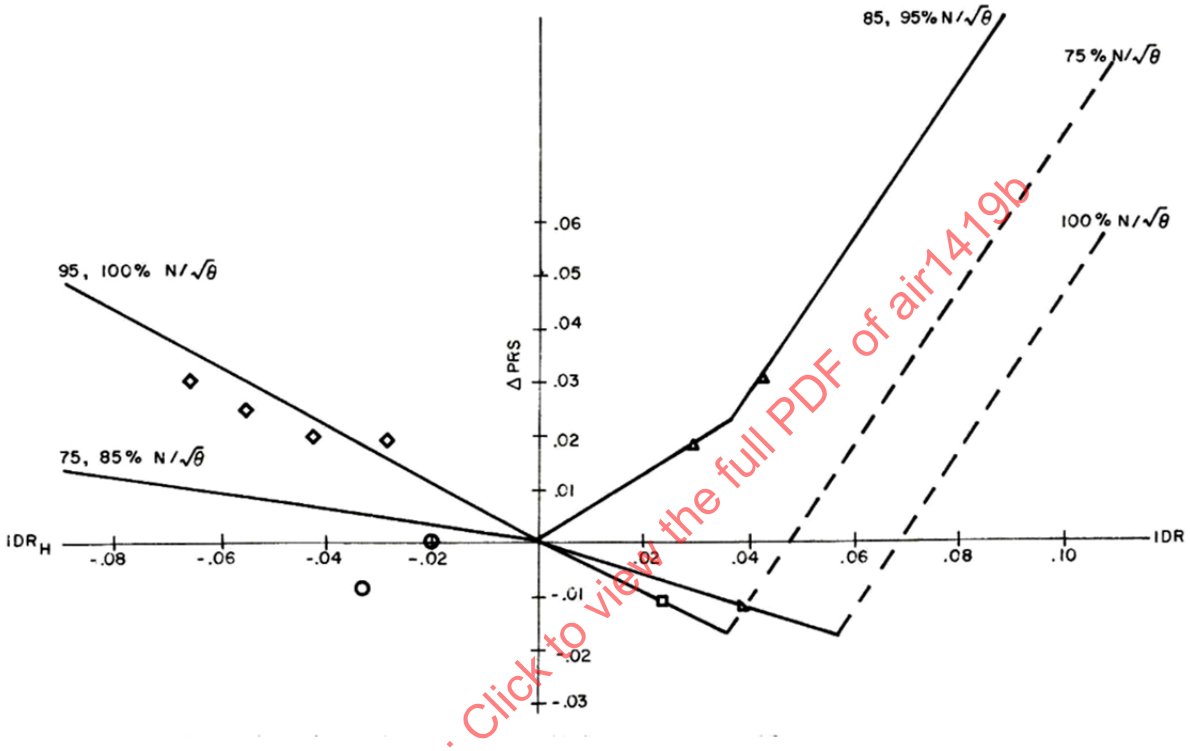

FIGURE 35 - LOSS OF STABILITY PRESSURE RATIO DUE TO HUB- AND TIP-RADIAL TOTAL-PRESSURE DISTORTION

As in the case of circumferential distortion sensitivities, CR is zero for the line segments which pass through the origin. The hub-radial distortion sensitivity is given in Figure 36. To obtain the tip-radial distortion coefficients, it is necessary to determine whether the level of distortion is such that the line segments pass through the origin or whether the lines intercept the ordinate. This determination can be made by reference to Figure 37, and will permit entry to Figure 38 for the appropriate tip-radial distortion sensitivity coefficients, that is, $K_{R_{T1}}$ and $C_{R_{T1}}$ are associated with R_1 while $K_{R_{T2}}$ and $C_{R_{T2}}$ are associated with R_2.

[1] A graded pattern, as opposed to a uniform square pattern, is one in which the total-pressure losses are faired to a minimum to avoid creating significant levels of turbulence due to screen edge mixing of a shear layer.

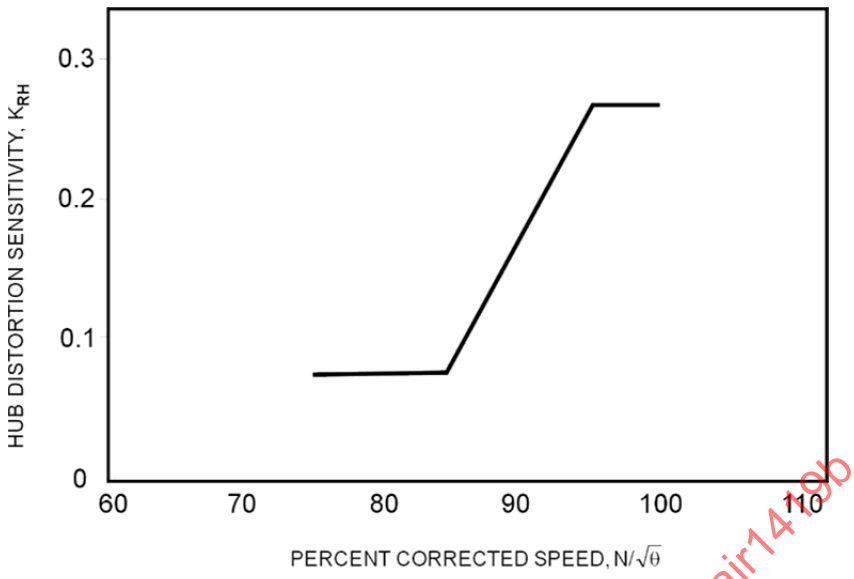

FIGURE 36 - HUB-RADIAL TOTAL-PRESSURE DISTORTION SENSITIVITY AS A FUNCTION OF SPEED

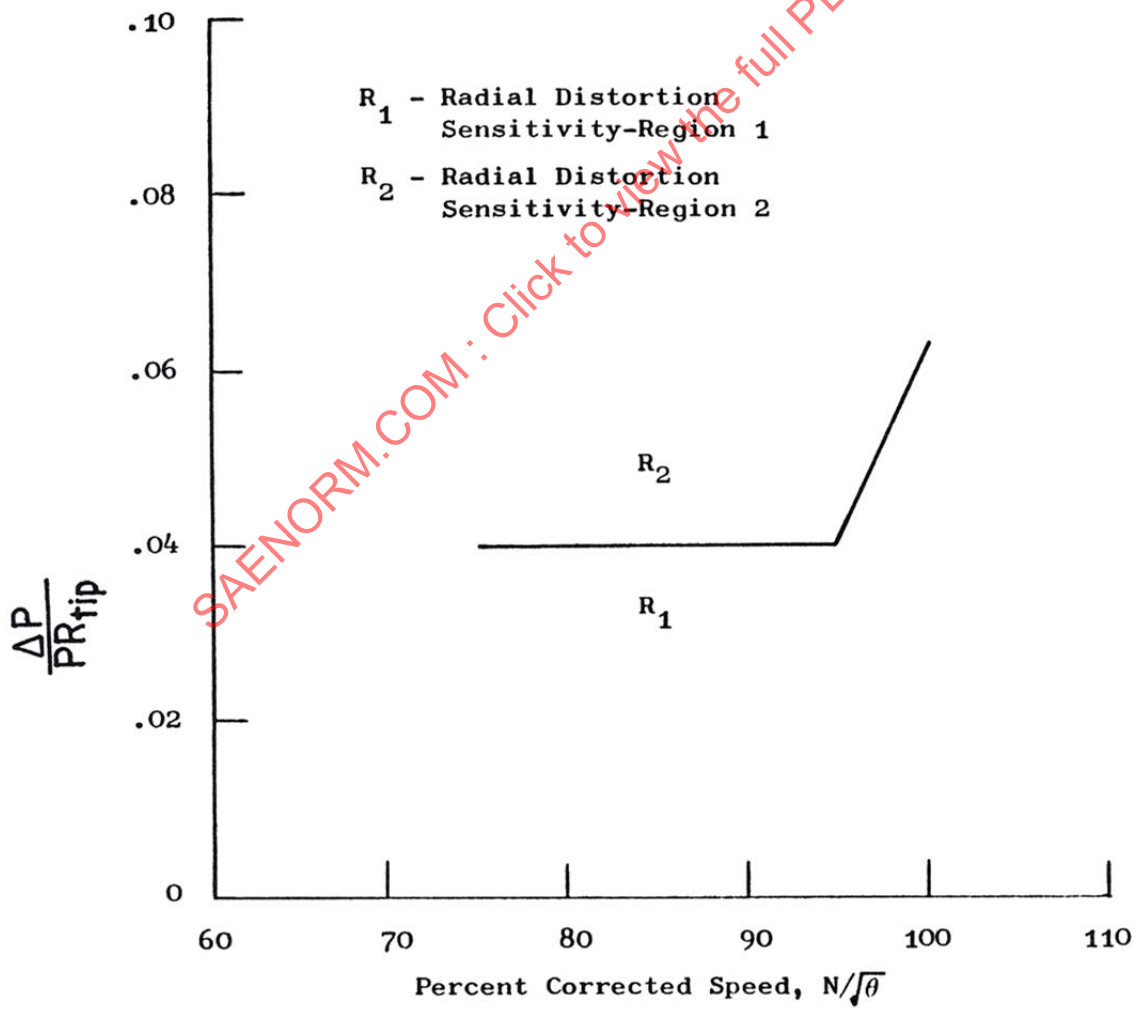

FIGURE 37 - TIP-RADIAL-DISTORTION LOGIC GUIDE AS A FUNCTION OF SPEED

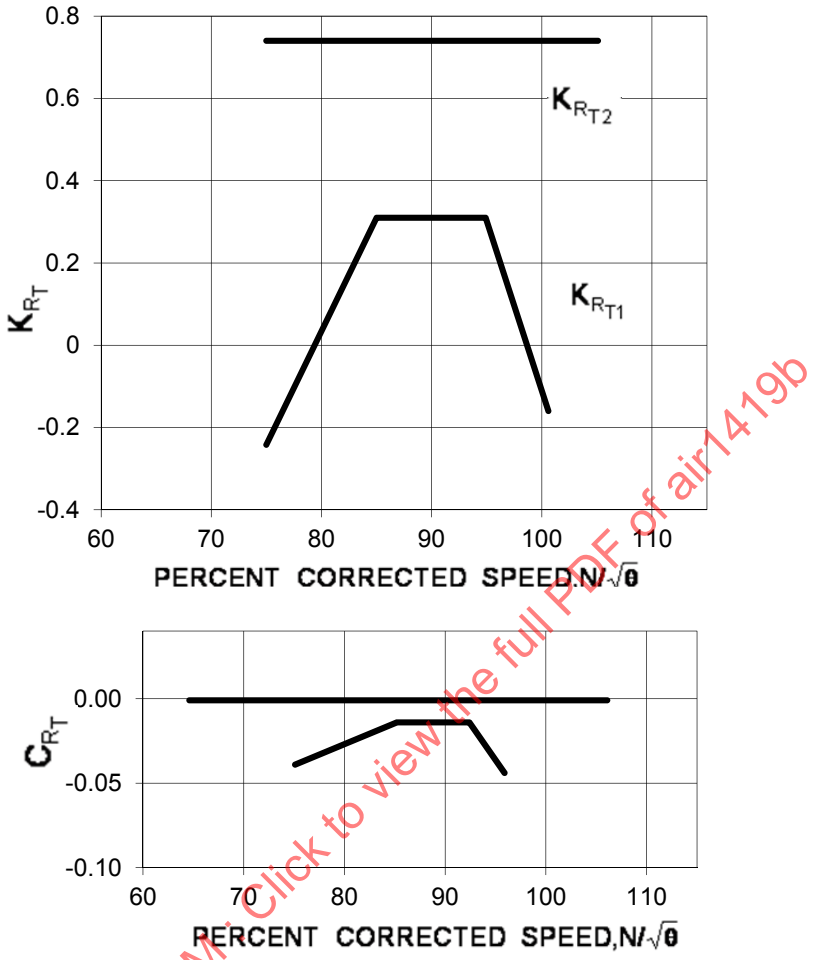

FIGURE 38 - TIP-RADIAL DISTORTION SENSITIVITY COEFFICIENTS AS A FUNCTION OF SPEED

4.5.2.4 Superposition Factor

Once the circumferential and radial distortion sensitivity coefficients have been determined, it is possible to determine the superposition factor b_p from data obtained by testing 180-degree one-per-rev + tip-radial combined distortion screens. This is accomplished through use of Equation 33 since the angular extent function EX_p is identically one. Hence, Equation 33 can be written in the form

$$b_P = \frac{\Delta PRS - KR_P\left(\frac{\Delta P}{PR}\right) + CR_P}{KC_P\left(\frac{\Delta P}{PC}\right) + CC_P} \quad \text{(Eq. 45)}$$

The results, expressed as a function of the ratio (ΔP/PR)/(ΔP/PC), are given in Figure 39 with corrected speed as a parameter. Based on experience and by iteratively examining correlations of aircraft patterns, the superposition function is forced to be less than or equal to one.

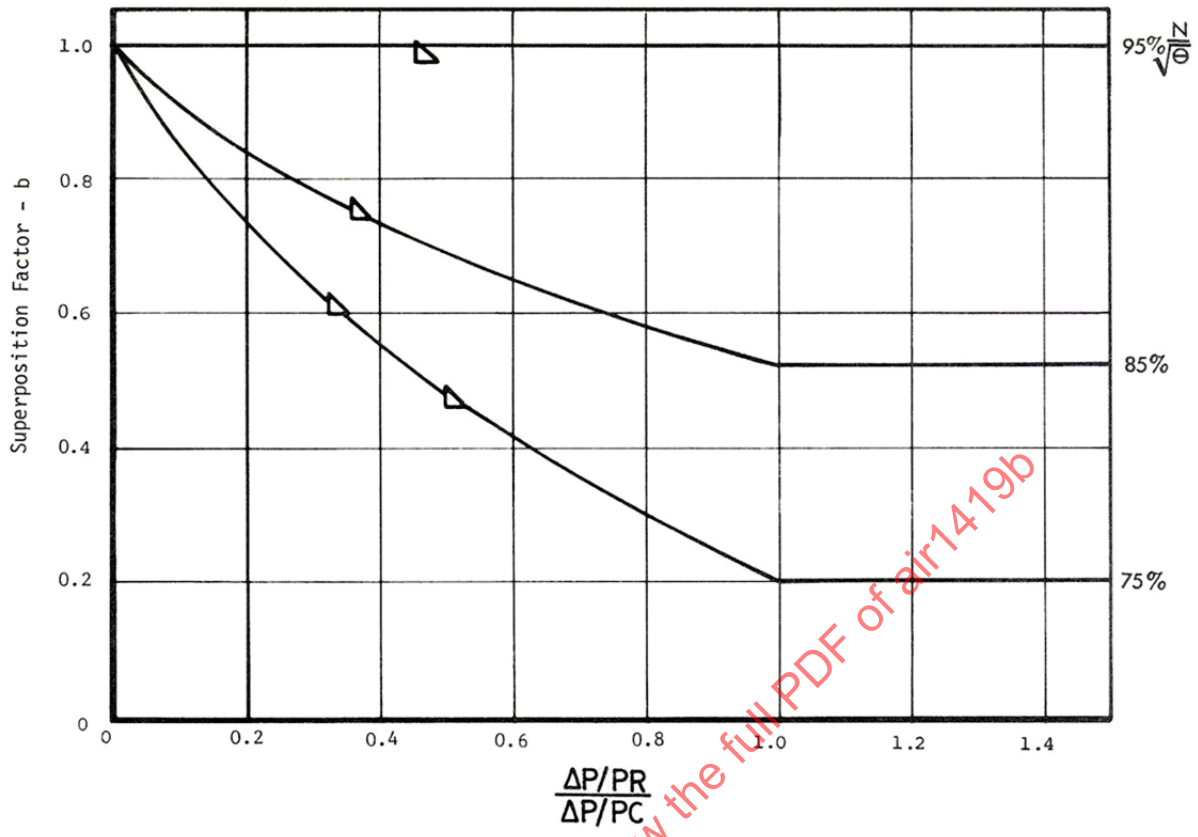

FIGURE 39 - COMBINED CIRCUMFERENTIAL AND RADIAL TOTAL-PRESSURE DISTORTION SUPERPOSITION FACTORS AS A FUNCTION OF SPEED

Extent Function

The extent function can be determined from the data obtained from testing the 135-degree one-per-rev + tip-radial and 90-degree one-per-rev + tip-radial screens, the previously determined circumferential and radial distortion sensitivities, and the superposition factor. Equation 33 now can be written in a form to permit solution for the extent function, EX_p:

$$EX_P = \frac{\Delta PRS - \left[KR_P\left(\frac{\Delta P}{PR}\right) + CR_P\right]}{b_P\left[KC_P\left(\frac{\Delta P}{PC}\right) + CC_P\right]} \quad \text{(Eq. 46)}$$

The results of these computations are shown in Figure 40 as a function of distortion angular extent with corrected speed as a parameter. The angular extent, θ^-, is determined by averaging the angular extents of the two rings giving the maximum value of ΔP/PC. By definition, the extent function has a value of one at 180 degrees. Further, based on experience and iterative examination of aircraft pattern correlations, the extent function is constrained from exceeding one.

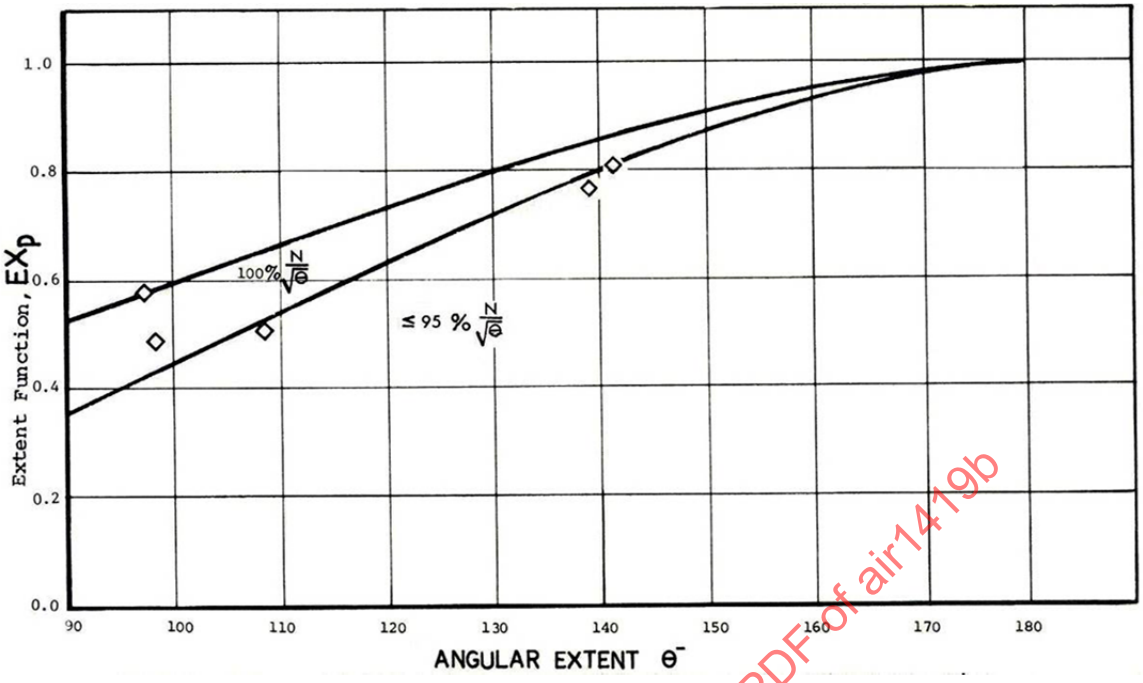

FIGURE 40 - 1/REV TOTAL-PRESSURE DISTORTION ANGULAR EXTENT FUNCTION

This methodology permits Equation 33 to be used for estimating the loss of stability pressure ratio due to any pattern which falls within the range of the parameters tested.

4.5.2.5 Coefficient Determination (Constant Corrected Flow)

Because compression components normally are tested at constant speed, the first step in developing the loss in stability pressure ratio correlation as a function of corrected flow follows the method outlined in the previous paragraph. Translation of the corrected speed results to a corrected flow form is accomplished using a flow/speed correlation. Generally, this is based on results obtained from cycle deck predictions.

4.5.2.6 Distortion Transfer and Generation Coefficients

The effect of inlet distortion on a compressor located downstream of the fictionalized fan can be estimated using Equation 33. However, two additional facets of the stability estimation process are encountered for such cases: (1) the transfer of total-pressure distortion through a fan, and (2) the generation of total-temperature distortion due to the change in total-pressure distortion through the fan component.

Because total-temperature is handled in a manner similar to total-pressure distortion, Equation 33 can be extended in the following manner for estimating the loss of stability pressure ratio of a high-pressure compressor (HPC) (see Reference 2.2.1):

$$\Delta PRS_{HPC} = \left\{ b_P EX_P \left[KC_P \left(\frac{\Delta P}{PC} \right)_{25} + CC_P \right] + \left[KR_P \left(\frac{\Delta P}{PR} \right)_{25} + CR_P \right] \right\}_{HPC} + S \left\{ b_T EX_T \left[KC_T \left(\frac{\Delta T}{TC} \right)_{25} + CC_T \right] + \left[KR_T \left(\frac{\Delta T}{TR} \right)_{25} + CR_T \right] \right\}_{HPC} \quad \text{(Eq. 47)}$$

where the terms in the first line of the equation are given in 4.5.2, except that $(\Delta P/PC)_{25}$ and $(\Delta P/PR)_{25}$ are the circumferential and radial distortions measured at the HPC inlet. The remaining terms in the equation are defined as follows:

S = Superposition function which accounts for coupling effects between total-pressure distortion and total-temperature distortion

b_T = Superposition function which accounts for coupling effects between the circumferential and radial components of total-temperature distortion

EX_T = Extent function which accounts for change in loss of stability pressure ratio due to the extent of the total-temperature pattern differing from 180 degrees

KC_T = Circumferential total-temperature distortion sensitivity

$(\Delta T/TC)_{25}$ = Level of HPC inlet circumferential total-temperature distortion

CC_T = Circumferential total-temperature distortion offset coefficient for sensitivity or portion of sensitivity lines not passing through the origin

KR_T = Radial total-temperature distortion sensitivity

$(\Delta T/TR)_{25}$ = Level of HPC inlet radial total-temperature distortion

CR_T = Radial total-temperature distortion offset coefficient for sensitivity or portion of sensitivity lines not passing through the origin

Since it is the high-temperature regions which cause the loss of stability pressure ratio, Equations 38, 39, and 40 can be used to quantify the levels of temperature distortion through use of the following substitutions:

$\frac{\Delta T}{TC}$ for $-\frac{\Delta P}{PC}$

T RING MAX_i for P RING MIN_i

T RING AVG_i for P RING AVG_i

T FACE AVG for P FACE AVG

$\frac{\Delta T}{TR}$ for $-\frac{\Delta P}{PR}$

The loss of stability pressure ratio for the high-pressure compressor can be estimated if the sensitivities and superposition functions are known and if the plane 25 distortion levels are known in terms of a plane 01 (engine inlet) distortion level. Hence, the following relationships can be written:

$$\left(\frac{\Delta P}{PC}\right)_{25} = f\left[\left(\frac{\Delta P}{PC}\right)_{01}\right] \quad \text{(Eq. 48)}$$

$$\left(\frac{\Delta P}{PR}\right)_{25} = f\left[\left(\frac{\Delta P}{PR}\right)_{01}\right] \quad \text{(Eq. 49)}$$

$$\left(\frac{\Delta T}{TC}\right)_{25} = f\left[\left(\frac{\Delta P}{PC}\right)_{01}\right] \quad \text{(Eq. 50)}$$

$$\left(\frac{\Delta T}{TR}\right)_{25} = f\left[\left(\frac{\Delta P}{PR}\right)_{01}\right] \quad \text{(Eq. 51)}$$

where Equations 48 and 49 represent total-pressure distortion transfer and Equations 50 and 51 represent total-temperature distortion generation. Both explicit and implicit distortion transfer and generation coefficients are illustrated in Figures 41 through 44. Equations 48 and 50 can be written in the following forms:

$$\left(\frac{\Delta P}{PC}\right)_{25} = CDTC_P\left[\left(\frac{\Delta P}{PC}\right)_{01}\right] \quad \text{(Eq. 52)}$$

$$\left(\frac{\Delta T}{TC}\right)_{25} = CDGC_P\left[\left(\frac{\Delta P}{PC}\right)_{01}\right] \quad \text{(Eq. 53)}$$

where $CDTC_p$ and $CDGC_p$ are the distortion transfer and generation coefficients, respectively, for circumferential total-pressure distortion. These coefficients are examples of explicit coefficients which are illustrated by the examples of Figures 41 and 42. The radial distortion transfer and generation coefficients are implicit coefficients (Equations 49 and 51) and are illustrated by the examples of Figures 43 and 44.

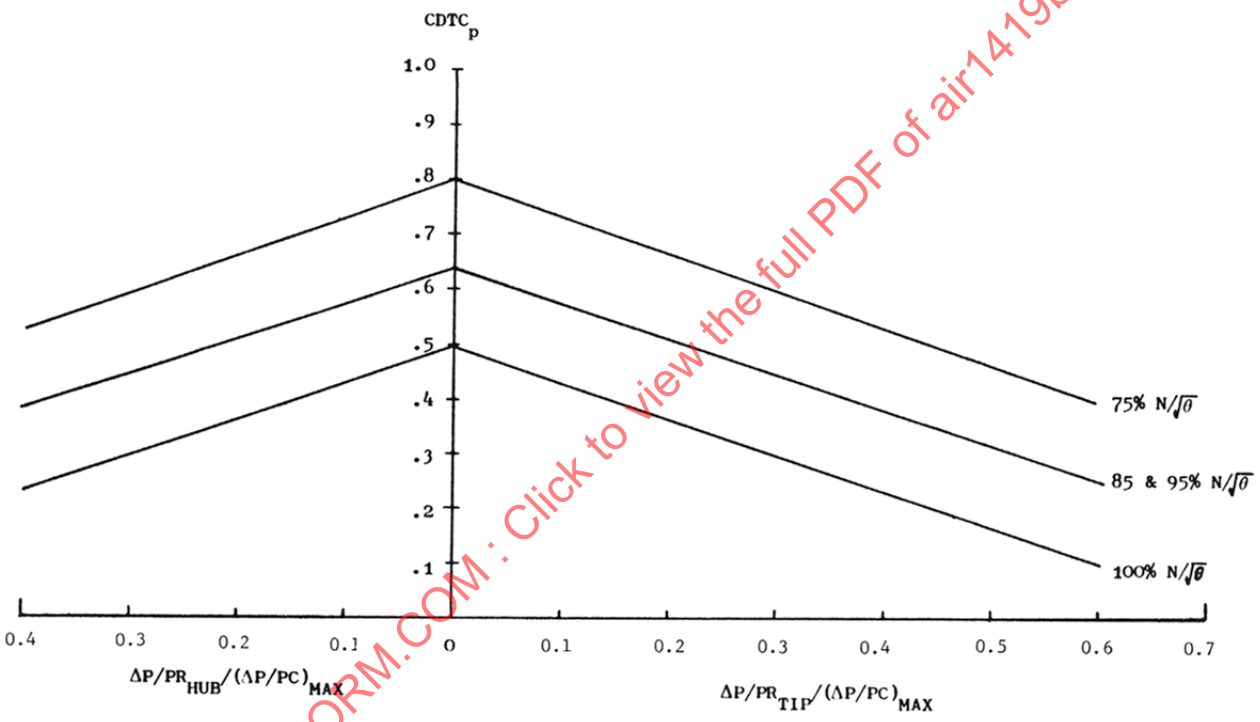

FIGURE 41 - CIRCUMFERENTIAL TOTAL-PRESSURE DISTORTION TRANSFER COEFFICIENT

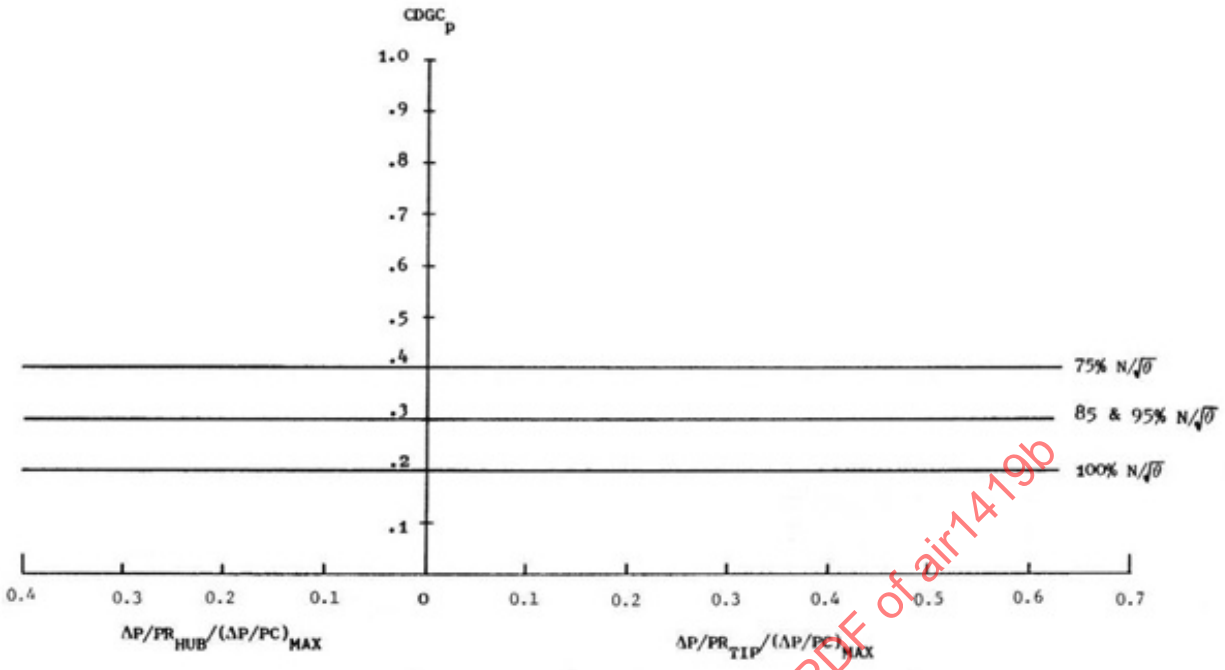

FIGURE 42 - CIRCUMFERENTIAL TOTAL-TEMPERATURE DISTORTION GENERATION COEFFICIENT DUE TO TOTAL-PRESSURE DISTORTION

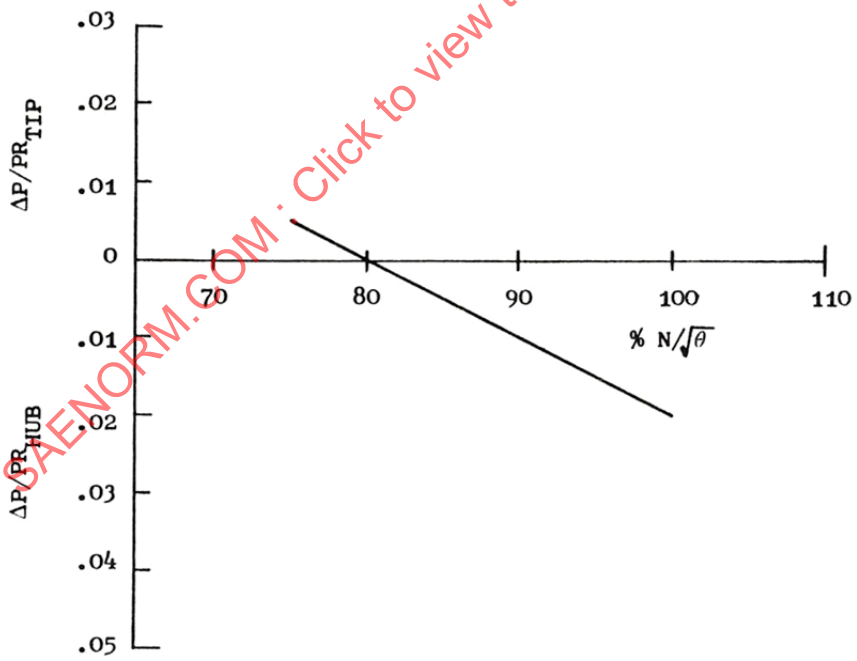

FIGURE 43 - RADIAL TOTAL-PRESSURE DISTORTION

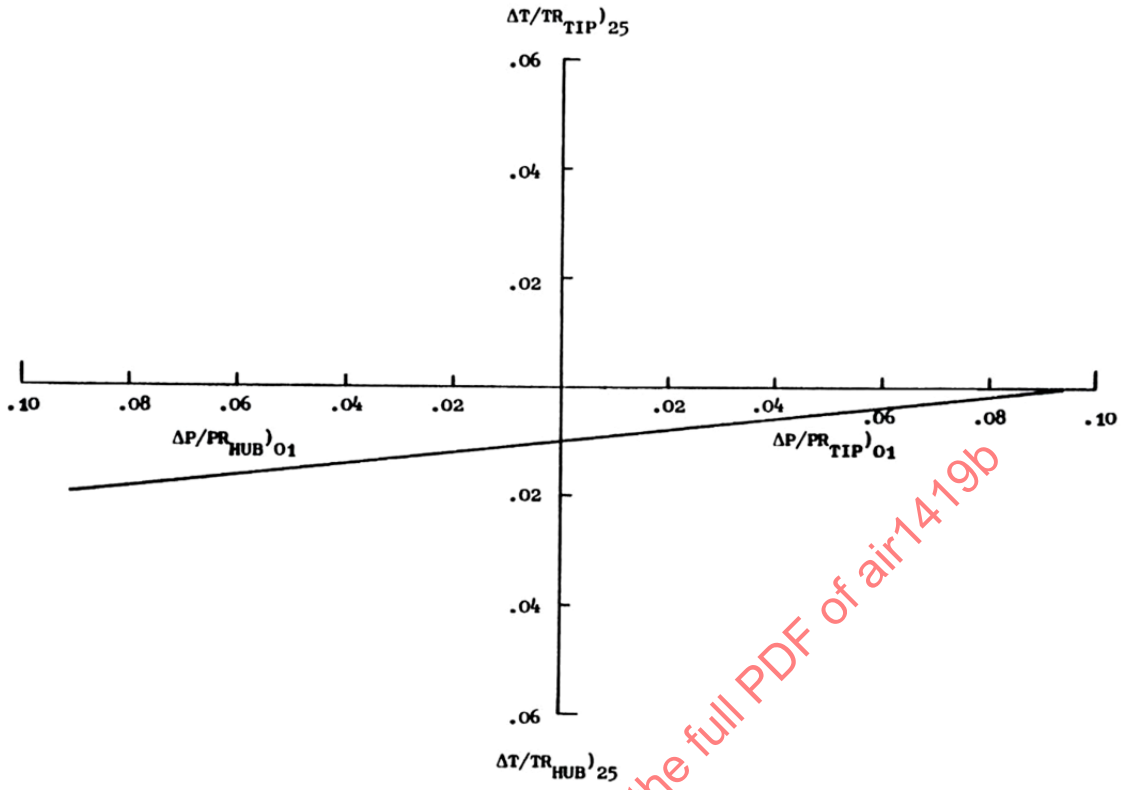

FIGURE 44 - RADIAL TOTAL-TEMPERATURE DISTORTION DUE TO RADIAL TOTAL-PRESSURE DISTORTION

Considerable effort is being exerted to determine temperature distortion effects on compression systems, temperature- and pressure-distortion superposition effects, and distortion transfer and generation coefficient definitions. Although the method discussed in these paragraphs represents the state-of-the-art, it has not yet been reduced to common practice.

4.5.3 Method C

In this method, Equation 21 is expanded to formulate regionally-averaged AIP total-pressure parameters, e.g., for the fan-inlet hub and tip regions, in terms of the ARP1420 descriptor elements. Loss of compressor stability pressure ratio at a given inlet corrected mass flow is correlated with the distortion parameters utilizing radial and circumferential sensitivities which are independent of the AIP pattern. The regionally averaged parameters with appropriate low-pass filtering (4.6.4) are used to define screening parameters directly applicable to inlet time-variant distortion (4.6.3).

The form of combinatorial algebra needed to correlate loss of compressor stability pressure ratio to the desired accuracy in a particular case depends on the complexity of the AIP pattern, compressor type (e.g., single or dual stream), and compressor radial and circumferential sensitivities. Downstream (high-pressure) compressor stability pressure ratio can be correlated explicitly with numerical AIP distortion descriptors through the use of upstream (low-pressure) compressor distortion transfer functions.

4.5.3.1 Definition of Terms

$\frac{\Delta PC}{P}, \frac{\Delta PR}{P}, \theta^{-}, MPR$ = Total pressure distortion elements defined in 4.1

ΔPRS = Overall loss of stability pressure ratio at constant corrected inlet flow

ΔPRS_c = Stability pressure ratio loss due to circumferential total pressure distortion

ΔPRS_R = Stability pressure ratio loss due to radial total pressure distortion

b = Stability limit line loss weighting or superposition factor

K_c = Circumferential distortion sensitivity

K_R = Radial distortion sensitivity

B = AIP distortion parameter weighting or superposition factor

DPC = Circumferential distortion parameter

DPR = Radial distortion parameter

DPS = AIP distortion screening parameter

θ_e^- = Effective distortion extent factor

α = A numerical exponent

$f(\theta_i^-)$ = Extent function

C_R = Radial offset term

I_R = Radial intensity parameter

ΔPRS_T = Loss of stability pressure ratio due to temperature distortion

$f(\theta)$ = Combined pressure and temperature distortion superposition and spatial orientation function

K_T = Temperature distortion sensitivity

DTC = Temperature distortion parameter

A_P, A_T = Pressure and temperature distortion transfer functions

4.5.3.2 Rationale

Equation 21 may be expressed for the full AIP or a tip or hub region at the AIP in the form:

$$\Delta PRS = \Delta PRS_C + b\,\Delta PRS_R \quad \text{(Eq. 54)}$$

Introducing circumferential and radial distortion parameters, DPC and DPR, for pure patterns

$$\Delta PRS_C = K_C(DPC) \quad \text{(Eq. 55)}$$

$$\Delta PRS_R = K_R(DPR) \quad \text{(Eq. 56)}$$

The terms K_C and K_R are empirically established circumferential and radial compressor sensitivities and are independent of the pattern. Then, for a combined distortion pattern

$$\Delta PRS = K_C(DPC) + b\,K_R(DPR) \quad \text{(Eq. 57)}$$

which may be written

$$\Delta PRS = K_C[(DPC) + B(DPR)] \quad \text{(Eq. 58)}$$

where:

$$B = \frac{b\,K_R}{K_C} \quad \text{(Eq. 59)}$$

The term B is a specified function of corrected flow and is independent of the pattern. Equation 58 may be used to define a screening parameter:

$$\text{DPS} = (\text{DPC}) + \text{B}\,(\text{DPR}) \quad \text{(Eq. 60)}$$

For pure circumferential distortion DPR = 0.

For pure radial distortion DPC = 0, B = 1.0.

Correlating Parameters

A full discussion of all possible expansions of DPC and DPR is beyond the scope of this discussion. Illustrative examples are provided below.

DPC

A general form of DPC, explicit in the ARP1420 elements for a region comprising j rings at the AIP (j ≤ N) is:

$$DPC = \frac{1}{j}\sum_j \left\{\left[1 - \left(\frac{\Delta PR}{P}\right)_j\right]\left(\frac{\theta_j^-}{\theta_e^-}\right) f(\theta_j^-)\left(\frac{1}{MPR_j}\right)^{\alpha}\left(\frac{\Delta PC}{P}\right)_j\right\} \quad \text{(Eq. 61)}$$

where

$$f(\theta_j^-) = \begin{cases} 1.0 \quad if \left(\dfrac{\theta_j^-}{\theta_e^-}\right) \le 1.0 \\ \left(\dfrac{\theta_e^-}{\theta_j^-}\right) if \left(\dfrac{\theta_j^-}{\theta_e^-}\right) > 1.0 \end{cases} \quad \text{(Eq. 62)}$$

depending on the shape of the circumferential pressure profile.

The effective distortion extent factor, θ_e^-, and multiple-per-rev exponent, α, depend on compressor dynamic response to circumferential extent and are specified functions of compressor inlet corrected flow. Descriptor elements are centered about the circumferential position surrounding the minimum total pressure in the region.

For classical one-per-rev circumferential patterns having θ^- extent terms greater than θ_e^-, DPC is equal to the ARP1420 circumferential distortion intensity descriptor element (ΔPC/P).

For an important class of inlet distortion where radial and circumferential total-pressure defects occur in the same region, and for that region where either radial intensity elements, $\left(\frac{\Delta PR}{P}\right)_i$, are small compared with the circumferential intensity elements, $\left(\frac{\Delta PC}{P}\right)_i$, or compressor radial sensitivity, K_R, is low, ΔPRS may be correlated with DPC alone. If, for example, this holds for the AIP, then $(DPC)_j = (DPC)_N$. For dual-stream low-pressure compressors (axial-flow fans), separate core flow (ID) and bypass flow (OD) DPC parameters appropriate to core engine and fan OD stability may be utilized.

DPR

The general correlation of radial distortion presents difficulties as ΔPRS_R may not be monotonic with DPR, as illustrated by Figures 45 and 46. In such cases, a method logic, analogous to that embodied in $f(\theta^-)$ for circumferential distortion, needs to be incorporated into DPR to enable a unique radial sensitivity, K_R, defined positive, to be used for correlating ΔPRS_R. A typical form applicable to hub and tip sensitive compressors may be defined such that:

$$DPR = |I_R - C_R| - |C_R| \quad \text{(Eq. 63)}$$

The term C_R is a radial offset term specified as a function of compressor-inlet corrected flow and represents a limiting value of the radial intensity parameter, I_R, and,

$$I_R = \frac{1}{2}\left[\sum_{i=4}^{5}\left(\frac{\Delta PR}{P}\right)_i - \sum_{i=1}^{2}\left(\frac{\Delta PR}{P}\right)_i\right] \quad \text{(Eq. 64)}$$

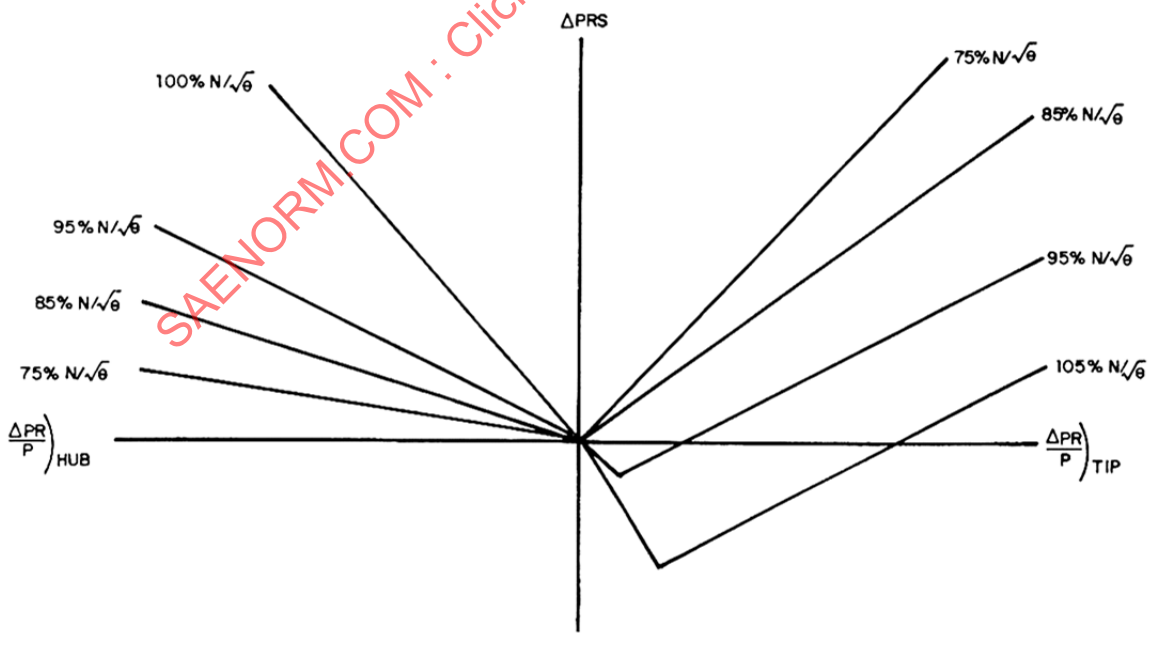

FIGURE 45 - EFFECT OF RADIAL DISTORTION ON A FAN DESIGNED FOR A TIP-RADIAL PROFILE

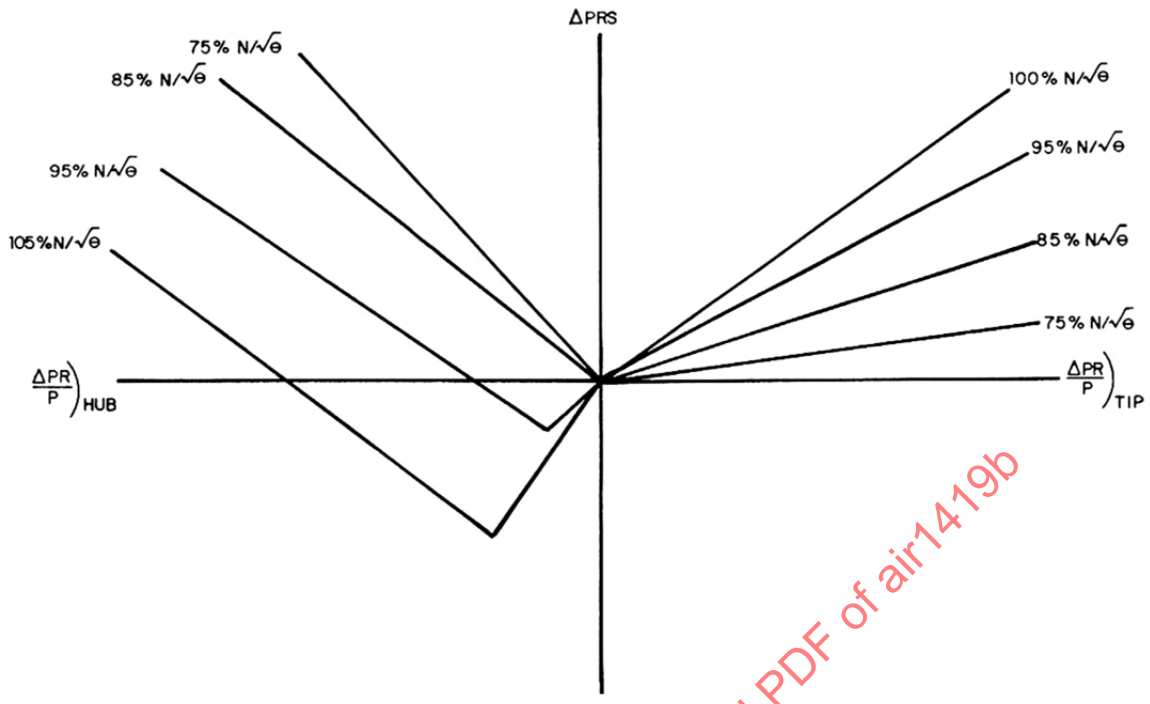

FIGURE 46 - EFFECT OF RADIAL DISTORTION ON A FAN DESIGNED FOR A HUB-RADIAL PROFILE

For tip-radial distortion, I_R is positive. For hub-radial distortion, I_R is negative. The computational logic caters to the experimental observation that ΔPRS_R may be negative, i.e., a degree of radial distortion may have a favorable effect on the stability limit line.

The application of Method C is conceptually similar to that of Method A (4.5.1) for circumferential, radial, and mixed inlet distortion patterns. Circumferential and radial sensitivities, K_C and K_R, are similar to those of Figures 25 and 30.

4.5.3.3 Downstream (High-Pressure) Compressors

Loss of stability pressure ratio due to total-pressure distortion may be correlated, as indicated above, utilizing distortion parameters defined at the high-pressure compressor (HPC) entry. This is not sufficient for determining the effect of AIP pressure distortion on installed HPC stability, however, because total-temperature distortion, created by the low-pressure compressor, can produce a significant loss of HPC stability limit line. Moreover, the spatial orientation between regions of high total temperature and low total pressure is also significant. Losses of stability pressure ratio due to pressure and temperature distortion may be additive or may cancel depending on their spatial orientations, intensities, and extents (Reference 2.2.2). These are all linked via the LPC distortion transfer characteristics to the AIP pressure distortion which, itself, may be time-variant.

A method for dealing with this complex problem is described below. For simplicity, it is assumed that only circumferential elements in the distortion are significant at the HPC entry - not an unreasonable assumption for engines having multistage low-pressure compressors. Otherwise, the method for DPS (4.5.3) may be utilized.

The total loss of HPC stability pressure ratio due to combined temperature and pressure distortion is:

$$\Delta PRS = \Delta PRS_P + f(\theta)\,\Delta PRS_T \quad \text{(Eq. 65)}$$

where $f(\theta)$ is a combined superposition and spatial orientation function defined at the HPC entry.

ΔPRS_p and ΔPRS_T correspond to losses of stability pressure ratio due to the total-pressure distortion and the total-temperature distortion, respectively. Defining pressure and temperature distortion parameters DPC and DTC and corresponding sensitivities as K_P and K_T such that:

$$\Delta PRS_P = K_P(DPC)$$
$$\Delta PRS_T = K_T(DTC) \quad \text{(Eq. 66)}$$

and introducing LPC distortion transfer functions

$$A_P = \frac{(DPC)}{(DPC)_{AIP}} \quad \text{(Eq. 67)}$$

$$A_T = \frac{(DTC)}{(DPC)_{AIP}} \quad \text{(Eq. 68)}$$

then, it may readily be shown that

$$\Delta PRS = [A_P\, K_P + f(\theta)\, A_T\, K_T](DPC)_{AIP} \quad \text{(Eq. 69)}$$

Usually, $A_p < 1.0$ and $A_T > 0$.

The square-bracketed term in Equation 69 can be regarded as an overall or composite sensitivity factor for correlating HPC stability pressure ratio loss with AIP distortion, allowing $(DPC)_{AIP}$ to be used as a screening parameter applicable to time-variant distortion. Thus, for core engine stability assessment, $(DPC)_{AIP}$ may be defined in the hub region of the AIP and related to the ARP1420 descriptor elements using, for example, a relation like Equation 61. It should be noted that the value of the composite sensitivity factor now depends on engine component matching.

4.5.4 Substantiation of Correlation Methods

The wide range of applicability of Equation 21 when expanded for special applications, as illustrated by the discussion of 4.5.1, 4.5.2, and 4.5.3, is more dramatically illustrated by the results shown in Figures 47 through 54. These results are taken from rig component and engine tests and cover a wide variety of compression components, including fans with one to three stages and compressors with eight to sixteen stages. Lines of ±0.02 ΔPRS (two standard deviations) have been superimposed about the line of perfect correlation. This tolerance value is generally accepted within the industry for inlet patterns that are critical for stability. It is clear that Equation 21 provides a framework around which the loss of stability pressure ratio for compression components can be correlated and represents the effects of inlet total-pressure distortion on stability limit line degradation.

4.6 Inlet Data Screening

The realities of establishing inlet/engine compatibility communication between the airframer and the engine manufacturer with their diverse needs and non-optimally time-aligned development programs cause inlet data screening to be a sensitive issue. With proper recognition of the requirements and constraints of each party, as discussed in the following paragraphs, a mutually beneficial dialogue can take place.

4.6.1 General Considerations

The requirement for a universal Aerodynamic Interface Plane flow distortion descriptor which will: (1) define the quality of the air supplied by the inlet and (2) describe the effect of the severity of the flow field upon engine stability, is in direct contrast to the requirement for engine-specific information to predict the effect of any distortion pattern upon engine stability. This dichotomy exists, especially when both the inlet and engine development programs start about the same time. Ideally, an inlet development program would be structured such that distortion sensitivity data would be available from engine component tests prior to the start of inlet development testing. The largest impediment to a “universal inlet distortion factor” is that, a priori, the engine manufacturer cannot predict how the radial distortion will couple with the circumferential distortion, nor whether a compression component will be hub- or tip-distortion sensitive.

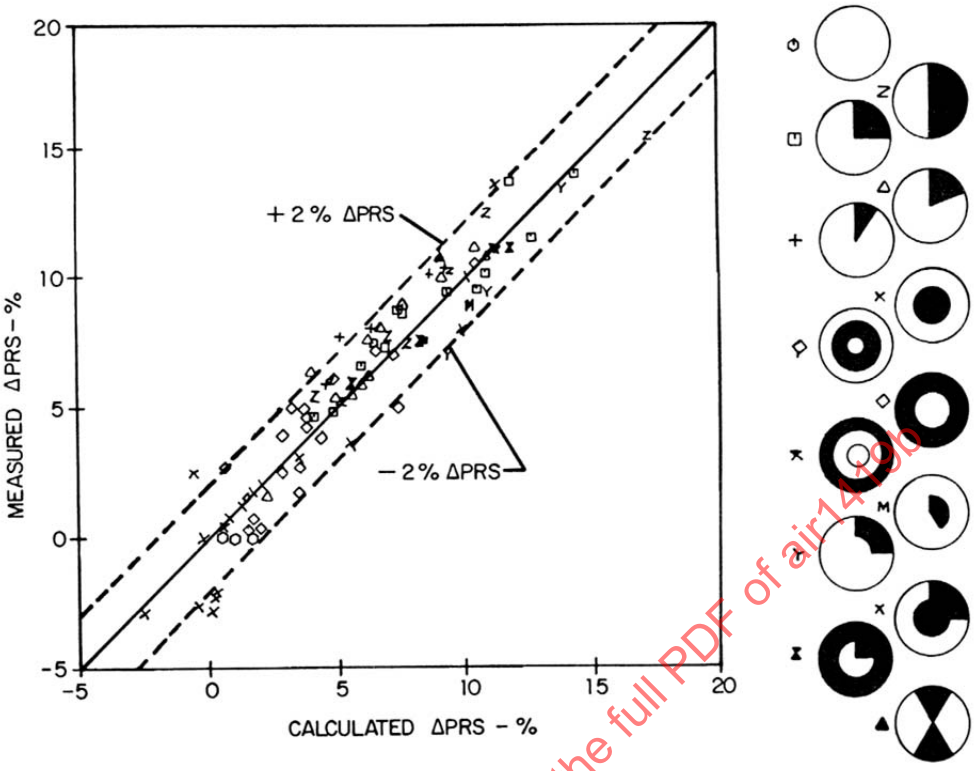

FIGURE 47 - ΔPRS CORRELATION OF J85 DATA

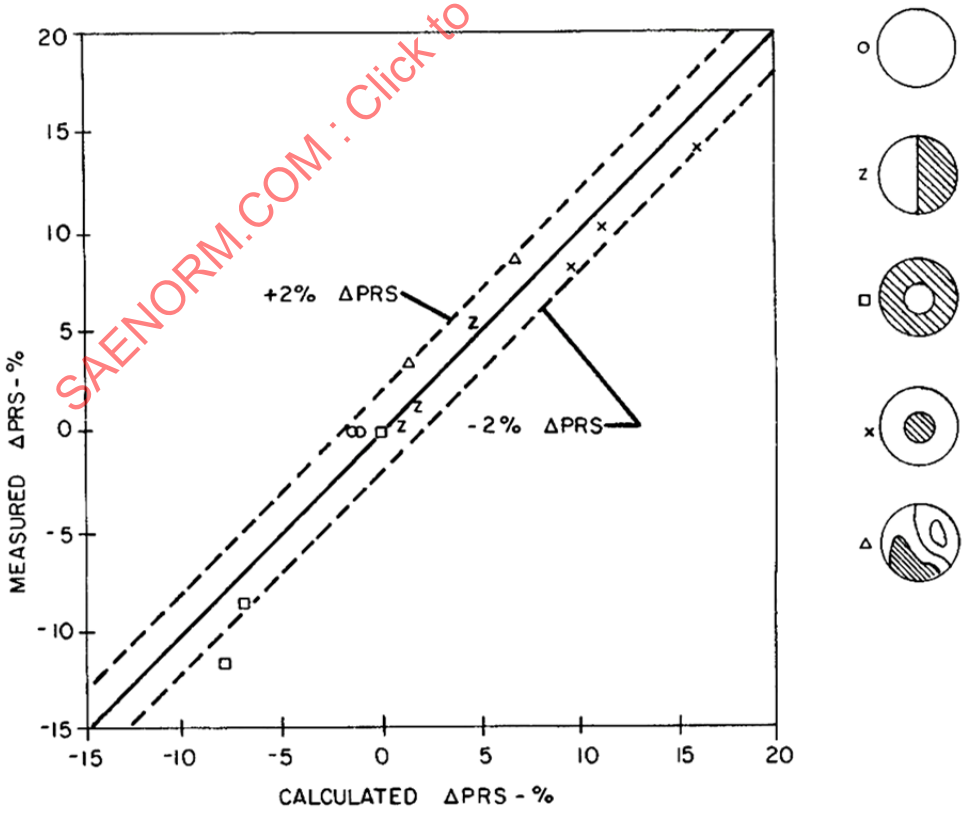

FIGURE 48 - ΔPRS CORRELATION OF A RESEARCH FAN

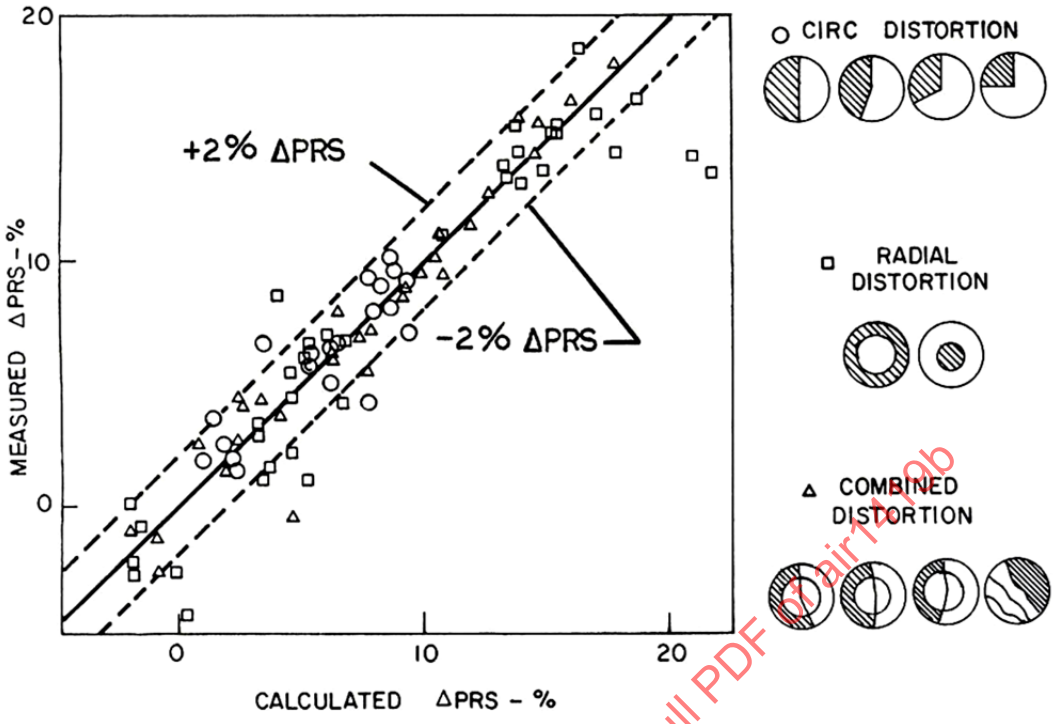

FIGURE 49 - ΔPRS CORRELATION OF F101 FAN

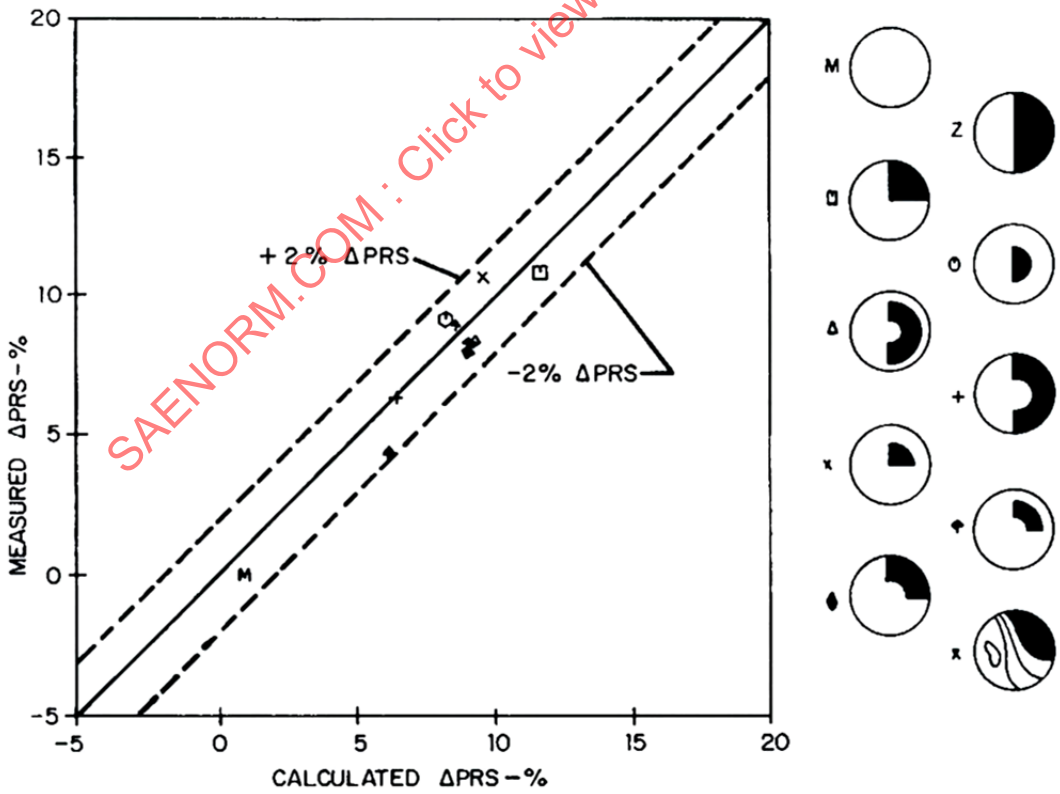

FIGURE 50 - ΔPRS CORRELATION OF J58 COMPRESSOR

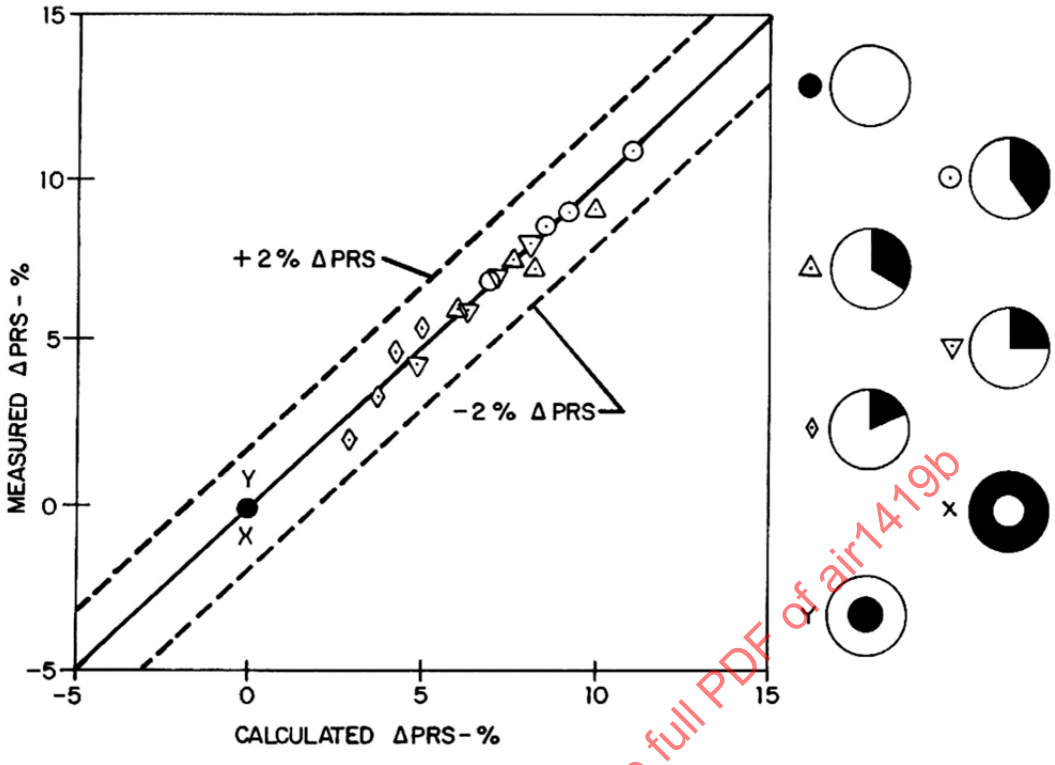

FIGURE 51 - ΔPRS CORRELATION OF A TURBOFAN COMPRESSOR

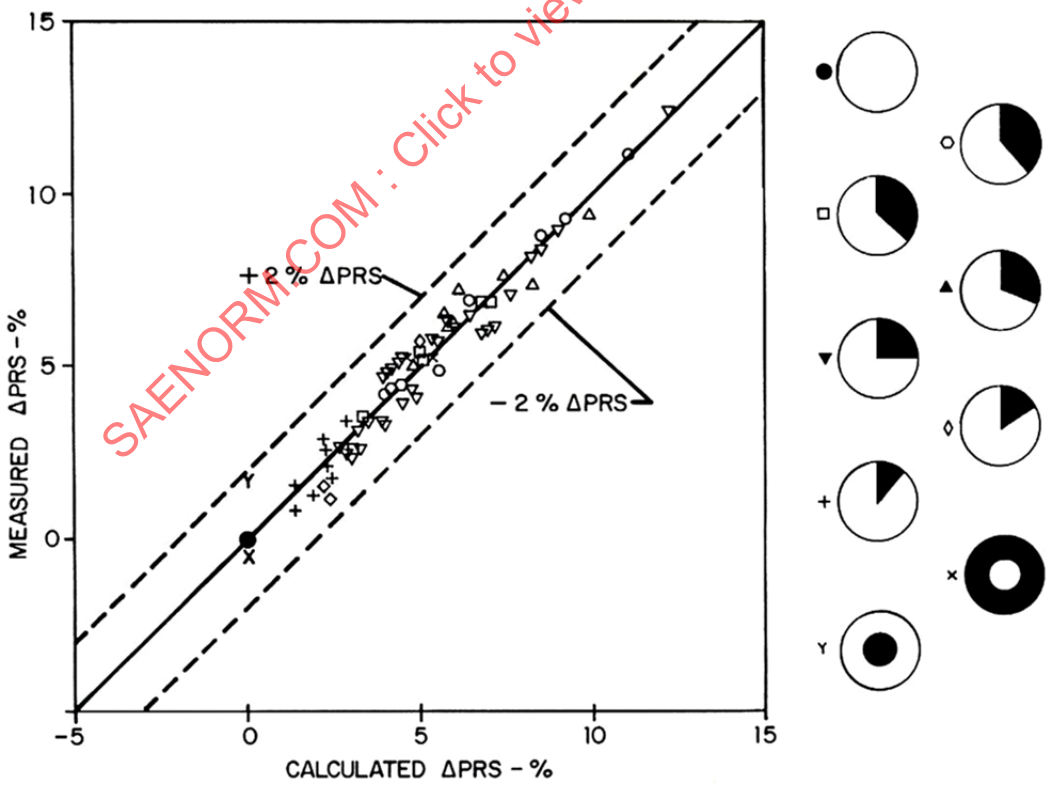

FIGURE 52 - ΔPRS CORRELATION OF A TURBOFAN CORE

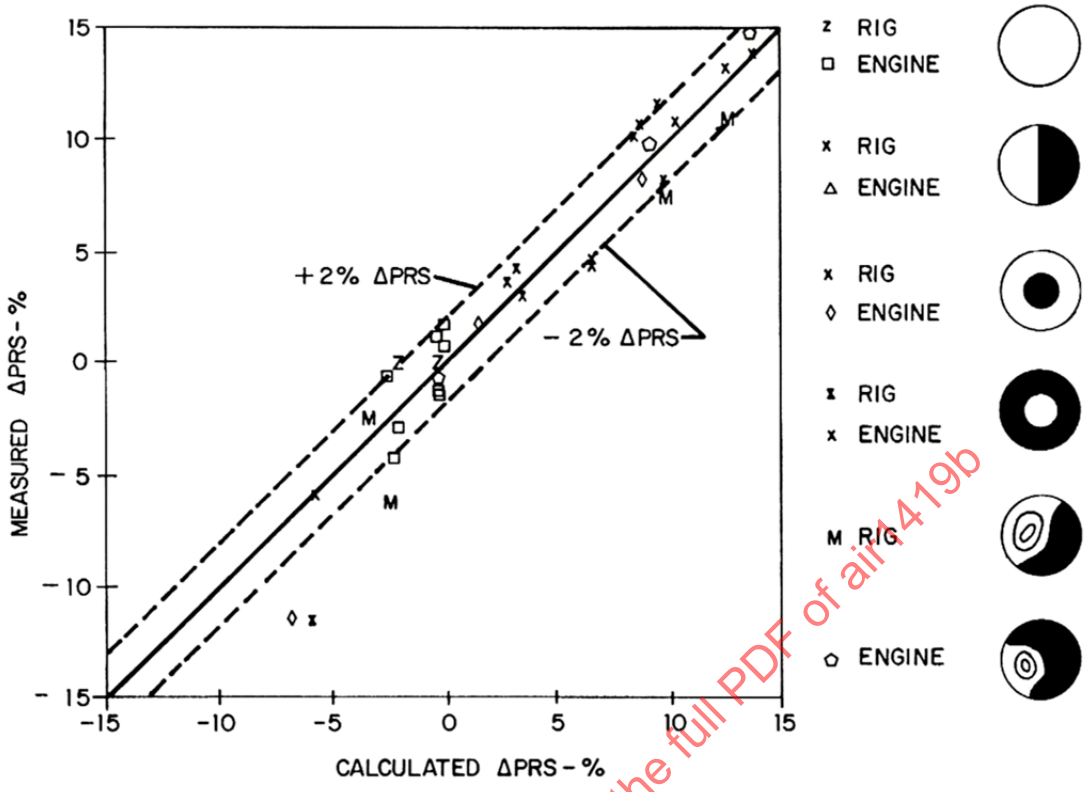

FIGURE 53 - ΔPRS CORRELATION OF F100 FAN

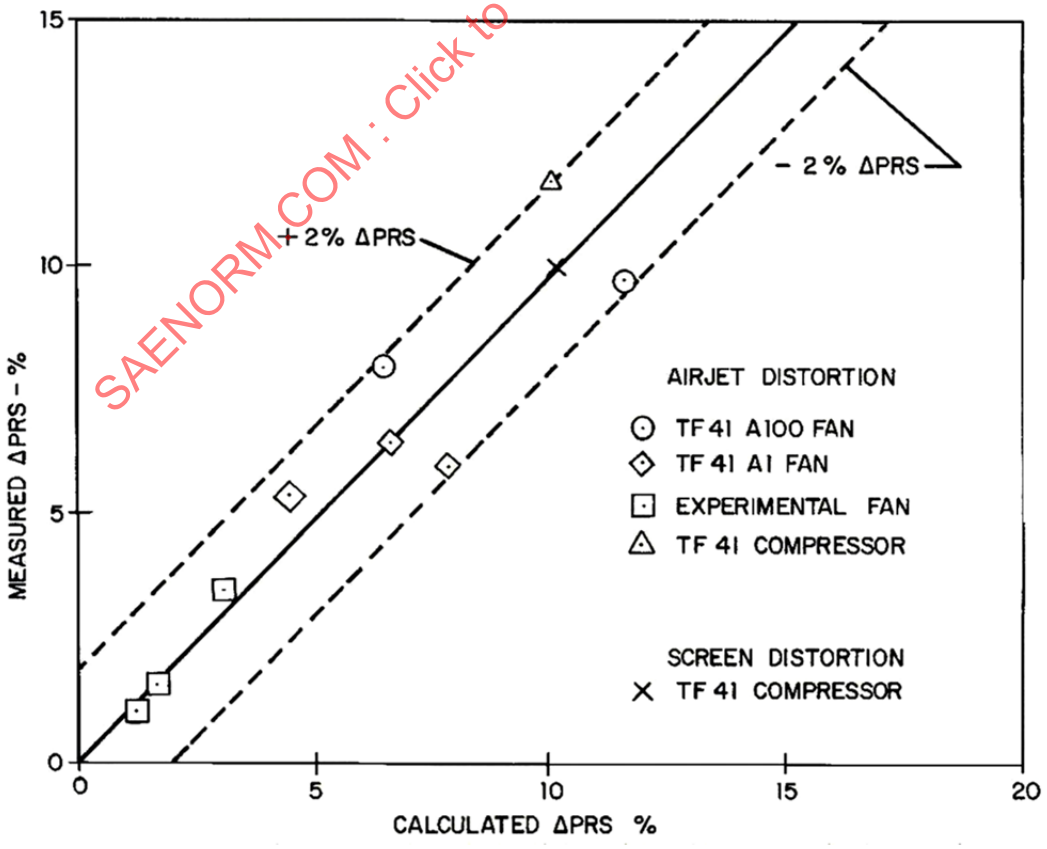

FIGURE 54 - ΔPRS CORRELATION OF TF41 FAN AND COMPRESSOR

4.6.2 Examples of Engine Dependency

If an engine were designed for a specific application, such as an inlet which might have a significant amount of outer-wall boundary layer, then the fan might be designed for a tip-radial profile. In this case, the effect of radial distortion, relative to the clean-inlet stability limit line on which the loss in stability pressure ratio (ΔPRS) is based, might take the form shown in Figure 45. Low values of tip-radial distortion may lead to negative values of ΔPRS and, hence, "gains" in stability margin relative to the clean (uniform) inlet flow condition.

On the other hand, if the fan were designed for a hub-radial profile, as might be produced by a centerbody, then the effect of radial distortion on the fan might take the form shown in Figure 46. In this case, low values of hub-radial distortion will lead to "gains" in stability margin relative to a clean inlet flow.

Because of the choice of types of engine, be it turbojet, augmented turbofan, or non-augmented turbofan and because the fan designer has the choice of designing for a uniform inlet profile or for hub- or tip-radial profiles of varying intensity, it is essentially impossible at this time to develop an inlet flow distortion screening parameter which is universal and quite independent of engine sensitivity parameters. To a lesser extent, the multiple-per-rev (MPR) factor is also an impediment to establishing a universal distortion screening parameter. Multiple-per-rev patterns have a dominant effect upon stress levels, and hence, the pressure ratio at which the "effective" stability limit line may be set. For example, a compression system may have been designed for an application that produces essentially a one-per-rev pattern, but at a subsequent date, it is used in a bifurcated-inlet-duct propulsion system with a two-per-rev pattern. The "effective" stability limit line may have to be reset so that stress limits are not exceeded or the compression component will have to be redesigned. In either case, the sensitivity to distortions of the same level will generally change.

By establishing communication between the airframer and the engine manufacturer sufficiently early in a program, it should be possible to develop meaningful inlet distortion screening parameters which will assure that the airframe manufacturer obtains optimal information from wind-tunnel testing efforts and will be able to provide the engine manufacturer with inlet patterns which can be used to influence compression system design.

The distortion-descriptor elements are independent of compression system characteristics. Since circumferential distortion always causes a loss of stability pressure ratio, minimization of the circumferential distortion intensity element will always be beneficial. Discussions with the engine manufacturer should indicate the most desirable radial profile for the given application, that is, whether a uniform profile or whether a hub, tip or a combination profile is desired and which component of distortion should be minimized.

4.6.3 Inlet Data Screening Techniques

Screening of time-variant inlet data identifies inlet patterns that cause the greatest loss of stability pressure ratio. It follows that screening parameters should be proportional to stability pressure ratio loss, and therefore, the screening parameters which use ARP1420 distortion-descriptors will have a form similar to the basic equation used for calculating ΔPRS.

Screening techniques have been used successfully with many different distortion descriptors. A separate screening parameter is used for each component of the compression system that can initiate loss of stability. Also, separate screening parameters may be used for the hub and tip regions of a fan. Each screening parameter usually will select a different inlet pattern from time-variant inlet data. A stability assessment, which includes all destabilizing influences, is used to select a set of critical patterns and associated operating conditions for use in engine stability verification testing.

If engine stability has been determined to the point where all terms have been defined in the equation used for estimating the loss of stability pressure ratio, then screening can be done on the basis of ΔPRS for each component. It is customary to provide guidelines representing the component distortion tolerance in the form of an allowable ΔPRS. These guidelines can be used to normalize the calculated values of ΔPRS to give the screening parameter shown in Equation 70. This screening parameter is similar to the current screening parameter ID. A value lower than 1.0 indicates that a level of inlet distortion is within the distortion allowance of the component, while a value higher than 1.0 indicates that the inlet distortion is greater than the distortion allowance of the component. In such cases, surge or stall would have a significant probability of occurrence and the stability stack-ups at these conditions would warrant closer scrutiny.

$$SCREENING\ PARAMETER = \frac{\Delta PRS}{Allowable\ \Delta PRS} \quad \text{(Eq. 70)}$$

The radial distortion at the interface plane usually is completely attenuated by the first compressor. Consequently, screening parameters for downstream compressors usually contain only terms that include circumferential distortion. A family of such screening parameters is described by the general Equation 71. The terms for each ring are summed (although not always) over the portion of the interface plane that measures the quality of the air that passes through the downstream compressor. For example, on a particular fan engine with a bypass ratio of one, the screening parameter for the compressor will be summed over the inner two rings of interface instrumentation containing five rings. The extent and multiple-per-revolution functions may be different for each compressor. The engine manufacturer usually can define such functions, based on past experience with similar compressors for use in early screening of inlet data. This form of screening parameter is similar to the existing screening parameters K_θ, KC_2 and DC_θ, insofar as all these parameters include circumferential distortion only and the units are in terms of inlet distortion rather than stability pressure ratio, i.e., the screening parameter is independent of engine sensitivity to inlet distortion. Here again, it is customary to provide guidelines showing the estimated engine distortion tolerance in terms of maximum allowable values of the screening parameter.

$$SCREENING\ PARAMETER = \sum_{i=1}^{R} \left(\frac{\Delta PC}{P}\right)_i f(\theta_i^-)\ f(MPR_i) \quad \text{(Eq. 71)}$$

For compressors that are sensitive to inlet radial distortion as well as circumferential distortion, a screening parameter of the form shown in Equation 72 could be used. If such a screening parameter represents the stability of a fan hub, the terms are summed over rings 1 and 2. If the screening parameter is for the tip of the fan, the summation is over the outer two rings of the interface plane. The term describing circumferential distortion includes extent and multiple-per-revolution elements. The radial term has a superposition factor “b” which describes the ratio of radial distortion sensitivity to circumferential distortion sensitivity. This screening parameter is the equivalent of the existing screening parameter Ka_2. Here again, the engine distortion tolerance can be described in the same units as the screening parameter.

$$SCREENING\ PARAMETER = \sum_{i=R}^{S} \left\{ \left(\frac{\theta_i^-}{MPR_i}\right)^2 \left(\frac{\Delta PC}{P}\right)_i + b\left[\left(\frac{\Delta PR}{P}\right)_i + C_i\right] \right\} \quad \text{(Eq. 72)}$$

The examples of screening parameters shown in Equations 70, 71, and 72 look different because they are tailored to different requirements. However:

a. They all use ARP1420 distortion-descriptor elements combined in the same manner as in the equation for calculating stability pressure ratio loss.

b. They all can be used for comparing inlet distortion to engine distortion tolerance.

Current practice is to calculate the distortion screening parameters in near-real time from the digitally acquired data and to identify the peak values. This procedure for high speed screening of inlet data is discussed in 8.4.1.

4.6.4 Inlet Data Filtering (Averaging)

Central to the issue of selecting dynamic inlet patterns for replication by screens, and thereby validating adequate engine distortion allowance using steady-state distortion patterns, is the thesis that a low total-pressure region must last long enough to cause a loss of stability pressure ratio. Therefore, by low-pass filtering analog probe data (or performing the equivalent running average on digitized probe data) in conjunction with the use of the engine manufacturer’s distortion computation algorithm, a distortion pattern may be selected for replication by a steady-flow distortion screen during engine testing.

The appropriate averaging time (Reference 2.2.3) can be selected by running an engine in a controlled dynamic-distortion environment such as that produced by a random-frequency generator or a turbulator. The loss of stability pressure ratio data are correlated versus averaging time using screen-determined distortion sensitivities to establish the filter cutoff frequency (averaging time) which produces the minimum difference between the measured and calculated (using the largest peak distortion just prior to instability) losses of stability pressure ratio.

It is important to note the relationship between “the steady-state inlet distortion level” associated with dynamic distortion levels and the steady screen-produced distortion which replicates the maximum dynamic distortion pattern. The steady screen-produced distortion will equal the maximum dynamic distortion level while the steady-state inlet distortion will be less, sometimes by as much as a factor of two. An example of the correlation between steady-state screen distortion and dynamic-distortion-induced instabilities (from three different sources) is shown in Figure 55, taken from Reference 2.2.4. It can be seen that when total-pressure data are properly filtered to remove high frequency data that do not contribute to loss in stability pressure ratio, dynamic distortion will produce the same level of stability-pressure-ratio loss as steady-state distortion of an equivalent magnitude.

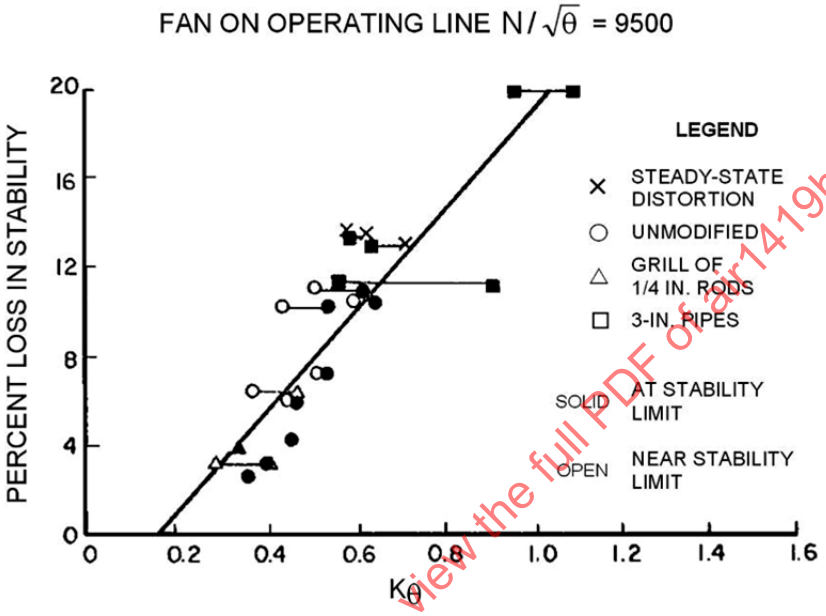

FIGURE 55 - STABILITY LIMIT LINE LOSS VERSUS INSTANTANEOUS SPATIAL DISTORTION

4.7 Independent Control of Variable Geometry

When compressor variable geometry is scheduled as a function of a defined engine operating parameter such as corrected rotor speed, stability margin can be defined by the ARP1420 method using compressor maps representing variable geometry in the scheduled position. Errors from the scheduled geometry setting can be accounted for by utilizing terms describing the effects of these errors on the stability limit line and operating airflow. Engines with fan geometry under the direct control of the pilot have been proposed for some applications. In such cases, the variable geometry setting is an independent variable adding a new dimension to compressor maps, stability margin definition, and stability accounting.

5. STABILITY ASSESSMENT

The overall purpose of a propulsion system stability assessment is to assure that the design meets the aircraft operational goals. It is a vital part of the propulsion system design and development process, providing the inlet and engine designers with data for defining operational capability and identifying any configuration changes needed, and the program manager with material for allocating development time and resources. To be effective, the stability assessment procedure must be timely, visible, and continuous from conceptual studies to operational service.

Stability assessment involves determining the inlet distortion and the baseline (essentially clean flow) engine stability, and accounting for the destabilizing influence of the AIP distortion as well as other engine operating and installation factors. AIP flow distortion may not be restricted solely to time-variant, spatial, total-pressure distortion. It is important at the outset of any stability assessment to identify when the AIP distortion can be accounted adequately in terms of total pressure alone.

The assessment of the influence of total-pressure distortion on engine stability forms part of a total procedure necessary to determine installed engine stability and stability margins. An assessment of all destabilizing effects must be made so that the contribution made by inlet distortion can be put in perspective. Stability assessments take various forms and are updated throughout the propulsion system design and development cycle. The methodology described in Sections 3 and 4 addresses the “classic” turbomachinery aerodynamic instability whereby constituent compressors stall and reduce engine airflow, to produce rotating stall, engine surge (oscillating reverse flow), or combinations of these post-stall instabilities. Other important aspects of engine aerodynamic stability include control system effects and afterburner stability, both of which may be affected by AIP distortion. Engine distortion tolerance depends on the stability margin allocated and available when other destabilizing factors, operating on compression component operating lines and stability limit lines, are taken into account.

This section discusses the impact of AIP total-pressure distortion on engine stability in the broader context of an overall stability assessment.

5.1 Stability Assessment Philosophy

The assessment method depends upon the anticipated severity of the stability problem (for example, new engine/new installation, established engine/new application, the input information available, and the degree of complexity and expense of the assessment). Distortion stability assessments are unique in that they are complex and not amenable to standardized “cookbook” treatment. As stated previously, the scope of the assessment depends on the status of the propulsion system development which dictates the quantity and accuracy of the component test data on which the assessment is based. Assessments will emphasize different facts: an assessment supporting the engine compression system designer’s needs might emphasize stability margin sensitivity to blade shape, spool matching, and flow-path configurational changes for an anticipated distortion pattern. An assessment supporting the inlet designer’s needs may stress the sensitivity of the engine to the various elements in the AIP distortion descriptor for various inlet configurations. The assessment may be largely empirical, i.e., engine tolerance to distortion may be derived through engine tests with suitable instrumentation, such as described in Sections 7 and 8, rather than being synthesized through the use of component test data and suitable engine computer simulations.

Although some features of distortion stability assessments make each assessment unique, assessment outputs are similar in that they provide estimates of stability margin utilization at critical points in the flight envelope and engine tolerance to distortion, and identify the margin required to achieve acceptable AIP distortion levels. All destabilizing effects must be considered to conduct a meaningful stability assessment. Destabilizing effects which influence both the component compressor operating lines and compressor stability limit lines have been compiled and are presented in Table 5. These factors may be random and/or non-random. Once numerical values for each significant factor have been determined, the stability assessment may proceed. Some of these factors are illustrated in schematic form in Figure 56.

The more significant operating line assessment factors for a given engine build are:

a. Deterioration

b. Bleed

c. Horsepower extraction

d. Reynolds number effects

e. Steady-state inlet total-pressure distortion and temperature distortion

f. PLA transient (including augmentor operation)

g. Variable geometry control tolerance and transients

h. Gas-path control system sensor(s) in distorted regions

The more significant stability limit line assessment factors are:

a. Deterioration

b. Reynolds number effects

c. Time-variant inlet-total-pressure and temperature distortion

d. Variable geometry tolerances and transients

TABLE 5 - STABILITY ASSESSMENT FACTORS

FACTOR	OPERATING LINE	STABILITY LINE
INLET DISTORTION:		
a. STEADY-STATE TOTAL-PRESSURE DISTORTION	X	X
b. TEMPERATURE DISTORTION	X	X
c. SWIRL DISTORTION	X	X
d. MAXIMUM INSTANTANEOUS TOTAL-PRESSURE DISTORTION		X
RAM RECOVERY	X	
HORSEPOWER EXTRACTION	X	
PLA TRANSIENT	X	
ENGINE DETERIORATION	X	X
FUEL CONTROL DETERIORATION	X	
DETERIORATION EFFECT ON TRANSIENT FUEL FLOW RATE	X	
FUEL CONTROL TOLERANCES	X	
VARIABLE GEOMETRY CONTROL TOLERANCES	X	X
ENGINE-TO-ENGINE VARIATION	X	X
ENGINE VARIATION EFFECT ON TRANSIENT FUEL FLOW RATE	X	
COMPRESSOR BLEED	X	X
REYNOLDS NUMBER EFFECTS	X	X
NOZZLE MATCHING EFFECTS	X	
HUMIDITY	X	X
CONTROL MODE	X	
BACK PRESSURE DISTORTION	X	X
COMPRESSOR INTERACTION EFFECTS	X	X
TRANSIENT VARIABLE GEOMETRY EFFECTS	X	X
PLA TRANSIENT HEAT TRANSFER	X	X

Steady-state effects of bleed, horsepower extraction and Reynolds number are contained within the engine digital simulations used to define the operating pressure ratio of the compression component at the selected operating condition.

Early stability assessment procedures used a direct algebraic summation of the worst possible combination of destabilizing factors to arrive at the required stability margin. As the list of identified destabilizing factors grew longer, the resulting demand on engine stability margin also grew, compromising performance and weight, and it became recognized that the probability of all worst cases occurring simultaneously was low. It has been established that some destabilizing factors should be summed statistically to establish more realistic stability-performance-weight trade-offs. This approach is justified in that the Root-Sum-Square (RSS) combination of the random effects retains the overall probability of the individual effects. One approach to statistical assessment is shown in Reference 2.1.1.3.

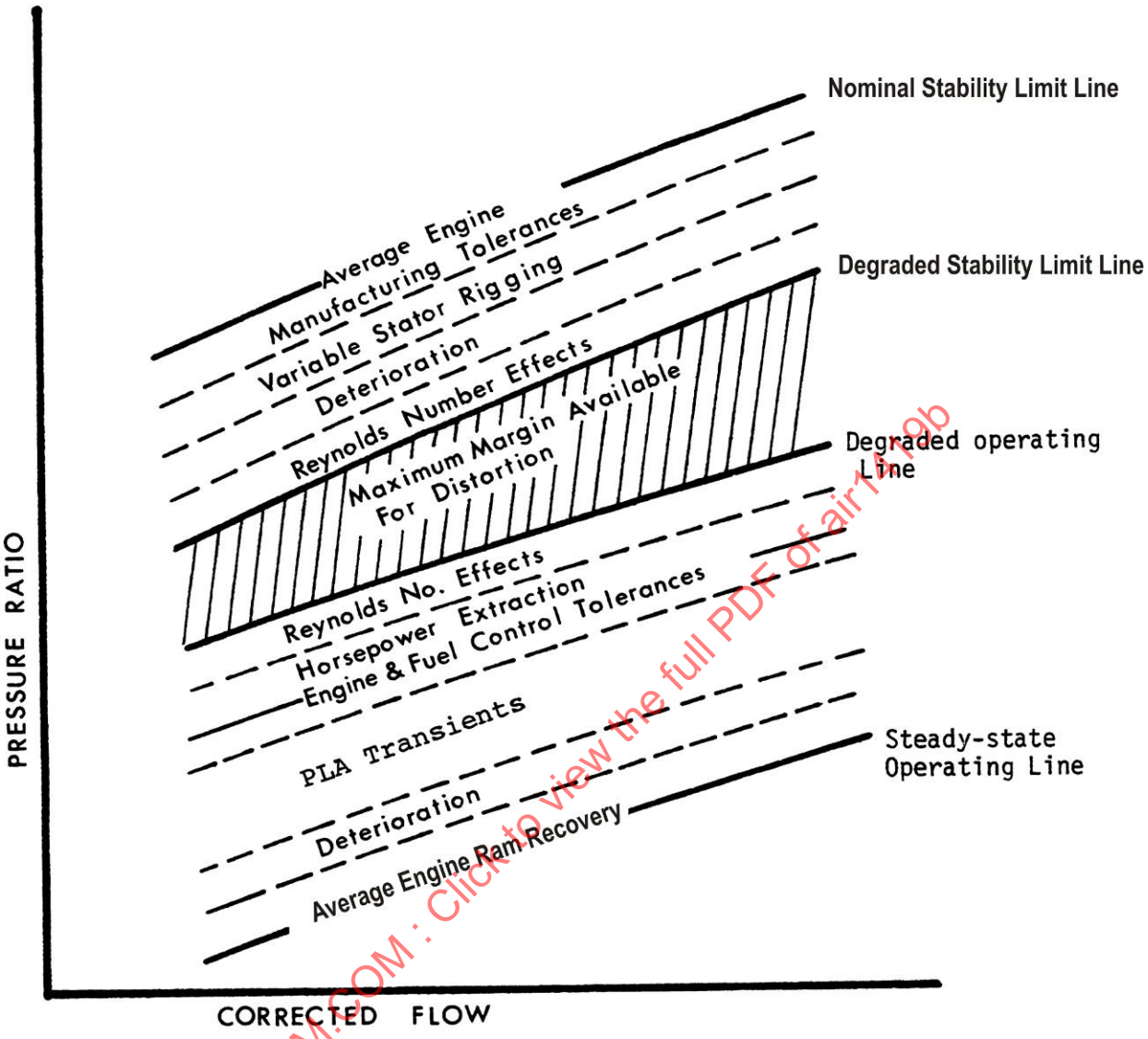

FIGURE 56 - TYPICAL COMPRESSOR DESTABILIZING FACTORS

For an individual compression component, the net stability margin is defined by the relation:

$$SM_{NET} = SM_{Baseline} - [(\Delta SM)_{NR} + (\Delta SM)_R] \quad \text{(Eq. 73)}$$

where:

$\Delta SM_{NR} = \sum_{i=1}^{n} (\Delta SM)_i$ = Total algebraic stability margin loss due to non-random factors

$\Delta SM_R = \pm \sqrt{\sum_{j=1}^{m} (\Delta SM)_j^2}$ = Total root-sum-square stability margin loss due to random factors (ΔSM_{RSS})

The loss in stability margin due to distortion is computed using the total-pressure distortion descriptors discussed in Section 4. Other destabilizing effects are evaluated from engine/control data obtained through testing and analysis. All destabilizing effects are combined to determine the net stability margin.

The limitations of current stability assessment procedures should be recognized in applying assessment results. Errors associated with total-pressure distortion assessment can occur because (1) the value of the distortion descriptor varies with the amount and accuracy of test data, (2) other AIP flow distortions, such as in-phase oscillations, vortex ingestion and swirl may exist and not be accounted for in the assessment, and (3) summations of individual effects may result in an oversimplification of the actual process.

5.2 Stability Assessment Procedure

The stability assessment process, Figure 57, is independent of the complexity of a particular assessment. The results identify the residual stability margins for the compression system components examined at the critical steady or transient operating points, the types and levels of distortion that are most likely to cause loss of engine stability, and the need for additional engineering activity. The assessment procedure depicted in the figure is an integration of background experience, test-derived information, and synthesis techniques concerned with accounting inlet flow distortion effects and other destabilizing factors. The procedure produces information that is analyzed either to forecast or evaluate the stability status of a propulsion system at critical flight operating points.

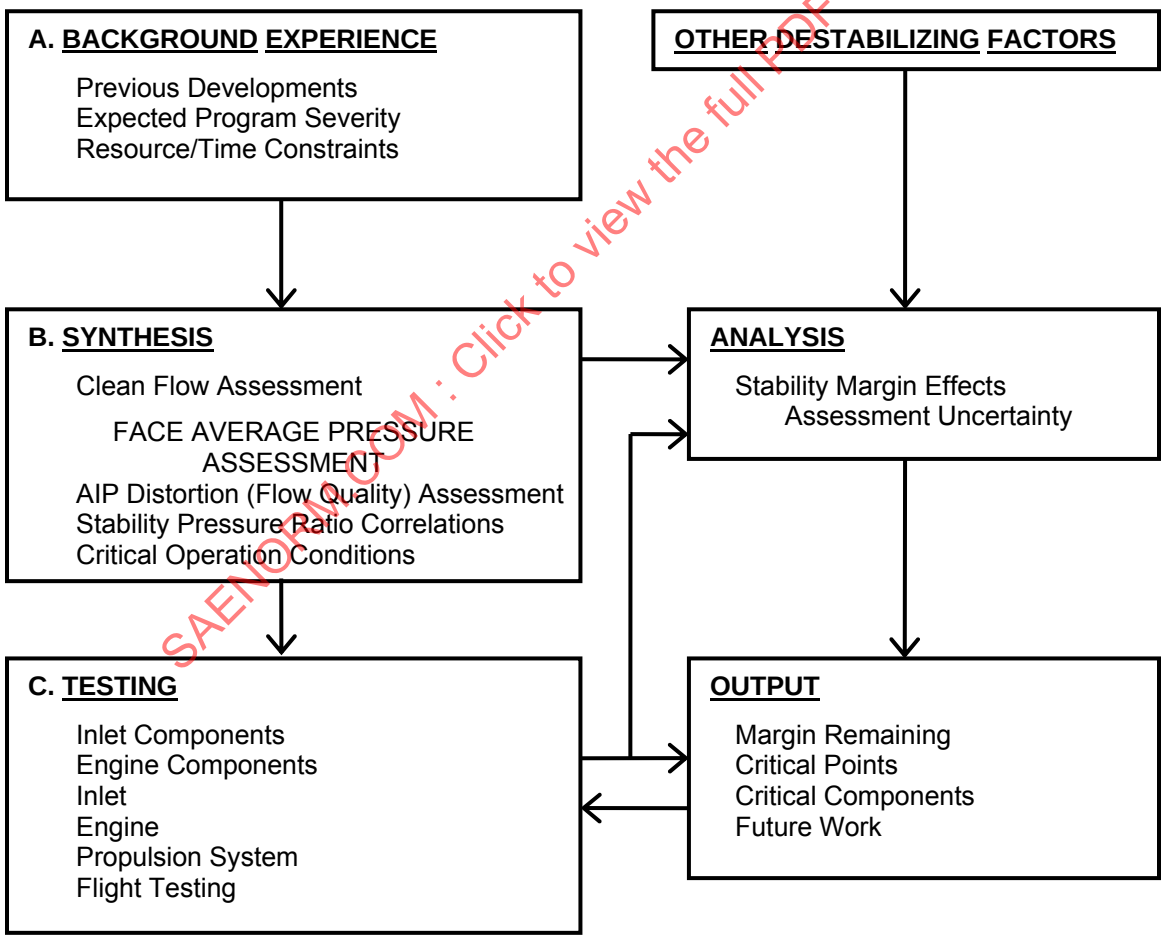

FIGURE 57 - STABILITY ASSESSMENT PROCESS

Blocks A, B, and C in Figure 57 provide the input data necessary to conduct the distortion assessment. Synthesis refers to the process of developing estimates of the effects of destabilizing factors through analysis of component test data and analytical predictions. In early development the synthesized items in Block B are usually based primarily on prior experience and analytical estimates. As development progresses, the synthesis activity relies more heavily on the expanding test data base, permitting the analysis activities to produce more accurate indications of stability margin. As development nears the qualification phase, testing objectives become more oriented toward stability evaluation, permitting the assessments to become, correspondingly, more oriented toward validating previous forecasts.

An example of the output section of the stability assessment process is presented for a fan/compressor propulsion system. In this example the propulsion system is assumed to be operating at an altitude flight condition where the inlet distortion is defined by the information contained in Figure 22.

An illustrative estimate for a fan operating at 98% inlet corrected airflow is presented in Figure 58. The baseline operating pressure ratio, PRO, is 3.0 and the baseline stability pressure ratio PR1 is 3.75. The baseline SM is:

$$SM_{Baseline} = \frac{PR1 - PRO}{PRO} \times 100 = \frac{3.75 - 3.0}{3.0} \times 100 = 25 \quad \text{(Eq. 74)}$$

The loss in fan stability pressure ratio due to inlet total-pressure distortion can be calculated using an expansion of Equation 21 in the following form:

$$\Delta PRS = b_P \, EX_P \left[KC \left(\frac{\Delta PC}{P} \right)_{max} + CC_P \right] + \left[KR_P \left(\frac{\Delta PR}{P} \right)_{max} + CR_P \right] \quad \text{(Eq. 75)}$$

This equation is similar to Equation 33 for a 1/rev pattern since MPR = 1.

The maximum circumferential distortion is the average of any two adjacent rings:

$$\left(\frac{\Delta PC}{P} \right)_{max} = \frac{1}{2} \left[\left(\frac{\Delta PC}{P} \right)_2 + \left(\frac{\Delta PC}{P} \right)_3 \right] = 0.0599 \quad \text{(Eq. 76)}$$

The circumferential extent is equal to the average of the extents of the two adjacent rings used to calculate the circumferential distortion and is equal to 177.6 degrees.

The maximum radial distortion occurs in the tip (ring 5):

$$\left(\frac{\Delta PR}{P} \right)_{max} = 0.0678 \quad \text{(Eq. 77)}$$

The value and source of the fan coefficients used in the calculation are given in Table 6. These coefficients apply at 95% corrected fan speed which corresponds to the matched-inlet corrected airflow of 98%.

$$\begin{aligned} \Delta PRS &= \{(1.0)(0.995)[0.46(0.0599) + 0] + [0.74(0.0678 - 0.038)]\} \times (100) \\ &= 4.9\% \end{aligned} \quad \text{(Eq. 78)}$$

The loss in stability margin due to inlet total-pressure distortion and the other assumed stability margin utilizations for this example are presented in Table 7.

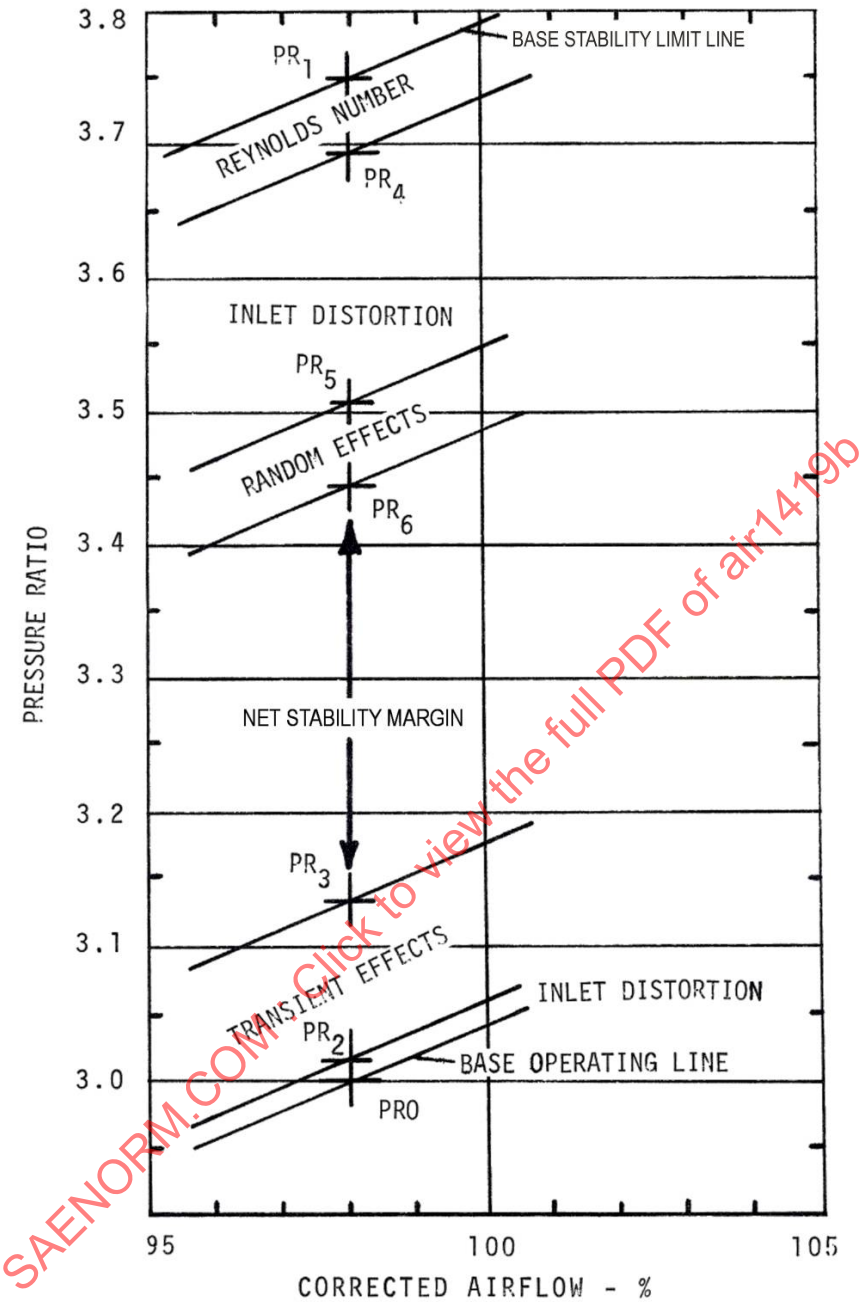

FIGURE 58 - FAN STABILITY ASSESSMENT EXAMPLE

TABLE 6 - FAN STABILITY-PRESSURE-RATIO LOSS COEFFICIENTS

COEFFICIENT	VALUE	SOURCE
KC_P	0.46	Figure 34
CC_P	0	since ΔPRS curves pass through origin of Figure 33
KR_T	0.74	Figures 37 and 38
CR_T	-0.038	Figures 37 and 38
B_P	1.0	Figure 39
EX_P	0.995	Figure 40

For the purpose of determining net or residual stability margin, it is assumed that the total random effects may be used to lower the stability limit line or raise the operating line. For this example, it is assumed that the stability limit line is lowered so that:

$$PR6 = PR5 - \frac{\Delta SM}{100} \times PRO = 3.507 - 0.0208 \times 3.0 = 3.44 \quad \text{(Eq. 79)}$$

The net or residual stability margin is then given by:

$$SM_{Net} = \frac{(PR6 - PR3)}{PRO} \times 100 = 10.3\% \quad \text{(Eq. 80)}$$

TABLE 7 - FAN STABILITY MARGIN ASSESSMENT

Destabilizing Factor	Assumed Cause	Pressure Ratio (PR) and Stability Margin Loss (ΔSM)
Non-Random (NR)	Operating Line Shift Due to AIP Total Pressure Distortion	$PR2 = 3.015$ $\Delta SM = \frac{PR2 - PRO}{PRO} \times 100$ $= 0.5$
	Operating Line Shift Due to 4% ΔP/P Augmentor Spike	$\Delta SM = 4.0$ $PR3 = PR2 + \frac{\Delta SM}{100} \times PRO$ $= 3.015 + 0.04 \times 3.0$ $= 3.135$
	Stability Line Loss Due to Reynolds Number, ΔPRS = 1.5	$PR4 = PR1 - \frac{\Delta PRS}{100} \times PR1$ $= 3.75 - 0.0015 \times 3.75$ $= 3.694$ $\Delta SM = \frac{PR1 - PR4}{PRO} \times 100$ $= 1.87$
	Stability Line Loss Due to Time-Variant AIP Distortion, ΔPRS = 5.0	$PR5 = PR4 - \frac{\Delta PRS}{100} \times PR1$ $= 3.694 - 0.05 \times 3.75$ $= 3.507$ $\Delta SM = \frac{PR4 - PR5}{PRO} \times 100$ $= 6.25$
		$TOTAL\ \Delta SM_{NR} = 0.5 + 4.0 + 1.87 + 6.25$ $= 12.62$
Random (R)	Operating Line Effects: - Variable Geometry Control Tolerances - Engine-to-Engine Variations	ΔSM=±1.1 ΔSM=±1.2
	Stability Line Effects of Engine-to-Engine Variations	ΔSM=±1.3
		$TOTAL\ \Delta SM_R = \Delta SM_{RSS}$ $= \pm\sqrt{(1.1)^2 + (1.2)^2 + (1.3)^2}$ $= \pm 2.08$

A similar example can be constructed for the compressor, where the effects of compressor inlet-total-pressure and total-temperature distortion need to be assessed taking into consideration the fan distortion transfer characteristics at fixed-throttle or transiently matched conditions. It is generally accepted that the data obtained from the two inner instrumentation rings, which are located in the core stream, are sufficient for developing core distortion sensitivities and distortion transfer correlations.

The results of an example calculation, illustrating the assumptions made, in a format suitable for comparison with the fan stability assessment are presented in Table 8. In this example, the residual fan stability margin is 10.30%, and the residual compressor stability margin is 3.27%. The critical component would appear to be the compressor. However, to proceed further, it may be necessary to calculate the probability of occurrence of an instability. This is discussed in Reference 2.1.1.3. At a given operating point, the critical component is that component having the highest probability of instability. It is important to note that the critical component at one flight, inlet, and engine operating condition need not be the critical component at other conditions. Because of this fact, stability assessments have to be conducted at several points throughout the operational flight envelope.

TABLE 8 - TYPICAL STABILITY MARGIN ASSESSMENT

DESTABILIZING EFFECTS	COMPONENT			
	FAN		COMPRESSOR	
OPERATING LINE	NON-RANDOM	RANDOM	NON-RANDOM	RANDOM
Inlet Distortion	0.5	-	0.7	-
PLA Transient	4.0	-	6.0	-
Variable Geometry Control Tolerances	-	±1.1	-	-
Fuel Control Tolerances	-	-	-	±1.15
Engine to Engine Variation	-	±1.2	-	±1.25
STABILITY LIMIT LINE				
Reynolds Number	1.87	-	0.36	-
Inlet Distortion	6.25	-	7.50	-
Engine to Engine Variation		±1.3	-	±1.35
TOTAL	12.62	±2.083	14.56	±2.169
BASE STABILITY MARGIN	25.0		20.0	
NET STABILITY MARGIN	10.30		3.27	

5.3 Distortion Stability Assessment

The above examples illustrate the impact of inlet-total-pressure distortion on the fan and compressor stability. The loss in fan stability margin due to AIP total-pressure distortion represented approximately 25% of the baseline fan stability margin, and the loss in compressor stability margin, due to the combined effects of total-pressure and total-temperature distortion at compressor entry, accounted for approximately 37.5% of the baseline compressor stability margin.

The distortion stability assessment procedure is shown graphically in Figure 59. As previously stated, the procedure is iterative and the level of confidence in the assessment increases through the propulsion system development process.

Section 4 describes the methodology involved in establishing ΔPRS and distortion sensitivities through correlations of compressor data. Typical data from which correlations are derived are presented in Figures 25 through 46.

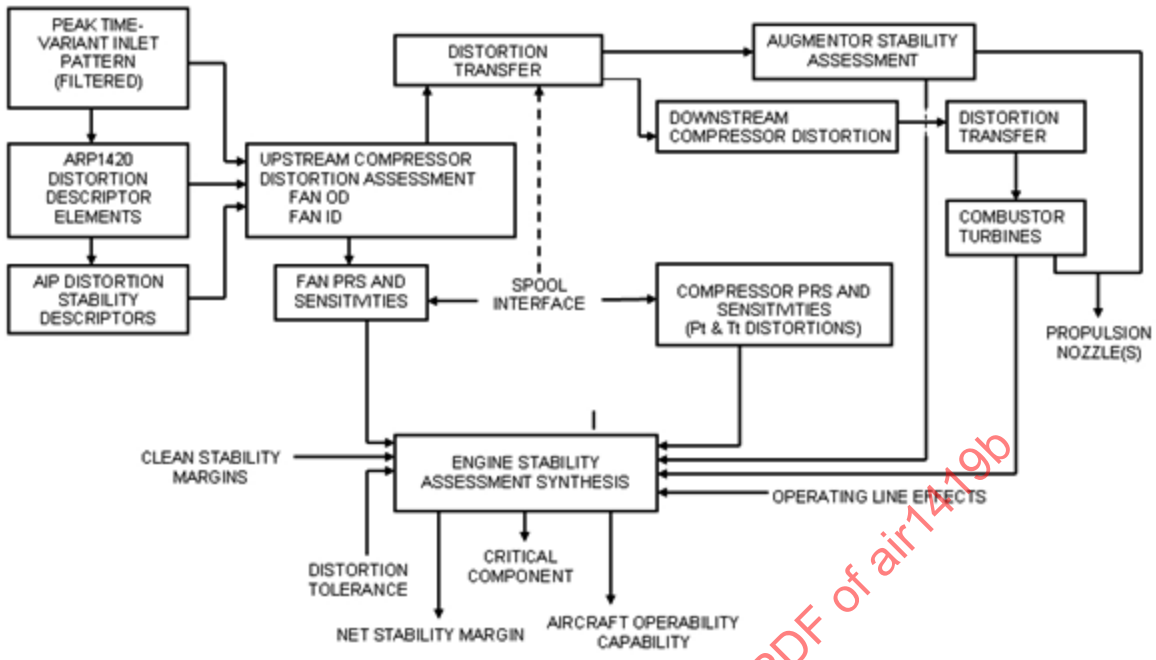

FIGURE 59 - DISTORTION STABILITY ASSESSMENT

5.3.1 Circumferential Distortion

The effect on the stability limit line of one-per-rev circumferential distortions (MPR = 1.0) of varying extents from rig tests of a three-stage compressor with distortion screens is shown in Figure 60. Similar examples, derived from engine tests, are shown in Figures 61 through 64 for the J85-GE-13 engine. Results for a two-per-rev circumferential distortion can be seen in Figure 65 (Reference 2.2.5). Each test result provides distortion response data. An example for one-per-rev circumferential distortions appears in Figure 66. The experimentally established ΔPRS are plotted here in terms of a distortion descriptor. The descriptor is represented by the product of the ARP1420 circumferential extent and intensity elements together with a correlation coefficient which varies with corrected airflow. The distortion descriptor is a special form of Equation 72, applicable to this compressor. The slopes of the correlation lines of Figure 66 represent the sensitivity of the compressor expressed in terms of the descriptor, i.e., screening parameter level as discussed in Section 4. Thus at 92% design airflow:

$$\frac{\Delta PRS}{100} = 1.54 \times Screening\ Parameter \qquad \text{(Eq. 81)}$$

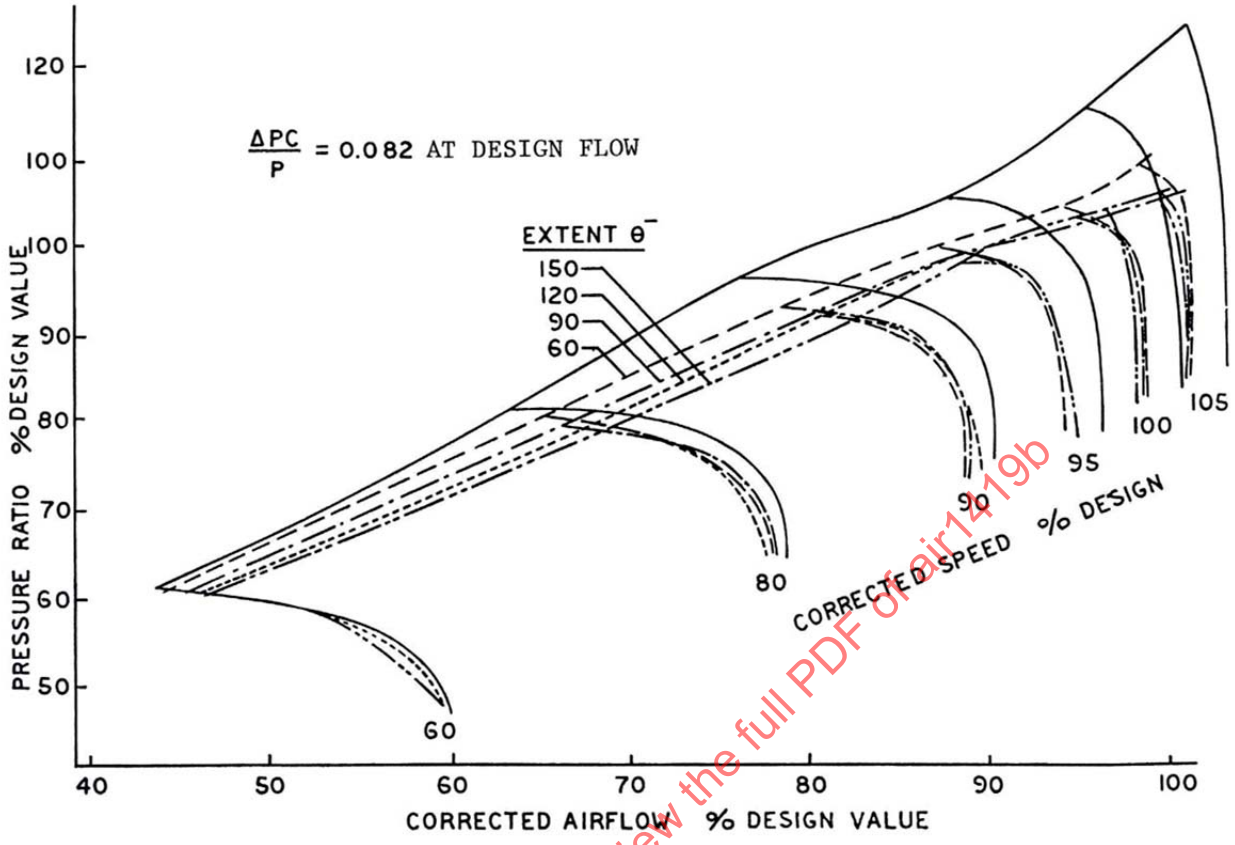

FIGURE 60 - EXAMPLE OF ONE-PER-REV SQUARE WAVE CIRCUMFERENTIAL TOTAL-PRESSURE DISTORTION

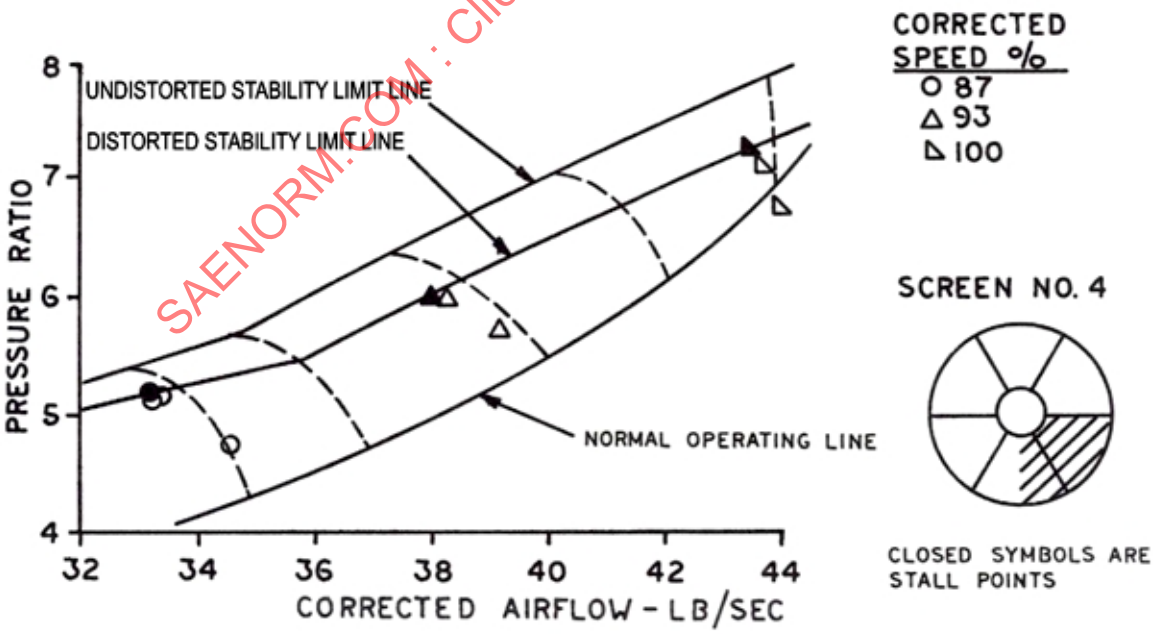

FIGURE 61 - EXAMPLE OF ONE-PER-REV CIRCUMFERENTIAL TOTAL-PRESSURE DISTORTION, 90-DEGREE EXTENT

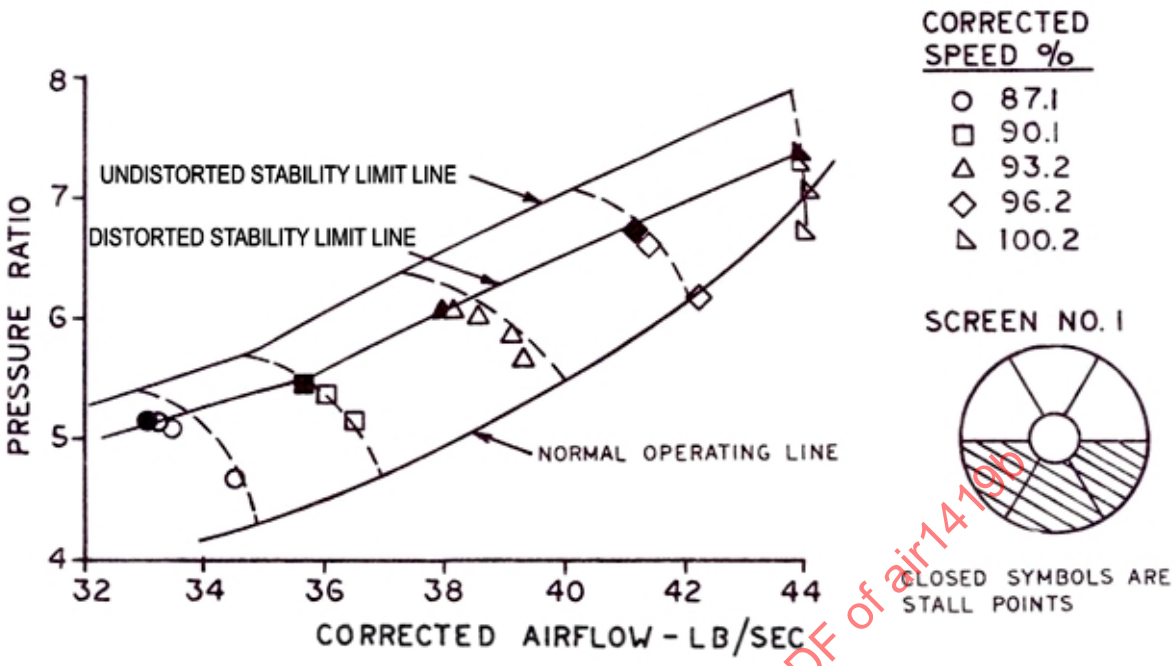

FIGURE 62 - EXAMPLE OF ONE-PER-REV CIRCUMFERENTIAL TOTAL-PRESSURE DISTORTION, 180-DEGREE EXTENT

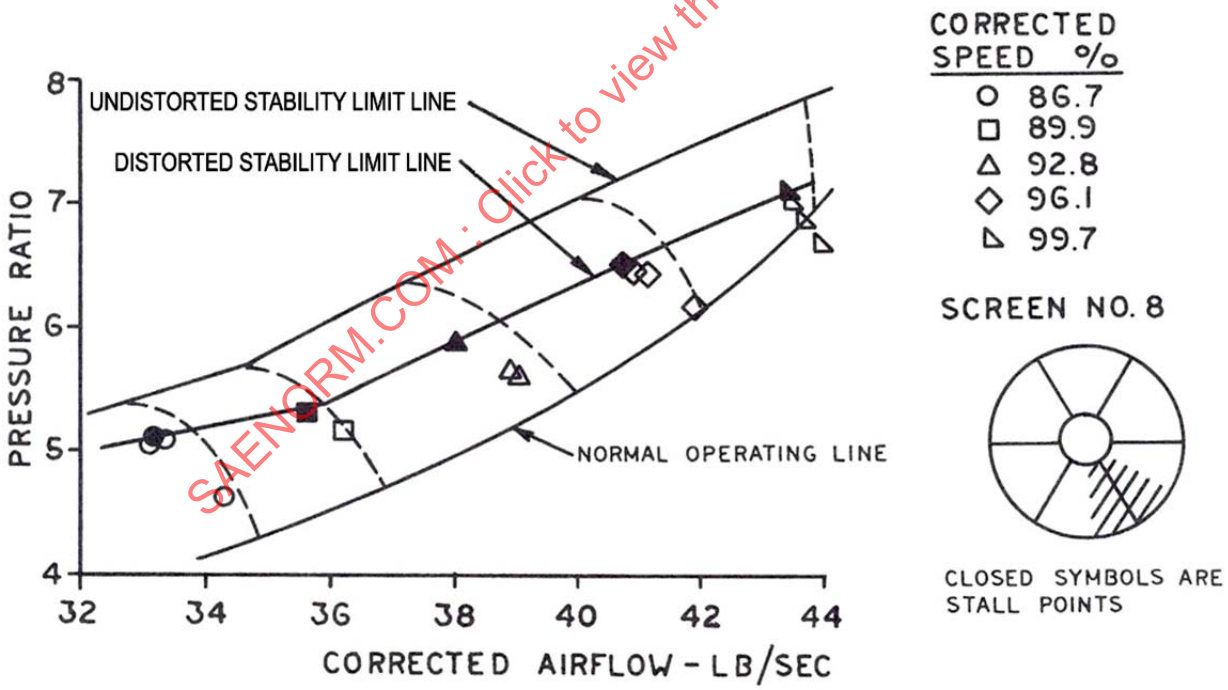

FIGURE 63 - EXAMPLE OF ONE-PER-REV CIRCUMFERENTIAL TOTAL-PRESSURE DISTORTION, 45-DEGREE EXTENT

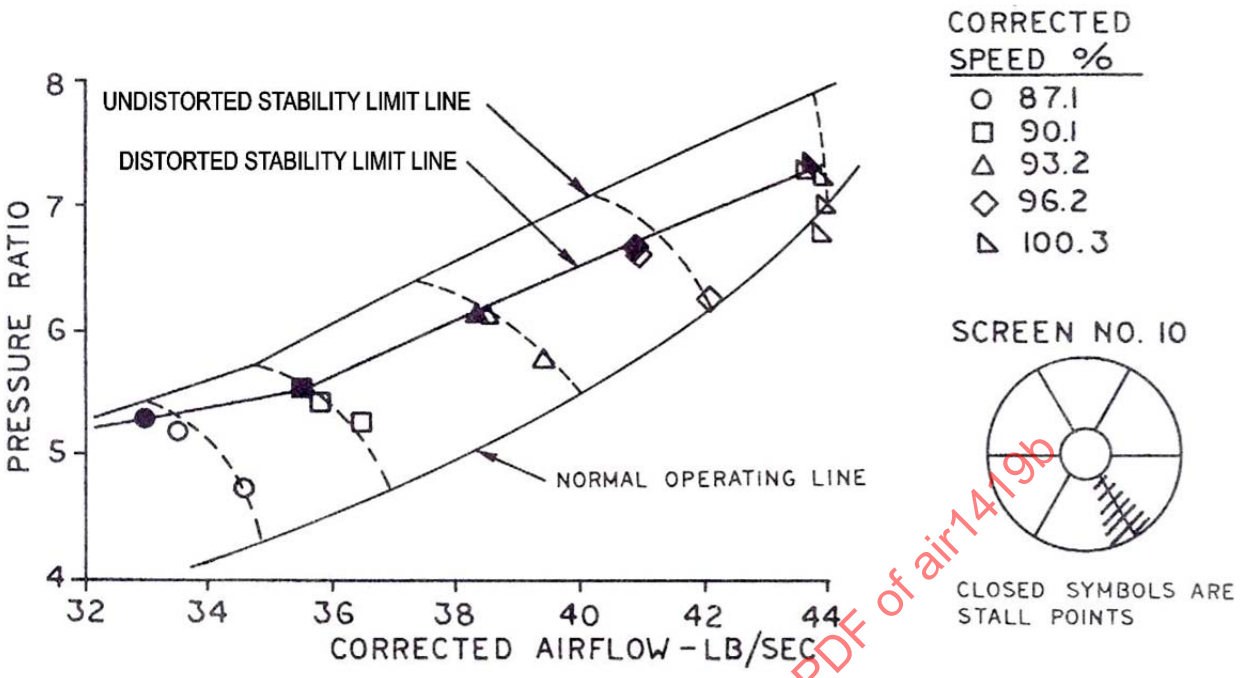

FIGURE 64 - EXAMPLE OF ONE-PER-REV CIRCUMFERENTIAL TOTAL-PRESSURE DISTORTION, 22-DEGREE EXTENT

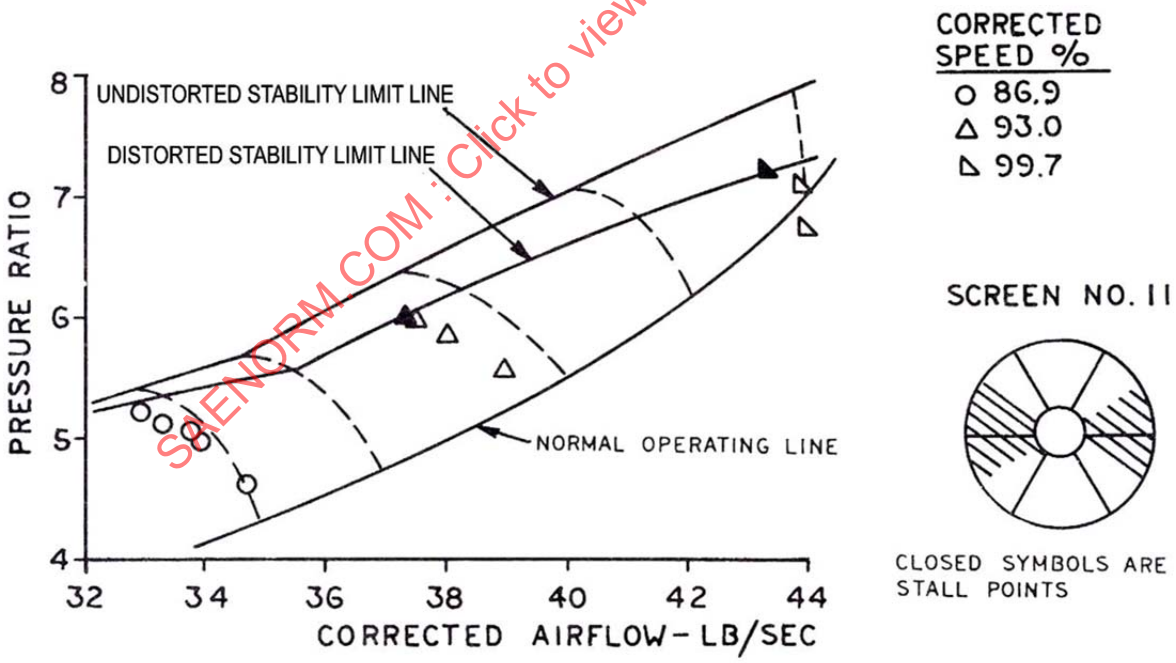

FIGURE 65 - EXAMPLE OF TWO-PER-REV CIRCUMFERENTIAL TOTAL-PRESSURE DISTORTION

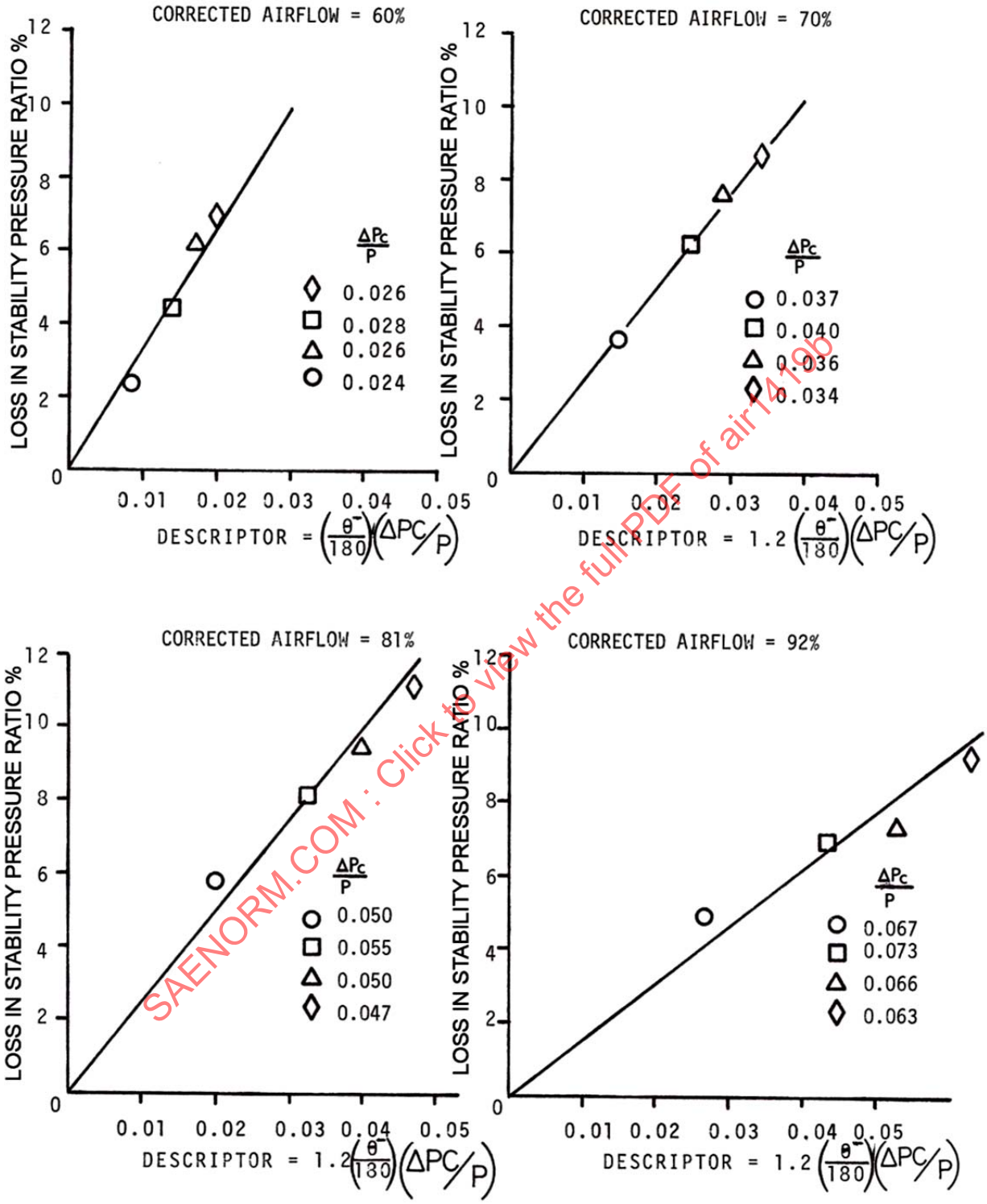

FIGURE 66 - COMPRESSOR SENSITIVITY TO ONE-PER-REV CIRCUMFERENTIAL TOTAL-PRESSURE DISTORTION

5.3.2 Radial Distortion

The effect on the stability limit line of a severe hub-radial distortion established from rig tests on a three-stage compressor can be seen in Figure 67. Results, derived from tests of the J85-GE-13 engine with hub-radial, mid-span, and tip-radial profiles, are shown in Figures 68 through 72 (Reference 2.2.5).

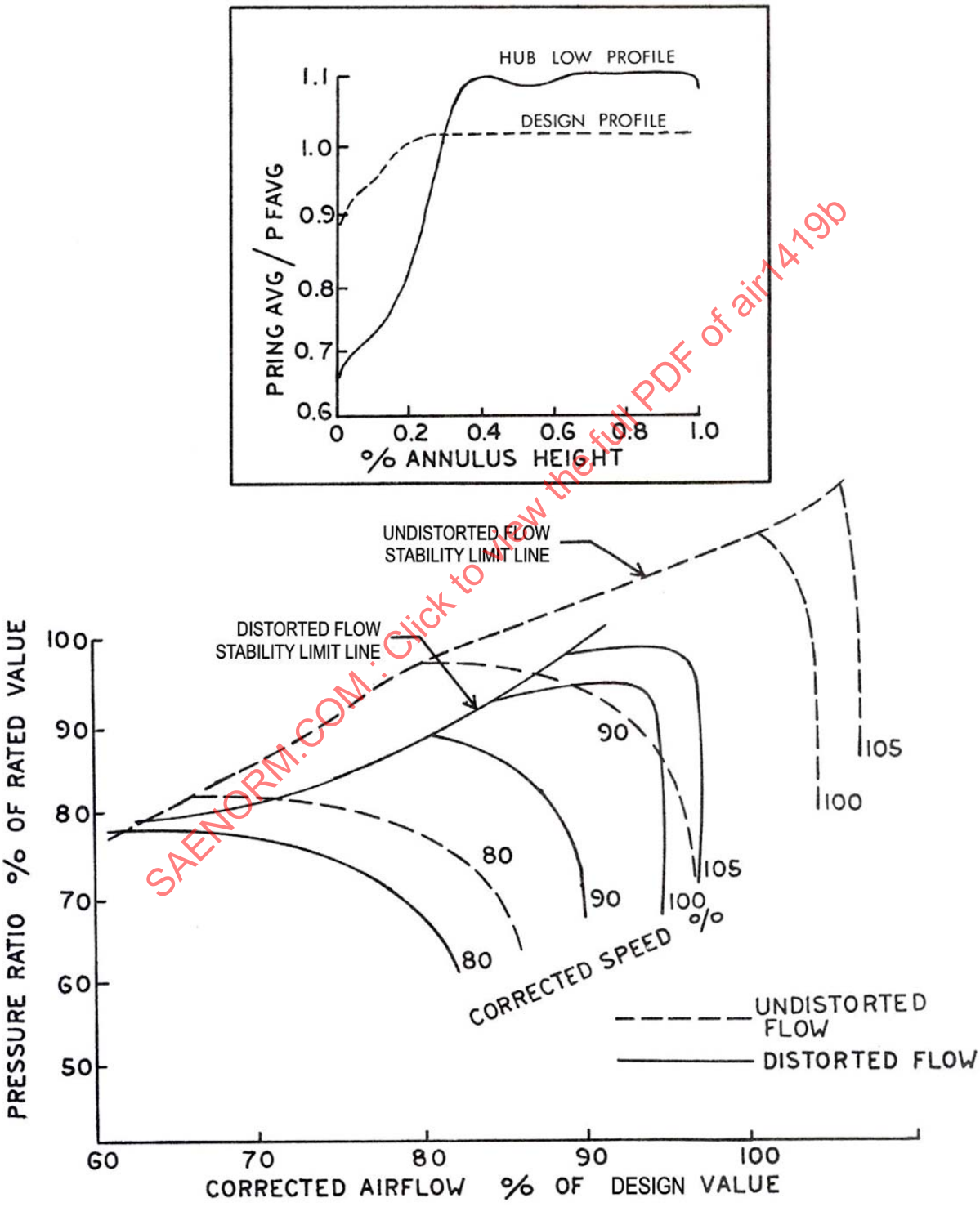

FIGURE 67 - EXAMPLE OF HUB-RADIAL TOTAL-PRESSURE DISTORTION

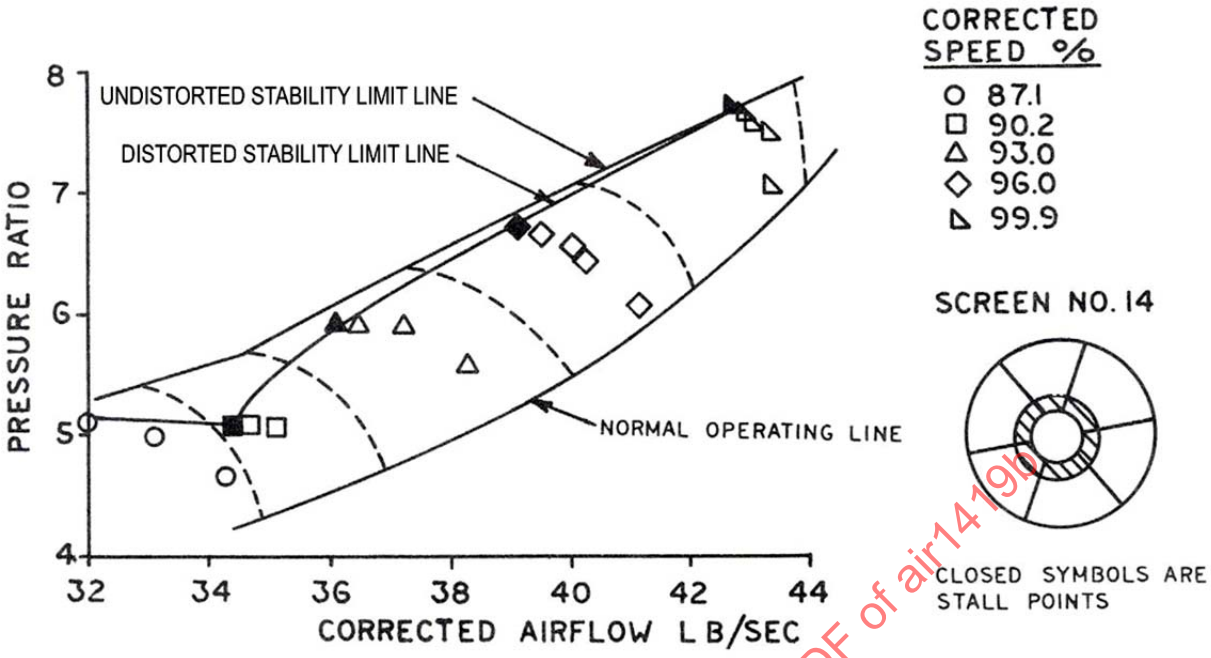

FIGURE 68 - EXAMPLE OF HUB-RADIAL TOTAL-PRESSURE DISTORTION, NARROW EXTENT

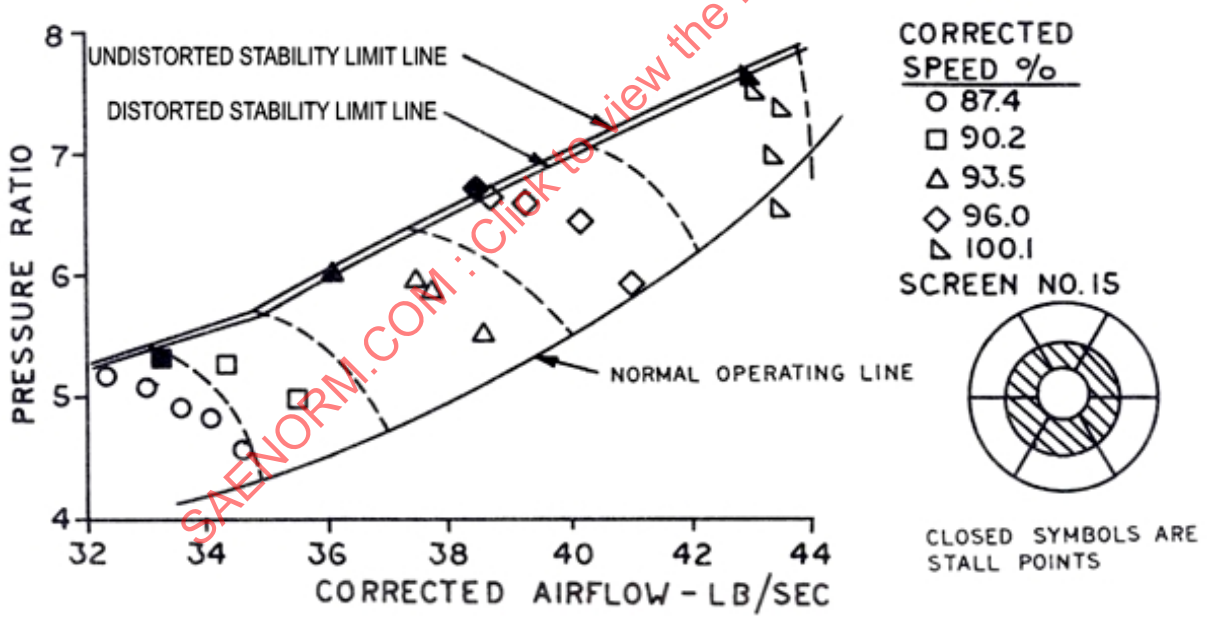

FIGURE 69 - EXAMPLE OF HUB-RADIAL TOTAL-PRESSURE DISTORTION, WIDE EXTENT

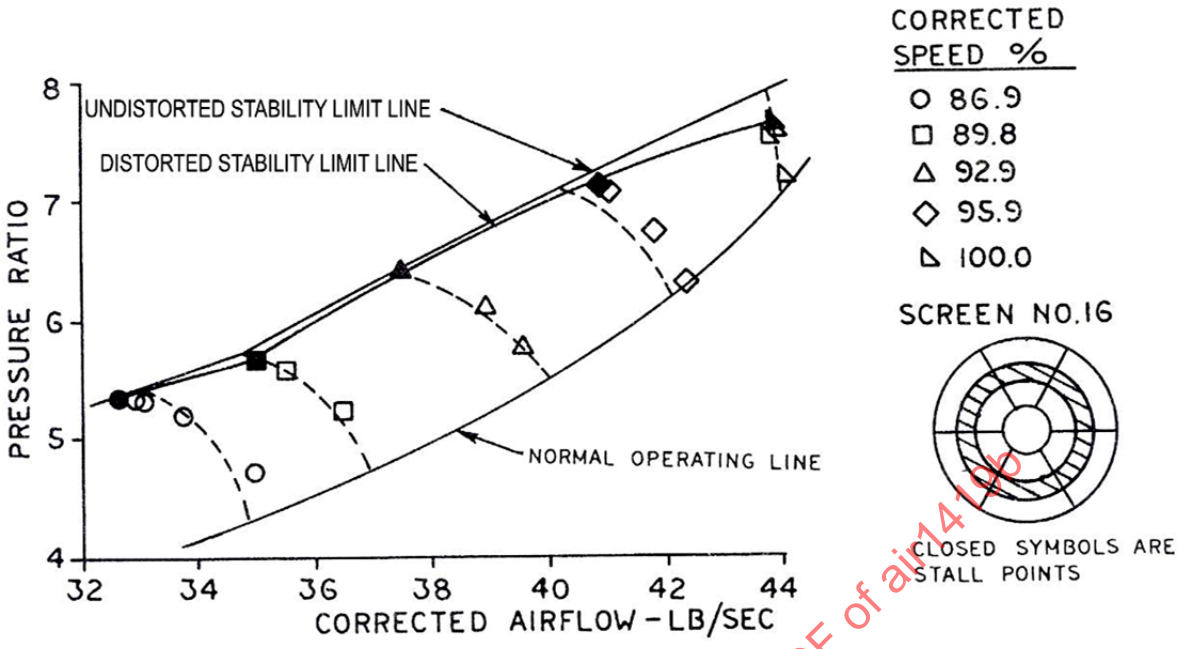

FIGURE 70 - EXAMPLE OF MID-SPAN-RADIAL TOTAL-PRESSURE DISTORTION

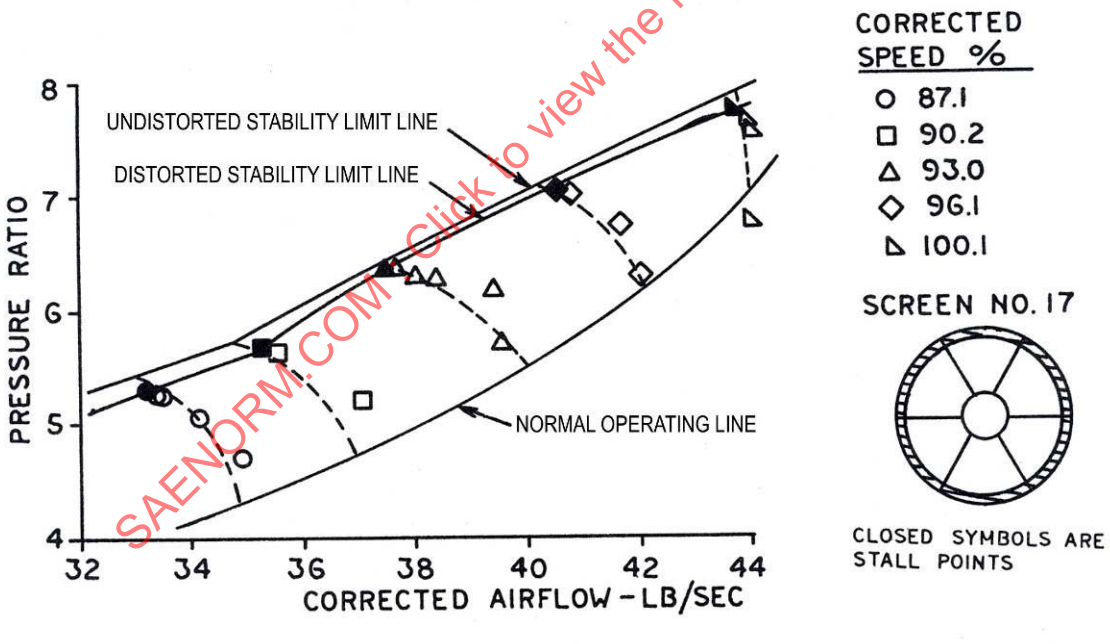

FIGURE 71 - EXAMPLE OF TIP-RADIAL TOTAL-PRESSURE DISTORTION, NARROW EXTENT

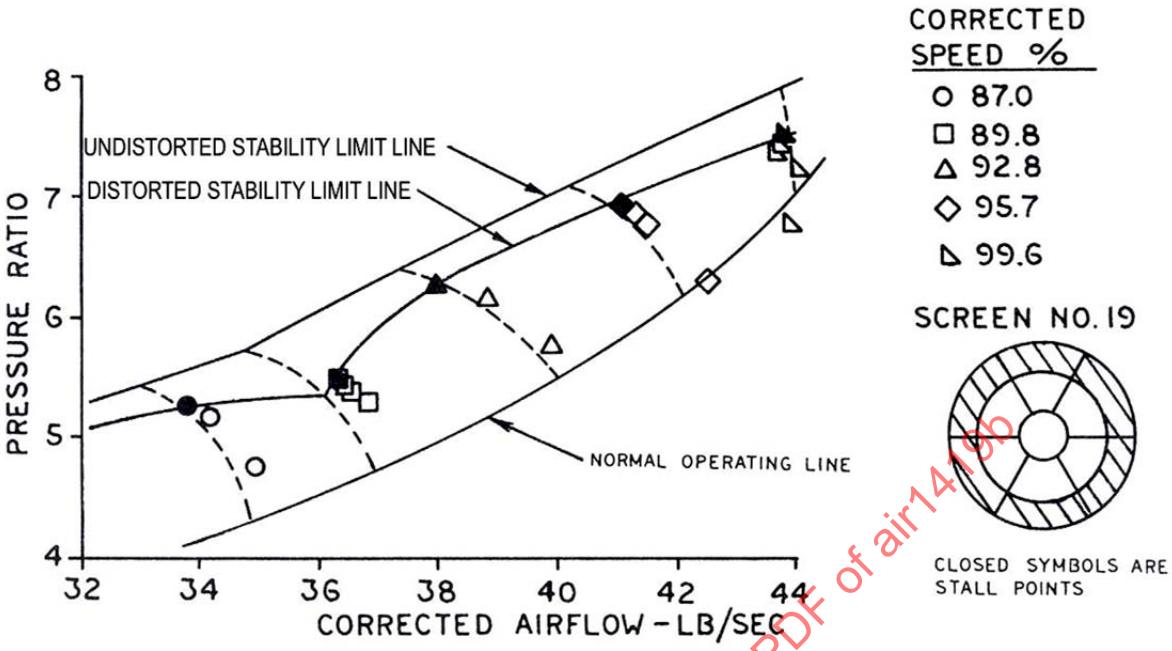

FIGURE 72 - EXAMPLE OF TIP-RADIAL TOTAL-PRESSURE DISTORTION, WIDE EXTENT

Correlations similar to those for circumferential distortion can be developed from these data. Since radial distortion effects can be favorable, it may be necessary to apply a methodology which accounts for the fact that ΔPRS changes are not monotonic (Section 4, Figures 45 and 46).

5.3.3 Combined Circumferential and Radial Distortion

The distortion patterns encountered during normal aircraft operation are a combination of circumferential and radial profiles. It is necessary that all correlation methodologies collapse data of this format. The loss in stability margin exhibited by the J85-GE-13 engine when combined inlet distortions were imposed on the engine is presented in Figures 73 and 74.

The examples point up the fact that acquisition of stability response data can be time-consuming and expensive. To minimize the work involved it is important to identify, from inlet tests, the major features of the AIP distortion early in the preliminary design and development phases of a program. Assessment procedures for turbofan engines are complex and involve developing a methodology to account for spool interaction and induced radial-flow and bypass-ratio effects through and at the exit from the fan.

Test data may not be available in the conceptual design, preliminary design, and early development phases of a new system. The baseline ΔPRS equation, Figure 23, is equally applicable to theoretical and semi-empirical stability assessment methods using the ARP1420 distortion descriptor elements. Theoretical and semi-empirical methods encompass spool, stage, and blade-row models incorporated into numerical computer simulations of the engine. These tools, together with background experience, provide a basis for stability assessment in early design and development phases of a program. The computer methods are applied in conjunction with steady and transient engine computer decks (Reference 2.1.1.4).

The results of a stability assessment, expressed in terms of an AIP distortion descriptor and compared with flight test results, are shown in Figures 75 and 76. Fixed-throttle engine operation appears in Figure 75, and throttle transient (accel) operation appears in Figure 76. The examples show that the fixed-throttle assessment correctly predicted the flight stability limit. The throttle transient results serve to illustrate the influence of AIP distortion on acceleration capability. Prior to flight test, such assessments may be used to identify critical inlet/engine compatibility conditions within the flight envelope.

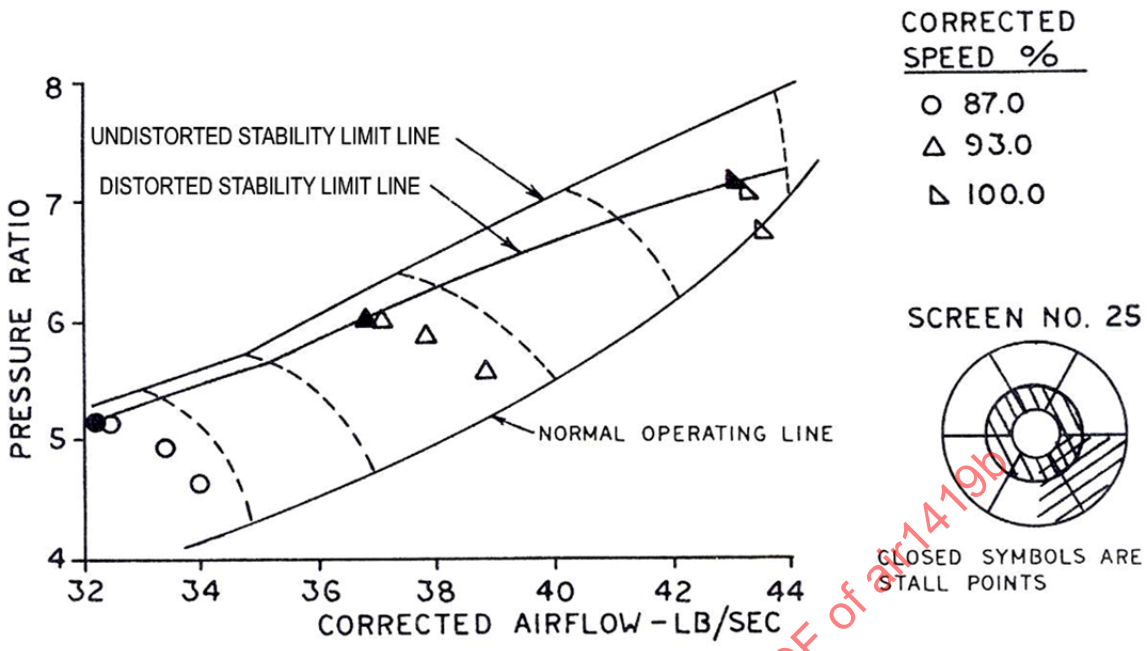

FIGURE 73 - EXAMPLE OF COMBINED HUB-RADIAL AND CIRCUMFERENTIAL TOTAL-PRESSURE DISTORTION

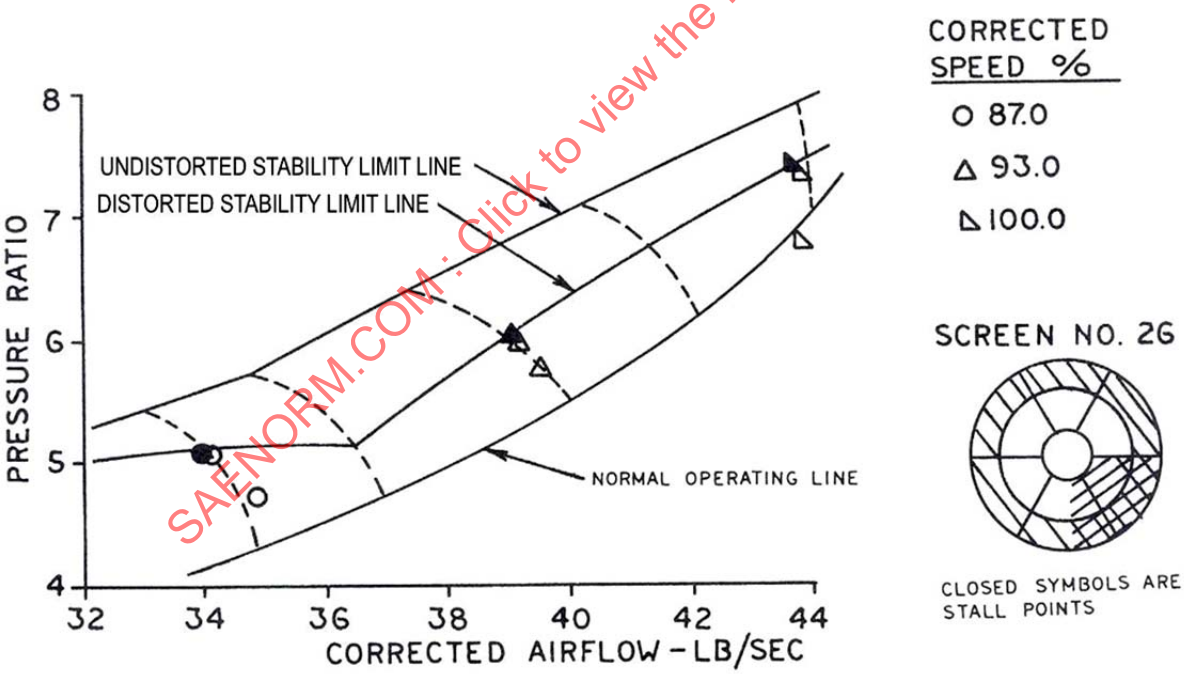

FIGURE 74 - EXAMPLE OF COMBINED TIP-RADIAL AND CIRCUMFERENTIAL TOTAL-PRESSURE DISTORTION

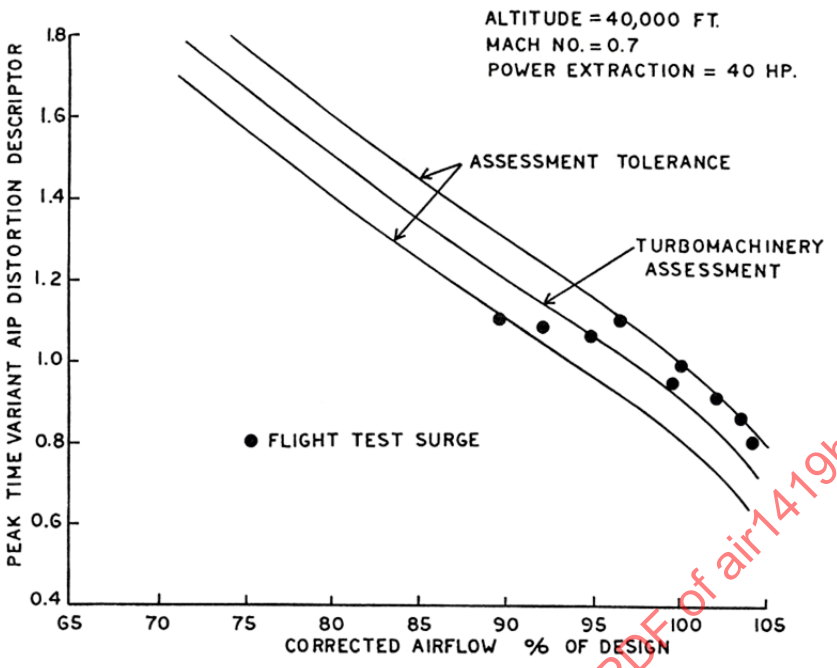

FIGURE 75 - COMPARISON OF DISTORTION STABILITY ASSESSMENT WITH FLIGHT TEST RESULTS FOR FIXED THROTTLE

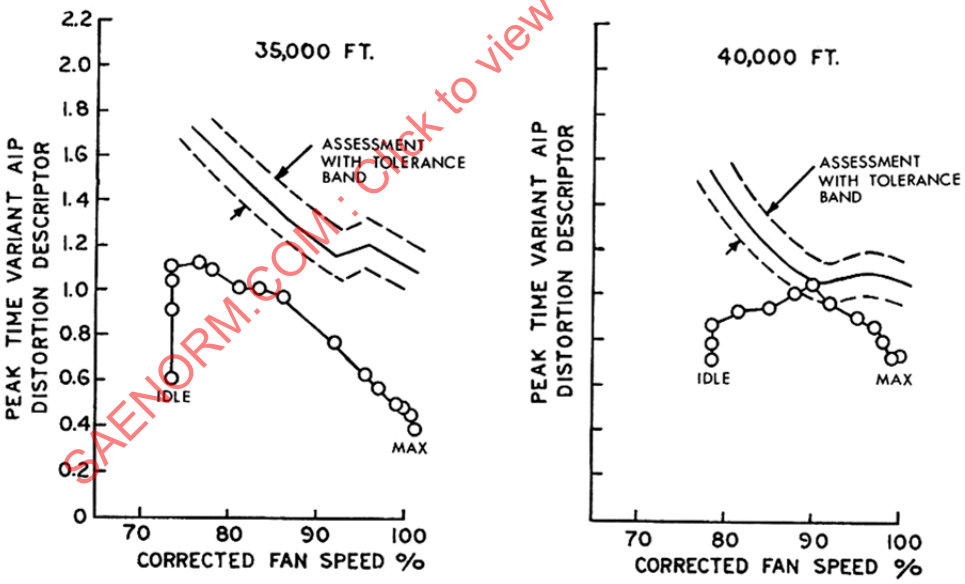

FIGURE 76 - COMPARISON OF DISTORTION STABILITY ASSESSMENT WITH FLIGHT TEST RESULTS FOR SNAP-THROTTLE TRANSIENTS - NO SURGES

6. PERFORMANCE ASSESSMENT

Propulsion system internal performance is assessed normally by evaluating inlet performance in terms of total-pressure recovery and installed engine performance at the corresponding value of AIP face-average total pressure, PFAV. Engine thrust, fuel consumption, airflow, and accel/decel times at appropriate inlet/engine operating conditions are established by treating the AIP airflow as an equivalent one-dimensional flow. Assessment procedures take into consideration changes in engine and matched engine-component performance resulting from losses of inlet total pressure, and account for control interactions.

In many cases where the AIP airflow pattern is substantially uniform so that spatial total-pressure distortion, PFAV fluctuations, and turbulence levels are low, these assessment procedures provide adequate performance accuracy. The effect of inlet flow distortion is small and well within experimental measurement scatter. Engine and engine component performance tests with simulated distortion are not usually necessary.

When the engine inlet airflow is distorted significantly, assessments of installed engine performance on a face-average total-pressure basis may be insufficient, and a procedure for accounting the effect of spatial total-pressure distortion, and perhaps flow unsteadiness, may be desirable. The assessment procedure adopted for a particular engine installation may, depending on the anticipated severity of the problem, involve synthesizing overall engine performance from estimated or empirical data using appropriate computer simulations, and from engine tests with simulated inlet distortion. The assessment of the effects of distortion then forms part of an overall assessment of installed engine performance at selected aircraft mission and powerplant operating conditions.

Distortion assessment procedures take different forms according to the type and development status of the propulsion system. They need to be constructed to account for the effects of changes in engine-component performance maps, component matching changes, and changes in control system pressure and temperature input signals (engine control interactions) resulting from modifications to flow profiles at intermediate stations throughout the engine. Results may be expressed directly as installed thrust, airflow, fuel consumption, and other relevant performance parameters for a defined AIP distortion pattern or, explicitly, as changes relative to face-average or equivalent uniform flow performance. It may be desirable for some purposes to widen the scope of the distortion assessment to correlate overall performance changes with relevant AIP distortion elements or combinations of those elements for a range of patterns and levels of distortion.

Practical difficulties arise in synthesizing and measuring performance changes specifically due to distortion. Accuracy problems are experienced since changes are derived from small differences between large estimated or measured flow quantities. These can cause uncertainties in assigning numerical values to threshold levels of distortion below which performance losses can be regarded as negligible, in establishing meaningful numerical performance/distortion sensitivity or trade factors, and in deciding on the extent of testing required to establish valid distortion response data.

6.1 Inlet Pressure Recovery and Distortion

Aspects of inlet performance relevant to engine performance assessments are discussed in terms of inlet type and location, the definition of AIP face-average total pressure, and distortion in the following paragraphs.

6.1.1 Inlet Type/Location - Distortion Characteristics

Average total-pressure recovery and distortion characteristics at the AIP differ markedly according to inlet type, location on the airframe, and mode of operation. Inlet designs of conventional powerplants range from relatively simple round-lip, short, straight duct configurations, appropriate to podded subsonic transport aircraft, to complex, sharp-lipped, long, curved duct configurations for highly integrated subsonic and supersonic combat aircraft.

The simple podded inlet designs are very efficient. They provide close to 100% recovery and virtually zero total-pressure distortion at most major performance points within the normal aircraft flight envelope. Total-pressure-defect regions are generally of the tip-radial or wall-boundary-layer type and are comparable to those observed in engine component and engine test facilities. Total-pressure distortion problems may need to be addressed at high inlet crossflow conditions to provide for emergencies outside the normal operational envelope.

The more complex inlet designs provide lower inlet recovery as a consequence of larger total-pressure-defect regions at the AIP. Distortion patterns generally contain radial and circumferential elements. Numerical inlet performance characteristics are used together with pattern data to establish the need for and to conduct quantitative assessments of engine performance in distorted flow. Data for three inlets are presented in Figures 77, 78, and 79. The steady or time-averaged inlet data are expressed in terms of ARP1420 recommended distortion descriptor elements and area-weighted face-average total pressure.

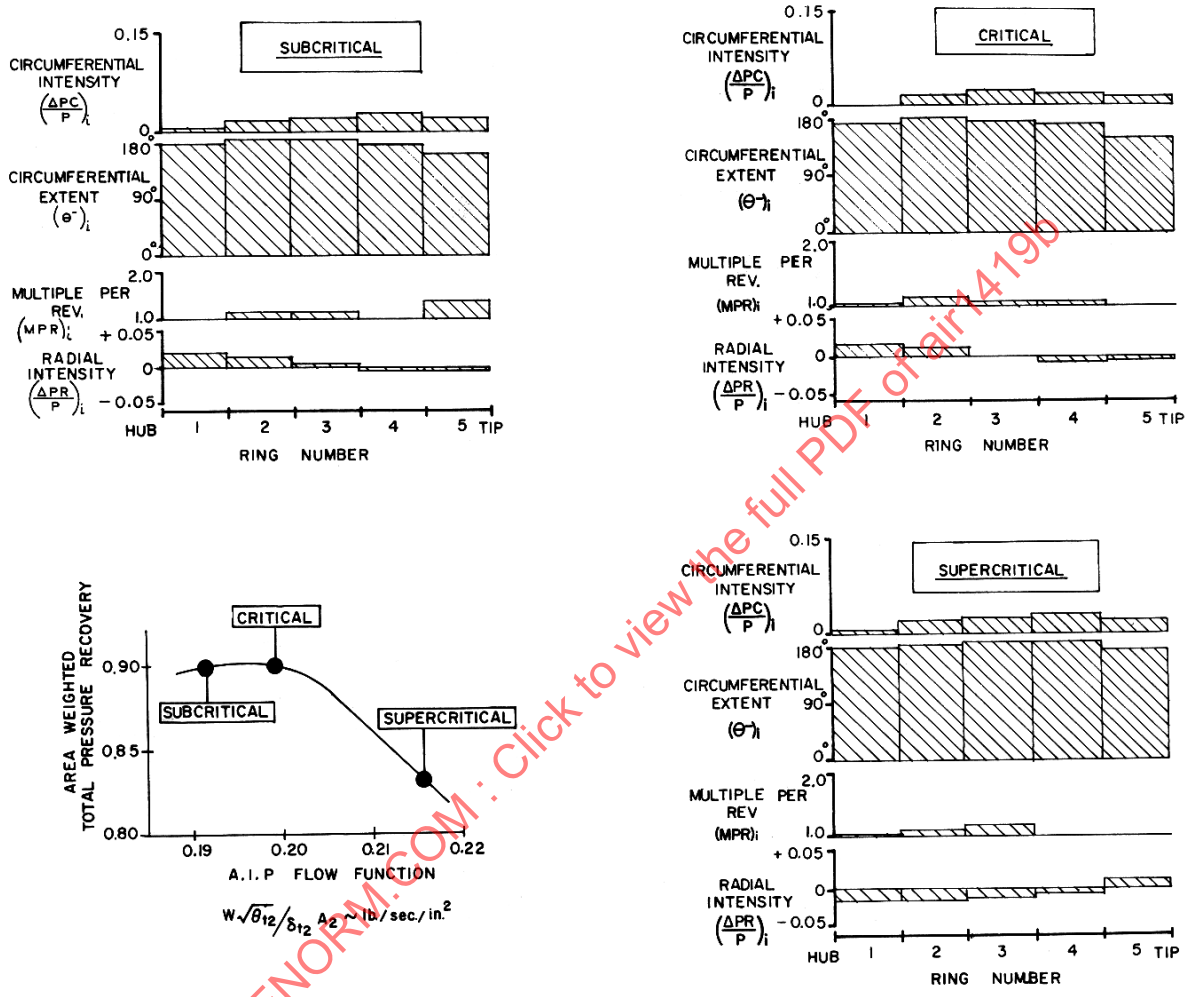

FIGURE 77 - SUPERSONIC, TWO-DIMENSIONAL, EXTERNAL-COMPRESSION INLET, MACH 2.0, CRUISE INCIDENCE, FIXED RAMPS

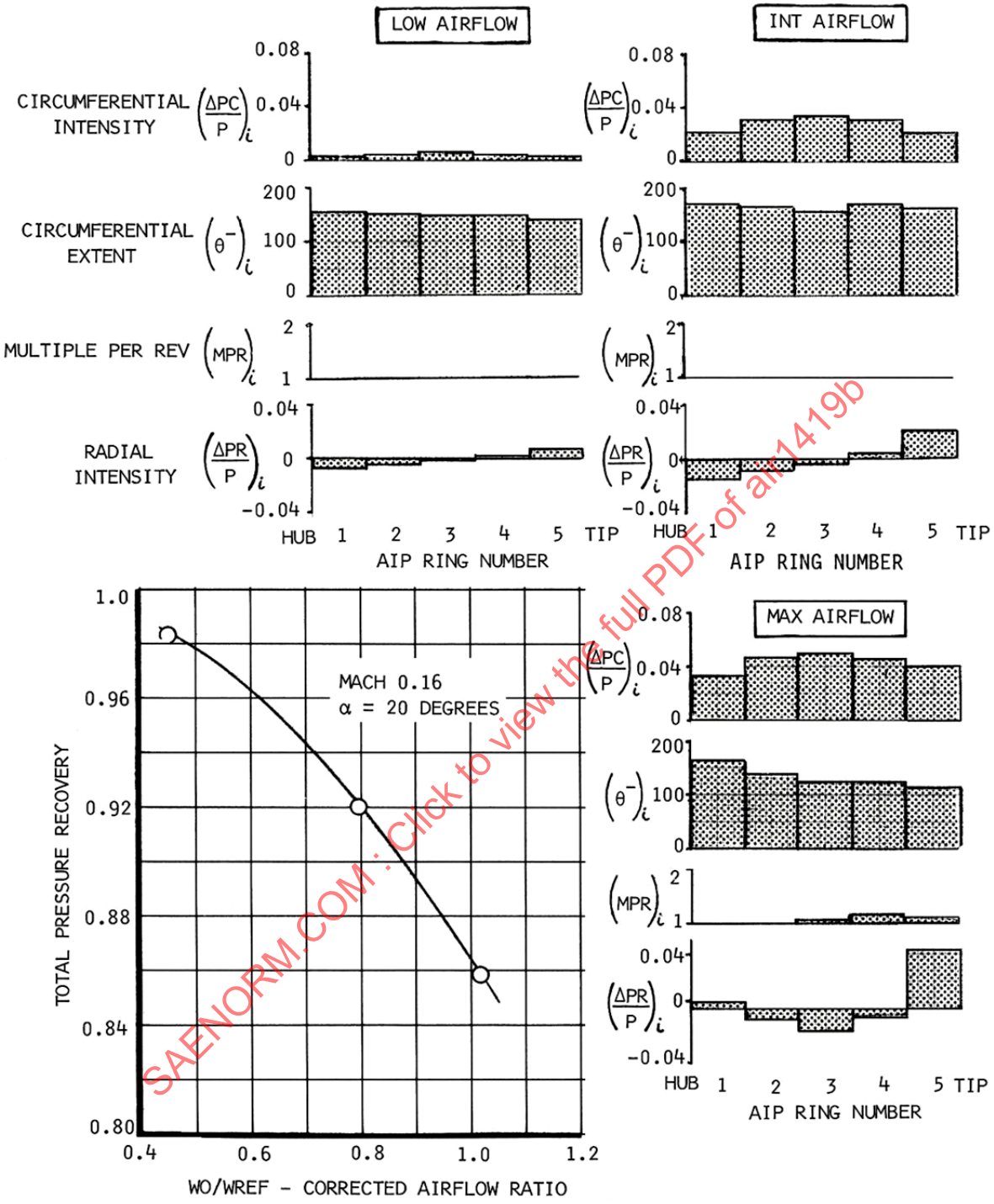

FIGURE 78 - SUPERSONIC, TWO-DIMENSIONAL, EXTERNAL-COMPRESSION INLET, DISTORTION CHARACTERISTICS DURING LOW-SPEED OPERATION

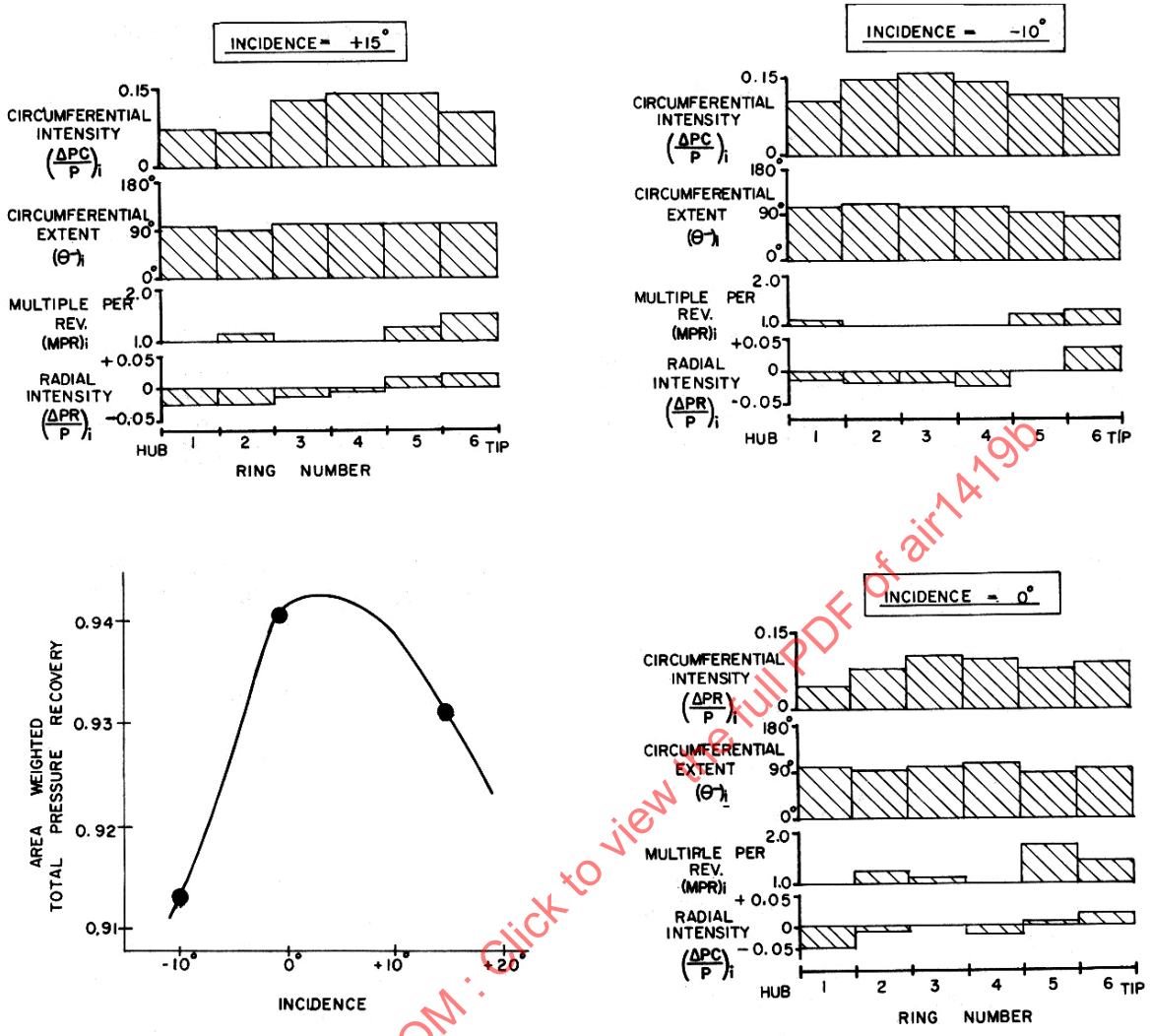

FIGURE 79 - SHORT SUBSONIC BIFURCATED INLET

The figures illustrate several features relevant to the assessment of installed engine performance. The long-duct supersonic inlet in a typical cruise configuration exhibits low radial and circumferential distortion (Figure 77). Installed engine performance is predominantly dependent on the face-average total-pressure level. An assessment of performance changes due to distortion is unlikely to be necessary in this case. Low speed data for a different supersonic inlet design are presented in Figure 78. Distortion elements are higher for the intermediate and maximum flow conditions. An assessment of performance changes due to distortion is likely to be necessary in this case. The short subsonic bifurcated inlet (Figure 79) exhibits peak recovery at cruise incidence, and the circumferential intensity elements are high. Both recovery and distortion deteriorate with incidence. An assessment of performance changes due to distortion may be required in this case also.

6.1.2 Face-Average Total Pressure

Alternate definitions of face-average total pressure are possible at the AIP in distorted flow conditions. This situation stems from the fundamental fluid mechanical difficulty of constructing a unique one-dimensional or equivalent face-average flow that can simultaneously account for mass flow, momentum, and energy-flux variations across the AIP. Definitions which are employed include flow-continuity, area-weighted (area-averaged), mass-flow-weighted, momentum-weighted, and entropy-derived face averaging. Differences in the numerical values of the alternate face-average definitions can be on the order of 1% of the face-average total-pressure level, depending on pattern shape.

Area-averaged total pressure is used widely throughout the Aerospace Industry, has considerable technical merit, is simple and easy to apply, and eases inlet and engine data acquisition and processing requirements. Area-averaging greatly facilitates the definition and quantification of distortion at the AIP, and is the recommended basis of ARP1420 guidelines. Alternative definitions, appropriate to a particular propulsion system development, such as mass-flow weighting for compressor efficiency accounting, can be related to the area-averaged value for defined AIP patterns.

When instrumentation rings are located at centers of equal area:

$$PFAV = \frac{1}{N}\sum_{i=1}^{N}(PAV)_i = \frac{1}{N}\sum_{i=1}^{N}\left[\frac{1}{360}\int_{0}^{360} P(\theta)_i d\theta\right] \quad \text{(Eq. 82)}$$

where N is the number of instrumentation rings and $(PAV)_i$ are the ring-average total pressures.

The numerical distortion descriptor elements are defined relative to the area-averaged AIP mean total pressure, PFAV. The above definition implies that:

$$\sum_{i=1}^{N}\left(\frac{\Delta PR}{P}\right)_i = 0 \quad \text{(Eq. 83)}$$

where $\left(\frac{\Delta PR}{P}\right)_i$ are the radial intensity elements.

ARP1420 guidelines for assessing installed engine performance in distorted flow conditions thus involve accounting for baseline uniform-flow performance using the area-averaged AIP total pressure, and performance changes due to distortion relative to this area-averaged datum.

In this context it may be noted that, by virtue of the area weighting involved, PFAV is related to the conservation of momentum flux at the AIP.

6.1.3 Inlet Data Acquisition

As time-averaged performance is of prime interest, it is usual to base assessments on steady-state AIP pressure data obtained from a low-response instrumentation array used for sub- and full-scale inlet tests (Section 8). Early assessments of inlet performance use small-scale inlet data, accounting for Reynolds number effects at defined performance conditions within the operational envelope. Testing at the maximum Reynolds number that is both practical and affordable is recommended. This practice places the data acquisition Reynolds number as close as possible to the flight Reynolds number, minimizing the extrapolation necessary to perform a Reynolds number correction to the steady state total-pressure-recovery data. This practice also improves the data acquisition accuracy by placing the pressure sensed by the transducers more toward the center of their operating range. Additionally, this would minimize any adjustments necessary to the subscale model geometry to account for differences between subscale and flight Reynolds numbers. For a given scale of inlet model there will be a minimum Reynolds number below which performance data would be unacceptable due to the issues mentioned above.

6.2 Engine Performance Data

Prior to discussing guidelines for procedures to assess the effects of distortion on performance, illustrative examples of the effects of distortion on engine and engine compression components are presented to highlight the main technical issues and candidate data needs. The data presented apply to time-averaged or steady-state distortion and performance.

6.2.1 Compression Components Response to Distortion – Examples

The upstream, low-pressure compressor or fan is unshielded from, and is most likely to be affected by, the inlet flow distortion. Significant changes in the fan performance map can occur.

Compressor rig tests with screen-simulated total-pressure distortion should include classical (square-wave) patterns and simulated aircraft inlet patterns (7.2). Tests using classical patterns provide information on the types of distortion to which the compressor is most sensitive. Tests are conducted for both stability and performance evaluations and usually include distortions more severe than those corresponding to aircraft mission performance points. The test data provide a basis for deriving compressor numerical performance/distortion sensitivity factors.

The results obtained from rig tests of a five-stage axial compressor with three classical time-averaged circumferential distortion patterns are presented in Figure 80. The multiple-per-rev elements were unity. At these levels of circumferential distortion, which are typical of those encountered in the mixed radial and circumferential patterns of inlets at cruise conditions, flow and efficiency losses were less than 1% and were of the order of the measurement accuracy. Area-averaged compressor performance was not greatly affected.

The results of a seven-stage axial compressor test with classical circumferential screen patterns are shown in Figure 81 (Reference 2.2.6). Screen details are presented in Table 9.

In this case the predominant distortion effect for the more severe patterns (screens 3 and 4) was loss of corrected flow, particularly close to the stability limit. Efficiency changes (not shown) also occurred. The data give an indication of the measurement scatter problem for less severe distortions (screens 1, 3, and 2 of No. 1).

The results of tests of the same seven-stage compressor with hub-radial and tip-radial patterns are shown in Figure 82. Classical and graded tip-radial patterns were tested. A mixed classical pattern consisting of the tip-radial and 90-degree circumferential screens was also tested. Screen data are presented in Table 10.

The dominant effects observed were loss of compressor corrected flow for the hub-radial distortion and a gain in corrected flow for tip-radial distortion when the compressor is unchoked. AIP distortion, tip-radial distortion in this case, does not necessarily produce losses in compressor corrected flow. The increase in corrected flow due to the graded tip-radial distortion, screen 21, was mitigated to some extent by adding the circumferential distortion element, screen 2, which had very little effect on flow when tested alone (Figure 81).

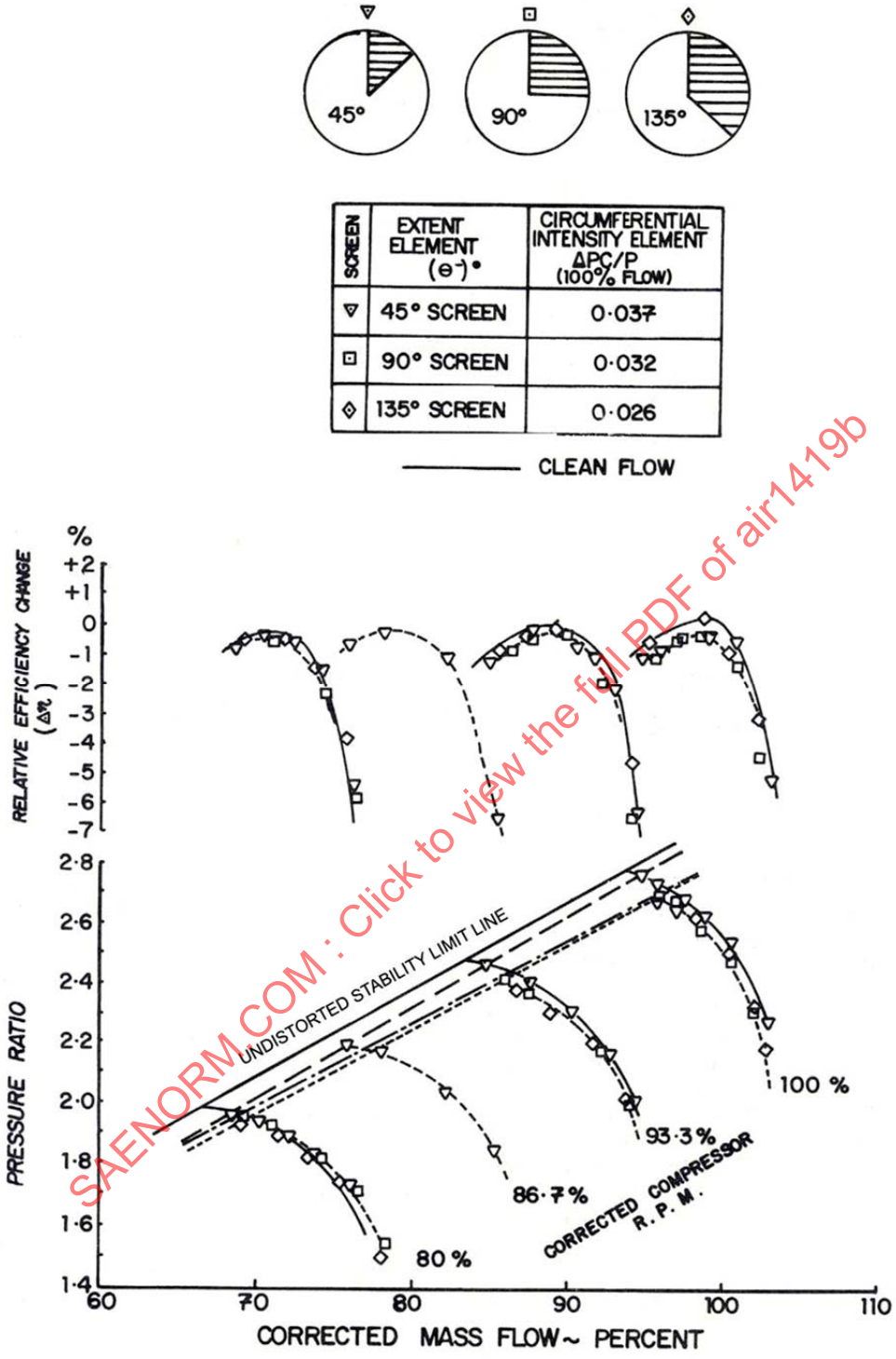

FIGURE 80 - EFFECT OF CLASSICAL CIRCUMFERENTIAL INLET DISTORTION PATTERNS

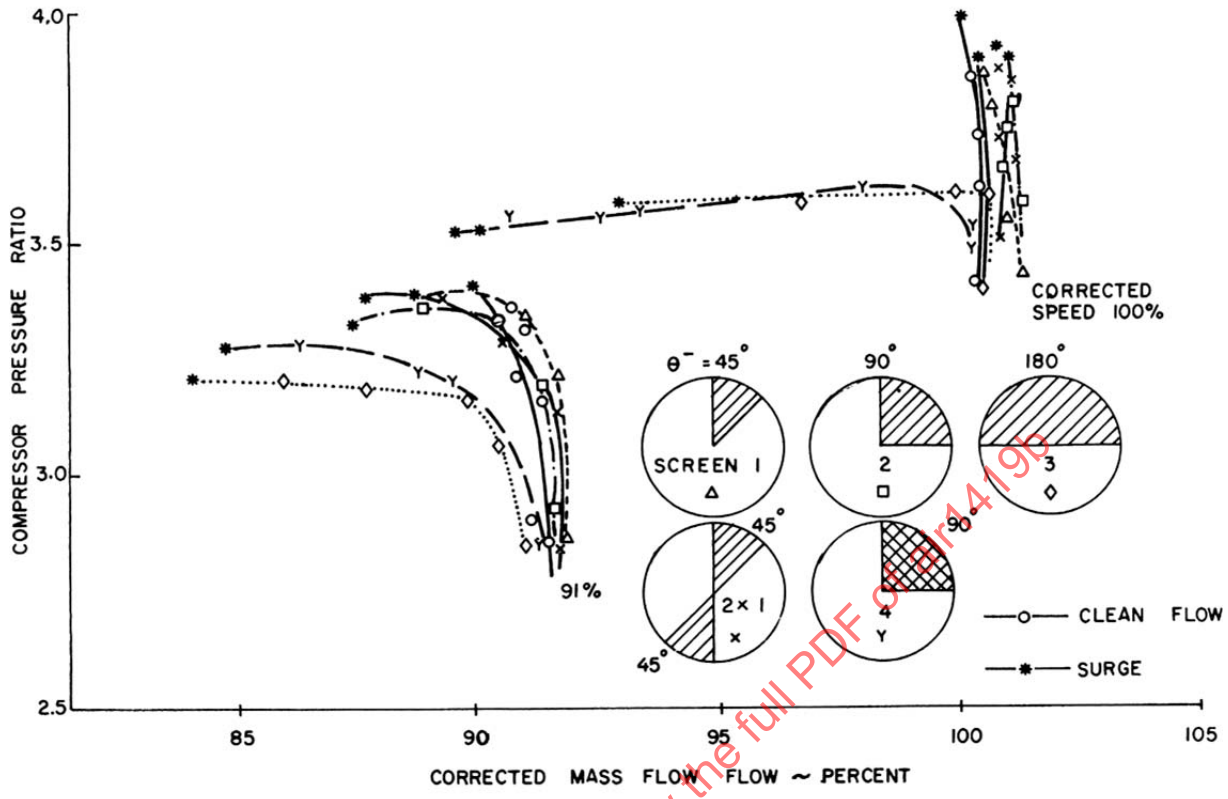

FIGURE 81 - RIG COMPRESSOR TESTS - CLASSICAL DISTORTION

TABLE 9 - CLASSICAL CIRCUMFERENTIAL SCREENS

Screen		Extent ($\bar{\theta}$), degrees	Intensity (ΔPC/P) (100% Flow)	Multiple-Per-Rev (MPR)
Clean Flow	O	-	-	-
1	Δ	45	0.06	1
2	□	90	0.044	1
3	◊	180	0.064	1
4	Y	90	0.07	1
5	X	2 X 45	0.046	2

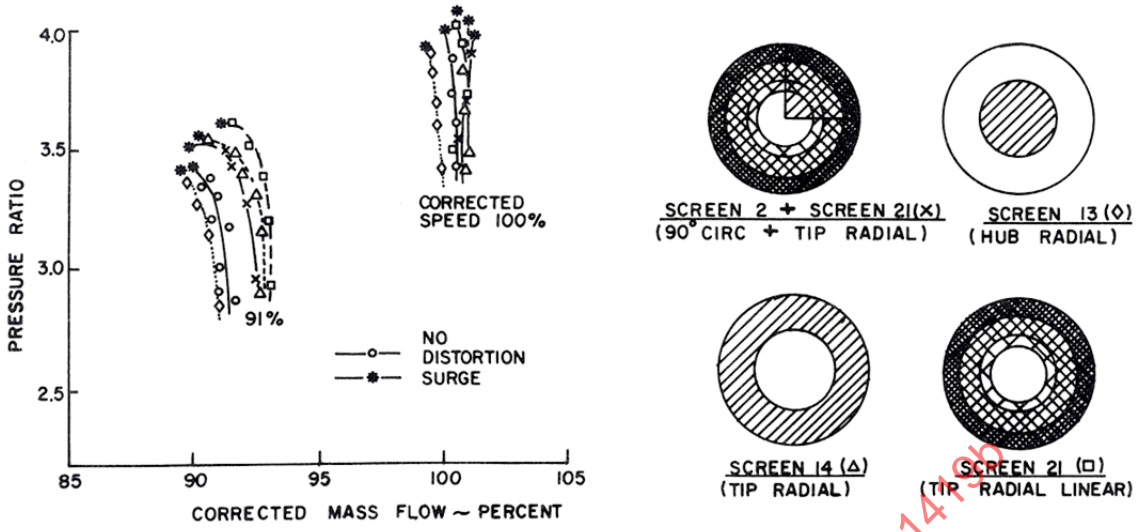

FIGURE 82 - RIG COMPRESSOR TESTS - RADIAL AND MIXED DISTORTION

TABLE 10 - RADIAL AND MIXED SCREENS

Screen		Distortion Type	Radial Intensity (ΔPR/P)						Radial Extent (Percent)
Clean	O	-	-						-
13	◊	HUB-RADIAL (CLASSICAL)	±0.04						50 (Area)
14	Δ	TIP-RADIAL (CLASSICAL)	±0.055						50 (Area)
21	□	TIP-RADIAL (LINEAR)	RING:	1	2	3	4	5	100
				-0.15	-0.03	+0.02	+0.06	+0.10	
2 + 21	X	MIXED	SCREEN 2 + 21						+100

The data illustrate several points relevant to the assessment of distortion effects on performance:

a. Testing with classical patterns provides important quantitative insights into compressor performance response.

b. Some distortion elements can have a favorable effect.

c. The interpretation of test data for moderate distortion levels can be occluded by data random error and repeatability scatter.

The combined tip-radial and circumferential distortion pattern (screen 2+21) results imply that upstream compressors should be tested with inlet patterns to determine the performance changes.

The results of testing on a three-stage turbofan are shown in Figure 83. The inlet pattern for this turbofan is illustrated in Figure 84. Overall fan performance was affected significantly, corrected flow and efficiency changes being approximately 2%. In this case, additional data relevant to changes in split-flow outer diameter (OD) and inner diameter (ID) performance characteristics and bypass ratio may be required for analysis.

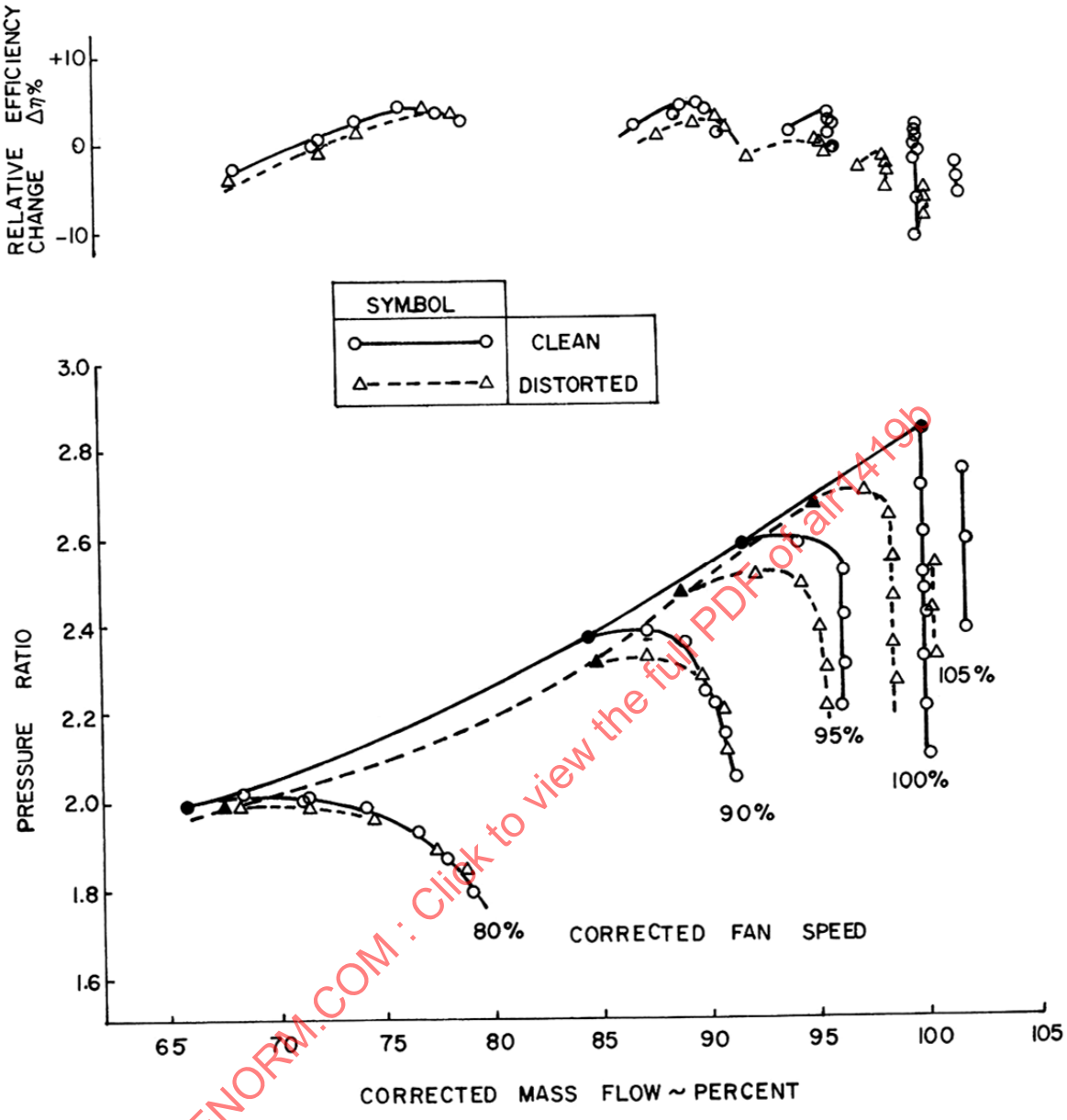

FIGURE 83 - RIG COMPRESSOR TESTS - SCREEN SIMULATED DISTORTION

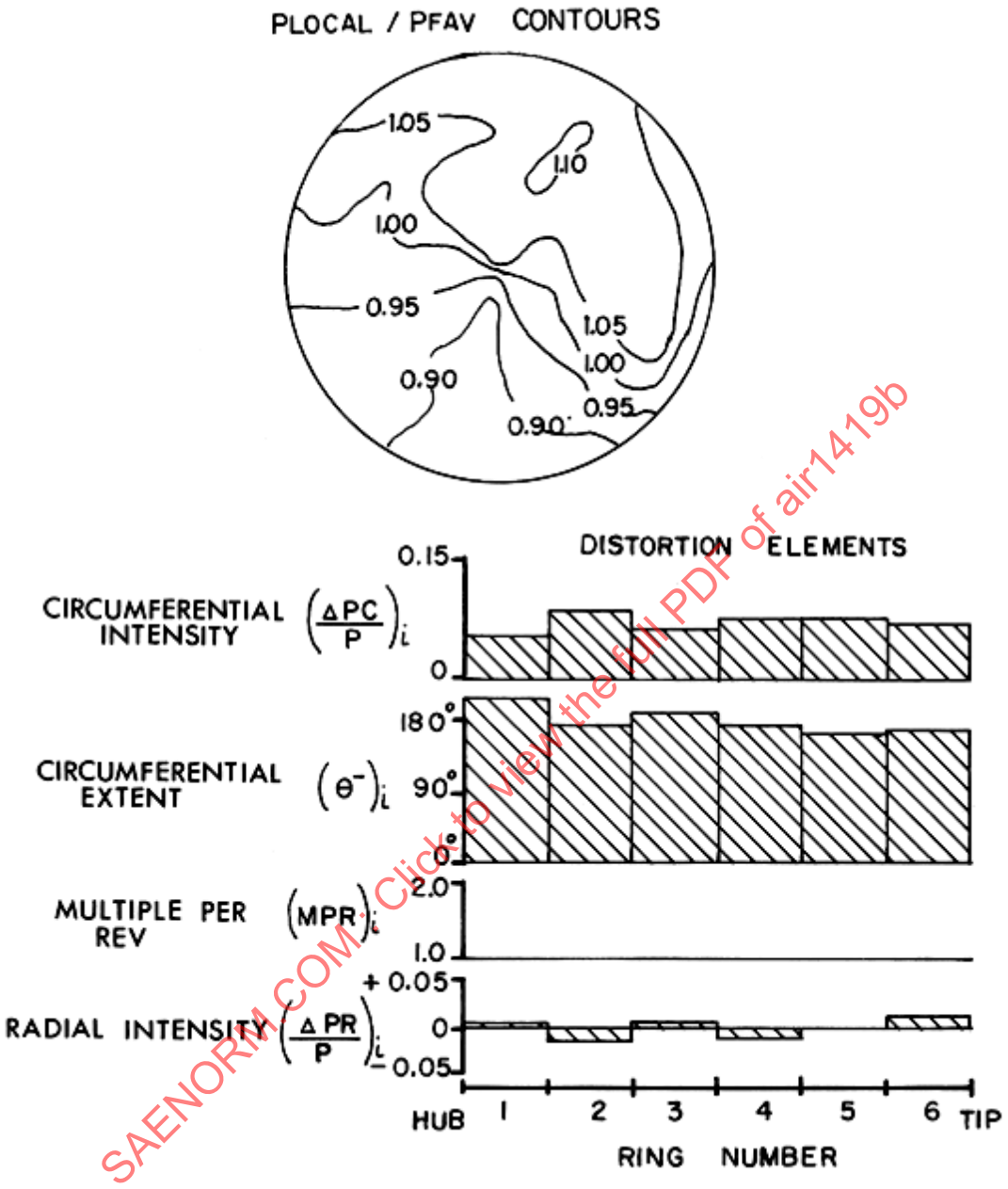

FIGURE 84 - SIMULATED INLET-DISTORTION SCREEN #1

The assessment procedures can use compressor test results in the form of modified performance maps for specified distortion patterns, as discrete changes due to those patterns, or as changes correlated with numerical distortion descriptors. An example correlation for a three-stage research compressor tested with a number of classical patterns is shown in Figure 85 (Reference 2.2.6). Fan corrected flow, pressure ratio, and efficiency changes for nominal matching of the operating line correlated well with radial distortion. Tip-radial distortions were favorable, and hub-radial distortions were unfavorable. Circumferential distortion elements were not dominant in this case. The particular distortion descriptor used for the correlation is defined by a combination of radial distortion elements:

$$\frac{(PAV)_{ID} - (PFAV)}{PFAV} = \frac{1}{N}\sum_{i=1}^{N}\left(\frac{\Delta PR}{P}\right)_i \qquad \text{(Eq. 84)}$$

where $\left(\frac{\Delta PR}{P}\right)_i$ are the radial intensity elements, and N denotes the number of instrumentation rings describing the ID region of the patterns. (For this example, N = 2, and $(PAV)_{ID}$ equals the average pressure in the ID region.)

If the major effects of distortion are not confined to the upstream compressor, then compression component distortion transfer data - principally total pressure and temperature data - may be required to assess the effect of AIP distortion on downstream components. Pattern and numerical distortion descriptors at the low-pressure-compressor exit would be required for this purpose.

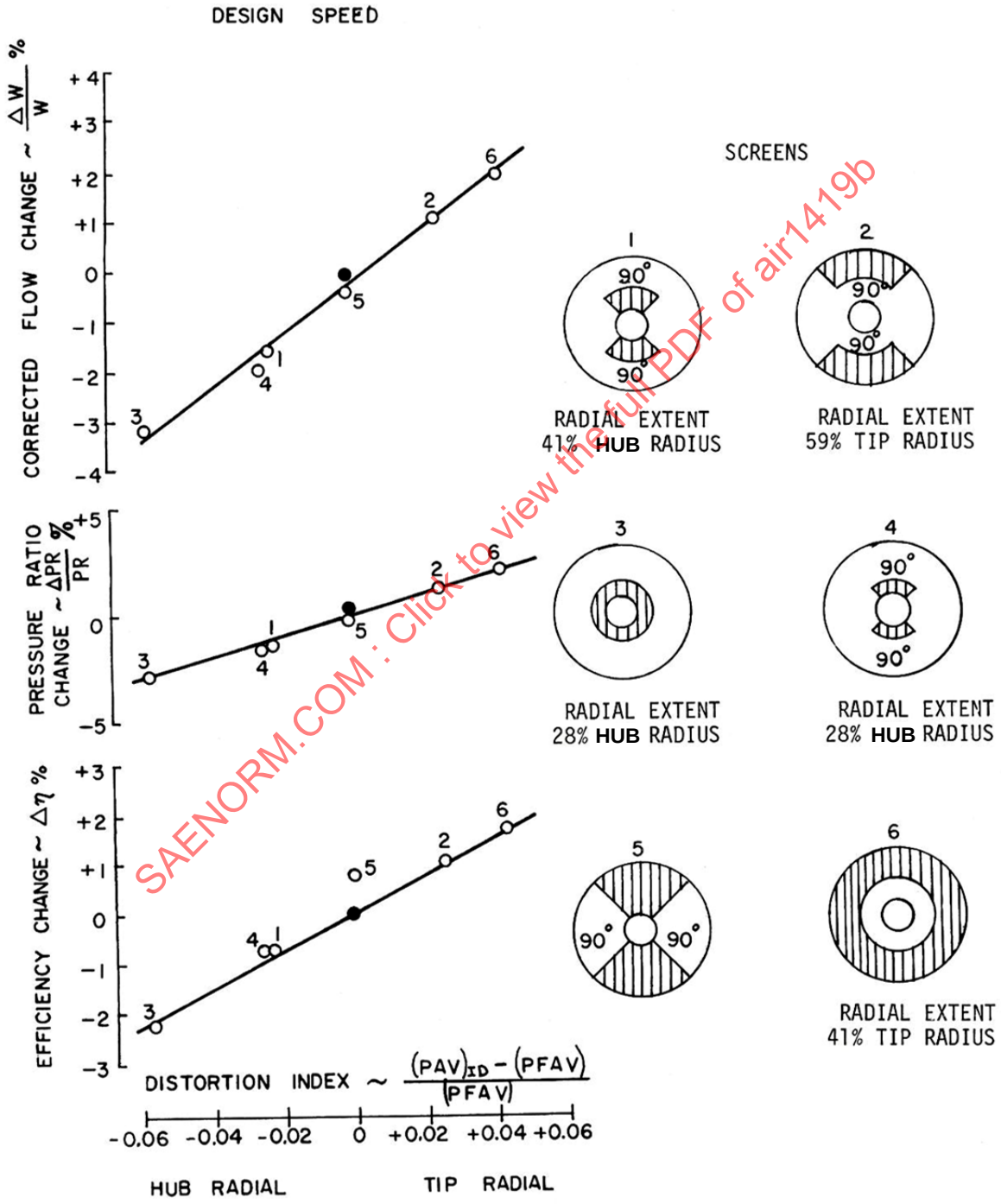

FIGURE 85 - DISTORTION EFFECTS ON THREE-STAGE FAN COMPRESSION

6.2.2 Engine Response to Distortion – Examples

Engine tests with total-pressure distortion play an important part in the assessment of performance changes due to distortion. The results of tests conducted in a direct-connect altitude test facility on a turbofan engine with inlet distortion simulated by a screen at Mach 0.9, 40 000 ft., standard day conditions appear in Figure 86. Data are presented in terms of changes in corrected fuel consumption and corrected gross thrust relative to tests with undistorted inlet flow. No significant trends in the corrected gross thrust and fuel flow changes due to distortion were observed in the data range from 70 to 100% corrected fan speed for this limited sample test case. Airflow changes were on the order of 0.5%.

Engine tests in both undistorted and distorted inlet flows are necessary to establish distortion effects. Individual data points can be misleading. A factor of some importance in the interpretation of the data is that of accounting for screen pressure loss which affects the engine test Mach number/altitude setting for a given nominal flight condition, the power extraction, and the intercomponent match. No corrections for engine final nozzle rematch were necessary in this choked nozzle operating case.

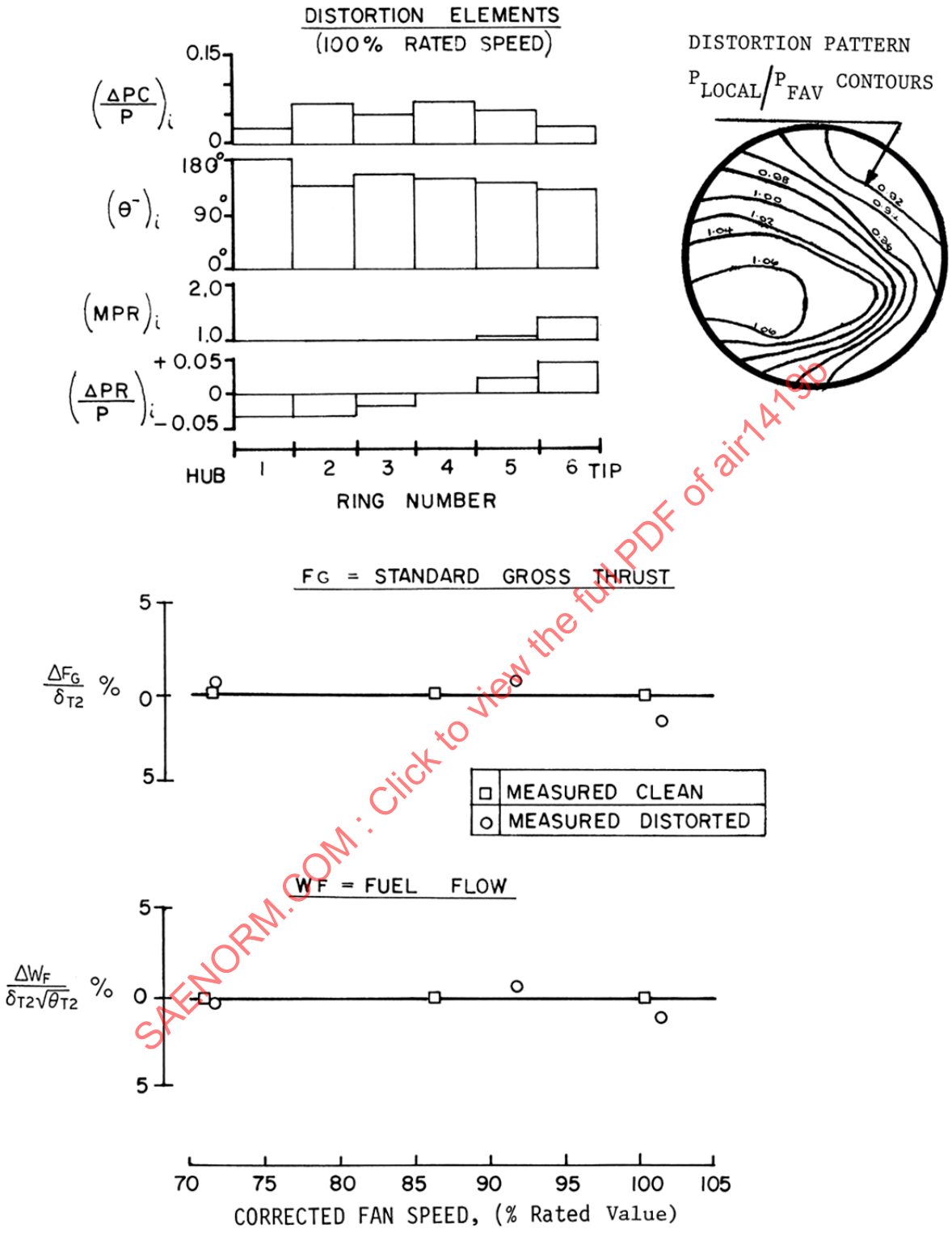

FIGURE 86 - TURBOFAN ENGINE PERFORMANCE WITH INLET DISTORTION

Results obtained from turbofan engine tests conducted on a sea-level test stand with a classical circumferential inlet distortion pattern can be seen in Figure 87. Significant changes in corrected gross thrust and specific fuel consumption were caused by the inlet screen. Specific fuel consumption increased by 6% and thrust decreased by 2% relative to undistorted-flow engine performance. These changes were not due solely to the effects of distortion, however, but to the combined effect of distortion and loss of inlet recovery which caused engine component rematching with the unchoked mixed-flow nozzle. Corrections to the measured results for the effect of the screen losses reduced the magnitudes of the performance changes so that they fell within the undistorted-flow engine-performance data scatter. Corrections for average total-pressure loss are necessary in order to isolate the effect of distortion if the screen loss does not correspond to that of the inlet loss. Tests with uniform screens designed to simulate the distortion screen pressure losses may be required to establish the appropriate corrections and validate cycle deck calculations.

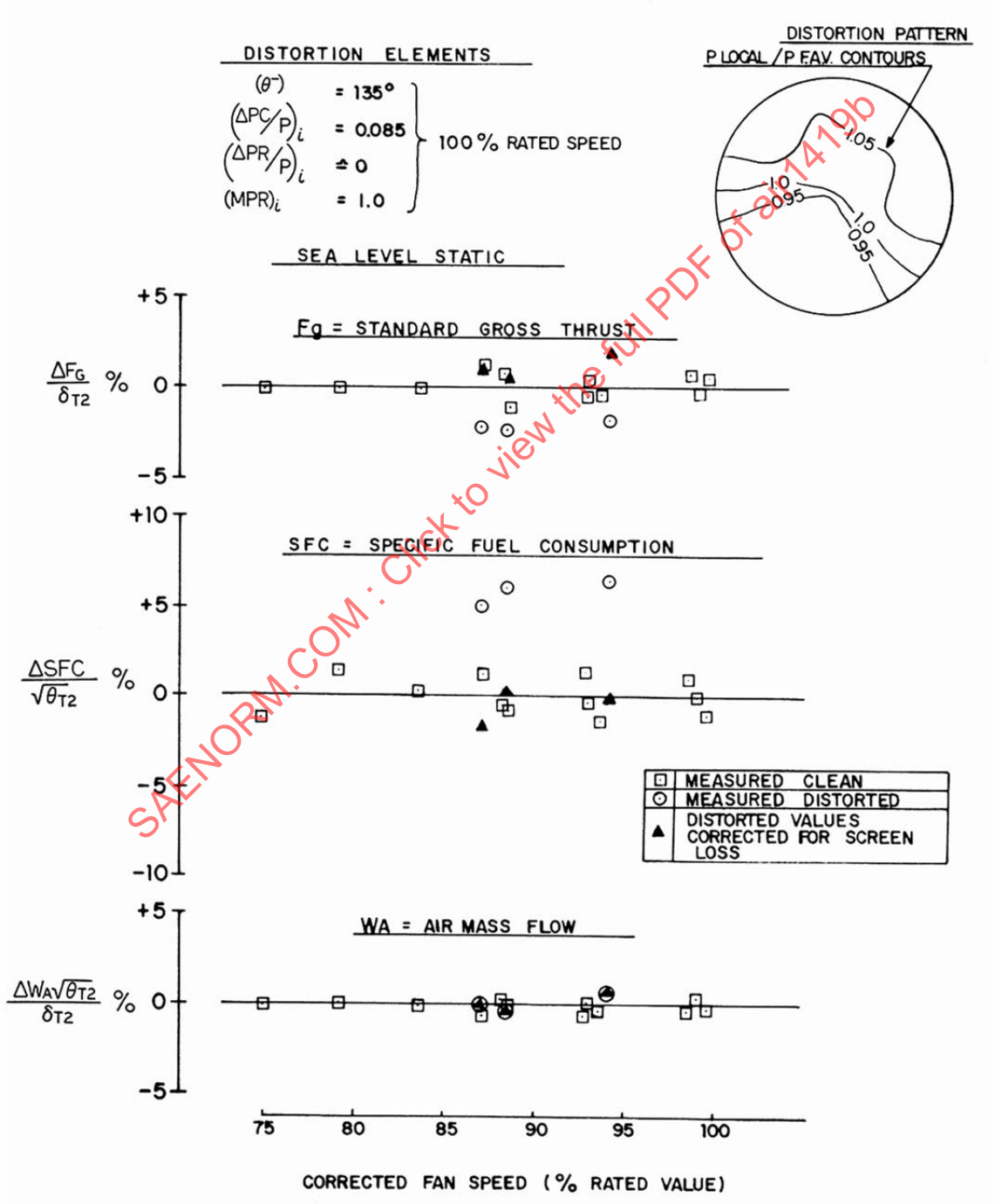

FIGURE 87 - TURBOFAN ENGINE WITH CLASSICAL CIRCUMFERENTIAL DISTORTION PATTERN

Inlet flow distortion can affect rated performance if the engine control employs discrete or local-flow parameter sensing, e.g., a local exhaust pipe total-temperature signal. In this case very significant changes in performance due to distortion can occur due to flow profile effects within the engine, created as a consequence of AIP distortion transfer. Circumferential total-temperature profiles at high-pressure (HP) compressor and low-pressure (LP) turbine exits for a turbofan engine operating at constant HP compressor speed behind the screen-simulated distortion can be seen in Figure 88. The distortion pattern is shown in Figure 89. Significant performance changes would result if the engine were controlled to a fixed temperature limit using a single local sensor. The performance change would depend on the sensor location relative to the distortion pattern. This, in fact, occurred, as can be seen in Figure 90. The changes in normalized specific fuel consumption, gross thrust, airflow, and LP and HP compressor speeds were very significant. The data, which were derived from sea-level-static tests, are uncorrected for screen loss, which was constant for all screen positions. The data points were obtained by rotating the screen. Results obtained from turbofan engine tests where a fan pressure ratio control was being investigated appear in Figure 91. Significant changes in fan operating line position were observed for various screen positions.

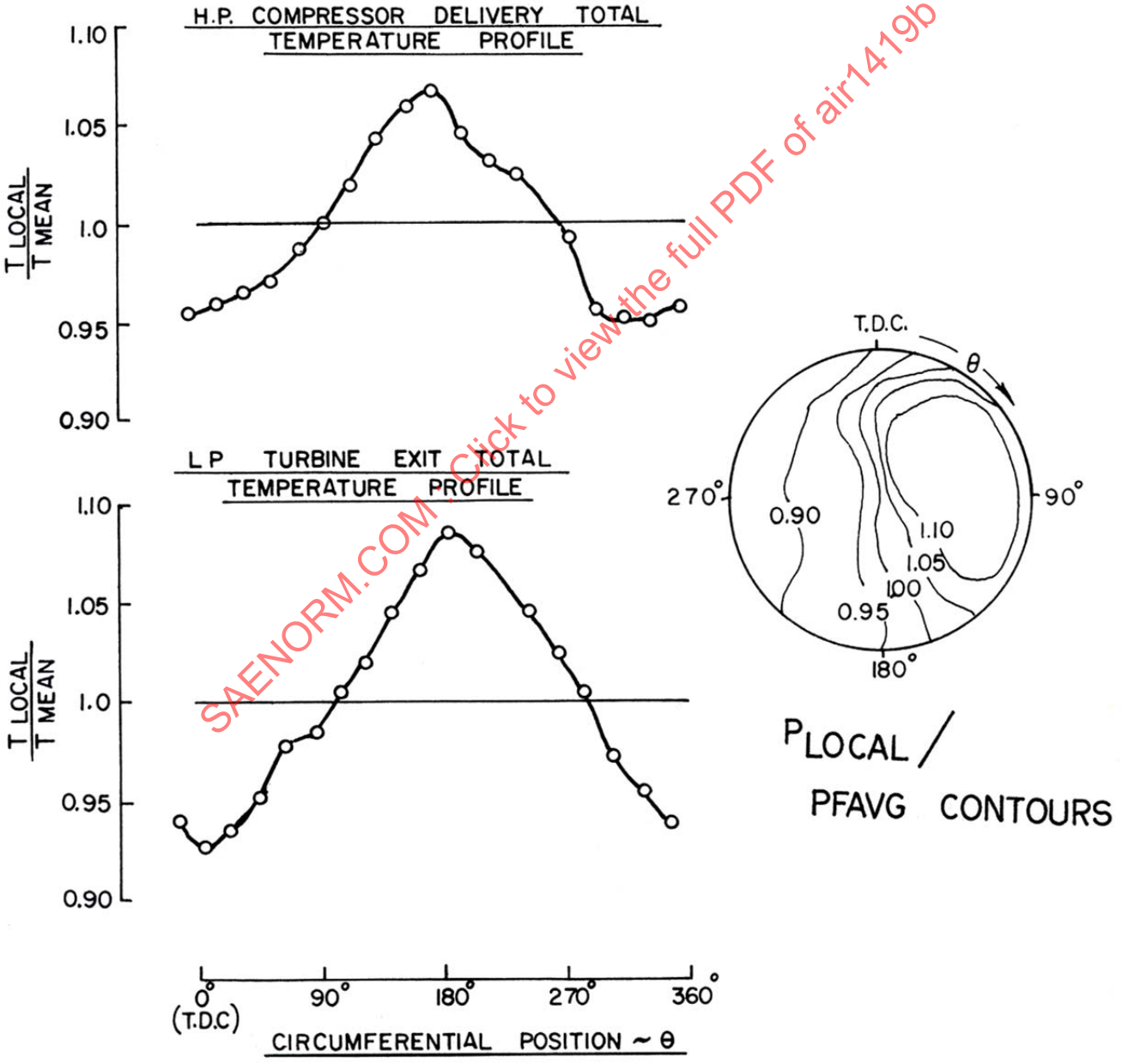

FIGURE 88 - TURBOFAN ENGINE PERFORMANCE WITH DISTORTION

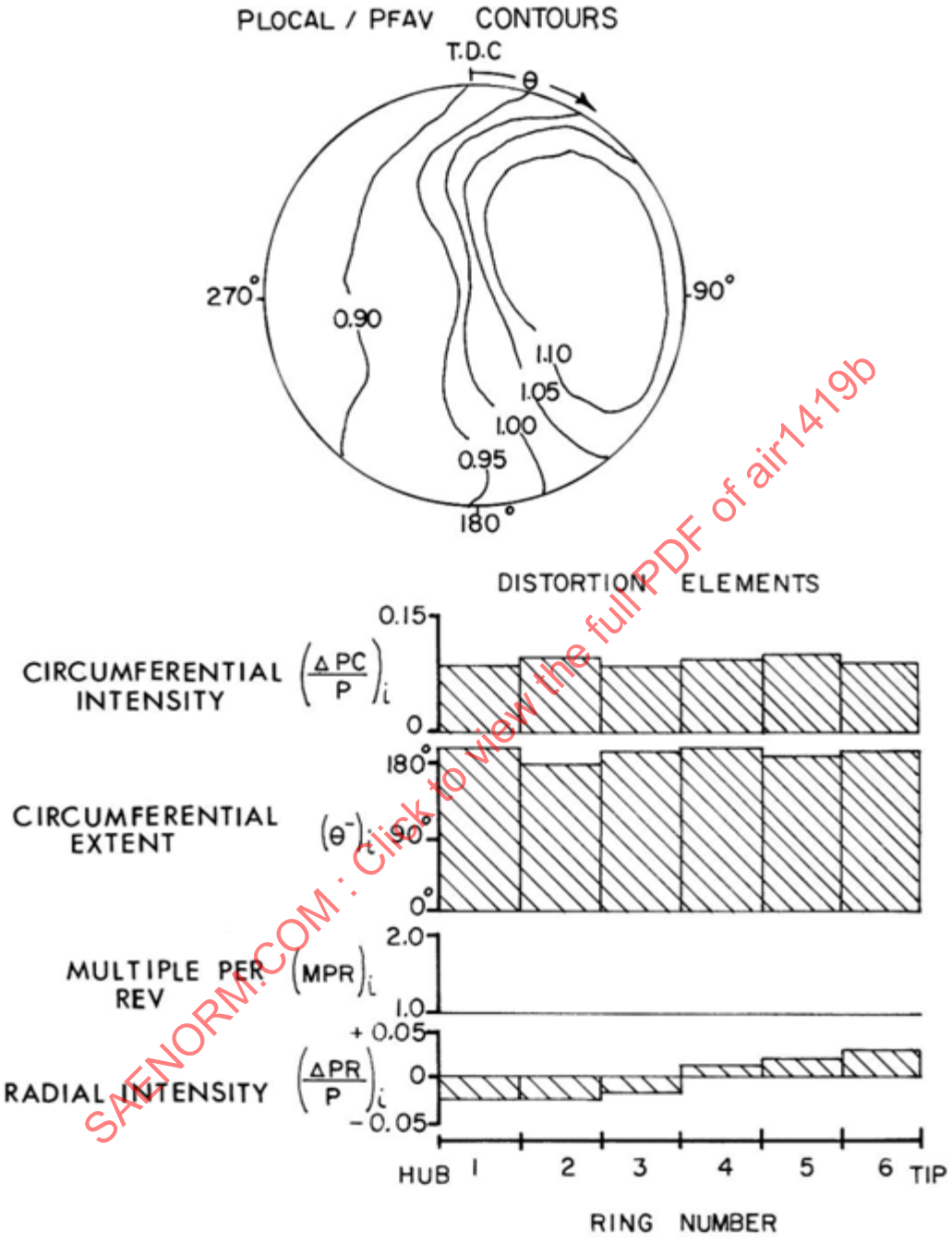

FIGURE 89 - SIMULATED INLET-DISTORTION SCREEN #2

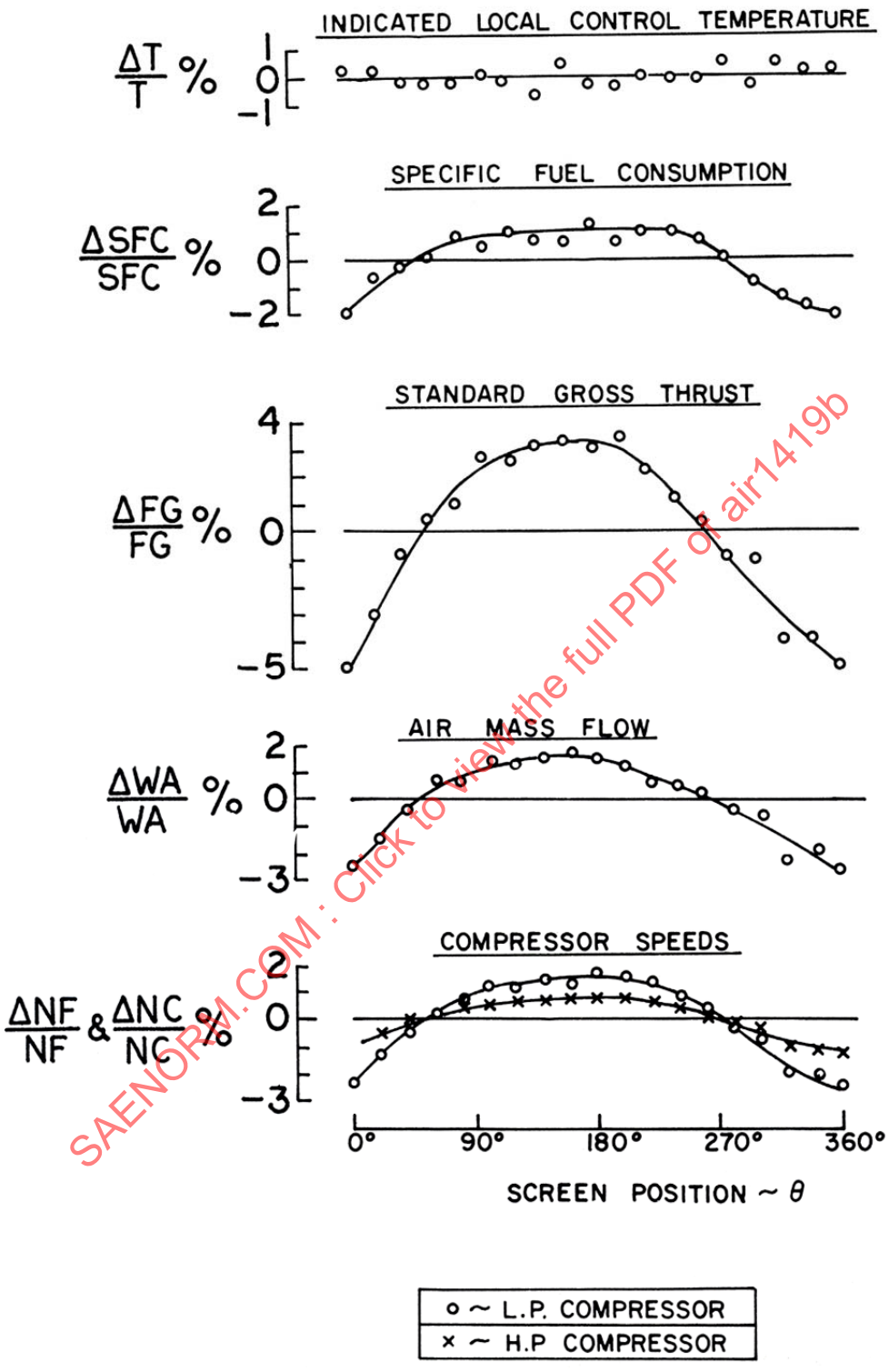

FIGURE 90 - TURBOFAN ENGINE PERFORMANCE - SCREEN POSITION EFFECT

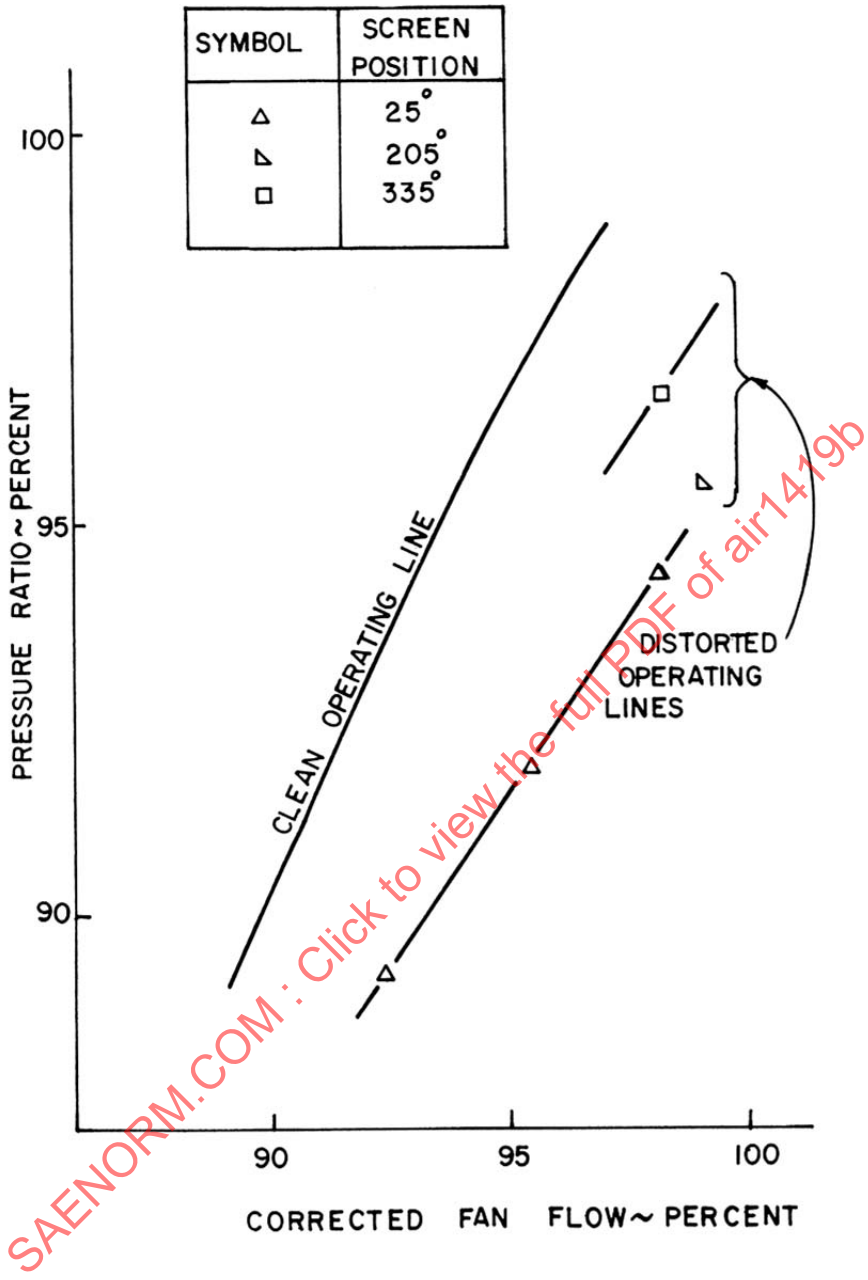

FIGURE 91 - EFFECT OF ENGINE SENSOR LOCATION

Compression system designs which incorporate variable geometry, e.g., variable stagger stator blading, may employ local flow sensors to schedule the geometry. In such cases, the effect of flow distortion on the schedule and the resultant change in component matching and overall engine performance should be evaluated.

The data illustrate that performance assessment procedures may need to account for circumferential distortion pattern position and that more than one screen position may need to be tested to cover multi-engine (mirror imaged) installations. Engine control mode and sensor selection studies should address the anticipated distortion characteristics. In view of the complexity of the question, engine tests would be necessary to account such effects with confidence.

6.3 Assessment Procedures

Procedures for assessing the effect of AIP total-pressure distortion on engine performance are part of the procedure for evaluating installed engine performance. A prime concern is to identify the technical need to account distortion effects explicitly. This need should be judged against performance and performance accuracy goals and the anticipated severity of the distortion problem. Each propulsion system should be considered on its own merits.

Assessment procedures for determining installed engine performance fall into two broad categories: Performance Synthesis and Performance Testing. Synthesis and testing activities interact. They are not sequential, and they evolve as updated information becomes available. A logic flow chart for the evaluation of installed engine performance is shown in Figure 92.

Performance synthesis activities include:

1. Assessments of baseline undistorted flow or uninstalled performance using estimated or empirical engine component data.

2. Assessments of installed performance based on AIP face-average pressure and engine component data.

3. Assessments of AIP distortion effects using component distortion response data.

Performance testing activities are organized to yield performance data for:

1. The uninstalled engine in undistorted flow. Programs may include sea level test stand and altitude test facility (ATF) testing.

2. The “installed” engine with simulated AIP distortion. Programs may include distortion tests on the sea level test stand and in the ATF with simulation of aircraft services, including bleed and power extraction.

3. The inlet plus engine. Programs may include sea level test stand and free-jet ATF testing.

4. The installed flight test engine.

Performance assessments are conducted at operational conditions defined in Table 11.

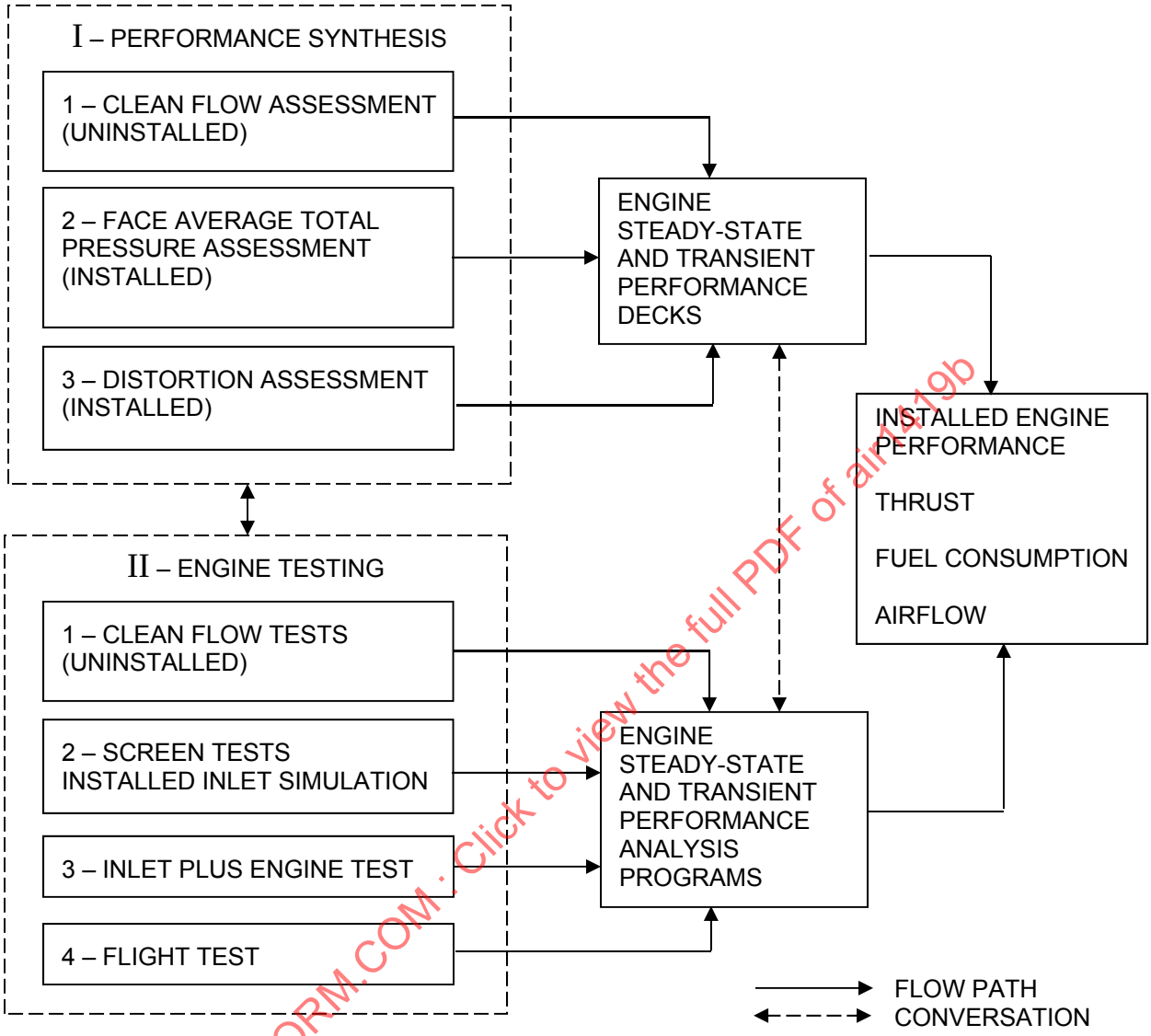

FIGURE 92 - INSTALLED ENGINE PERFORMANCE ASSESSMENT GUIDELINE

TABLE 11 - OPERATIONAL CONDITIONS

Aircraft	Inlet	Engine
Temperature	Configuration	Power Level
Altitude	Bleed	Service Bleeds
Flight Speed	Reynolds No./Scale	Power Extraction
Attitude (α, β)	Mass Flow	Afterburner
Thrust (Drag) Level		Thrust Reverse

6.3.1 Performance Synthesis

Synthesis methods are organized into steady-state and transient computer programs, or performance and handling decks, which incorporate engine component performance maps and matching and control logic in mathematical models of the engine. Treatments of uninstalled and installed engine performance based on AIP face-average total pressure are well established. For example, steady-state and transient performance presentations for digital computational programs are presented in Reference 2.1.1.4. Other relevant data are presented in References 2.1.1.5, 2.1.1.6, and 2.1.1.7.

In assessing installed performance on a face-average inlet pressure basis, engine rematching due to changes in inlet pressure level and in non-dimensional engine performance parameters is taken into account. The non-dimensional component performance maps correspond to undistorted AIP flow conditions. This implies that the effects of distortion on the non-dimensional performance maps (in particular, compressor maps) are assumed to be negligible. Rematching effects due to distortion are assumed to be small. Changes in engine internal flow profiles and distortion effects on the control system are assumed not to occur.

Synthesis outputs at matched inlet flow conditions are installed thrust, airflow, fuel consumption, aircraft performance parameters, and engine gas generator performance and control parameters.

The extent to which explicit distortion assessment procedures are incorporated into a performance synthesis methodology will depend on the particular propulsion system and initial assessments of the magnitudes of the performance changes likely to be involved. Experience may, for instance, indicate that distortion will not affect installed engine performance significantly and that detailed assessments will not be required. The quality of information on the inlet and engine available during the conceptual studies and preliminary design phases of the power-plant development will be relevant.

6.3.1.1 Inlet Recovery Guidelines

The need to account for distortion is indicated by the level of inlet recovery. A level close to 100% indicates a low performance effect, while low levels mean that distortion effects might be significant. This stems from the fact that recovery and distortion levels are often correlated in the inlet data. Loss of recovery may be used in face-average performance synthesis programs to establish performance sensitivity factors - Δ(Thrust)/ΔPFAV, Δ(Fuel)/ΔPFAV - at a given operating condition. Losses may be expressed relative to a standard inlet recovery schedule.

A first assessment of the effects of distortion on turbofan engines can be made by representing the AIP distortion as an equivalent OD (bypass) and ID (core) square-wave, radial, total-pressure distortion. Inlet OD and ID recovery factors may then be defined and input to engine performance decks incorporating split-flow fan characteristics, i.e., separate bypass and core-flow performance accounting methodology. Estimated distortion patterns and actual inlet patterns, if available, can be used, and parametric studies can be conducted. The OD/ID split line may be taken as the radial stream-tube corresponding to the matched engine bypass ratio.

$$\left(\frac{A_{core}}{A_{overall}}\right)_{AIP} = \frac{1}{1+BPR} \quad \text{(Eq. 85)}$$

For an ID (core) region having n instrumentation rings in the ID flow, the average ID total pressure is related to the face-average total pressure by:

$$\frac{(PAV)_{ID}}{PFAV} = \frac{1}{n}\sum_{I=1}^{n}\left[1-\left(\frac{\Delta PR}{P}\right)_i\right] \quad \text{(Eq. 86)}$$

and for the OD (bypass) region having (N-n) rings in the OD flow, the average OD total-pressure is given by:

$$\frac{(PAV)_{OD}}{PFAV} = \frac{1}{N-n}\sum_{i=n+1}^{N}\left[1-\left(\frac{\Delta PR}{P}\right)_i\right] \quad \text{(Eq. 87)}$$

where $\frac{n}{N}(PAV)_{ID} + \frac{(N-n)}{N}(PAV)_{OD} = PFAV$ and $\left(\frac{\Delta PR}{P}\right)_i$ are the distortion radial intensity elements.

The procedure is illustrated in Figure 93.

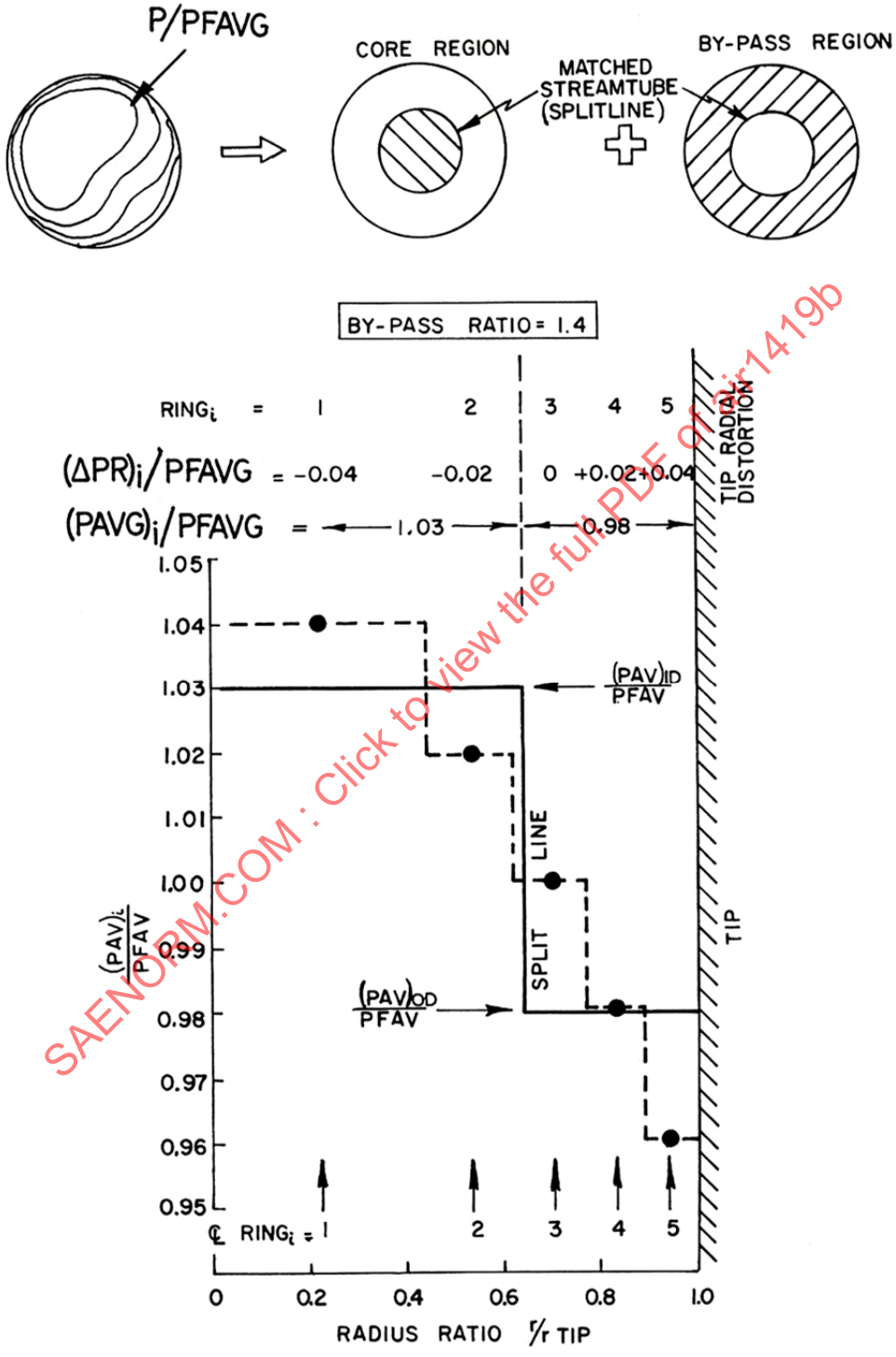

FIGURE 93 - SPLIT-FLOW AIP DISTORTION ANALYSIS EXAMPLE

An example performance synthesis output for a separate-flow two-spool turbofan engine operating at sea-level static, standard-day conditions, is given in Table 12. Thrust data for engine operation either at constant fan speed or constant jet pipe (LP turbine exit) total temperature are provided for cases where the inlet total-pressure loss is confined either to the bypass or the core flow region of the AIP (square-wave radial pattern). A local pressure loss of 10% was assumed. The effects on thrust are expressed in terms of thrust loss sensitivity factors and are compared to uniform flow thrust loss factors. Significant differences occur in the engine total thrust sensitivity, depending on the location of the total-pressure defect region and engine control mode. In this example, hub-radial distortion nearly doubled the thrust loss factor in the temperature-control mode. Data on engine internal temperature, pressure, spool speed, flow, bypass ratio, and fuel consumption changes can also be obtained as outputs.

TABLE 12 - TURBOFAN THRUST LOSS SYNTHESIS

ENGINE CONTROL MODE	CONSTANT FAN SPEED 100%			CONSTANT JET PIPE TEMPERATURE		
INLET RECOVERY LOSS REGION	OVERALL (UNIFORM LOSS) 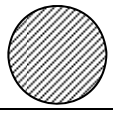	CORE 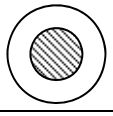	BY-PASS 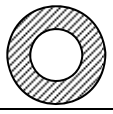	OVERALL (UNIFORM LOSS) 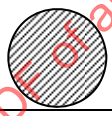	CORE 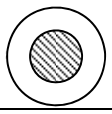	BY-PASS 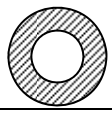
LOCAL RECOVERY LOSS ~ PERCENT	10 (DATUM)	10 (ID) 0 (OD)	0 (ID) 10 (OD)	10 (DATUM)	10 (ID) 0 (OD)	0 (ID) 10 (OD)
DISTORTION $\frac{PFAV - PAV_{ID}}{PFAV}$ $\frac{PFAV - PAV_{OD}}{PFAV}$	0 0	+0.0615 -0.0427	-0.0604 +0.0456	0 0	+0.0615 -0.0427	-0.0593* +0.0466
PFAV RECOVERY ~ PERCENT	10	4.1	5.7	10	4.1	5.6
THRUST LOSS ~ PERCENT	15.8	5.9	9.6	16.4	13.1	3.4
THRUST SENSITIVITY $\frac{THRUST\ LOSS\ \%}{PFAV\ RECOVERY\ LOSS\ \%}$	1.58 (DATUM)	1.54	1.73	1.64 (DATUM)	3.3	0.62
RADIAL DISTORTION $\frac{PAV_{ID} - PAV_{OD}}{PFAV}$	0	-0.104	+0.106	0	-0.104	+0.106
THRUST SENSITIVITY CHANGE ~ PERCENT	0	-0.04	+0.15	0	+1.66	-1.02

*Different bypass ratio from constant speed case due to engine component rematch

The example, which can be generalized to cover other distortion cases, illustrates three points of general interest:

a. Turbofan performance synthesis programs can provide valuable and timely quantitative indications of the effect of distortion on engine performance for defined AIP patterns - inlet type or parametric patterns - and engine control modes.

b. Performance changes can be correlated with numerical distortion descriptors (results in Table 12 may be expressed as differences).

c. Such correlations are only valid for a specified class of distortion so that care is required when attempting generalized correlations. Different results would be obtained for different ID/OD total pressure distributions.

Appropriate provisions for engine component rematching at specified propulsion system operating conditions should be included in the computational system.

6.3.1.2 Distortion Data Use

The assessment outlined above accounts for engine component rematching and control interactions but uses undistorted or clean-flow component non-dimensional performance maps and excludes the potential effects of distortion on engine control sensing in the mathematical modeling.

Assessments of the performance effects of AIP distortion can be updated during the development phase when the effects of distortion on engine component performance maps - in particular those of the compression system - are available from component rig and engine tests. Distortion test results then can be used in higher-order mathematical models appropriate to the powerplant under development.

Numerical assessment programs using empirical distortion data should provide for the following inputs:

a. Numerical AIP distortion descriptor elements.

b. Performance-related AIP distortion parameters. (These combined descriptor elements are not necessarily the same as those for stability assessments.)

c. Performance changes within compressor, main combustion, turbine, afterburner, and nozzle components.

d. Control system effects.

A logic flow chart illustrating alternate procedures for synthesizing engine performance changes due to distortion is shown in Figure 94. The main points of this procedure are:

a. Distorted compressor performance maps, available from compressor rig tests with a given AIP distortion pattern, can be directly input to the steady-state computer programs (Reference 2.1.1.4) as an alternative to the undistorted flow map, to enable matched thrust, fuel consumption, airflow and other engine performance variables to be determined. The impact of distortion can be established by comparing face-average assessment outputs. This procedure is an important turbofan assessment option where ID/OD rematching is important. Split-flow fan performance characteristics are required in this case.

b. Compressor distortion-response data for a given AIP pattern can be expressed incrementally as changes in corrected airflow, $\Delta W\sqrt{\theta_t}/\delta_t$, and efficiency, $\Delta\eta$, for specified compressor operating conditions. The increments may be functions of several relevant compressor flow variables, for example, Nc and PR (Figure 82). Separate terms for ID and OD flows may be necessary for assessing turbofans. The component performance increments may be used as input data to the engine matching program to provide absolute or normalized engine performance with inlet distortion.

c. Compressor flow and efficiency increments may be correlated with the distortion descriptors at specified compressor operating conditions provided a suitable background of component testing has been conducted. Correlated changes may be input to the engine matching program. This procedure is straightforward for turbojet engine assessments. However, care is required in turbofan applications to assure correct ID/OD matching. Distortion transfer data applied to downstream components provide similar input data to the engine matching program, which may need to provide for estimating the effects of flow profile changes on engine control functions.

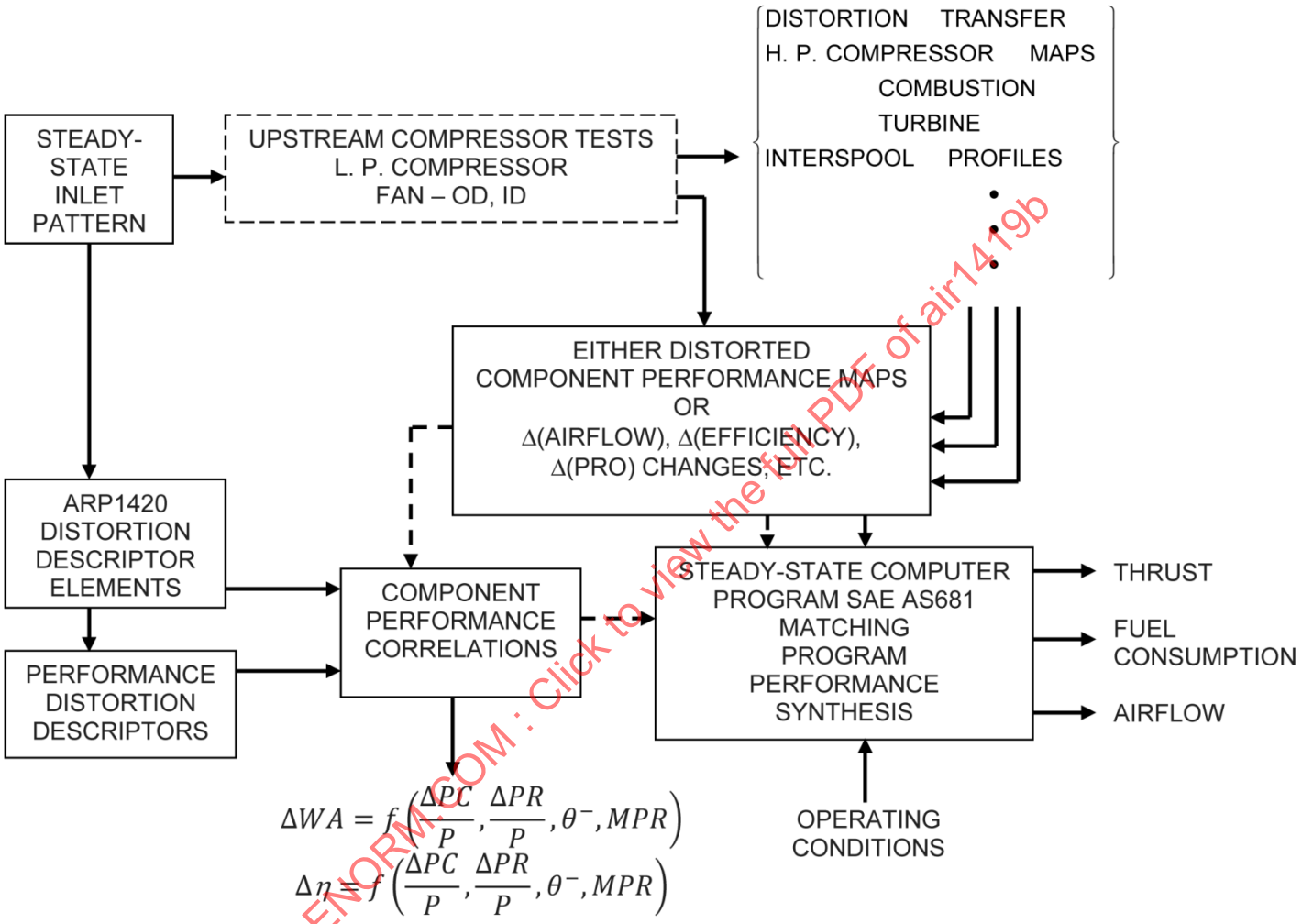

FIGURE 94 - STEADY-STATE PERFORMANCE ASSESSMENT WITH INLET DISTORTION

A flexible approach to the organization of performance synthesis procedures should be adopted whenever possible in order to facilitate program options.

6.3.2 Performance Testing

Engine and engine component tests with distortion provide data essential for the assessment and validation of distortion effects on installed engine performance. Component and engine test data acquisition should be regarded as complementary processes. Test planning and implementation guidelines are presented in Section 7 together with a discussion of available test techniques.

General points relevant to data acquisition for performance assessments are:

a. Engine tests provide data for installed components and extend rig experience to include the effects of component interactions (rig-engine interference terms).

b. Engine tests provide development data on flow profile/control system sensor interactions for appropriate patterns and pattern positions, which may affect control system design.

c. Measurement repeatability and accuracy in rig-component and engine tests are primary considerations as the quantification of performance changes due to distortion essentially involves measuring small differences between large quantities. The validity of performance loss/distortion data correlations and the amount of testing required to establish meaningful performance changes rest heavily on the measurement technology employed. Assessments should be accompanied by uncertainty analyses.

d. AIP distortion patterns tested for performance should correspond to inlet patterns representative of prime mission performance points.

e. The need for tests at distortion levels high enough to produce measurable performance changes should be considered.

f. The effects of screen loss on engine rematching, in particular for unchoked nozzle operation, need to be isolated if distortion-induced performance changes are to be accounted for explicitly. This may require uniform screen testing through the requisite test flow range.

g. Adjustments to nominal test conditions (for example, screen inlet pressure levels) may be required to account for screen losses over the test flow range and provide controlled performance assessment data.

Assessment data acquired from inlet-plus-engine ground facility tests, flying test beds, and flight development prototype aircraft are included implicitly in measurements made with gas path instrumentation. The quality of flight-test performance assessment data will depend on the extent to which instrument calibrations include the effects of AIP distortion. The increased trend towards the use of on-board diagnostic and monitoring data systems provides means for acquiring engine performance in service operation.

6.4 Time-Variant Distortion

Current methods of accounting for the effects of steady-state total-pressure distortion at the AIP on steady-state engine performance use time-averaged data from the low-response instrumentation located at the AIP. Available information is insufficient to define the effect of time-variant AIP total pressure distortion and PFAV fluctuations on steady-state engine installed thrust, fuel consumption, and airflow. At typical mission performance points, AIP distortion data indicate that turbulence levels are low and the performance effect minimal.

Data available from compression component rig tests indicate that the time-averaged performance may be affected by time-dependent flow (References 2.2.7 and 2.2.8). Random AIP flow fluctuations may cause losses of corrected flow in the order of 1% ± 0.5% RMS total-pressure amplitude (filter range 0 to 1500 Hz). The test results indicate that compressor performance responds to a wider turbulence frequency range than compressor stability.

7. DISTORTION TESTING

Tests provide the technical data base for the development and verification of the stability and performance assessments discussed in Sections 5 and 6. The validity of the assessments depends on the quality of the data base generated during the test effort. A program, with techniques defined in terms of the instrumentation, data management, equipment, procedures, and analysis and communication of results, should be established by all involved parties to assure maximum utilization of the data.

The primary objectives of distortion tests are to define the flow distortion characteristics of the inlet and to quantitatively determine the effects of distortion on the stability and performance of the engine. The scope of the test effort must be tailored to the specific needs of the propulsion system. The extent and type of the tests must be balanced with regard for system requirements, program milestones, program risk assessments, program schedules, and cost constraints. Tests may be required on inlet and aircraft components, engine and engine components, and the propulsion system. Information acquired from these tests decreases the risk of incompatibility between the inlet and engine as propulsion system development progresses (Figure 95).

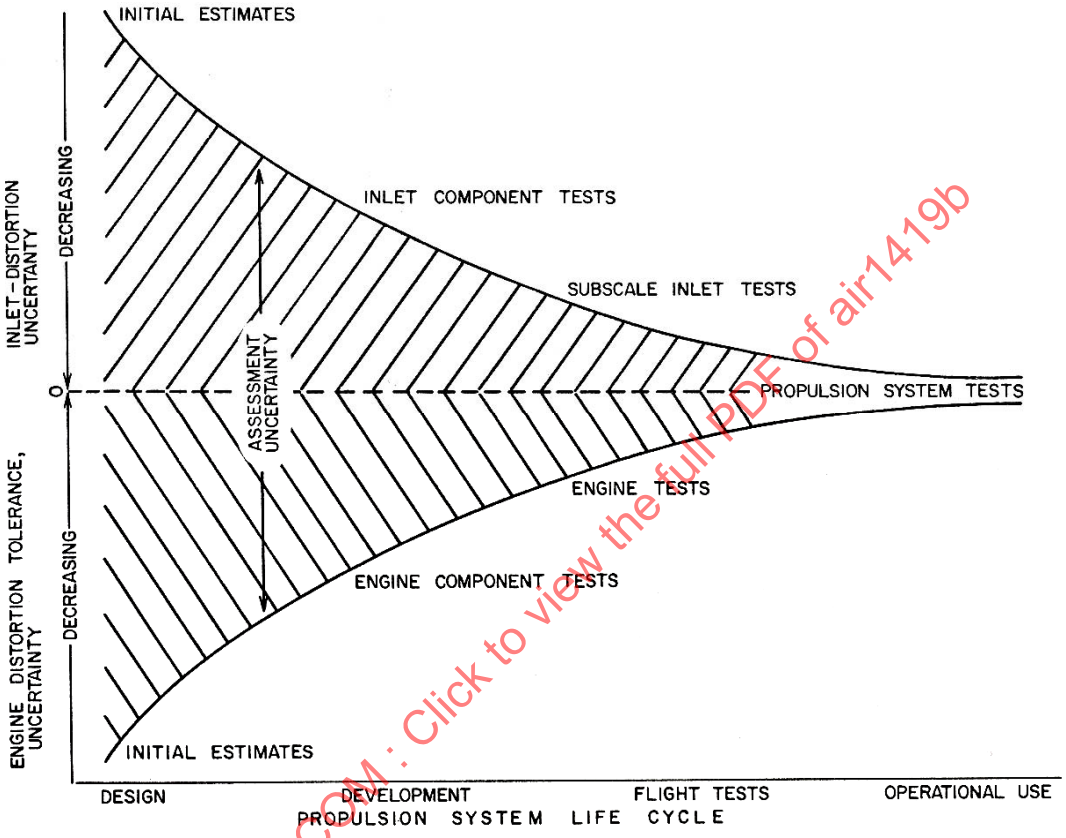

FIGURE 95 - DISTORTION ASSESSMENT UNCERTAINTY DURING PROPULSION SYSTEM LIFE CYCLE

7.1 Inlet and Aircraft Component Tests

A purpose of the inlet system is to supply the desired quantity and quality of air to the engine. A well-constructed inlet development program is necessary to identify appropriate performance, weight and cost trades. The tests required depend on the degree of complexity and risk associated with individual designs. Highly integrated systems, involving significant advances in the state-of-the-art, may require tests that extend over a period of years. With a concomitant engine development program, time phasing and appropriate information exchanges become critical to the development of an optimal system. In less complex programs, or where a higher degree of technical risk is acceptable, limited tests over a relatively short time period may be adequate.

A checklist, identifying test objectives during various stages of the inlet development program, is given in Table 13. Appropriate wind tunnel models, test facilities, major independent test variables, and data requirements are summarized. Tests are grouped in three major categories: (1) inlet development tests, (2) inlet verification tests, and (3) full-scale, inlet-engine compatibility tests. Individual aircraft development programs may require the use of various combinations of these tests.

Inlet/aircraft models of differing scales are tested in a number of facilities to acquire inlet data. Model scale, Reynolds number, and facility type can all introduce uncertainties in the data. Tests with short subsonic inlets have indicated that the distortion in flight may be significantly different from the distortion measured in scale model tests due to the effect of engine pumping, Reynolds number, and other wind-tunnel-to-flight differences. Data in Reference 2.2.9 show that engine pumping substantially reduces distortion following separation at high angles of attack. It appears that these effects are most significant in close-coupled installations such as those utilized in commercial aircraft. Programs on conventional supersonic inlets indicate that, with sufficient attention to detail, good correlation can be obtained between subscale and full-scale model tests for selected inlet configurations (References 2.2.10 to 2.2.12). The data indicate that Reynolds number effects on inlet distortion due to model scale and/or tunnel conditions were negligible at static and subsonic conditions, provided Reynolds number is sufficiently high to preclude non-representative flow and separation in the inlet duct. Full-scale test article data at high Reynolds number showed higher total-pressure recovery and slightly lower distortion compared to results with sub-scale models. Comparable results were obtained in both blowdown and continuous wind tunnel facilities.

Flight test and wind tunnel results are compared in Reference 2.2.12. Distortion patterns recorded during flight tests were found to be similar to wind tunnel results obtained during static, subsonic and supersonic operation. Flight data resulted generally in slightly higher total-pressure recovery and slightly lower total-pressure distortion than recorded during comparable wind-tunnel conditions. These differences were smaller than the differences recorded among different aircraft at comparable operating conditions. Results, comparing data from full-scale inlet/engine tests with data from “cold pipe” (no engine present) tests, indicated that the effects on total-pressure recovery and distortion were negligible. The latter result is attributed to good simulation of the acoustic impedance of the engine achieved by locating the choking station (used for airflow control) close to the AIP.

7.1.1 Inlet Development Tests

Small-scale inlet test results are used to define the inlet/forebody configuration. Tests to evaluate the inlet in terms of the flow quality at the AIP, to evaluate inlet drag, to identify appropriate trades, and to optimize performance are described in this section.

7.1.1.1 Internal Performance

Internal performance (defined by total-pressure recovery and distortion at the AIP, airflow, and the inlet operating stability limits) is obtained from (1) isolated-inlet tests, (2) subsonic-supersonic inlet/forebody tests, and (3) low speed inlet/forebody tests. These tests are described separately in Table 13. However, no single test accomplishes all the stated objectives. In practice, the design process is iterative and requires more than one wind tunnel entry. Each test generates data that are used to modify the configuration for the next test. Tests are conducted with small-scale models to permit the use of less expensive test facilities. To a great extent, model size is determined by wind tunnel capability, but the model should be at least 1/10 scale to achieve accurate geometric similarity. Typically, the allowable projected frontal area of models required to simulate the downstream aerodynamic environment should be approximately 1% of the cross-sectional area of the test section. The allowable model size for tests in which only the inlet conditions need be simulated can be approximately 15% of the cross-sectional area of the test section. Of paramount importance during the conduct of any inlet test is the accurate measurement of inlet mass flow. This parameter is the primary correlation variable between various types and categories of tests and from subscale to full scale.

CFD and empirical methods are usually employed to estimate initial inlet performance. Initial inlet tests may be performed with an isolated inlet model in a facility that permits frequent access to the model. Geometry, flight Mach number and engine airflow are duplicated. The tests update the initial configuration evaluation and performance estimates. Alternate geometries (ramp, sideplate, diffuser, internal line, cowl lip) are evaluated. Limited dynamic instrumentation is used to identify potential distortion problems. The tests provide sufficient data to permit detailed configuration development.

An example of an isolated-inlet test facility is shown in Figure 96. The subsonic diffuser model was built to evaluate the internal performance of various inlet duct configurations. Total pressure recovery, steady-state distortion, and RMS pressure levels were measured by a 40-probe rake mounted at the simulated engine face station. Internal components could be changed easily to evaluate different diffusers. Other low-cost techniques are also available for investigating subsonic diffusers. One method, employing an altitude chamber as a vacuum source, is described in Reference 2.2.13.

Inlet/forebody models, tested at low speed, subsonic and supersonic conditions, are configured with a forebody, a wing stub, if required, any forward control surfaces, and other aircraft features which affect the flow forward of the inlet. Flow-field tests are performed to measure the local Mach number and the flow direction of the air entering the inlet. For some tests, the inlet is replaced by a rake of flow-field probes and is tested over the Mach number and attitude range. Flow-field data are used to optimize inlet placement and orientation. CFD has largely replaced this type of testing.

TABLE 13 - INLET AND AIRCRAFT COMPONENT TESTS

Model/Facility/Test Variables	Data	Objectives
Inlet Development Tests		
A. Isolated Inlet Model 1. Inlet Alone (Scale > 0.1) 2. Blowdown Wind Tunnel 3. Mach, Inlet MFR, Geometry	Steady-State AIP Pressures Limited Turbulence Engine Airflow	Inlet Sizing Internal Diffuser Lines Cowl/Sideplate Arrangements Initial BLC Configurations Bypass/Auxiliary Inlet Configurations Inlet Stability Characteristics Buzz Frequencies/Amplitude Ramp Configurations Inlet Shielding Devices for Radar Cross Section (RCS)
B. Subsonic-Supersonic Inlet/Forebody Model 1. Inlet/Forebody with Fwd A/C Control Surfaces/Wing Stub (Scale > 0.1) 2. Blowdown Wind Tunnel 3. Mach, α, β, Inlet MFR, Bleed Airflow, ECS Airflow, Geometry	Steady-State AIP Pressures High-Response AIP Pressures Engine, Bleed, ECS Airflows Static Pressure Distribution	Initial Subsonic/Supersonic Inlet Performance and Distortion Characteristics Boundary Layer Gutter Development Inlet Flow Field Inlet-to-Inlet Interdependence Inlet Control Sensor Locations Inlet Control Schedules Maneuver Envelopes Bleed Separation & Exit Configurations A/C Control Surface Vortex Ingestion Bypass Configurations ECS Scoop Configurations Inlet Shielding Devices for RCS Inlet Stability Limits External Stores Inlet/Engine Airflow Matching
C. Low-Speed Inlet/Forebody Model 1. Same Model as B.1. Above 2. Low Speed, Continuous Wind Tunnel 3. Mach, α, β, Inlet MFR, Geometry	Steady-State AIP Pressures High-Response AIP Pressures Engine Airflow Static Pressure Distribution	Initial Static/Take-off (Mach < 0.2) Performance & Distortion Characteristics Auxiliary Inlet Arrangements Ground Plane Effects Crosswinds Nose Gear Wake Ingestion Wing Slat Effects Off-Schedule Ramp Geometry High α/β Operation to Support A/C Stall Investigations
D. Drag Models 1. Complete Aircraft Model with Appropriate Portions of Inlet on Force Balance (Scale < 0.1), Forebody Model, or Aerodynamic Model to Obtain Spillage Drag 2. Continuous and/or Blowdown Wind Tunnel 3. Mach, α, β, Geometry	Inlet Drag Components External Static Pressures	Drag Data to Support Inlet Configuration Trades and to Estimate Installed Performance
Inlet Verification Tests		
1. Inlet/Forebody with Fwd A/C Control (Scale ≈ 0.2) 2. Continuous Wind Tunnel 3. Mach, α, β, Inlet MFR, Bleed Airflow, ECS Airflow, Geometry	Steady-State AIP Pressures High-Response AIP Pressures Engine, Bleed, ECS Airflows Static Pressure Distribution	Critical High-Response Distortion Patterns and Levels Reduced Bleed Requirements Inlet Performance Over Flight and Maneuver Envelopes Wake/Vortex Ingestion Envelopes Duct Loads – Hammershock Weapon Bay Doors – Spoilers External Stores Refined Control Schedules External Pods, Scoops Inlet Shielding Devices for RCS Refined Inlet Control Sensor Locations Bypass Door Operation
Inlet/Engine Compatibility		
1. Full-Scale Inlet Model and Prototype Inlet Control, Prototype Engine and Control Tests Consist of 3 Phases: a. Inlet Alone b. Inlet Plus Inlet Control (No Engine Present c. Inlet Plus Inlet Control (Engine Present) 2. Continuous Wind Tunnel 3. Mach, Limited α, Inlet MFR, Geometry, Distortion	Steady-State AIP Pressures High-Response AIP Pressures Inlet/Engine Airflows Inlet Static Pressures Full Engine Instrumentation	Inlet/Engine Compatibility Demonstration Inlet Control Operation Inlet Control Response Rates Engine Control Sensitivity to A/C Distortion Inlet Stability Limits Engine Throttle Transients Hammershock Loads Vortex Ingestion Engine Distortion Tolerance Flight Test Instrumentation Checkout

More than one series of inlet/forebody tests may be necessary to acquire the internal performance data. Tests are conducted over the full range of flight conditions from static operation to high Mach number. A full complement of low- and high-response AIP instrumentation is employed to obtain distortion data. All parts of the aircraft that affect the inlet internal operation are duplicated.

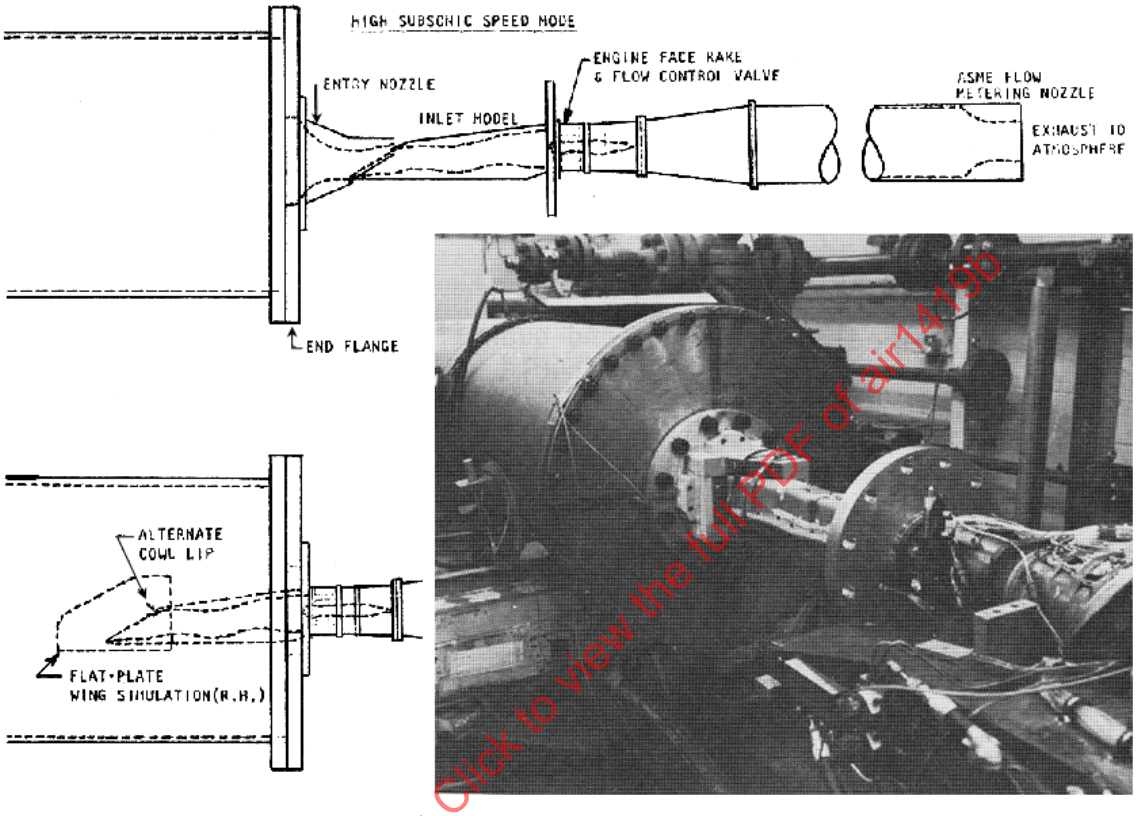

FIGURE 96 - SUBSONIC DIFFUSER MODEL FOR INVESTIGATING INTERNAL PERFORMANCE

As an example, a 0.10-scale B-1 model with a single nacelle dual-inlet design mounted to a complete fuselage forebody with stub wings is shown in Figure 97. A weapons bay just forward of the nacelle is simulated. This model was used to determine the effects of weapons bay doors and external stores on inlet performance. Tests were conducted to define inlet performance in detail, identify the effects of the aircraft and adjacent inlets, define the inlet control requirements, and provide data to refine the initial design.

Diagnostic testing in a low-speed (Mach 0.2) wind tunnel can also be of value for screening configuration changes. Use of the low-speed tunnel permits the use of a large-scale model in a continuous flow environment. Flow visualization tests of the diffuser can be conducted. In addition, AIP steady-state instrumentation can be used as an evaluation tool. These tests permit assessment of inlet changes in the presence of a flow field and are relatively inexpensive.

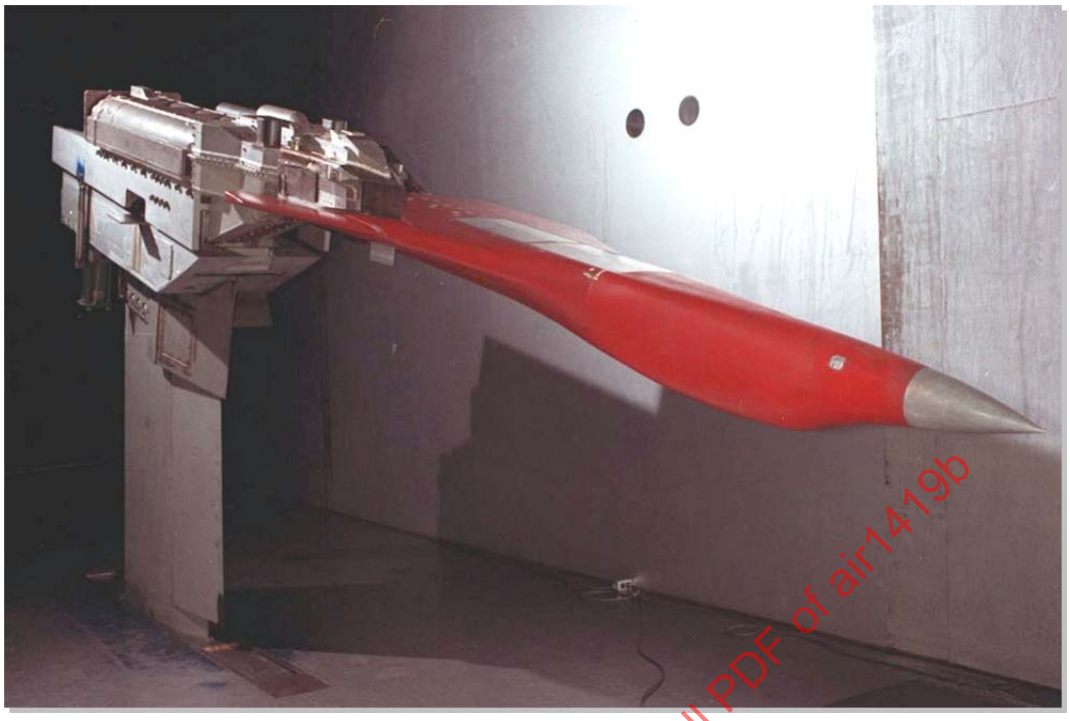

FIGURE 97 - INLET/FOREBODY WIND TUNNEL MODEL

7.1.1.2 External Performance

The tests described above define and quantify the factors which affect internal performance. Concurrently, tests should be conducted to evaluate external performance which includes all drag items chargeable to the inlet (inlet spillage drag, bypass drag, bleed drag, and any interference effects of the inlet flow on aircraft drag). Because testing requires a complete aircraft model and the external flow field is important, the model is generally smaller than the internal performance model. It is designed with several internal balances and extensive static pressure instrumentation to evaluate the drag associated with the inlet. These tests provide drag data to evaluate configuration changes resulting from the internal performance tests as well as providing data for overall aircraft performance assessments.

As an example, a 0.07-scale B-1 inlet drag model is shown in Figure 98. This model represents the left-hand dual inlet nacelle mounted to the fuselage forebody. Fuselage structural mode control vanes, stub wings, and the opposite-side flow-through nacelle are simulated. Model drag is measured by an internal force balance supporting the metric portion of the system. The model provides incremental inlet drag data for installed engine performance calculations.

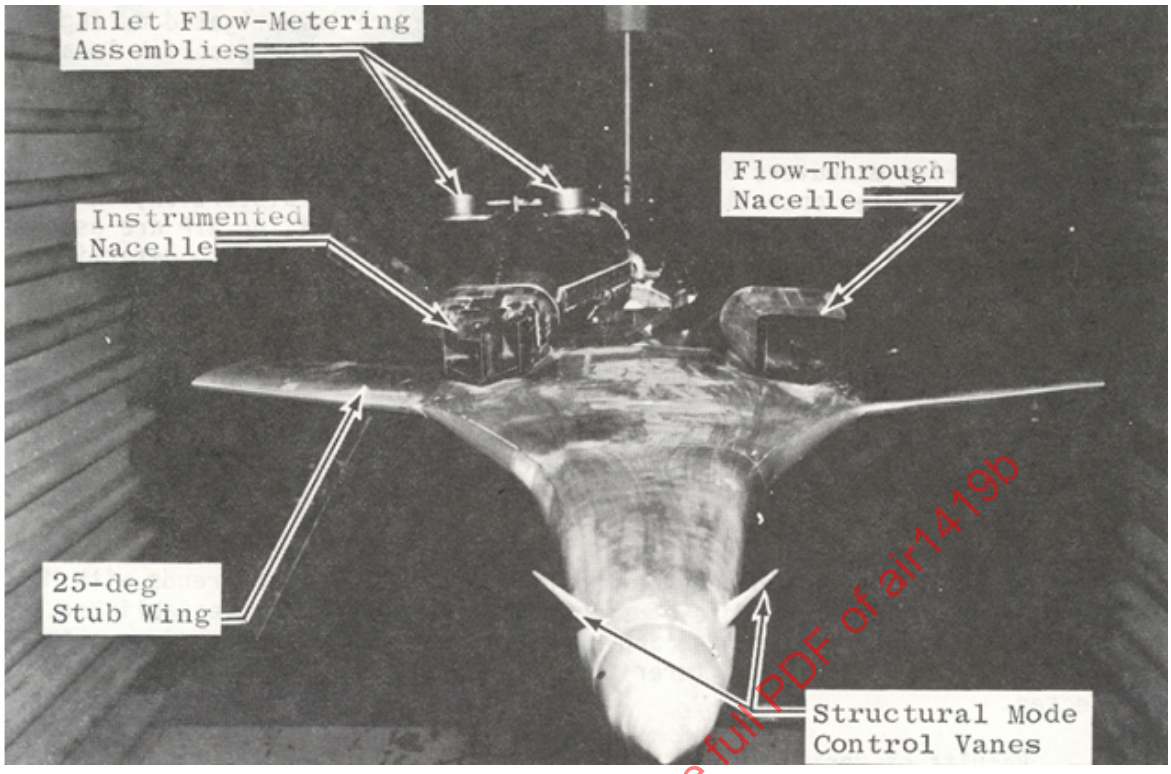

FIGURE 98 - INLET DRAG WIND TUNNEL MODEL

7.1.2 Inlet Verification Tests

This test phase provides the final subscale evaluation of inlet internal performance. Model size is usually 15% scale or larger to assure that all forebody and other parts of the airframe which may influence the inlet flow field are represented. The overall purpose of verification tests is to define the inlet performance characteristics throughout the required Mach number, angle-of-attack, sideslip angle, and corrected airflow ranges. Items that affect the inlet are optimized. The model should fully represent each configuration item that has a potential influence on inlet operation. This requires that all scoops, vents, exits, and protuberances be simulated. As an example an F-18E/F model, constructed for this type of testing, is shown in Figure 99.

Auxiliary air induction systems, environmental control system inlets, radar cooling circuit scoops, gun bay purge devices and any system exhausts that may influence the inlet flowfield are evaluated during the tests. Flow and recovery characteristics are established as functions of speed and angle of attack. The effects of wake and shock ingestion from adjacent structures are evaluated. Typical items include flight-test or production noseboom, landing gear, auxiliary tanks and pods. An evaluation of aircraft protuberances should be made. Items include angle-of-attack vanes, total-pressure and total-temperature probes, and antennae.

FIGURE 99 - 0.176-SCALE F-18E/F MODEL USED FOR INLET VERIFICATION TESTS

Alternative inlet control-sensor locations are investigated during the tests. Several options can be evaluated simultaneously to establish locations that best provide the desired signals. Boundary-layer-bleed systems should be refined to minimize inlet drag. The inlet bypass system maintains satisfactory inlet operation during maneuvers while minimizing the total system drag (inlet spillage and bypass) for non-maneuvering conditions. Calibrated mass-flow measurements are required. Inlet operation in buzz is investigated. Distortion, in-phase pressure oscillation amplitudes, and frequency content at the AIP are used to evaluate engine response. Static pressure loads are obtained to determine structural design criteria for the inlet.

Instrumentation for the inlet verification test phase is comprehensive. Low- and high-response static-pressure taps are located in the bleed and bypass systems and in the diffuser. The AIP is fully instrumented with both low- and high-response total-pressure probes. Static pressure taps at the AIP can provide further useful information. High-response instrumentation may be required in auxiliary air induction systems to determine if pressure oscillations occur.

Digitized peak time-variant distortion data will provide patterns for stability evaluation by the engine manufacturer. Distortion trends with Mach number, angle of attack, angle of sideslip, and mass flow are established. Inlet recovery, stable-airflow range, and steady-state distortion data are obtained for use by the engine manufacturer to determine whether engine performance is affected.

Results of verification tests are used to establish the final design of the inlet, including control schedules, bleed and bypass requirements, and external flow field effects. Definitive flow distortion and recovery levels are obtained for the final design.

7.2 Engine and Engine Component Tests

Engine and engine component tests are required to develop and verify the initial (design phase) assessments of the effects of inlet distortion on engine performance and stability. The tests that may be required are based on three engine-inlet AIP flow conditions: uniform, steady flow (7.2.1), steady-state distorted flow (7.2.2), and time-variant distorted flow (7.2.3).

Candidate engine and engine component tests are shown in Table 14. The primary objective and data requirements for each type of test are outlined. Since inlet flow distortion may affect the basic aerodynamics of a number of engine components as well as interactions between those components and the engine control system, testing of the engine components (primarily the compression system components) and the engine is usually required.

TABLE 14 - ENGINE COMPONENT AND ENGINE TESTS

OBJECTIVES	TESTS	DATA
Develop Flow Stability Define Descriptor(s) Define Control Sensor Locations Evaluate Off-Schedule Geometry Evaluate Bleed Effects Evaluate Reynolds Number Effects	Compressor Rig/Diffuser Test with Classical and Flight Patterns	Stability Pressure Ratio Airflow Efficiency Exit Profiles Distortion Sensitivities Control Tolerance Distortion Transfer
Define Spool Interactions	Dual Spool or Engine Tests with Distortion Burner Rig Tests with Distortion	Spool Supercharging Bypass Ratio Shifts Speed Mismatch Stability Pressure Ratio Airflow Efficiency Exit Profiles Distortion Transfer Distortion Sensitivities
Evaluate Compressor-Burner Interactions Define Control Sensor Locations	Burner Rig Tests with Distortion	Burner Pressure Loss Exit Temperature Profiles Exit Pattern Factor Rich/Lean Fuel/Air Limits
Define Augmentor Stability Define Control Sensor Locations	Augmentor Rig Tests	Exit Total Pressure and Temperature Pressure Transients Rumble and Screech Light and Blowout
Define Control System Destabilizing Effects	Engine Tests with PLA Transients and Flight Trajectory Transients Fuel System Stability Checks	Linkage Rates Travel Limits and Lags Compressor Operating Lines Fuel Pressure Pulsations Control Tolerance
Define Engine Stability and Performance	Engine Tests with Classical Patterns and Flight Patterns Installation Effects at Critical Flight Conditions	Stability Limits Airflow(s) Efficiency(ies) Distortion Transfer Speed(s) Thrust Specific Fuel Consumption (SFC)
Define Response to Time-Variant Distortion	Engine Tests with Time-Variant Distortion	Stability Limit Critical Compressor Airflow
Define Response to Special User Requirements	Engine Tests with: Water Ingestion Steam Ingestion Hot Gas Ingestion	Stable Operating Range

Direct-connect test facilities provide controlled inlet flow conditions to the engine and are generally used for developing and verifying compressor and engine stability and performance. It is neither technically nor economically feasible to obtain sufficient data for in-depth assessments from free-jet or flight tests of the propulsion system.

Inlet flow distortion may significantly affect engine mechanical integrity and life. Experience indicates that distortion may increase the risk of exceeding turbine nozzle and blade temperature limits, promote forced compressor rotor vibration and coupled blade-disk-mode excitation, increase stator stress loads, and affect compressor flutter onset limits (References 2.2.14 to 2.2.17). During engine tests with inlet distortion it is necessary to ensure that engine component stress and temperature limits are not exceeded. The aeromechanical limits of the engine components, such as the compressor operating limits shown in Figure 100 (Reference 2.2.17), must be considered in test program planning.

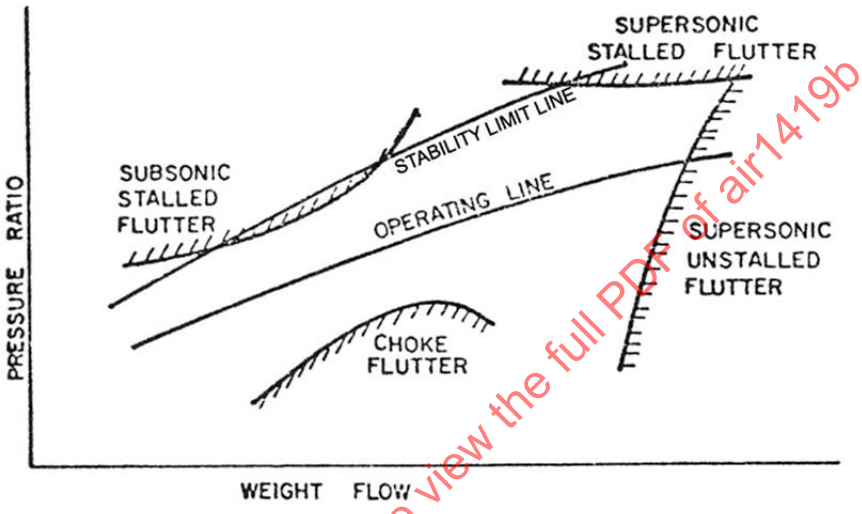

FIGURE 100 - COMPRESSOR MAP SHOWING BOUNDARIES OF FOUR TYPES OF FLUTTER

7.2.1 Uniform Steady-State Inlet Flow

Testing with uniform and steady inlet flow establishes the baseline performance and stability of the engine and engine components. Uniform steady-state inlet flow conditions are defined as those conditions having low steady-state and time-variant total-pressure and total-temperature distortion. Studies (Reference 2.2.18) have defined uniform steady-state flow quality goals as:

$$\frac{P_{MAX} - P_{MIN}}{P_{AVG}} < 0.01 \qquad \text{(Eq. 88)}$$

$\left(\frac{\Delta P}{P}\right)_{RMS}$ < 0.01 in the frequency range 0 to 1000 Hz;

$$\frac{T_{MAX} - T_{MIN}}{T_{AVG}} < 0.005 \qquad \text{(Eq. 89)}$$

$\left(\frac{\Delta T}{T}\right)_{RMS}$ < 0.005 in the frequency range 0 to 1000 Hz.

Compressor rig tests usually take place early in an engine development program and precede engine tests. They provide a flexible means for evaluating the effects of distortion over a range of throttle conditions using comprehensive instrumentation.

An example of a typical single-spool, single-discharge compressor rig is shown in Figure 101. The facility includes a large intake plenum, an inlet bellmouth, and a low-volume, quick-opening throttle valve. The first two items provide high quality airflow at the compressor face and the third allows rapid surge recovery. The rig tests define the performance of the test compressor from open throttle settings to the stability limit throttle setting at each of several constant rotational speeds. The test results are presented as a compressor map defining performance in terms of flow pressure ratio, efficiency, and stability limit. If the test compressor is an integral unit of a multiple-compressor-compression system, such as a dual-spool engine, then aerodynamic coupling effects between the spools (spool interference) may need to be accounted in the test set-up and procedures.

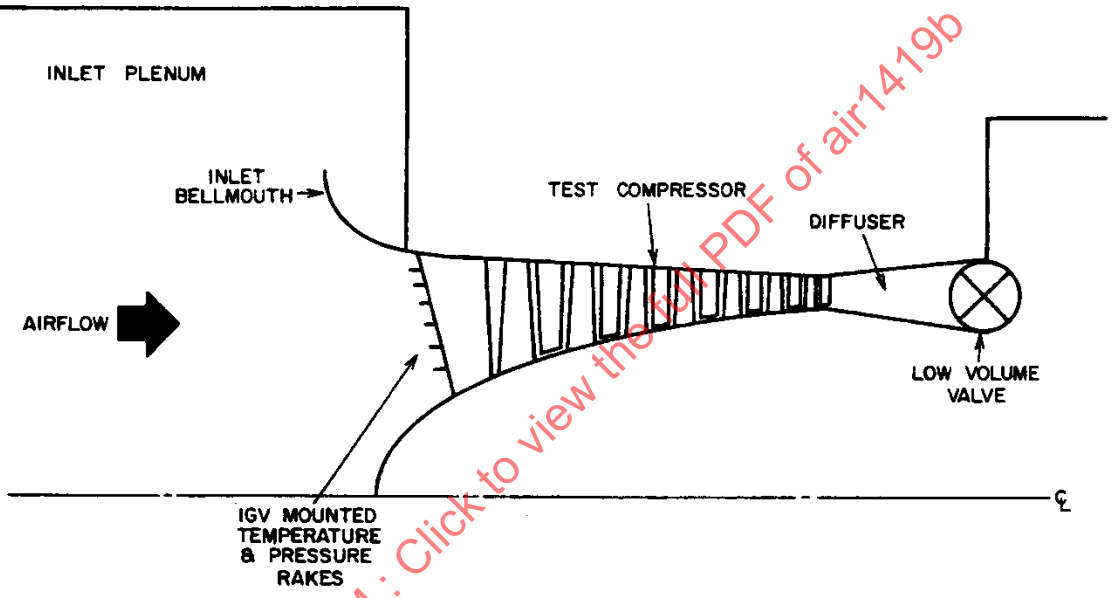

FIGURE 101 - SINGLE-SPOOL COMPRESSOR FACILITY

A schematic of a dual-spool rig used to characterize the stability of a fan/low-pressure unit and its corresponding high-pressure compressor appears in Figure 102. Dual-discharge rigs are necessary for testing fan/low-pressure units, with close attention paid to simulating the expected discharge flow schedules. Variances in these schedules can cause significant changes in unit performance and stability characteristics. A schematic of the test section of a typical dual-discharge rig designed to independently vary fan and low-pressure-compressor discharge-flow schedules appears in Figure 103.

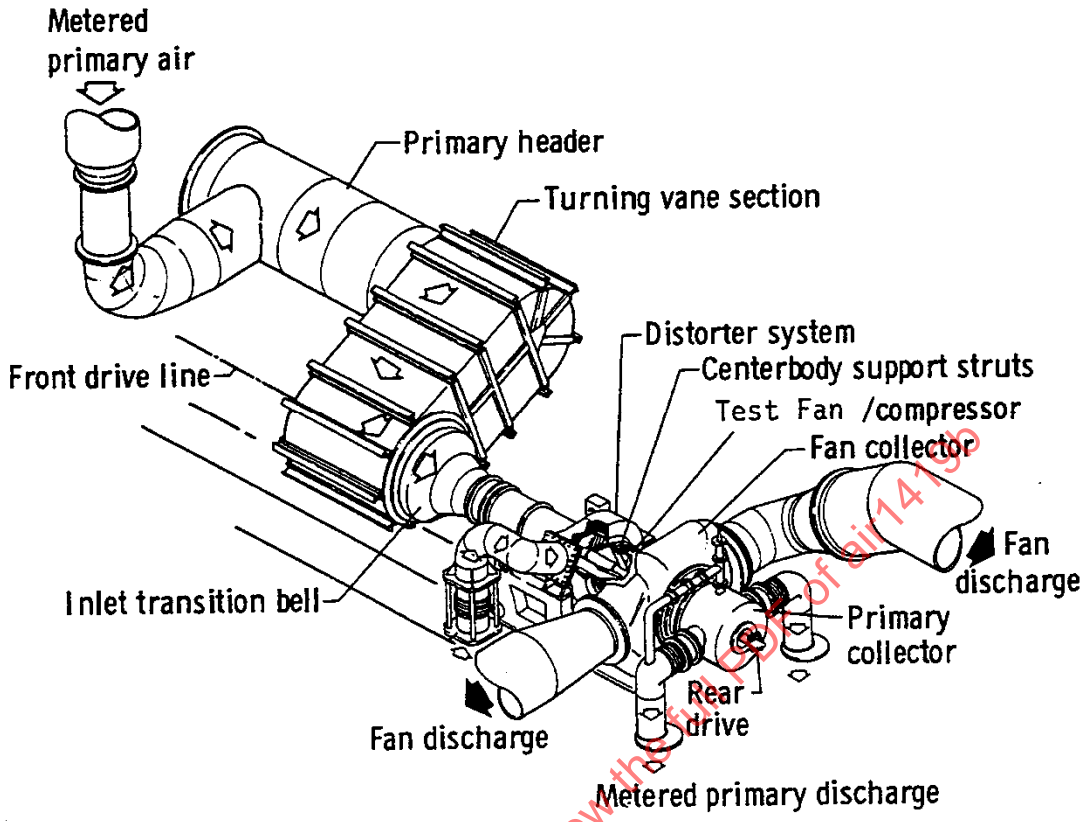

FIGURE 102 - DUAL-EXHAUST, DUAL-SPOOL COMPRESSOR FACILITY

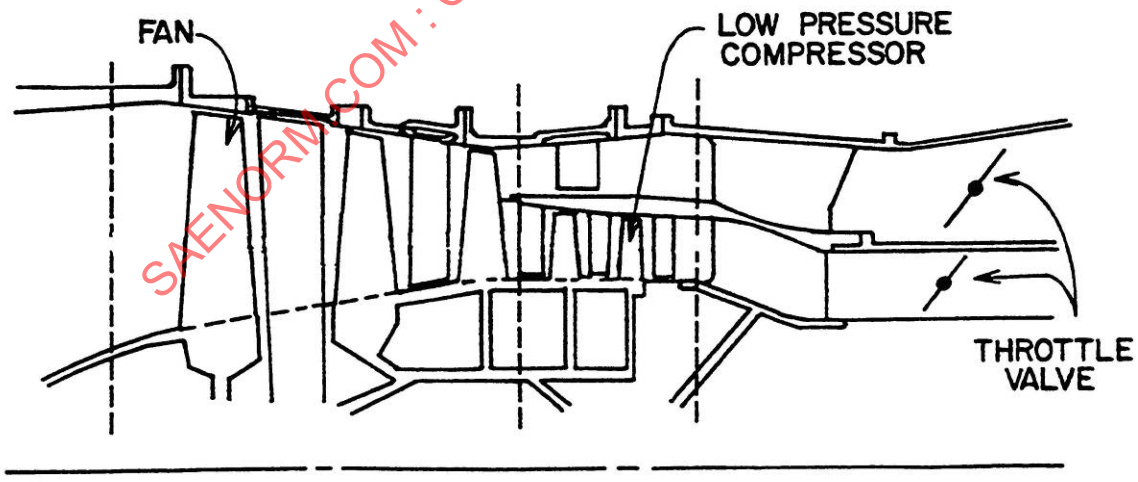

FIGURE 103 - DUAL-DISCHARGE COMPRESSOR FLOWPATH

Engine tests define overall performance and stability, verify the results of component tests (e.g., compressor rig tests), and ascertain the effects of component interactions on engine system stability and performance. Tests are conducted to assess the effects of the engine operating environment and the effects of the engine operating condition. Environmental considerations include the effects of flight Mach number, altitude, Reynolds number, nonstandard day conditions, external engine thermal environment, and flight transients where performance or stability characteristics vary prior to the achievement of engine thermal equilibrium. Typically, the engine operating characteristics are established with and without engine air bleed and power extraction, with control system variations representative of control tolerances, and in steady-state and transient nonaugmented and augmented control modes.

Direct-connect sea-level and altitude test facilities can be used for engine baseline testing. A typical direct-connect engine test installation in an altitude test facility is illustrated in Figure 104. The salient features of the installation are a critical-flow airflow-measuring venturi, a large inlet plenum, and a bellmouth at the engine inlet duct to provide uniform steady flow to the engine. Flow straighteners are fitted in the inlet plenum to ensure that the flow is uniform.

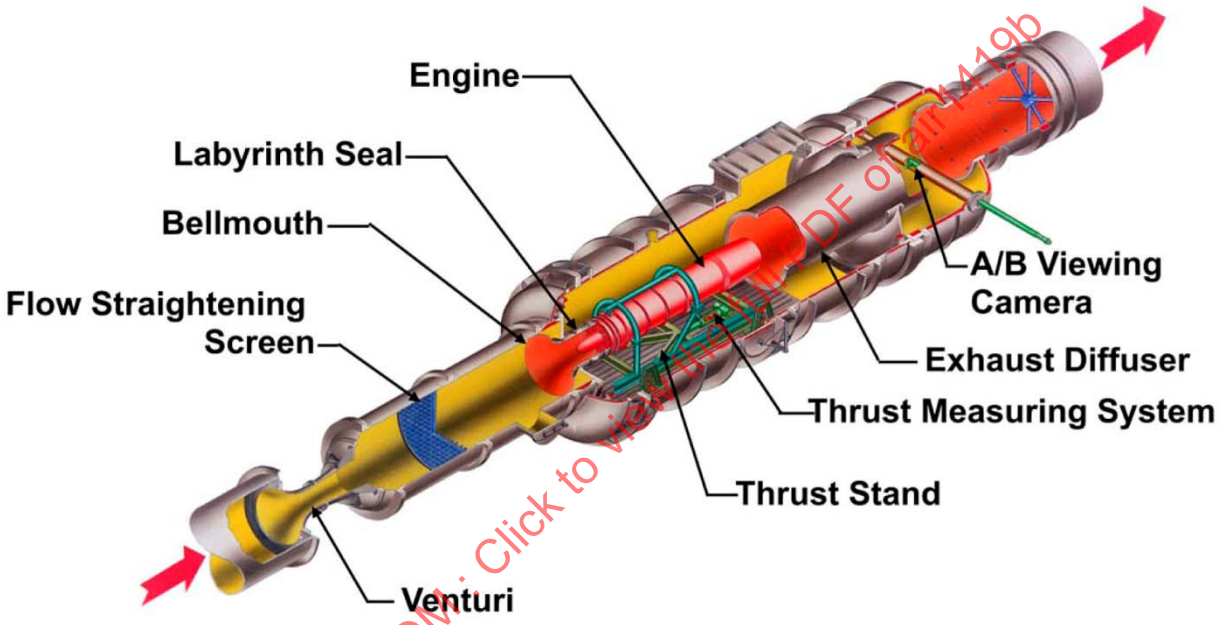

FIGURE 104 - TYPICAL DIRECT-CONNECT ENGINE TEST INSTALLATION FOR BASELINE STABILITY AND PERFORMANCE TESTING

7.2.2 Steady-State Total-Pressure Distortion

Tests with steady-state inlet total-pressure distortion define the effects of classical and composite distortion patterns on engine and engine component performance and stability. Testing with classical patterns establishes the basic sensitivity characteristics of the engine. Testing with composite patterns establishes performance changes and the loss in stability attributable to flight type inlet-distortion patterns. Composite patterns are based on inlet test results at selected operating conditions. The established practice in industry is to simulate peak time-variant distortion patterns with steady-state patterns, thus avoiding the need for extensive compression system development testing with high-response instrumentation and data-acquisition systems. Compressor and engine testing with steady-state total-pressure distortion can be accomplished in the direct-connect installations described for testing with uniform inlet flow conditions using steady-state distortion generators located approximately one engine diameter forward of the compressor inlet.

Distortion levels up to 30% $(P_{max} - P_{min})/P_{avg}$ generally are sufficient for most steady-state distortion testing needs. The time-variant component, $\Delta P_{rms}/P_{avg}$ (0-1000 Hz), should be less than 1% and total-temperature distortion, $(T_{max} - T_{min})/T_{avg}$, should not exceed 1/2%.

7.2.2.1 Screens

Wire-mesh screens are used to generate steady-state total-pressure distortion at the compressor and engine inlet, Figure 105. Screen systems have several significant advantages. They are relatively simple to fabricate and use. Once calibrated, screen systems may be used with limited AIP instrumentation in different facilities having identical engine inlet configurations. Rotatable distortion screen assemblies may be used to obtain detailed distortion data from a minimum number of installed sensors (AIP and engine internal sensors) at a stabilized engine/environmental test condition and to assess engine control system interactions at a constant engine power level position. An example of a rotatable distortion screen assembly used for engine testing is illustrated in Figure 106.

FIGURE 105 - TYPICAL CLASSICAL AND AIRCRAFT PATTERN DISTORTION SCREENS

Techniques have been developed to aid in the definition and design of screen configurations that result in desired total-pressure distortion patterns. Selected inlet distortion patterns usually can be established to required accuracies to within two to four screen tailoring test iterations. Screens have undesirable operating characteristics in that their pressure losses are dependent on the screen porosity (blockage) and approach velocities, so that the simulation of a number of inlet distortion patterns requires a screen change with a consequent loss of test time.

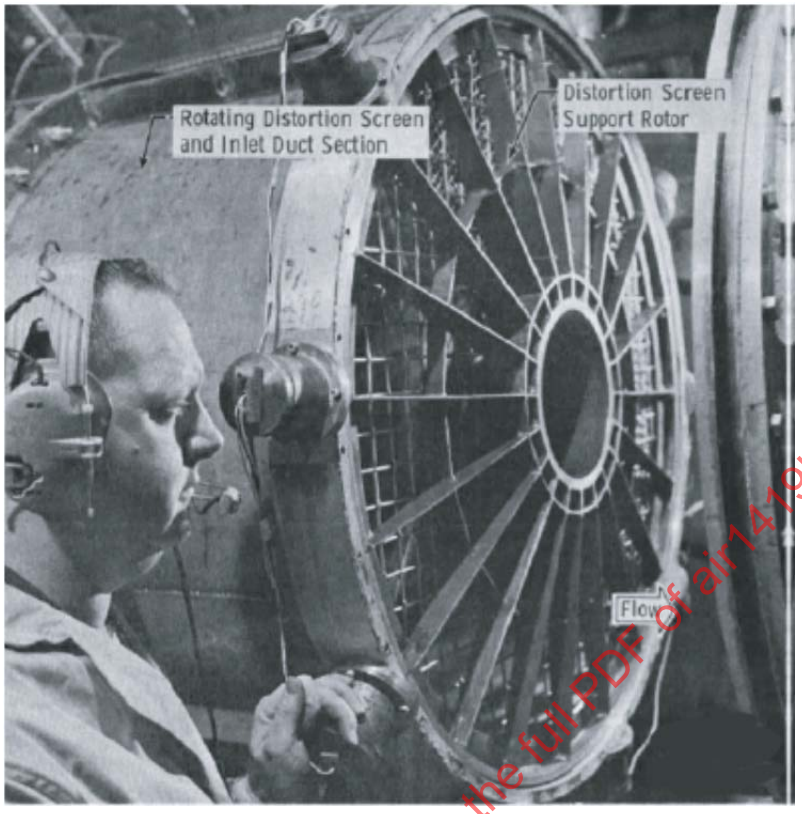

FIGURE 106 - ROTATABLE DISTORTION SCREEN ASSEMBLY

7.2.2.2 Air Jet Distortion Generators

An airjet system can be used as an alternative steady-state distortion generator. Airjet-distortion generators use a counterflow (to the primary engine inlet airstream) air jet system in which the jet flow momentum cancels part of the primary compressor inlet airstream momentum with an accompanying total-pressure loss. The flow distortion pattern is varied by remotely controlling the jet flow rate and distribution.

A typical airjet distortion generator (Figure 107) is reported in Reference 2.2.19. The system includes a secondary (airjet) air temperature conditioning system (to match the temperature of the primary engine airstream), an airjet nozzle array (56 equally spaced flow nozzles), and a computerized airjet nozzle flow control system to provide “dial-a-pattern” capability. Defined parametric or flight-related patterns can be established within approximately 90 s during testing to approximately the same accuracy limits obtainable with a screen distortion generator (2% rms error on a probe-by-probe basis). The airjet system provides a capability for producing variable-amplitude and variable-pattern steady-state distortion at a fixed engine operating condition or a constant distortion level and pattern over a range of engine airflow without hardware changes.

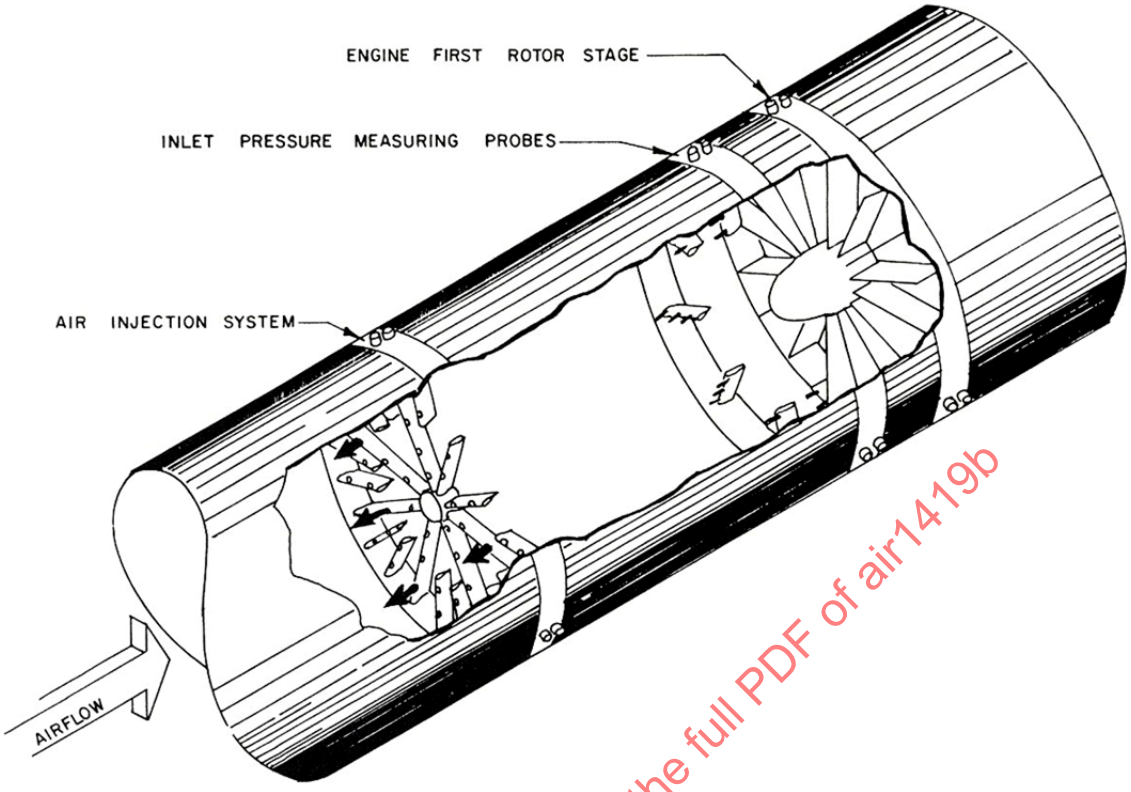

FIGURE 107 - SCHEMATIC OF AIRJET DISTORTION GENERATOR

The airjet distortion generator requires the use of a full AIP steady-state total-pressure probe array and a secondary air supply system. The time-variant distortion levels obtained with the airjet system may be higher than comparable levels obtained with screen systems, necessitating the use of high-frequency-response inlet instrumentation (Reference 2.2.19). Similar airjet distortion generators are reported in References 2.2.20 and 2.2.21.

7.2.2.3 Compressor Tests

Initial assessments of compression system sensitivity to inlet distortion usually are determined by compressor rig testing. A typical test sequence starts with a baseline test conducted with a “clean inlet” configuration, as discussed in 7.2.1. The test facility is then modified to include distortion-producing devices, and distorted-flow compressor maps are produced for each distortion pattern.

Total-pressure distortion at the inlet of a multi-component system is converted to combined pressure and temperature distortion at the inlets of down-stream compression-system components. It may be desirable, therefore, to test HP compressors with both pressure and temperature distortion patterns. A schematic of an airjet distortion system which accomplishes this objective by injecting high-temperature, high-pressure air at appropriate angles to the inlet flow is presented in Figure 108. The injection angle determines the degree of pressure distortion included in the pattern. Another system for producing temperature and pressure distortions involves the use of hydrogen burners in combination with screens (Figure 109).

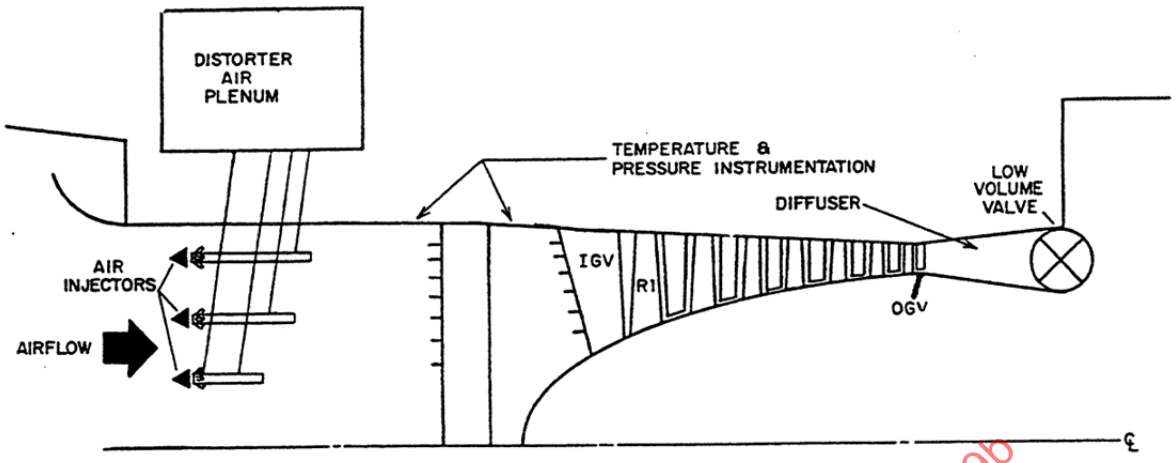

FIGURE 108 - COMPRESSOR RIG TEST WITH AIRJET DISTORTION GENERATOR INSTALLED

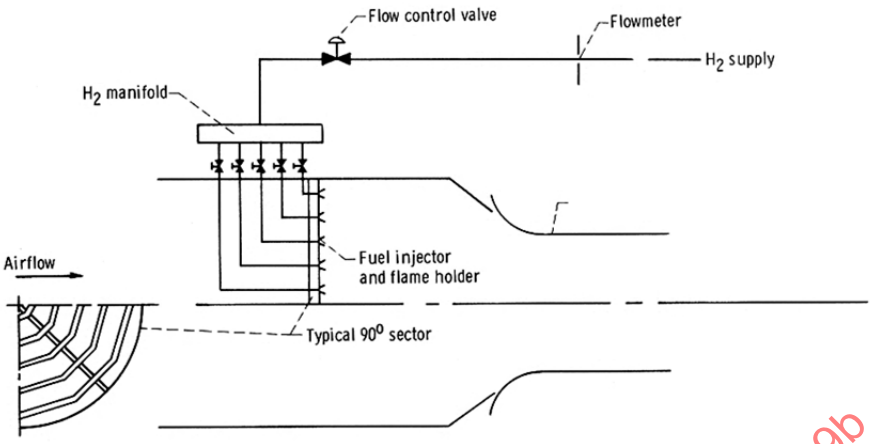

(a) Schematic of installation.

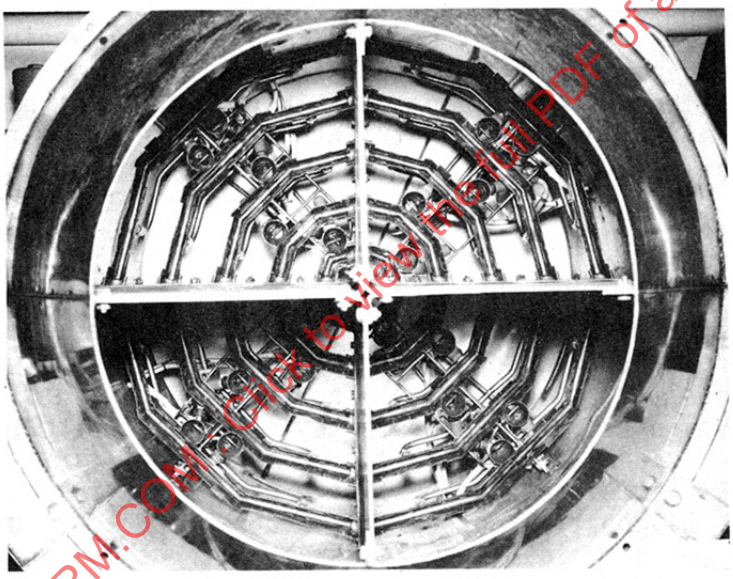

(b) Photograph looking upstream.

FIGURE 109 - TEST CONFIGURATION FOR TEMPERATURE DISTORTION TESTING

The compressor rig test results are analyzed to assess compressor sensitivity to each inlet distortion pattern. The typical test sequence involves testing with classical patterns (Figure 105) such as “pure” 180-degree-circumferential, tip-radial, and hub-radial patterns and then proceeding to more complex patterns such as graded-radial patterns, combined radial and circumferential patterns, and two per rev patterns. The classical pattern test data serve to define basic compressor distortion sensitivities and offset coefficients, while the complex pattern data allow generalized sensitivities to be derived.

Testing on a compressor rig imposes constraints which may affect the applicability of the rig test results to a complete engine. Insofar as practical, the compressor rig should include a simulation of downstream components if these are anticipated to affect the distortion sensitivity of the compressor. Aeromechanical constraints may prohibit testing with high levels of distortion, and rig drive-power limitations may preclude testing above design speed.

7.2.2.4 Engine Tests

Engine tests are conducted to establish the overall effects of AIP total-pressure distortion on engine performance and stability, verify installed compressor sensitivity coefficients and distortion transfer characteristics, and confirm initial distortion assessments. Tests at selected environmental operating conditions are performed over a range of fixed-throttle settings and PLA transients (accel/decel rates) with representative customer bleeds and power extractions. Diagnostic tests with the normal control functions muted can be carried out, and classical or parametric patterns can be tested to determine the distortion sensitivity characteristics of multi-spool compression systems using heavily-instrumented engines. For qualification or certification testing, test matrix requirements are generally limited to specified engine and environmental “rating” conditions using flight-type distortion patterns.

Engine tests with steady-state inlet flow distortion are performed in the test installations used for baseline clean-flow engine performance and stability test assessments, modified to include a selected steady-state distortion generator. An engine inlet-airflow metering system, such as a critical-flow venturi, forward of the inlet plenum provides accurate engine airflow measurements while testing with the steady-state distortion generator. Engine-installed compressor loading test techniques to assess installed compressor stability limits may be employed (7.4).

7.2.3 Time-Variant Total-Pressure Distortion

Tests with time-variant inlet total-pressure distortion may be required to assess the effect of random- and discrete-frequency pressure fluctuations on compression-system stability and performance. Time-variant distortion analysis techniques are similar to steady-state techniques, except that the inlet data are filtered via analog and/or digital data processing systems to match the compression system dynamic response characteristics. The objective of the tests is to correlate surge or stall events with the maximum time-variant distortion level producing the instability. A “low-pass” filter with a cutoff frequency of 1/2 to 1 times the compressor rotor speed is sufficient to assess the response of most current engines (Reference 2.2.22).

7.2.3.1 Random Frequency Generators

An example of a random frequency generator installation is shown in Figure 110. A critical-flow convergent-divergent nozzle with a variable-position centerbody is used to generate turbulent flow by interaction of a shock wave and a boundary layer in the same manner as turbulent flow is generated in an aircraft inlet. A turbulence attenuation screen located downstream of the venturi may be used to modify the characteristics of the turbulent flow system. The centerbody may be offset to obtain asymmetric distortion patterns. The random frequency generator (RFG) should simulate the length/volume characteristics of the aircraft inlet duct from the inlet throat to the compressor face.

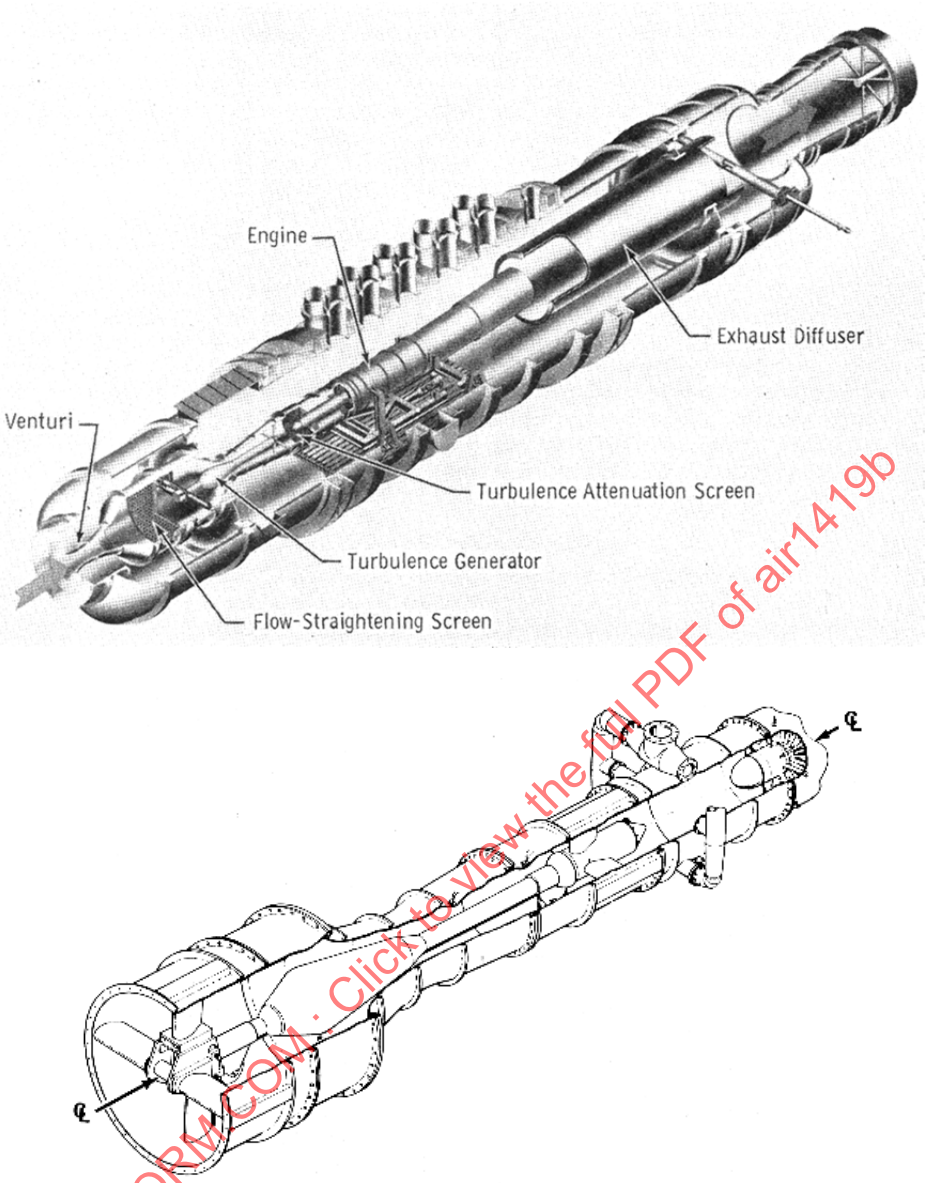

FIGURE 110 - TYPICAL RANDOM FREQUENCY GENERATOR TEST INSTALLATION FOR ENGINE STABILITY ASSESSMENT

Random frequency generators may be designed to simulate specific inlet configurations. The two-dimensional random frequency generator reported in Reference 2.2.3 (Figure 111) is designed to produce distortion patterns which are similar in shape, level and dynamic content to those obtained from two-dimensional inlet models. Testing an engine with the generator provides a means for evaluating pressure-distortion sensitivity and transfer characteristics as well as engine/control performance in a realistic environment prior to inlet/engine and flight testing. The random frequency generator consists of a duct with a cross-sectional area of 39.85 in^2 and 18.5 ft long. The upper and lower duct walls each consist of three articulated ramps that may be positioned remotely using screw jacks. Changing the flow channel geometry by positioning these ramps induces distortion via boundary layer separation and shock/boundary layer interaction. Distortion level and extent are controlled by the particular geometry of the ramp positions and airflow. The turbulence level and ratio of unsteady to steady-state distortion are controlled by a full-span monoporosity screen located just behind the aft ramp. The distortion levels produced by the RFG are, in general, controllable and repeatable.

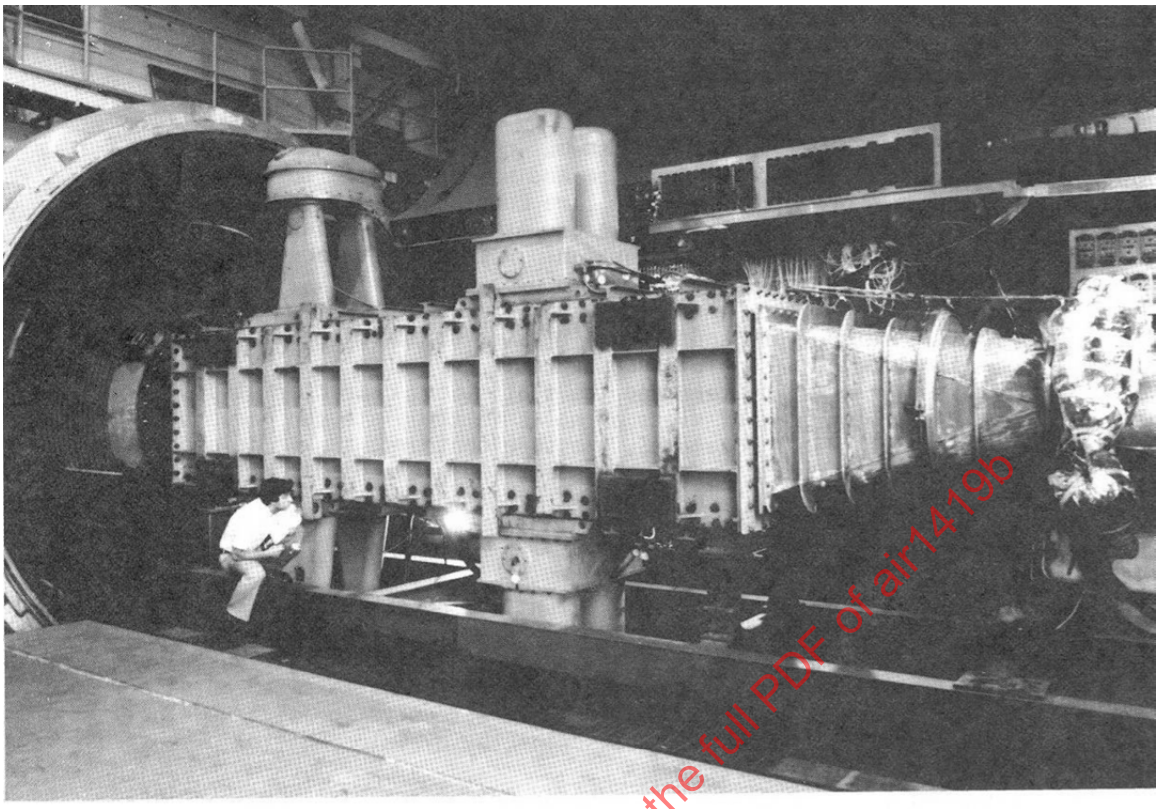

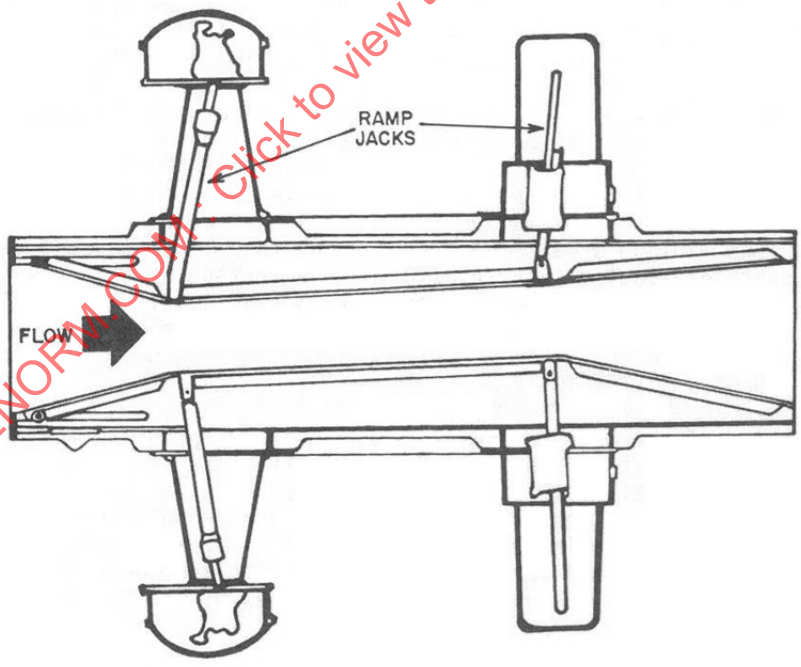

FIGURE 111 - RANDOM FREQUENCY GENERATOR DESIGNED TO SIMULATE FLOW CONDITIONS OF TWO-DIMENSIONAL INLET CONFIGURATION

Typical RFG test results are shown in Figure 112. The data were acquired with an analog recording system and were digitized for off-line analysis. The data were filtered to a time constant nearly equal to one engine revolution. The curves show (a) 1 s of data with an engine stall near 0.80 s and (b) calculated distortion parameters and face-average pressure in an expanded region from 0.75 to 0.85 s.

Another method for generating AIP time-variant distortion involves the use of a perforated plate simulator designed to reproduce the AIP steady-state total-pressure distortion pattern and the statistical characteristics of the inlet flow. An arrangement of slots or holes in the plate can be adjusted to reproduce steady-state and local RMS pressure contours, amplitude probability density, and spectral density characteristics (Reference 2.2.23). High-response AIP instrumentation is required to develop the simulator.

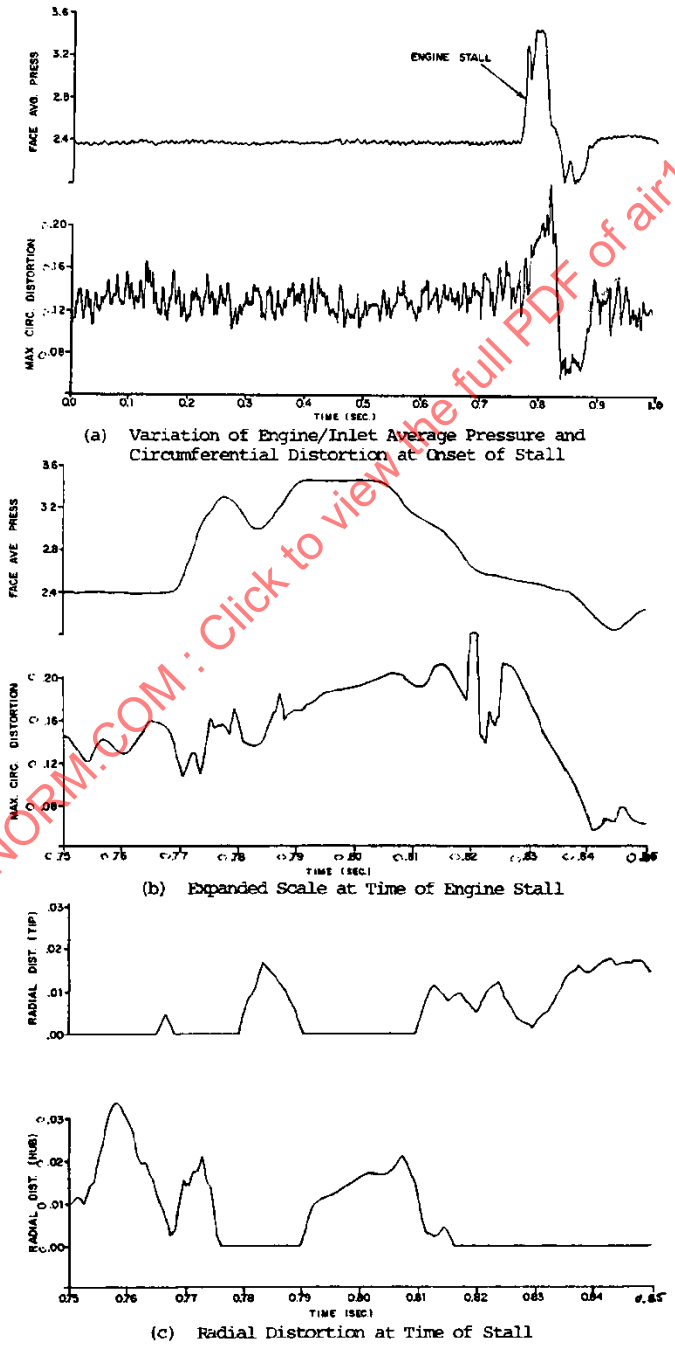

(a) Variation of Engine/Inlet Average Pressure and Circumferential Distortion at Onset of Stall

(b) Expanded Scale at Time of Engine Stall

(c) Radial Distortion at Time of Stall

FIGURE 112 - TYPICAL ENGINE TEST RESULTS OBTAINED WITH A RANDOM FREQUENCY GENERATOR

7.2.3.2 Discrete Frequency Generators

Discrete-frequency pressure fluctuations occur in an aircraft inlet duct due to turbulence and as a result of inlet instability, such as buzz, or as a result of duct resonances. The propagation characteristics, the surge, and the performance effects of the planar inlet pressure fluctuations may be determined using discrete-frequency generators. They are effective tools for evaluating time-variant analytical models which describe the dynamic behavior of compressors.

Several types of discrete frequency generators have been developed. The air jet distortion generator designs reported in References 2.2.20 and 2.2.21 have discrete frequency pressure pulse capabilities. A rotor/stator flow blockage design is reported in Reference 2.2.24. The generator consists of a rotor installed between matched stator assemblies. The output frequency of the generator is controlled remotely by varying the speed of the rotor. The amplitude of the pressure fluctuations can be varied by changing the solidity (blockage) of the rotor/stator assemblies. A similar design concept, the Planar-Pressure-Pulse Generator (P^3G) is reported in Reference 2.2.8. The P^3G is a choked-flow device which uses a single-stage rotor and stator combination to sinusoidally modulate the minimum area. The frequency of the planar waves is governed by the rotor-to-stator spacing (Figure 113). An advantage of this device is its ability to produce planar waves with peak-to-peak amplitudes of 10 to 30% of the mean total pressure over a frequency range from 420 to 800 Hz.

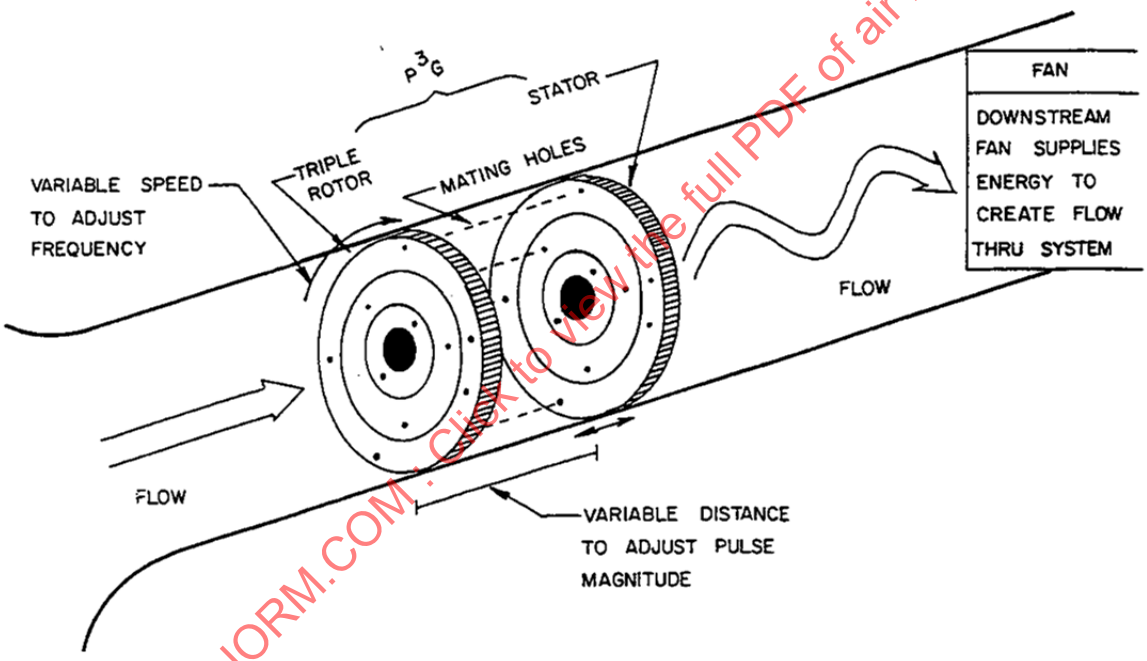

FIGURE 113 - SCHEMATIC OF PLANAR PRESSURE PULSE GENERATOR

7.3 Propulsion System Tests

Testing of the integrated inlet/engine system prior to installation in the flight test aircraft provides the first verification of installed performance and inlet/engine compatibility. Tests on a representative system may be carried out on a sea-level-static test stand, in an altitude propulsion wind tunnel, or on a flying test bed, depending on installation and program requirements. Flight testing demonstrates and verifies the performance and compatibility of the propulsion system over flight/maneuver envelopes of the flight test aircraft.

The types of test, primary test objectives, and basic data requirements which may be needed for system development are shown in Table 15. Primary considerations for the selection of the desired test techniques for specific programs include: (1) test model availability and cost, (2) test condition/matrix requirements, (3) data and instrumentation system considerations, and (4) test facility requirements/limitations.

TABLE 15 - PROPULSION SYSTEM TESTS

Objective	Tests	Data
System Performance and Stability Verification at Sea-Level Static	Static Tests with Simulated Ground Plane and Forebody	Stability and Performance Time-Variant Distortions Inlet Recovery Stability Pressure Ratio Crosswind Effects Distortion Transfer Power Transients
Pre-Flight Performance and Stability Verification at Altitude	Altitude Test Cell/Propulsion Wind Tunnel Tests with Simulated Flight Envelope	Time-Variant Distortion Reynolds Number Effects Inlet Recovery Stability and Performance Inlet Stability Range (Buzz – Unstart – Supercritical) Failure Modes Transients Control Interactions Distortion Transfer
In-Flight Performance and Stability Verification over Flight and Maneuver Envelopes	Ground and Flight Test Development in Aircraft	Stability and Performance Inlet Distortion at Critical Flight Conditions Additional Pattern Data Bank Aircraft Dynamics Weapon Firing Reingestion Behavioral Statistics Control Interactions

7.3.1 Static Tests

Static tests of the inlet/engine system can provide an early indication of inlet/engine operation at take-off. Test configurations represent the aircraft as closely as possible and include simulation of the ground plane, adjacent aircraft structure or adjacent engine, as appropriate. Tests enable the effects of the external environment on the flow quality at the AIP to be established at static or near-static conditions.

The General Electric Peebles Cross-Wind Facility (Figure 114) was designed for testing large turbofan engines and determining the effects of winds ranging from quartering tailwinds to headwinds. The facility is composed of 13 individually controlled fans capable of creating uniform-velocity flows ranging from 15 to 78 knots, and has a capability for ground plane simulation and ground vortex suppression.

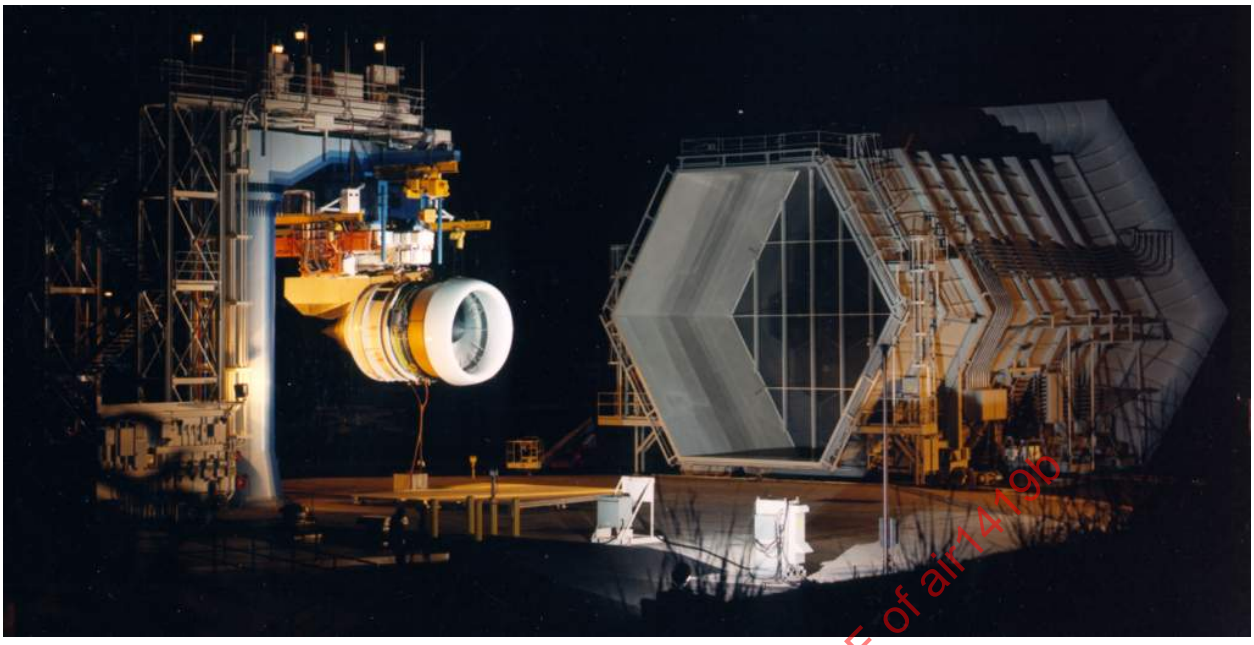

FIGURE 114 - PEEBLES CROSSWIND FACILITY

7.3.2 Wind Tunnel Tests

In aircraft programs involving significant advances in the state-of-the-art, inlet/engine tests in a wind tunnel can prove to be a cost-effective way of demonstrating inlet/engine compatibility prior to the start of flight testing.

Inlet tests with a cold pipe installation (no engine present) can be conducted to determine the full-scale inlet characteristics over a wide range of inlet mass flow ratios. These tests provide airflow calibrations for subsequent use in tests with the engine. Although complete aircraft maneuver envelopes cannot be explored, tests with off-schedule inlet geometry can be conducted to simulate distortion characteristics observed during previous sub-scale tests throughout the maneuver envelope. The effects of known external disturbances (external weapons, control vanes, weapon bay doors and others) can be simulated. If variable geometry inlets are employed, programs usually include a second, cold-pipe phase consisting of development tests of the inlet and inlet control system. Use of the actual aircraft control system, if timing permits, can be an effective means of system checkout and of minimizing the flight test development program, particularly for supersonic aircraft. The third test phase includes all three elements: inlet, inlet control system, and engine including the engine control system. Emphasis is placed on demonstrating inlet/engine compatibility over a complete range of equilibrium operating conditions and engine throttle transients at critical flight conditions. Techniques for intentionally stalling the engine to determine structural loads and to verify the system stability limits can be employed. Engine distortion limits can be explored by off-scheduling inlet geometry to generate high distortion levels. The use of flight test instrumentation and data reduction procedures during these tests can be an effective means of reducing the required effort during the flight test program. A successful program requires a high degree of coordination among the parties involved.

A schematic of a typical free-jet engine test facility is presented in Figure 115. The test facility is configured to duplicate the inlet environmental operating conditions at selected points in the flight and maneuver envelopes for defined propulsion system operating conditions. A propulsion wind tunnel test installation is shown in Figure 116.

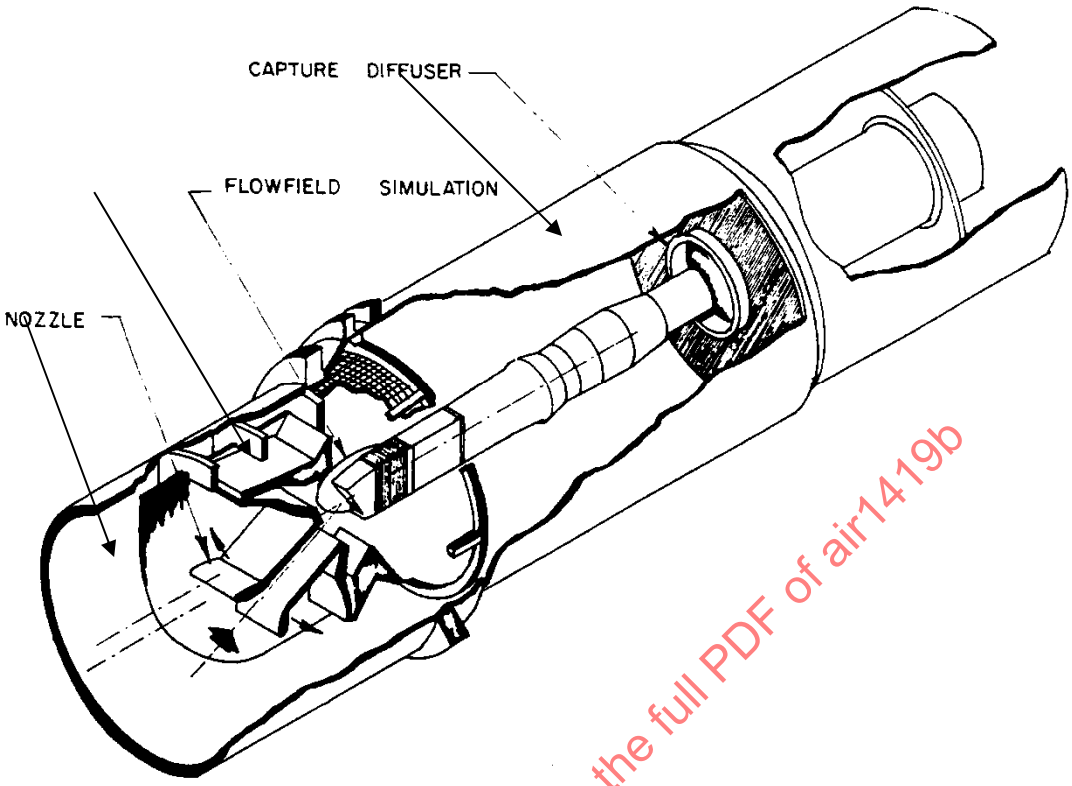

FIGURE 115 - FREE-JET PROPULSION-SYSTEM TEST INSTALLATION SCHEMATIC

FIGURE 116 - PROPULSION-SYSTEM TEST INSTALLATION IN PROPULSION WIND TUNNEL

Model size requirements have a significant effect on the selection of desired propulsion system test techniques. The historical growth in engine airflow requirements has led to increased test facility airflow requirements. Semi-free jet (inlet simulator) techniques can be used where test facility limitations exist. Semi-free jet tests may be used to produce inlet/engine interface flow conditions to a high degree of fidelity over the operating range of the propulsion system. An example of an inlet design simulating an aircraft inlet system downstream of the initial compression shocks of an external compression inlet is reported in Reference 2.1.1.8. The basic concepts of the simulator are illustrated in Figure 117.

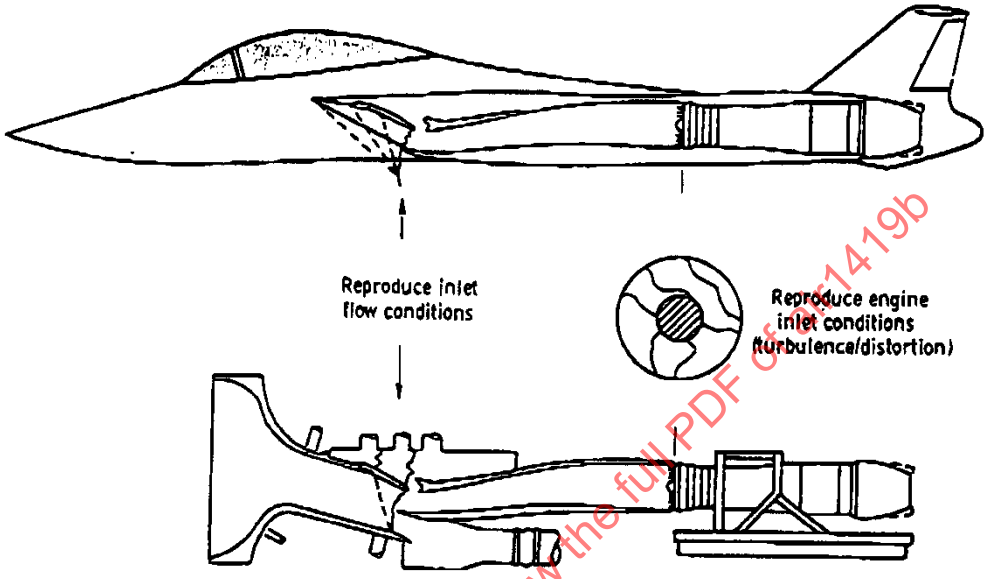

FIGURE 117 - SCHEMATIC OF INLET SIMULATOR

7.3.3 Flight Tests

Flight tests are oriented to demonstrate propulsion system operational goals and to provide verification of system performance, stability, and mechanical integrity over the aircraft flight and maneuver envelopes. Since installed stability margin is usually not measured in flight, propulsion system stability is demonstrated by operating to the aircraft-engine stability limits. Flight tests will gradually expand the envelope from low speed to supersonic conditions and from nominal to extreme altitudes and attitudes. Typical conditions which are tested are listed in Table 16.

Both steady-state and high-response instrumentation may be used at the AIP. In addition, the engine(s) can be instrumented to permit measurement of internal engine performance and in-flight thrust. Flight testing provides the opportunity to verify performance and distortion levels predicted from wind tunnel data (Reference 2.2.8). Sufficient instrumentation should be provided to identify any propulsion problems encountered during the flight test program.

TABLE 16 - FLIGHT TEST CONDITIONS

GROUND OPERATION FOD Screens Static Taxi Operations Crosswinds Runway Conditions
LOW SPEED OPERATION Rotation and Takeoff Approach and Landing Crosswinds Auxiliary Inlet Transients A/C Stall Characteristics Thrust Reverser
AIRCRAFT TRANSIENT OPERATION Accelerations Decelerations Automatic/Manual Inlet Controls Emergency Procedures
SUBSONIC PERFORMANCE Throttle and Augmentor Transients A/C Maneuvers A/C Control Surface Effects Weapons Bay Door Operation Weapon Release External Stores
SUPERSONIC PERFORMANCE Inlet Control – Automatic/Manual Throttle and Augmentor Transients A/C Maneuvers Emergency Procedures A/C Control Surface Effects External Stores

The comprehensive wind tunnel testing described in 7.1, 7.3.1, and 7.3.2 will have provided the data to identify and correct any major system deficiencies prior to flight test. It is possible, however, that problems may be encountered during the early part of the flight test program due to ground facility constraints. Wind-tunnel size limitations prevent complete duplication of the aircraft and may limit incidence and sideslip to less than the aircraft limits, and rapid changes in aircraft attitude or in-flight conditions cannot be simulated properly. Significant areas need to be explored during the flight test program, particularly with respect to flight dynamics. The flight test program provides the opportunity to evaluate refinements to the propulsion system design in terms of their effects on aircraft performance and inlet/engine compatibility. For example, inlet geometry may have a significant impact on aircraft trim drag. Minor changes to inlet geometry schedules may improve performance with essentially no adverse effect on distortion. The flight test program should be structured to explore those areas where interaction between the propulsion system and the aircraft may not have been fully tested during wind tunnel tests.

Correlation of flight test and wind tunnel data provides a data bank for evaluating future modifications to the system and for the development of new aircraft. Examples of correlations between scale model and flight data appear in References 2.2.11 and 2.2.12, and several examples of sub-scale to full-scale comparisons appear in Reference 2.1.1.9.

7.4 Stability Assessment Verification

Test verification of the validity of stability assessments is based on a building block concept. The quantitative evaluation of all destabilizing factors cannot be assessed during a single engine or engine component test. Consequently, stability assessments at program milestones are based on the test data available at that time. Hence, test programs must be carefully controlled to maximize the applicability of test results. Stability assessments are based on experimental audits at defined propulsion system operating conditions.

Stability margin destabilizing factors for a typical turbine engine compressor are shown in Figure 118 (Section 5). Normally, qualification/certification test engines are not subjected to intentional surge because of the hazard of structural damage and delays in engine qualification/certification testing. Consequently, the compressor stability limit line and engine stability margin requirements must be determined during component and engine development test programs conducted with qualification/certification components. Verification of the operating line excursions caused by control requirements and distortion effects may be obtained during the qualification/certification test. Engine operation in the region above the maximum predicted operating line but below the anticipated stability line(s) should be accomplished whenever practical.

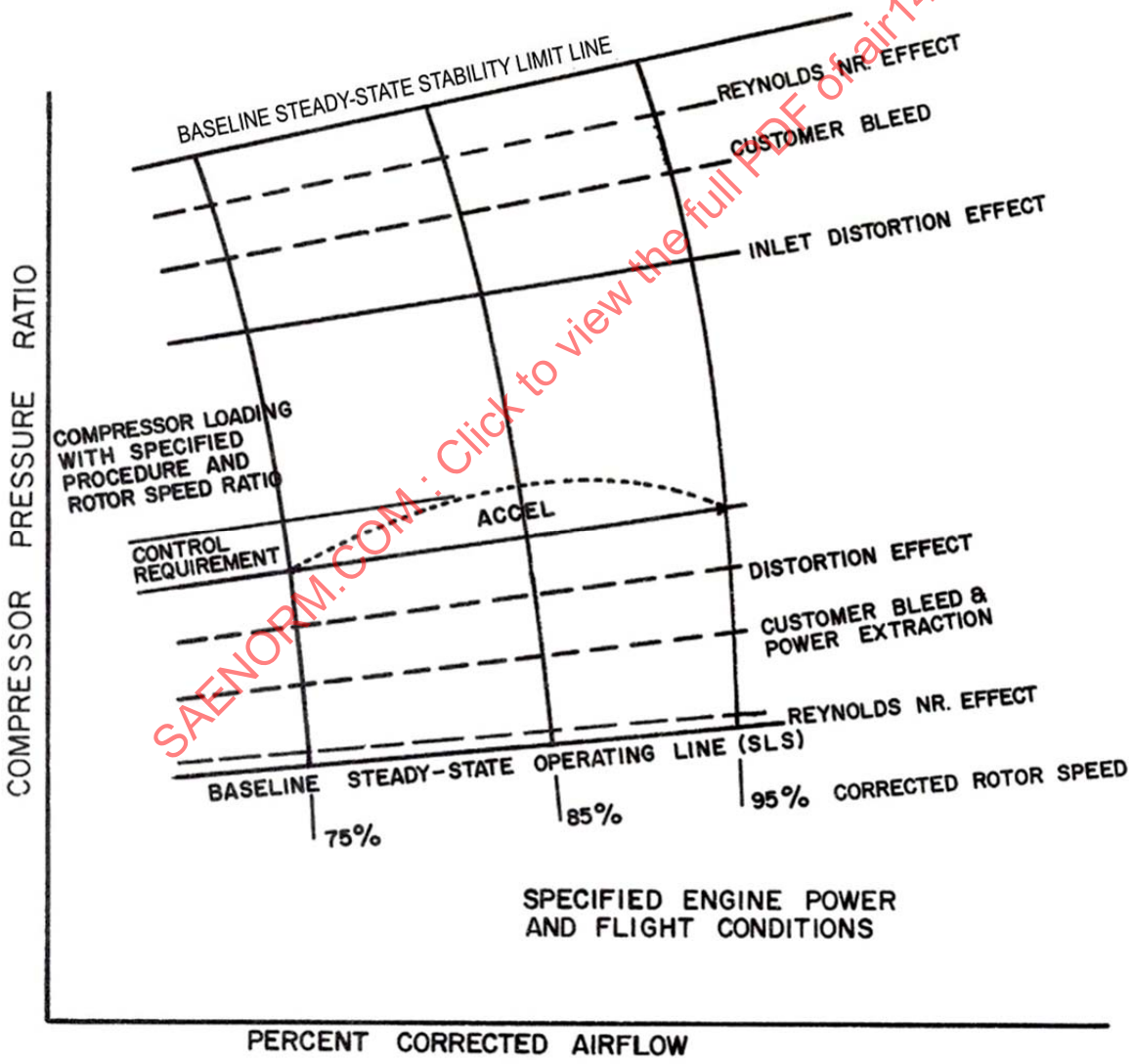

FIGURE 118 - TYPICAL TEST DATA BASE/TEST MATRIX REQUIREMENTS FOR STABILITY ASSESSMENT VERIFICATION

A test assessment methodology intended to demonstrate remaining margin is illustrated in Figure 119. In the example shown, an equivalent maximum operating line is established to account for the estimated internal effects (engine quality and deterioration) margin allocations of the stability assessment. By using the equivalent maximum operating line, a portion of the remaining margin (estimated net margin available to assure stable operation) can be demonstrated during engine testing (Figure 120) without subjecting the engine to surge.

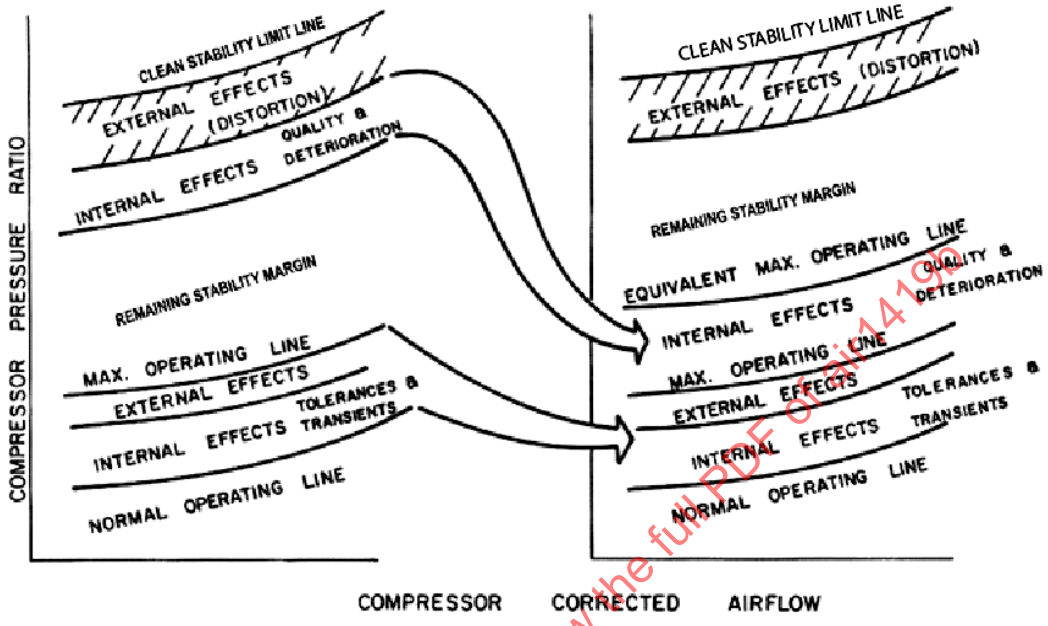

FIGURE 119 - STABILITY ASSESSMENT TEST VERIFICATION METHODOLOGY

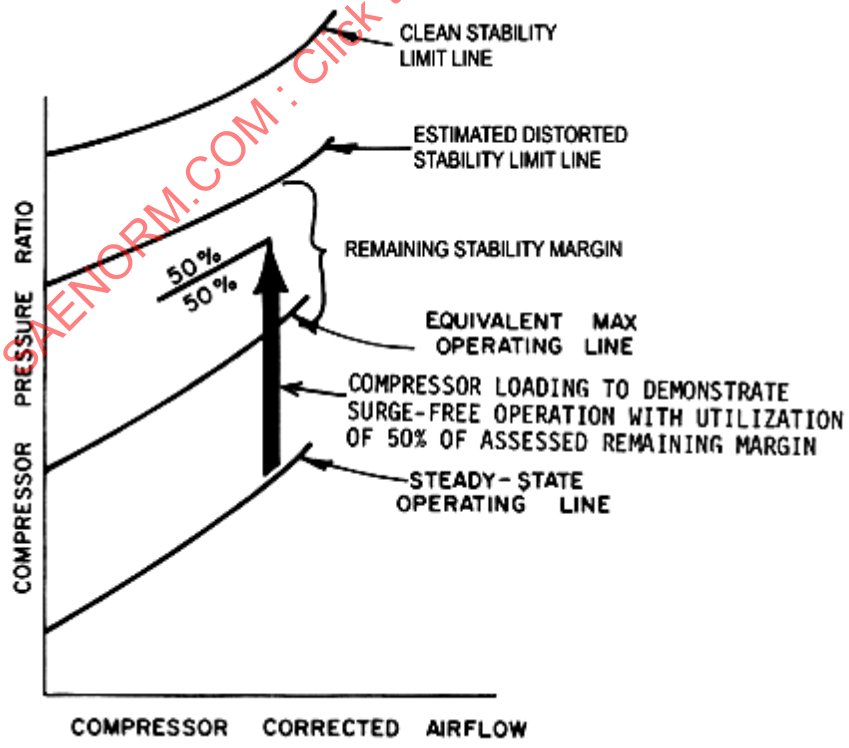

FIGURE 120 - TEST PROCEDURE TO DEMONSTRATE AVAILABLE MARGIN

Several installed compressor loading techniques are available for this purpose. These techniques can be divided into two general classifications, transient and steady-state loading methods. The most extensively used transient technique is the fuel step method which is based on the use of a controlled transient fuel step to increase the compressor ratio above the normal transient or equilibrium operating line. This technique usually requires only minor test equipment modifications, but does require transient measurements. Steady-state loading techniques include flow-blockage methods such as “inflow bleed” or mechanical blockage systems (Figure 121). Use of either system is straightforward with single fixed-geometry rotor configurations. By simultaneous use of both systems, selected rotor speed ratios can be controlled during loading of dual rotor configurations, as illustrated in Figure 122.

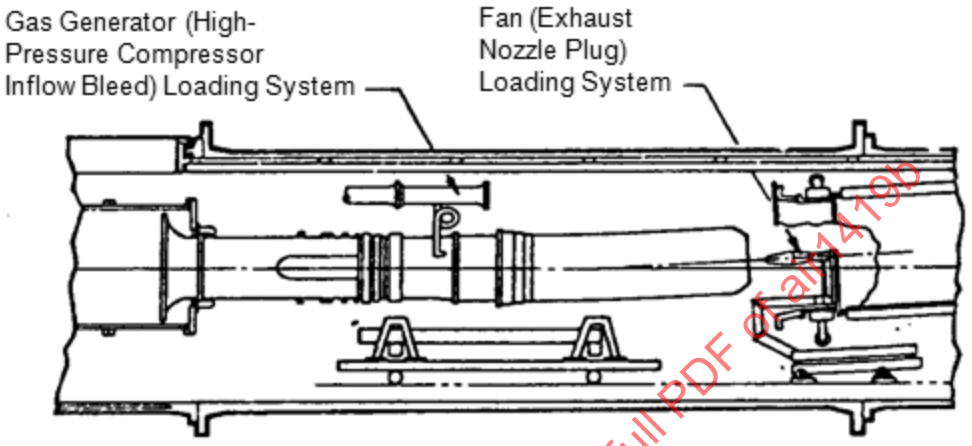

FIGURE 121 - SCHEMATIC OF TEST HARDWARE FOR SIMULTANEOUS LOADING OF FAN AND GAS GENERATOR HARDWARE

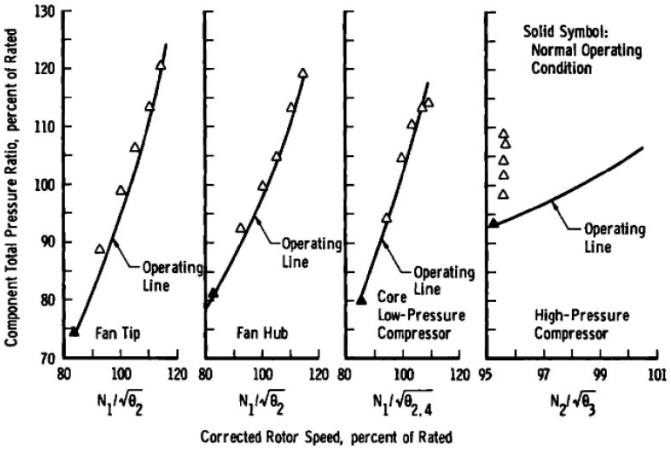

(a) High Pressure Compressor Inbleed Loading with Corrected Rotor Speed, $N/\sqrt{\theta}$ = 95.6 Percent

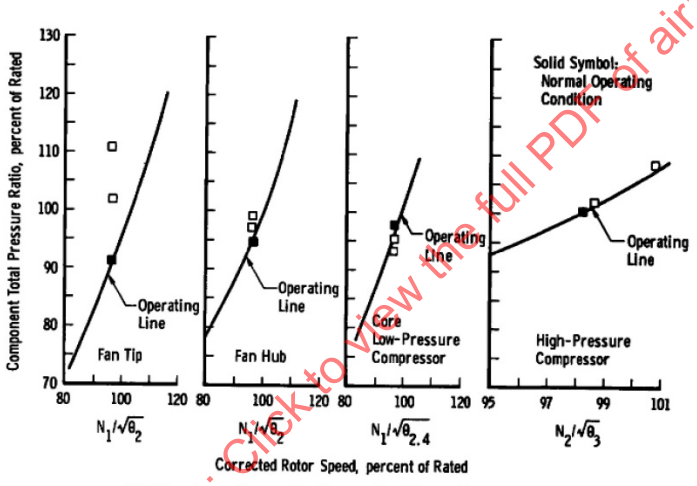

(b) Fan Loading with Corrected Low-Pressure Compressor Rotor Speed, $N/\sqrt{\theta}$ = 96 Percent

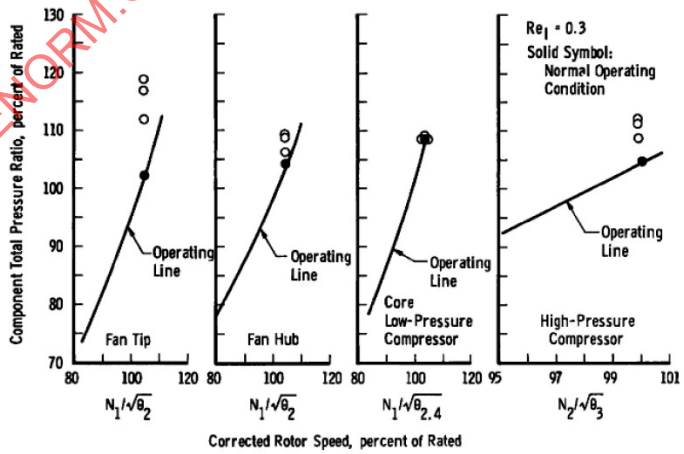

(c) Simultaneous Loading of Fan and Compressor

FIGURE 122 - COMPRESSOR OPERATING CHARACTERISTICS DURING COMPRESSOR LOADING OPERATIONS

Defined engine and environmental boundary conditions are necessary for engine stability tests. Typical criteria are listed in Figure 123. The inlet/engine interface criteria are based on a projected flight condition (mission requirement) and are specified using a point-by-point distortion pattern definition. Other environmental criteria which require definition are the projected aircraft service requirements such as compressor bleed and power extraction. Engine operating conditions are defined in terms of corrected rotor speed, corrected rotor speed ratio, engine service bleeds, and control mode operation. The operating condition matrix should be organized on a building block concept. Baseline data are established first; then the various destabilizing factors (Reynolds number, inlet distortion, control mode, and aircraft service requirements) are evaluated.

INLET	ENGINE
Corrected Airflow	Corrected Airflow
Altitude	Altitude
Mach Number	Total Pressure
Ram Recovery	Total Temperature
Angle of Attack	Distortion Pattern (Point-by-Point Definition)
Angle of Yaw	

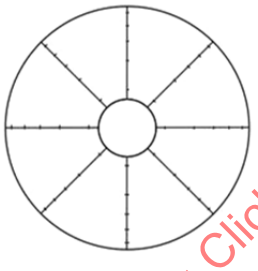

Instrumentation Definition

Circumferential Location

Individual Probe Values, P_{local}/P_{avg} at Corrected Airflow Value

Installation Interface Conditions (Aircraft Service Requirements)

Customer Bleed

Power Extraction

Engine Operating Conditions

Corrected Rotor Speed

Corrected Rotor Speed Ratio

Engine Service Bleeds (Intercompressor, Anti-Ice)

Control Function – Steady-State (SS), Transient

Control Operating Mode – Afterburning, Non-Afterburning

FIGURE 123 - ENGINE AND ENVIRONMENTAL CONDITION CRITERIA FOR TEST VERIFICATION OF STABILITY ASSESSMENTS

7.5 Performance Assessment Verification

Test verification of performance assessments may be required to validate the effects of inlet flow distortion on engine thrust, fuel consumption, and airflow. The most significant engine test objective is, in many cases, the evaluation of engine/control system interactions and engine-rotor-speed rematch characteristics with inlet flow distortion. For example, maximum-power engine performance may be control-limited at different engine operating conditions with or without inlet distortion; or engine performance at a selected thrust level may vary due to rotor speed rematch (Section 6).

Performance tests are conducted on defined engine and environmental boundary conditions, as discussed for stability assessments (Figure 123). The effects of inlet distortion may be assessed directly in terms of installed thrust, airflow, and fuel consumption for a defined AIP distortion pattern, or in terms of thrust, airflow, and fuel consumption changes relative to uniform inlet flow performance for the defined pattern. Because the impact of inlet flow distortion may be small relative to experimental measurement uncertainties, it may be desirable to conduct tests in a back-to-back mode (with and without a defined inlet distortion pattern) to minimize the effect of measurement bias errors. Back-to-back testing with and without inlet distortion screens may not always be practical in direct-connect test installations because test operations must be interrupted to manually install the inlet distortion screen. For specific applications, specialized test configurations may be used to provide an “on-line” inlet distortion screen change capability. A screen changer assembly successfully used for small engine testing is illustrated in Figure 124. The operating time required to change screens is on the order of one-half second. Engine power is reduced during the screen change transition period to reduce the possibilities of engine operational instabilities during the screen change transient.

The air jet distortion generator is also a potential tool for back-to-back testing with and without inlet flow distortion. Transitions from uniform inlet flow conditions to defined inlet flow distortion patterns may be accomplished in time periods on the order of 90 s with the engine operating at a fixed power level.

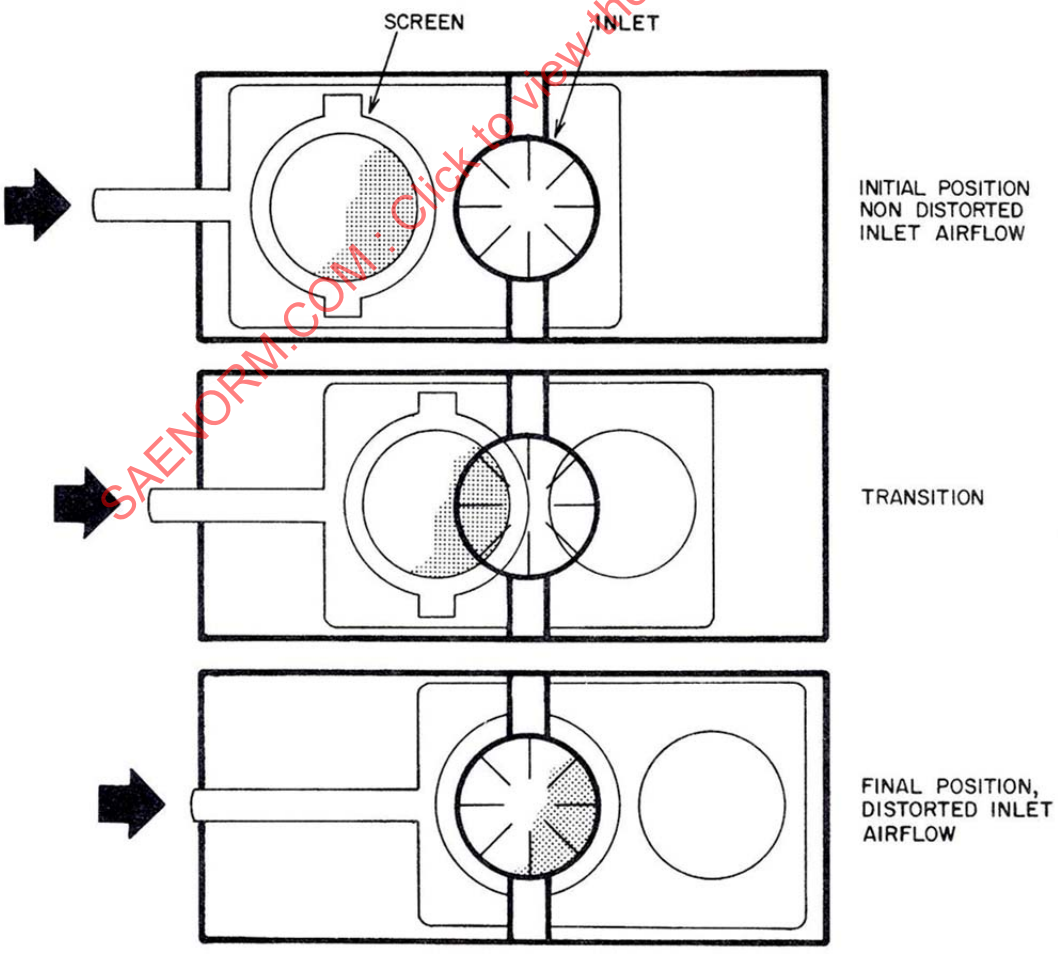

FIGURE 124 - SCREEN CHANGER ASSEMBLY

Two basic engine thrust measurement techniques are used for engine performance assessments in ground test facilities. Both can be employed for distortion tests and are comparable in terms of measurement uncertainty with uniform (undistorted) flow engine tests. Use of both techniques simultaneously provides maximum understanding and the best assessment of engine thrust. The external force balance method (Figure 125A) requires assessment of the flowstream force at the inlet of the thrust-stand-mounted engine inlet duct. The measurement uncertainty of the stream force is higher in a non-uniform flow field and may significantly affect thrust measurement uncertainties during testing with inlet flow distortion. The internal force balance method (Figure 125B) is an alternative way of testing to assess the effects of inlet distortion on engine thrust performance. Engine fuel flow and engine exhaust ambient pressure measurement uncertainties usually are not impacted by inlet flow distortion so that conventional measurement techniques may be used to assess engine performance with and without inlet flow distortion.

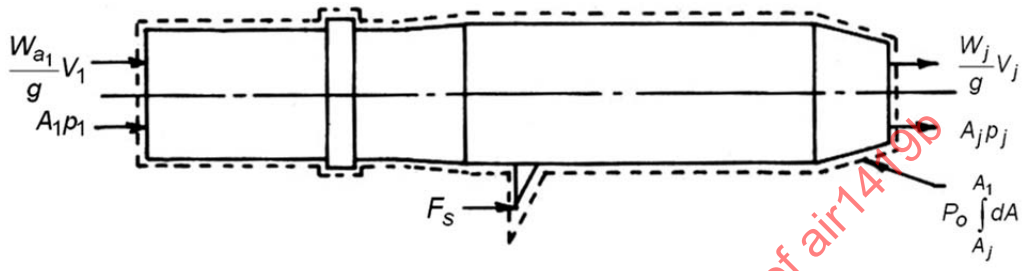

$$\sum F_X = C$$

$$\frac{W_{a_1}}{g}V_1 + A_1p_1 + F_s - P_o\int_{A_j}^{A_1}dA - \frac{W_j}{g}V_j - A_jp_j = 0$$

$$\frac{W_j}{g} = V_j + A_j(p_j - p_o) = \frac{W_{a_1}}{g}V_1 + A_1(p_1 - p_o) + F_s$$

$$F_{j_s} = \frac{W_j}{g}V_j + A_j(p_j - p_o)$$

$$F_{j_s} = \frac{W_{a_1}}{g}V_1 + A_1(p_j - p_o) + F_s$$

FIGURE 125A - EXTERNAL FORCE BALANCE SYSTEM

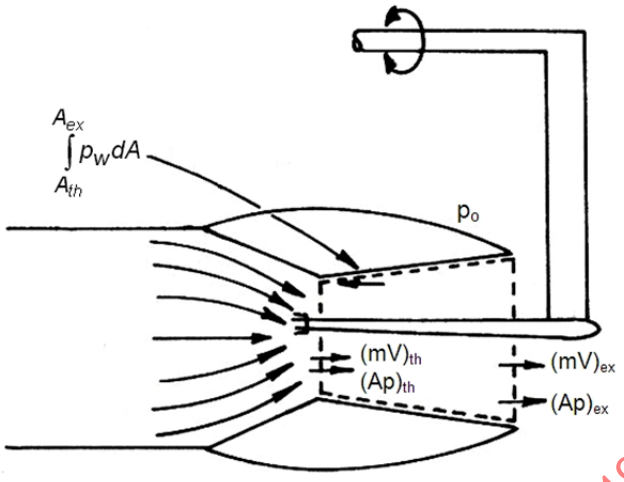

$$\sum F_X = 0$$

$$\sum F_X = \int_0^{A_{th}} \frac{(mV)_{th}}{A} dA + \int_0^{A_{th}} p_{th} dA - \int_{A_{th}}^{A_{ex}} p_w dA - \int_0^{A_{ex}} \frac{(mV)_{ex}}{A} dA - \int_0^{A_{ex}} p_{ex} dA$$

$$F_j = \int_0^{A_{ex}} \frac{(mV)_{ex}}{A} dA + \int_0^{A_{ex}} p_{ex} dA - A_{ex} p_o$$

$$F_j = \int_0^{A_{th}} \frac{(mV)_{th}}{A} dA + \int_0^{A_{th}} p_{th} dA - \int_0^{A_{ex}} p_w dA - A_{ex} p_o$$

FIGURE 125B - INTERNAL FORCE BALANCE SYSTEM

FIGURE 125 - ENGINE THRUST MEASUREMENT TECHNIQUES IN GROUND TEST FACILITIES

8. INTERFACE INSTRUMENTATION AND DATA MANAGEMENT

Instrumentation, data acquisition systems, data editing, and data reduction techniques necessary to acquire total-pressure distortion and performance test data are described. Since not all aircraft systems will have the same requirements, examples are presented to serve as a guide.

Inlet/Engine Aerodynamic Interface Plane

The inlet/engine aerodynamic interface plane (AIP) is the instrumentation station used to define total-pressure recovery and distortion interfaces between the inlet and engine. As described below, the selection and configuration of the AIP are dependent upon the nature of the program and the specific design of the inlet and engine. The AIP definition, as stated in ARP1420, must be agreed upon by all involved parties and should remain invariant throughout the test program.

AIP Location

The location of the AIP is a function of the details of engine and inlet design for a particular installation. The guidelines presented in ARP1420 are listed in Table 17 for convenient reference. In general these guidelines suggest that the AIP be located within a few inches (full-scale) of the compressor face. This will permit location of the AIP rake downstream of takeoff or bypass doors and other inlet variable geometry. In some cases it may be feasible to locate the instrumentation in the fan inlet guide vane (IGV) leading edge to minimize the effect of rakes upstream of the IGVs on the engine. In other cases it may be difficult to locate a rake close to the engine face. One example is an engine without IGVs and with a rotating bullet nose. In such a case, it may be more reasonable to locate the rake forward of the bullet nose providing the inlet is sufficiently long. During engine distortion tests with installations where the AIP is located appreciably forward of the first blade row, the inlet diffuser contours between the AIP station and the first blade row should be duplicated. Photographs of AIP instrumentation locations in several flight test aircraft are shown in Figures 126 through 128. Each installation has advantages and disadvantages that must be weighed against program objectives.

TABLE 17 - ARP1420 GUIDELINES FOR LOCATION OF THE AIP

1. The AIP should be located in a circular or annular section of the inlet duct.
2. The AIP should be located as close as practical to the engine-face plane. The engine-face plane is defined by the leading edge of the most upstream engine strut, vane, or blade row.
3. The AIP should be located so that all engine airflow, and only the engine airflow, passes through it. The distance between the inlet auxiliary air systems and the AIP should be such that the effect of the auxiliary air systems on distortion is included in the measurements at the AIP.
4. The AIP location should be such that the engine performance and stability are not measurably changed by interface instrumentation.

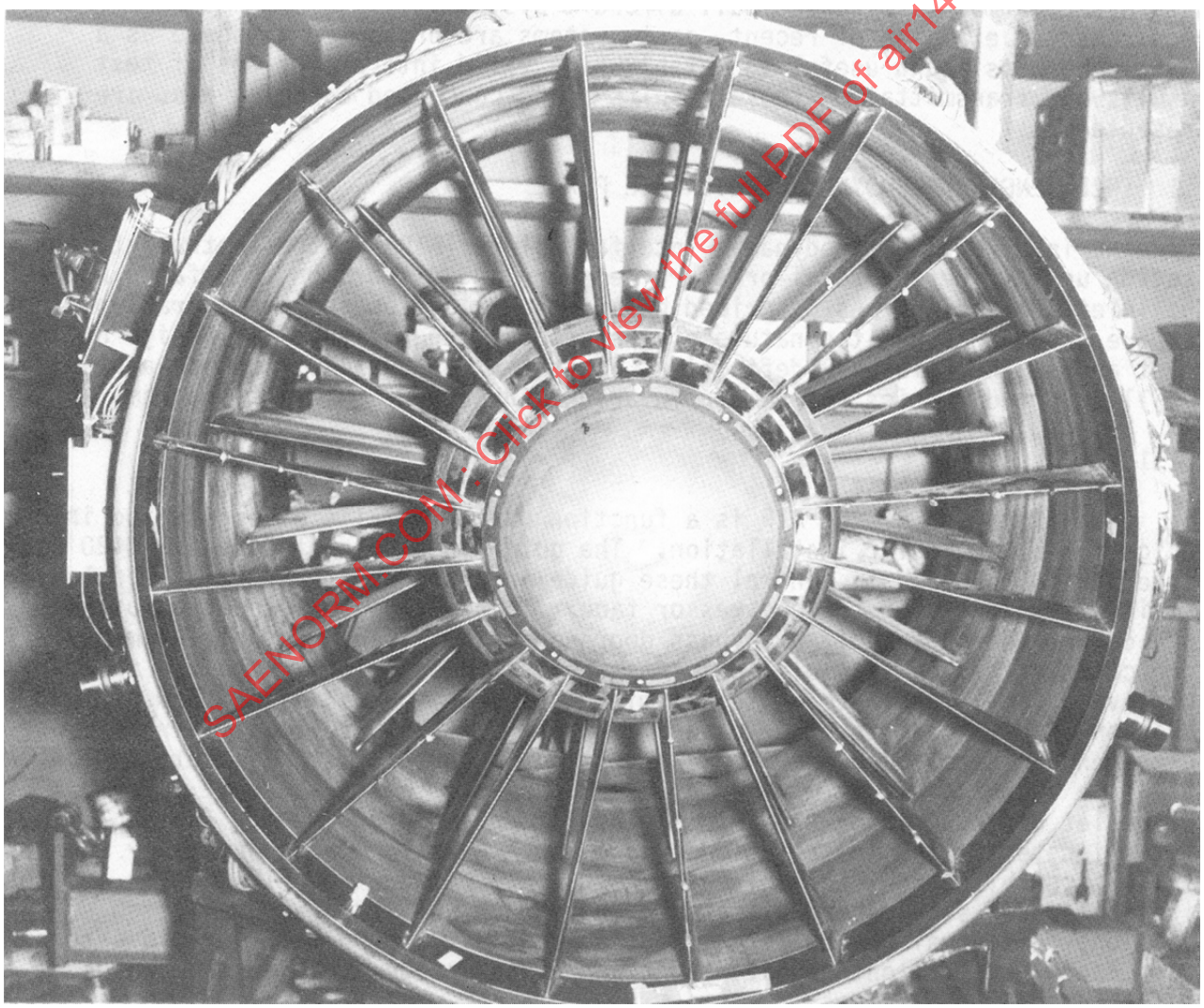

FIGURE 126 - AIP INSTRUMENTATION INTEGRAL WITH IGVS

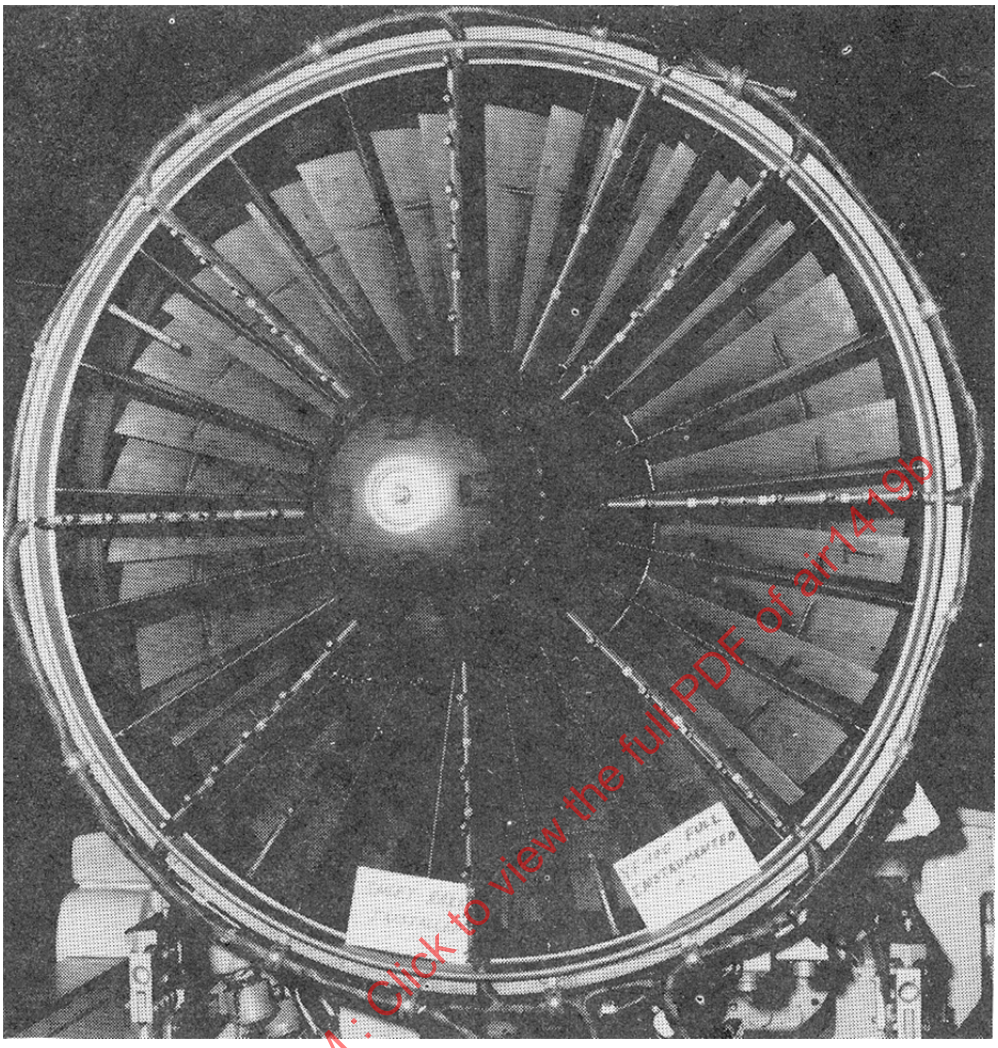

FIGURE 127 - AIP INSTRUMENTATION MOUNTED ON AIRCRAFT RAKES JUST FORWARD OF IGV LEADING EDGE

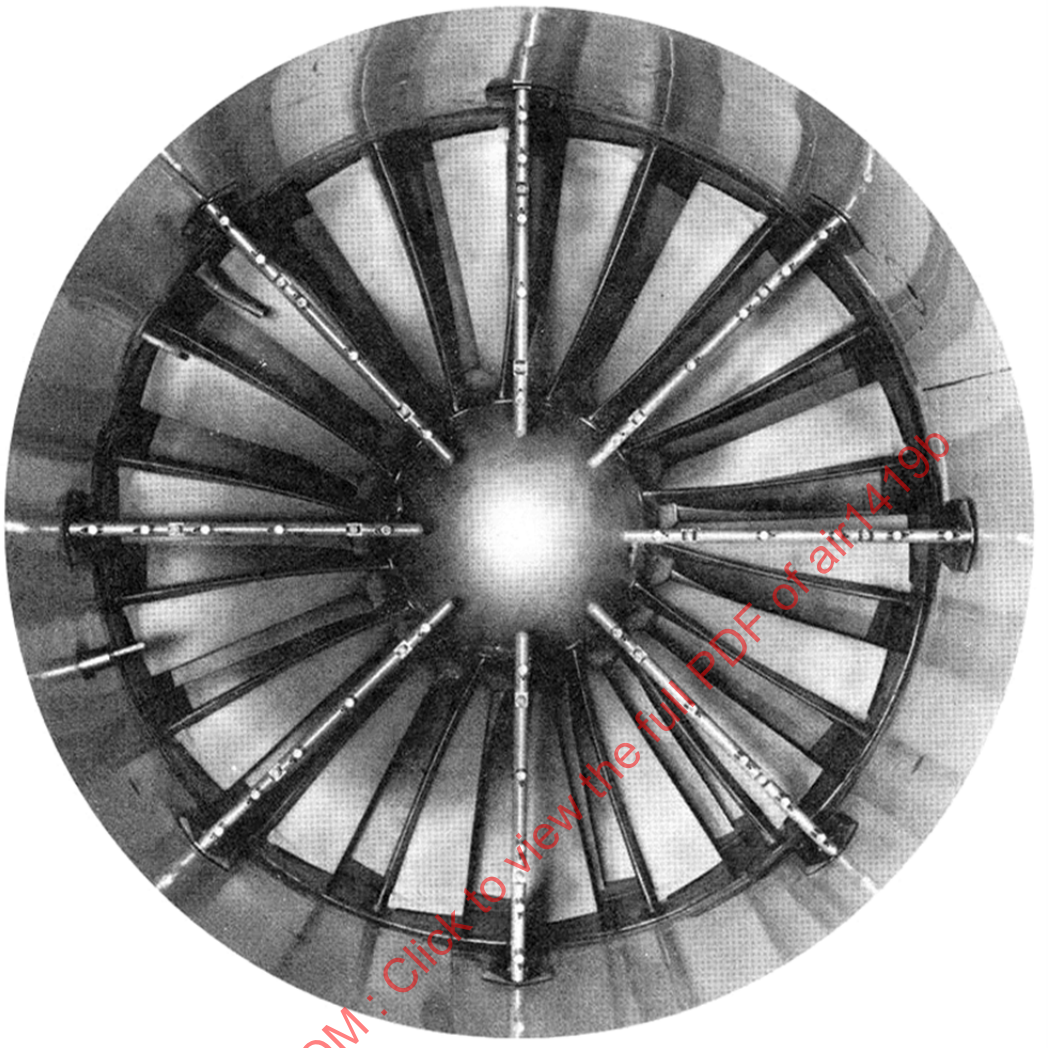

FIGURE 128 - AIP INSTRUMENTATION MOUNTED ON AIRCRAFT RAKES INSTALLED UPSTREAM OF THE BULLET NOSE

Probe Location and Density

Selection of the number and location of probes at the AIP is a compromise between accuracy of the pattern measurement and problems associated with data acquisition system complexity and rake-induced flow blockage. Studies have been conducted (e.g., Reference 2.2.25) in which specific patterns were evaluated using different rake arrangements. The general conclusion is that, for a typical pattern, a 40-probe (8 rakes of 5 probes each) arrangement like the one shown in Figure 129 is the minimum density of instrumentation required for reasonably accurate measurements.

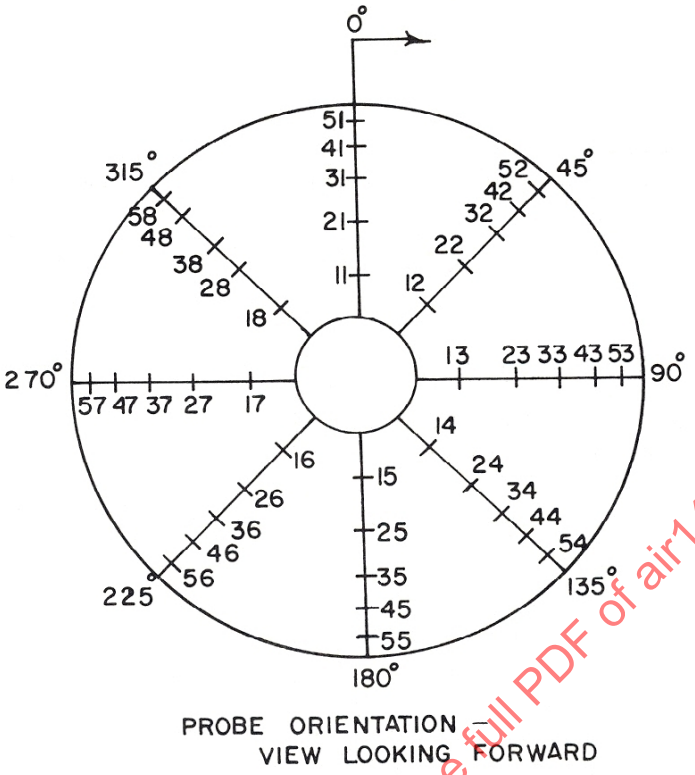

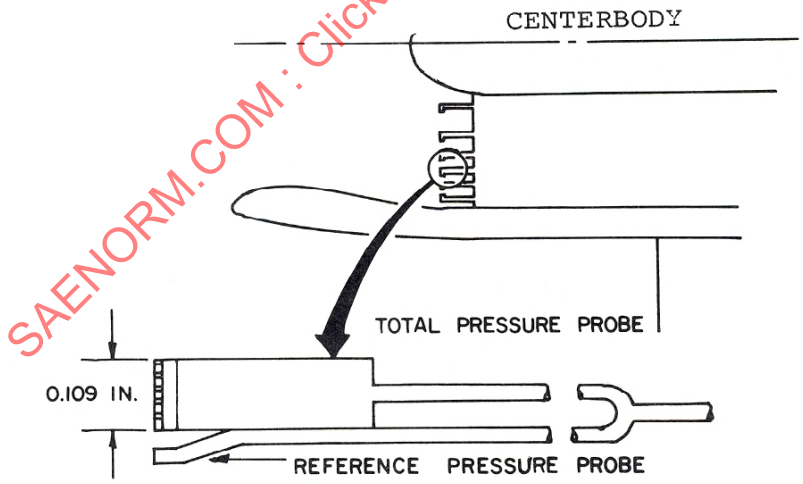

FIGURE 129 - TYPICAL 40-PROBE/RAKE ARRANGEMENT

The 40-probe AIP rake is normally used because it provides sufficient characterization for inlet distortion and performance purposes in the F-15/16 class of aircraft. More complex inlets can produce additional flow content which may require more probes to define the higher multiple-per-rev content. Such higher MPR content generally has a more significant impact on compression component aeromechanics (high cycle fatigue) than on engine operability.

For engine programs with rakes integrated with engine vanes, probe locations are dictated by engine strut design and may differ from the equal area location methodology used in wind tunnel tests. This can cause differences between flight and ground test results. This discrepancy is noted in AIR5687 (Reference 2.1.1.9). The wind tunnel test rake should be designed, if possible, to match the flight test rake (may be difficult to accomplish if the engine design is not known).

As an example, the pattern shown in Figure 130 was evaluated in the Reference 2.2.25 study. The pattern is highly distorted circumferentially, with relatively low radial distortion. Several probe/rake configurations were used in the study. Each probe/rake configuration was rotated through 360 degrees in 20 degree increments, and pressure readings were taken at each probe position for each incremental rotation. Circumferential and radial distortion factors, K_θ and KRAD, were computed from each set of data. The results are plotted in Figure 130 where ΔK_θ is the maximum K_θ minus the minimum K_θ realized for a given probe/rake combination. At least eight rakes are required to define the circumferential distortion. The large percentage errors in radial index are primarily due to the low levels of radial distortion.

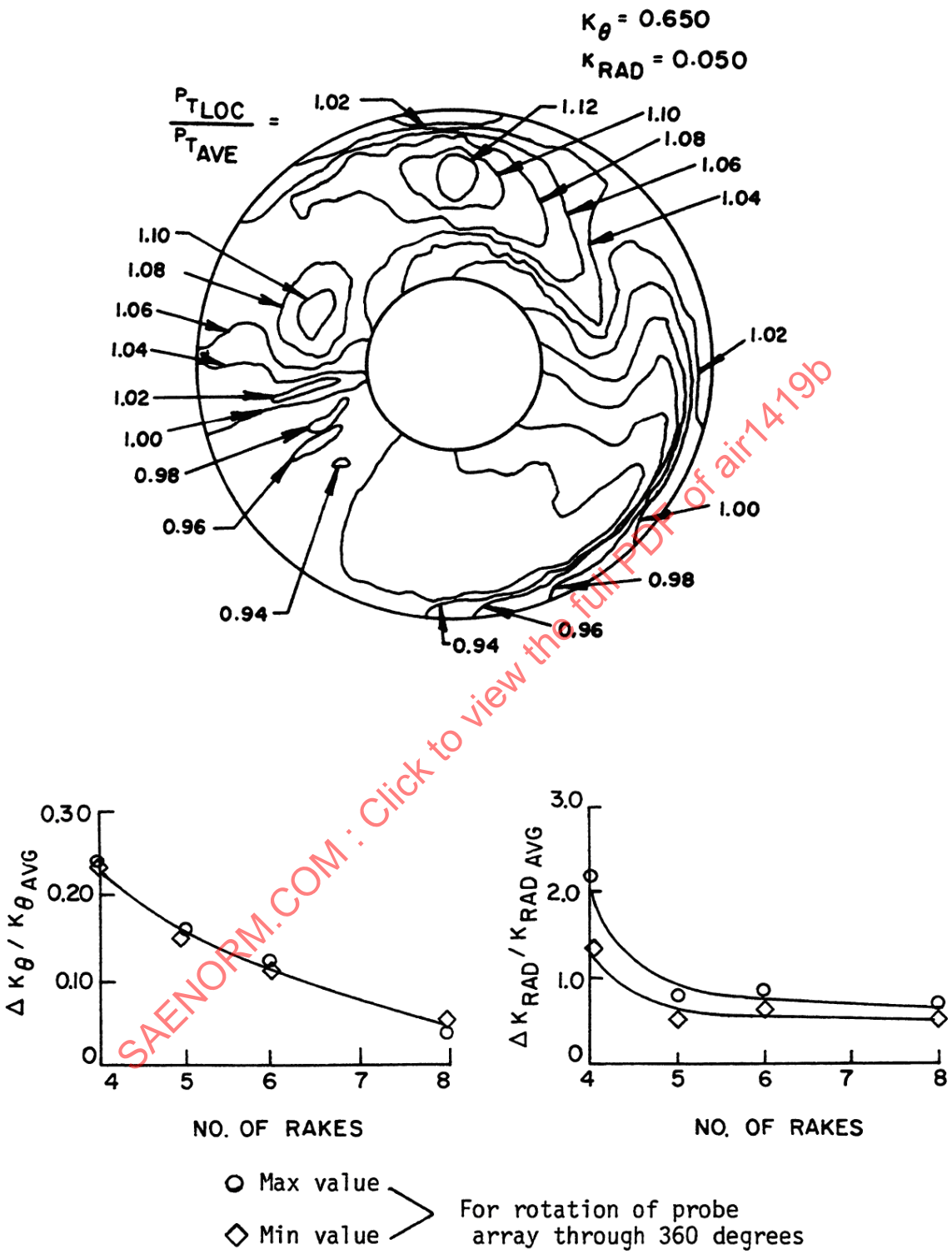

FIGURE 130 - DISTORTION FACTOR DEPENDENCE ON PROBE/RAKE CONFIGURATION

For a particular installation, the type of pattern anticipated may influence the rake selection. For example, an inlet with a strong radial distortion may require more than five probes per rake. A bifurcated inlet may require that special attention be given to the circumferential location of the rakes in relation to the trailing edge of the bifurcation.

Generally, the probes should be of such design that both the steady-state and dynamic components of total pressure can be recovered (see 8.2.1). This can be accomplished with various combinations of rake-mounted transducers, close-coupled transducers and signal conditioning equipment. Technology in probe design and placement is reviewed in Reference 2.2.26.

Considerable research effort has been expended to investigate accuracies to which instantaneous distortion parameters can be defined with various rake and probe configurations. It has been found that reasonably accurate values of engine face distortion parameters can be obtained with fewer than 40 total pressure probes, particularly when sufficient knowledge exists to select a proper data fill procedure. Using this approach, the optimum probe location for any given number of probes is dependent on the particular distortion pattern and the descriptor to be used.

In addition to the steady-state and high-response total-pressure probes, flow that contains bulk or localized swirl may require special probes to provide information about flow angularity at the AIP. More information about swirl is provided in Reference 2.1.1.10.

8.1 Applications

The preceding paragraphs have described the general requirements for probe location and arrangement. Examples presented below illustrate a variety of probe locations and arrangements employed in recent aircraft programs.

Large subsonic transports are not usually subjected to high angle-of-attack conditions. This point, when combined with the small range of aircraft cruise speed, usually permits an inlet to be designed with a minimum of engineering resources. Important exceptions include initial climbout and crosswind operation. For example, scale-model testing of the Boeing 747 inlet indicated that the total-pressure defect was restricted to the fan tip. As a result of these data and the constraint imposed by a rotating bullet nose on the engine, flight tests were conducted using partial span rakes cantilevered from the inlet wall. These rakes extended well into the high-pressure region of the inlet.

The full-span, high-response rake shown in Figure 131 was used by Pratt and Whitney in a JT9D/747-100 nacelle flown on a B-52 test aircraft evaluating thrust reverser induced stalls (Reference 2.2.27). The rake has a bearing-supported ring at the hub to accommodate the rotating hub. This type of installation is useful in exploring reverser or crosswind related patterns, which may be substantially different from flight patterns.

A 40-probe array was used throughout the B-1A development program. The program included 0.10-, 0.20- and full-scale inlet tests as well as flight tests. Small differences in angular location were necessary among these models due to the evolving nature and availability of particular IGV locations. Probes were integral with the leading edge of the IGVs, and attempts were made to align the probes with the flow streamlines. Both steady-state and high-frequency total-pressure signals were generated from single transducers at each location during the flight test.

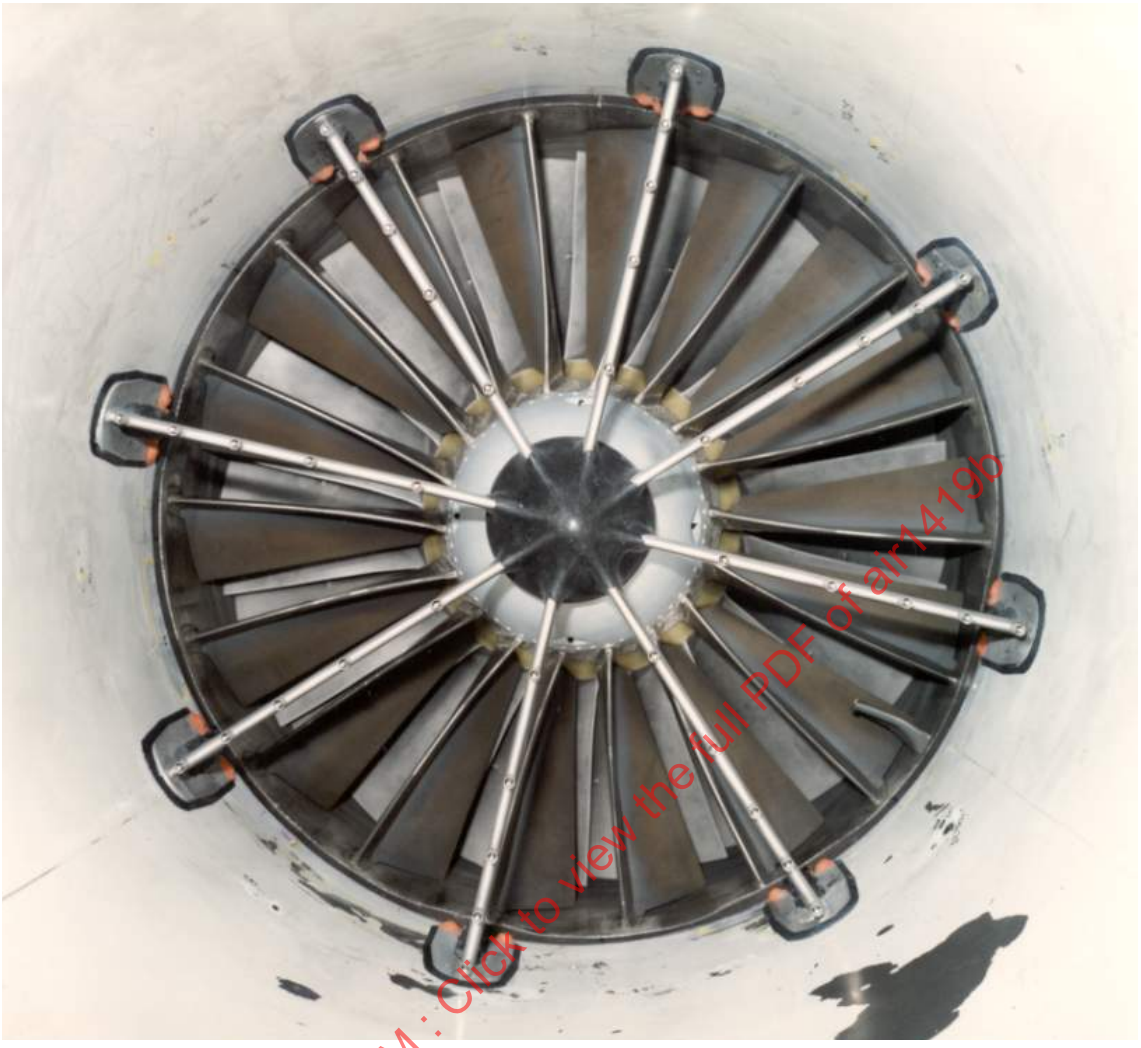

FIGURE 131 - FULL SPAN NON-IGV ENGINE INLET RAKES

On fighter aircraft programs, AIP instrumentation is also used to define both total-pressure recovery and appropriate distortion descriptors. Inlet geometry can be variable, and the aircraft is frequently required to perform highly dynamic maneuvers. The Integrated Propulsion Control System (IPCS) Program (Reference 2.2.28) employed the 40-probe array shown in Figure 129 to evaluate inlet performance and distortion using an F-111 aircraft. The AIP was located approximately four inches upstream of the leading edge of the inlet guide vanes. A photograph of the AIP rake is shown in Figure 132, and the design is discussed in 8.3.2.

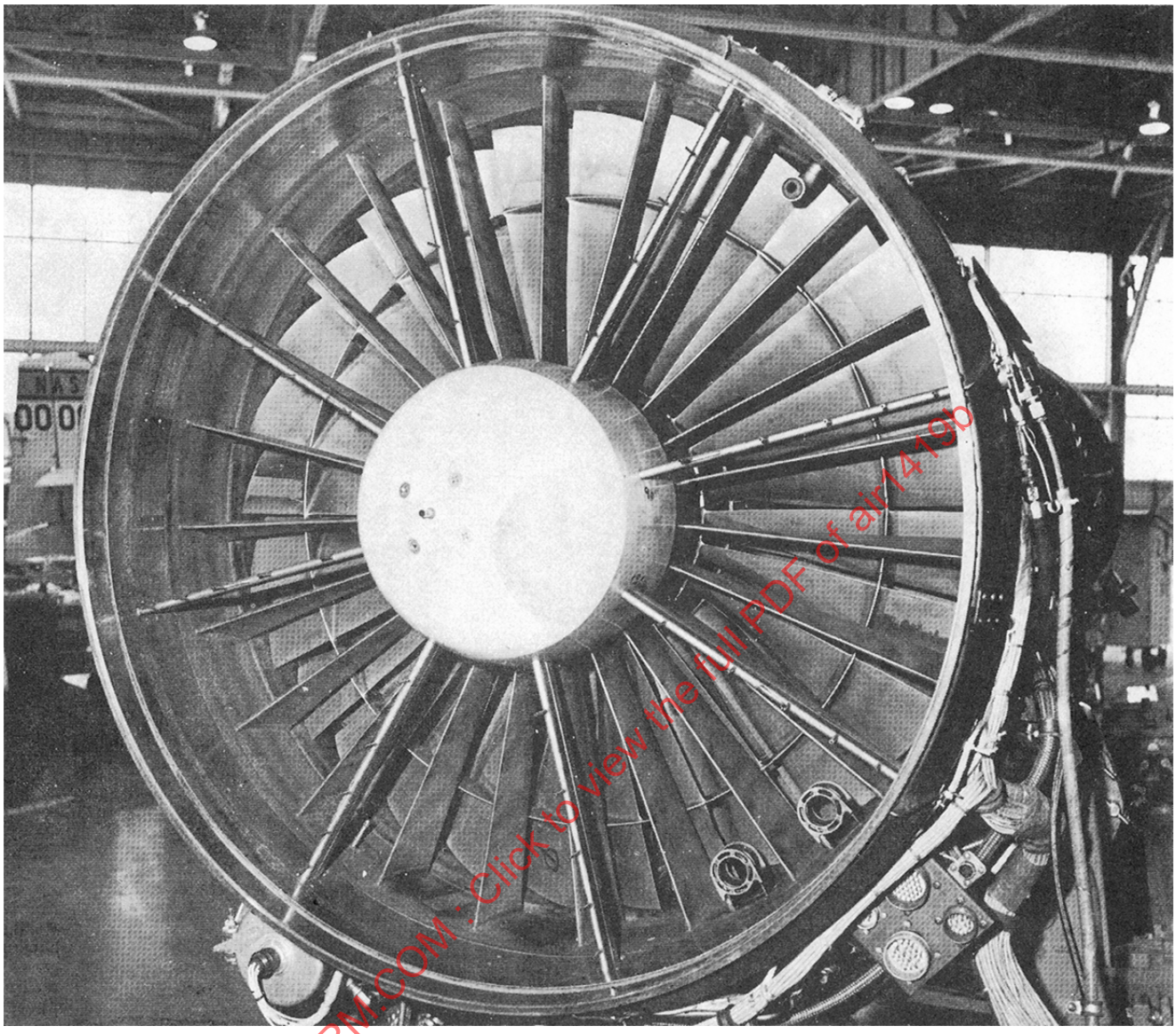

FIGURE 132 - COMPRESSOR FACE RAKE

The F-15 program employed a 48-probe arrangement on subscale and full-scale wind tunnel test programs as well as during the flight test program. The double probe configuration used for full-scale tests is shown in Figure 133. Dynamic transducers were installed in the airframe assembly in a manner that permitted replacement without engine removal. Pressure was sensed 4.5 in upstream of the leading edge of the IGVs. Steady-state pressures were sensed at the same inlet station with the transducers installed in a controlled environment in the bullet nose.

The HiMAT and F-16 provide two examples of programs where no AIP data were recorded during initial flight tests of highly maneuverable aircraft. However, both programs employed engines with well-developed stability characteristics, and the inlets were modeled after proven designs.

Another example, a subscale XFV-12A, used a 40-probe array in wind tunnel tests to identify inlet-distortion characteristics of a VSTOL fighter/attack aircraft.

In summary, AIP instrumentation for each system was judged on its own merit, balancing costs and technical objectives against risks. However, it is evident that whenever relatively new inlet/aircraft concepts are programmed in conjunction with the development of a new engine, inlet/engine compatibility characteristics are of sufficient concern to warrant the use of the 40-probe 8 × 5 total-pressure rake located as close as possible to the engine inlet. It is this preference that is expressed in ARP1420.

8.2 Transducer/Probe Characteristics

A transducer/probe configuration must meet two basic requirements to properly resolve the fluctuations produced by turbulent flow: (1) the transducer must have a nominally flat response up to frequencies in excess of the highest frequency of interest, and (2) the probe must be smaller than the characteristic size of the eddy producing the highest frequency of interest. Both of these requirements are discussed in Reference 2.2.29 and are summarized in the following paragraphs.

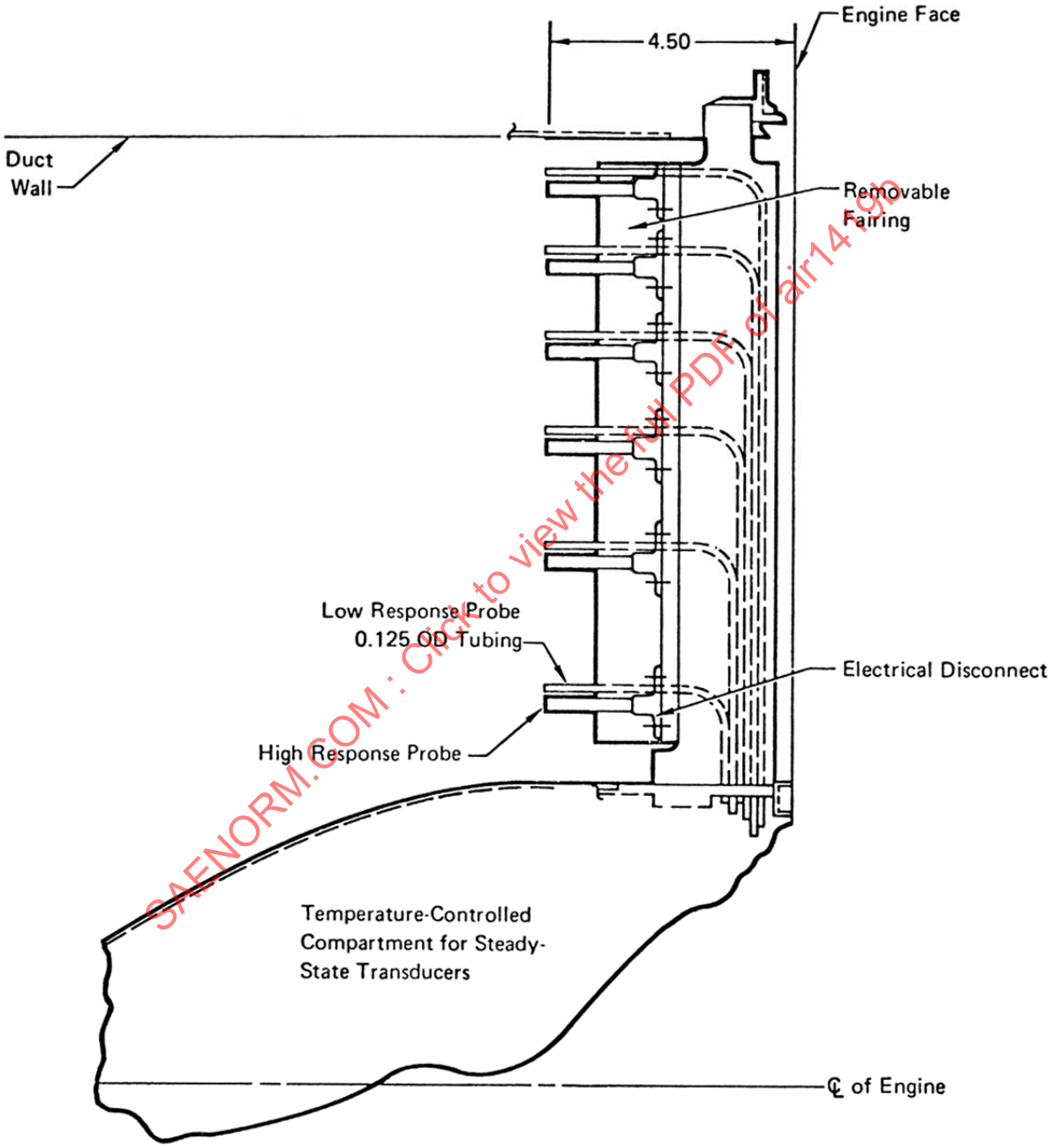

FIGURE 133 - F-15 RAKE CONFIGURATION

8.2.1 Frequency Response

Studies of the effect of time-varying flow on compressors such as the one described in Reference 2.2.4 have shown that distortion at frequencies corresponding to the appropriate design RPM of the critical compression unit has a significant impact on stability. In addition, higher frequency fluctuations, up to 2000 Hz, have been shown to affect compressor pumping characteristics (6.4). A flat transducer response also requires that the natural frequency of the transducer be two to three times higher than the highest frequency of interest to avoid problems in signal amplification. Further, the transducer must be sufficiently close to the measurement location that frequencies of interest are not affected by the installation.

8.2.2 Probe Size Criteria

Spatial averaging of the total-pressure fluctuations occurs as the eddy characteristic size becomes commensurate with the transducer or probe diameter. The result is that the measured auto-power spectral density at high frequencies is less than the actual auto-power spectral density.

Consider a turbulent flow with convective velocity, U_c. In the free-stream, an eddy would propagate with the flow velocity.

$$U_C = f_U \lambda_U \quad \text{(Eq. 90)}$$

where f_u is one frequency component and λ_u is its associated characteristic wave length. Suppose it is desired to resolve an eddy of characteristic wave length λ_u using a transducer of diameter D such that $D<<\lambda_u$.

The characteristic length of the eddy is L = 1/2 λ_u, shown in Figure 134. As a rule of thumb, the sensor size should be at most one-tenth the size of the phenomenon under examination. Hence,

$$D = \frac{L}{10} = \frac{\lambda_U}{20} \quad \text{(Eq. 91)}$$

Then,

$$f_U = \frac{U_C}{20\ D} \quad \text{(Eq. 92)}$$

where f_u is interpreted to be the highest frequency to which a turbulent flow can be resolved. Two important conclusions can be drawn from the above equation:

1. The upper frequency limit for a given velocity and accuracy of resolution can be increased by using smaller diameter transducers.

2. The upper frequency limit for a transducer of a given size and accuracy of resolution decreases as the velocity decreases.

For a given frequency component, as the wave length becomes commensurate with the transducer diameter, both high and low values of the property being measured will be located simultaneously over the transducer surface, illustrated in Figure 134. The values will tend to average out each other. In essence, this is the concept of “spatial averaging.” Hence, the spatial averaging of turbulence that occurs during any measuring process in a turbulent flow depends upon the interrelationship of flow velocity, highest frequency of interest, and transducer diameter.

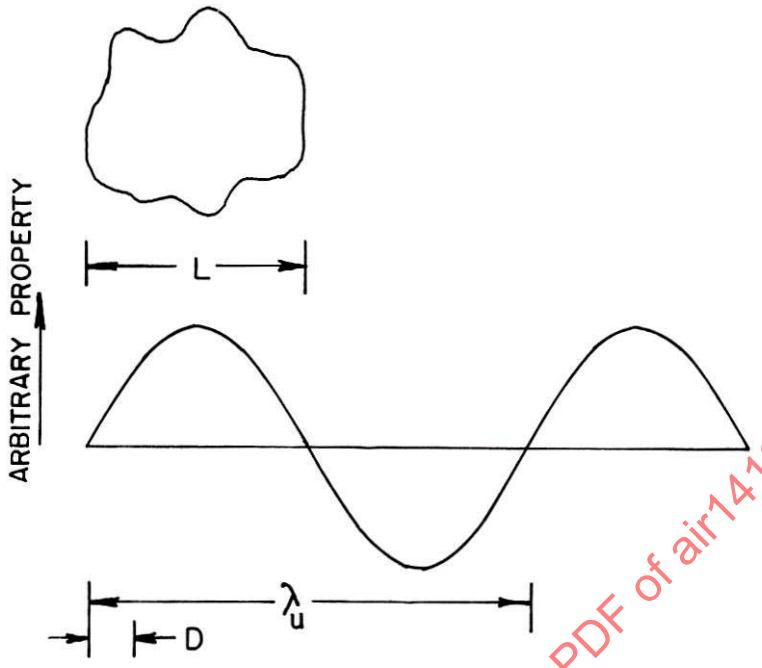

FIGURE 134 - SKETCH ILLUSTRATING THE EFFECT OF PROBE SIZE

Equation 92 is derived from theoretical considerations and is intended to provide a quick, order-of-magnitude estimate of the limiting frequency. Experimental data have been evaluated and are presented in Reference 2.2.29 for specific probe sizes. Effects of probe diameter on spatial averaging are shown in Figure 135. Typical smoothed auto-power spectra, ϕ, were obtained from the total-pressure fluctuations at a flow velocity of 236 ft/s. The spatial averaging effect is quite apparent, and as expected, the smallest diameter probe gives the highest auto-spectral values.

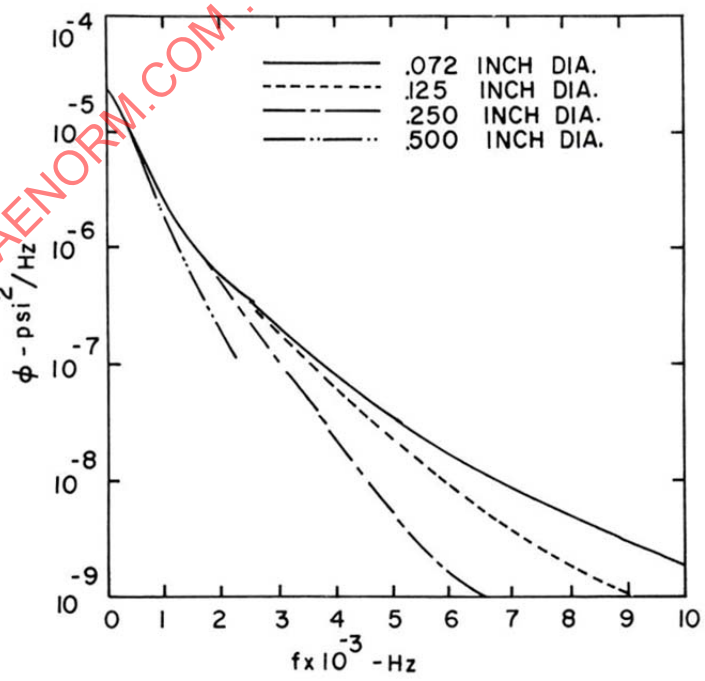

FIGURE 135 - EFFECT OF TRANSDUCER DIAMETER

Finally, the limiting frequency for which 90% or more of the actual total-pressure power spectra is resolved is given in Figure 136 as a function of the convective velocity for several commonly used transducer diameters. These data show a limiting frequency approximately three times that given by the equation above. Typically, the convective velocity will be of the order of 200 to 600 ft/s. Transducers in the 0.06- to 0.125-in diameter range are available. As shown in Figure 136, it is possible to acquire data over the frequency range of interest for stability evaluation. Scaling criteria, discussed in 8.3.3, are also applicable to transducer/probe characteristics.

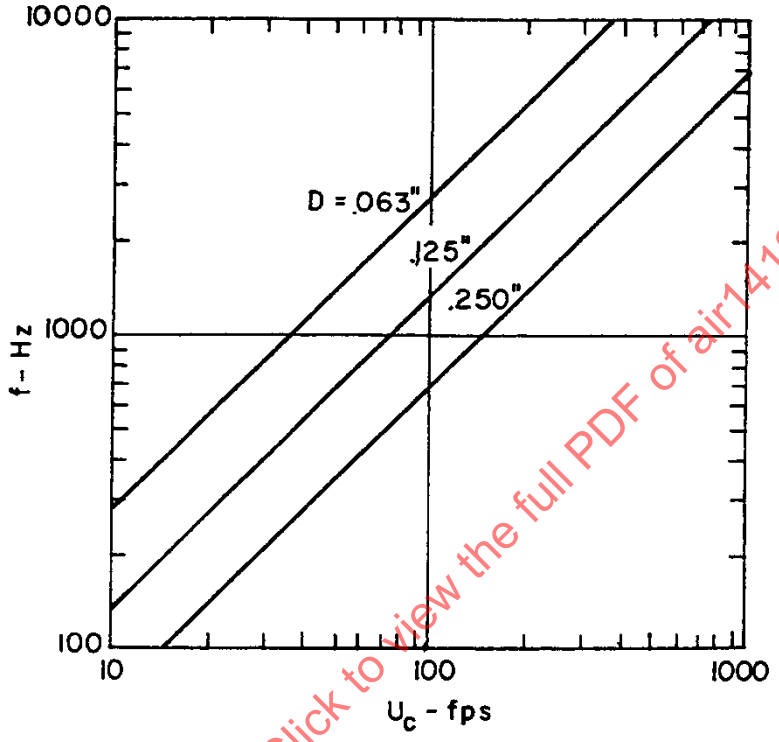

FIGURE 136 - FREQUENCY BELOW WHICH AT LEAST 90% OF SPECTRAL FUNCTION IS SENSED

8.3 Data Acquisition System

Foresight in configuring appropriate data acquisition systems can result in large dividends in subsequent data reduction and analysis tasks. Recording techniques are described, and guidelines are provided for system accuracy, frequency response, and data record length.

8.3.1 General Description

The data acquisition system consists of the hardware and software required to sense and record the data. The details of the system requirements will depend on the specific high-response transducer selection, sampling rate and data accuracy. The signal from the transducers is generally low level (less than 50 mv), and the voltage is proportional to the sensed pressure. Each analog signal, filtered if necessary, is input to a digital data acquisition system. Each transducer is simultaneously digitally sampled and recorded at a rate consistent with the filtering requirements and the maximum frequency of interest. A time code is included for each sample. The design of one system is described in Reference 2.2.30.

8.3.2 System Accuracy

A high degree of accuracy in the pressure measurement is necessary in order to quantify the distortion. Small differences between pressures become significant in the distortion descriptors presented in Section 4. The problem is made more difficult by the large range of inlet pressure levels encountered at different flight conditions. For example, pressures as high as 34 psi will be measured at Mach 1.2, sea level, and the pressure will drop to 2.8 psi during operation at Mach 0.9, 50 000 ft. These required pressure ranges make the accurate measurement of even steady-state pressures difficult.

Individual steady-state pressures (signals time-averaged to attenuate frequencies greater than 0.5 Hz) should be recovered with an error not to exceed ±0.5% (± two standard deviations) of the absolute pressure being measured. Individual dynamic absolute pressures (containing data to at least the highest frequency of interest) should be recovered with an error not to exceed ±2.0% (± two standard deviations) of the absolute pressure being measured for stability and ±5.0% (± two standard deviations) for performance. These errors include all errors introduced by the sensing, recording, playback, and processing systems from the point where the pressure signal is being measured to the point where it appears as an output pressure.

Measurement of dynamic or time-varying absolute pressure is more difficult because transducers with adequate frequency response and sufficiently small size are sometimes not accurate enough and often exhibit temperature sensitivity. This is especially true for subscale or small full-scale applications. Technical advances have provided significant transducer miniaturization, resulting in a relatively small transducer that accommodates an absolute gauge with an integrated heater to eliminate temperature sensitivity. These transducers are suitable for many full-scale applications. In full-scale applications where the temperature-controlled absolute transducers cannot be used it is generally necessary to apply some form of in-flight calibration to achieve the accuracy goals stated above. This is particularly true when the operating temperature ranges in an exposed inlet rake are considered. The following paragraphs discuss calibration methods that have been used.

The dynamic content of inlet total pressure is small compared to the overall pressure level. Turbulence RMS levels of less than 3% of average AIP steady-state total pressure are typical. This leads to the idea of separately measuring the high- and low-frequency components of total pressure in applications where the thermally controlled absolute transducers are not applicable (due to size, cost, etc.). Accuracy can then be improved by tailoring transducer and signal conditioning ranges to maximize resolution for each of the individual components. Low frequency response measurements can be made with larger, more accurate transducers located remotely in environmentally controlled areas to increase accuracy.

Several different approaches have been used to improve accuracy. The following paragraphs describe four: (a) the use of a rake which mechanically zeros a high-frequency-response, differential-pressure transducer, (b) post-test correction of average pressure using accurate steady-state measurements, (c) analog or digital summing of low- and high-frequency measurements and (d) use of a thermally-controlled absolute pressure transducer.

In testing an F-111 aircraft, NASA/DFRC used a rake which provided transducer zero-shift data by mechanically applying a reference pressure to both sides of the transducer diaphragm (Reference 2.2.31). The concept is shown in Figure 137. A solenoid-operated pneumatic actuator positioned the center rod in either the “zero” or “data” position. In the “data” position the transducer was connected to the rake probe. In the “zero” or “null” position the reference pressure was vented to both sides of the diaphragm. This rake was used in a number of flight test programs (Reference 2.2.28) with reference pressure a function of flight condition to minimize the component measured by the high-response transducer.

The major advantage of this approach was that only one low-frequency-response transducer is required instead of 40. This reduces data acquisition and maintenance costs. There are, however, two significant disadvantages: (1) it is difficult to prevent leakage in the rake seals, particularly under high-temperature flight conditions, and (2) the steady-state measurements are made with the high-frequency-response transducers.

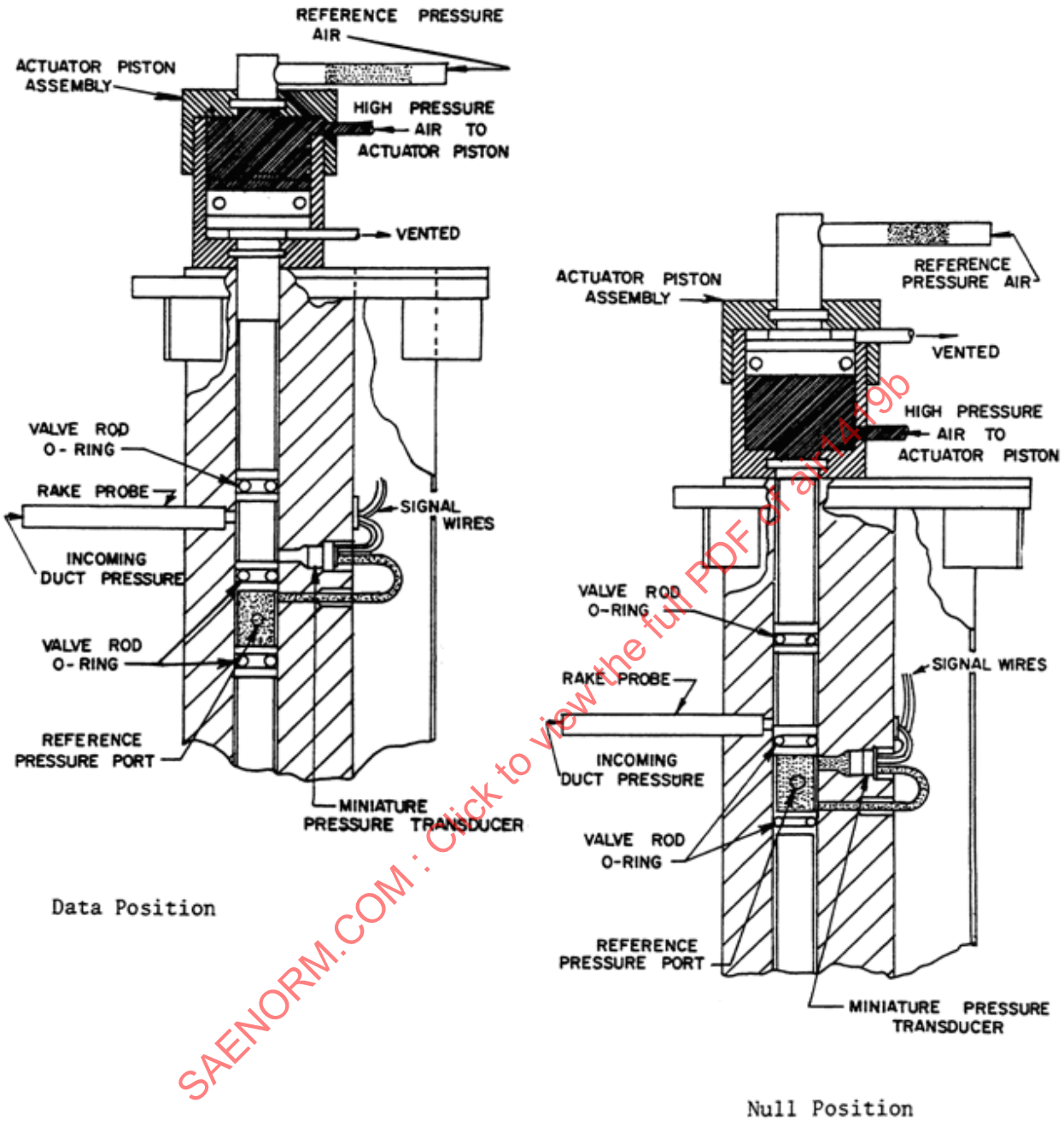

FIGURE 137 - NASA DRYDEN FLIGHT RESEARCH CENTER RAKE

A variation of this approach (Figure 138) was used during the B-1 flight test program. Instead of venting the reference pressure to both sides of the diaphragm, the sensed pressure was routed to both sides to provide a “zero” measurement. Additionally, the back side of the transducer was routed to a pressure regulated to 5.0 psi above the reference pressure. This required a three-way pneumatic valve for each transducer. Valves were cycled once per minute throughout the flight with the zero and calibrate positions held for 2 s each. In order to maintain signal resolution, provisions were also incorporated to change gains as a function of free stream total-pressure level. Although the data reduction effort becomes a little more involved, considerable success was achieved in measuring both low- (quasi-steady state) and high-frequency total-pressure components with a miniature transducer. (Success in this case means obtaining wind tunnel and flight test results that were consistent with each other.)

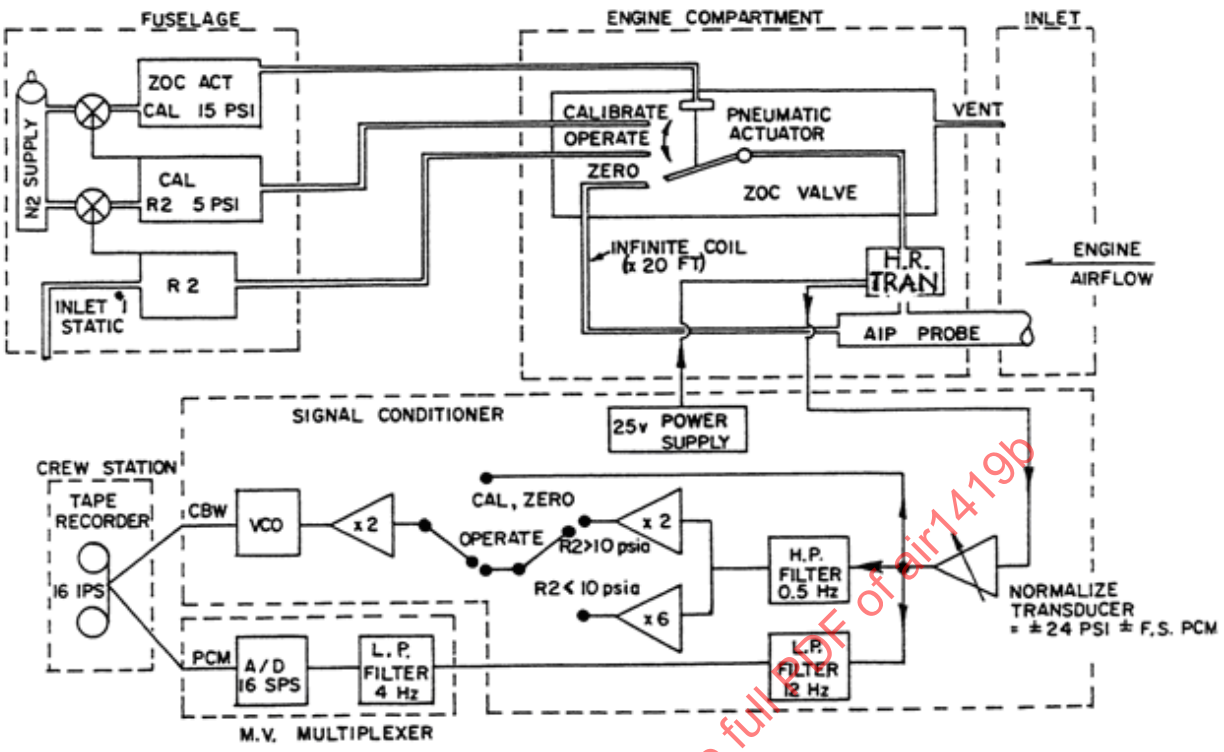

FIGURE 138 - B-1 FLIGHT TEST DATA ACQUISITION SYSTEM

A second approach, used in inlet/engine testing at NAPC and AEDC, involved the use of a rake having separate probes for steady-state and high-frequency-response measurements (Figure 139). In the post-event data processing, the time average of the high-response data for each probe was corrected to the steady-state value measured at the same time. With this approach, only the dynamic pressure fluctuations were measured with the high-frequency-response transducer. As with the zeroing rake, it requires significant post-event processing. This method also requires additional steady-state transducers. In addition, there is a measurement defect associated with using side-by-side probes (Reference 2.2.32).

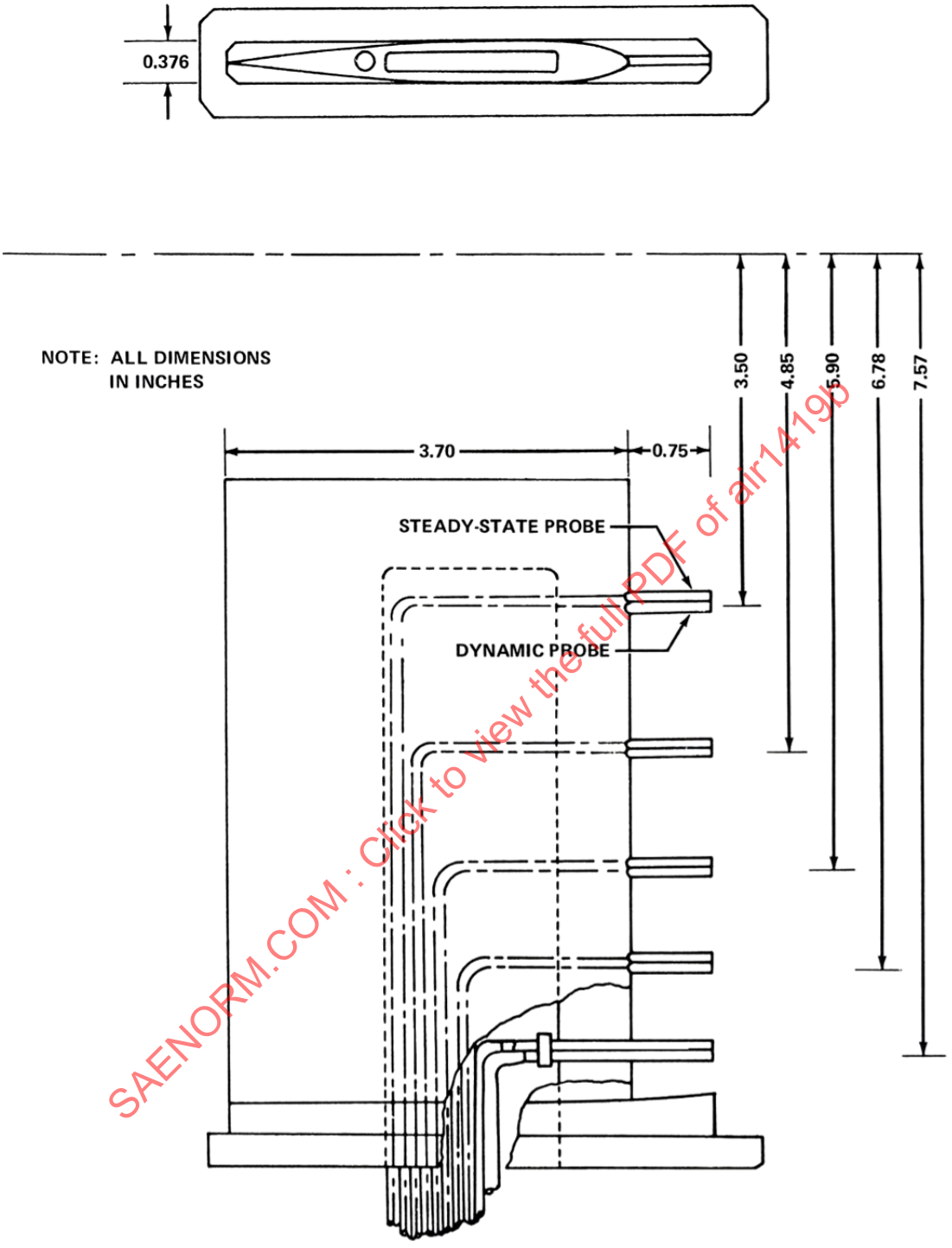

FIGURE 139 - DOUBLE PROBE RAKE CONFIGURATION

A third approach is similar to the second in the use of separate probes for steady-state and dynamic measurements. The difference is that the output of the low-frequency “steady-state” transducer is low-pass filtered and electrically added to the high-pass-filtered output of the high-frequency-response transducer. This process, as used in a Boeing wind tunnel test program, is illustrated in Figure 140. A similar system was used in F-15 flight testing. This approach reduces the data reduction effort and provides an electrical signal with the full frequency content which can be used in subsequent processing. Care must be taken to ensure high accuracy in the filtering and summation circuits to avoid degraded accuracy in the resulting pressures. Recent applications which use a combination of separately measured steady state and dynamic measurements utilize a digital data acquisition, filtering and recording system.